AD NUMBER

AD860679

LIMITATION CHANGES

TO:

Approved for public release; distribution is unlimited.

FROM:

**Distribution authorized to U.S. Gov't. agencies and their contractors;
Administrative/Operational Use; JUL 1969. Other requests shall be referred to Army Aviation Materiel Labs., Fort Eustis, VA.**

AUTHORITY

USAAMRDL ltr 23 Jun 1971

AD

USAAVLABS TECHNICAL REPORT 69-41

STUDY OF AN ADVANCED CONTROL SYSTEM FOR SMALL FREE-TURBINE ENGINES

By

Thomas L. Soule
Donald E. Anschutz
Melvin L. Perkins

June 1969

U. S. ARMY AVIATION MATERIEL LABORATORIES
FORT EUSTIS, VIRGINIA

CONTRACT DAAJ02-68-C-0041
HAMILTON STANDARD
DIVISION OF UNITED AIRCRAFT CORPORATION
WINDSOR LOCKS, CONNECTICUT

278

DISCLAIMERS

The findings in this report are not to be construed as an official Department of the Army position unless so designated by other authorized documents.

When Government drawings, specifications, or other data are used for any purpose other than in connection with a definitely related Government procurement operation, the United States Government thereby incurs no responsibility nor any obligation whatsoever; and the fact that the Government may have formulated, furnished, or in any way supplied the said drawings, specifications, or other data is not to be regarded by implication or otherwise as in any manner licensing the holder or any other person or corporation, or conveying any rights or permission, to manufacture, use, or sell any patented invention that may in any way be related thereto.

Trade names cited in this report do not constitute an official endorsement or approval of the use of such commercial hardware or software.

DISPOSITION INSTRUCTIONS

Destroy this report when no longer needed. Do not return it to the originator.

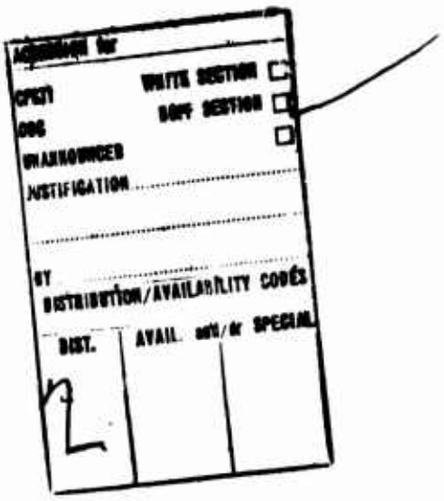

DEPARTMENT OF THE ARMY
U. S. ARMY AVIATION MATERIEL LABORATORIES
FORT EUSTIS, VIRGINIA 23604

The research described herein was conducted by Hamilton-Standard Division of United Aircraft Corporation under U. S. Army Contract DAAJ02-68-C-0041.

Appropriate technical personnel of this Command have reviewed this report and concur with the conclusions contained herein.

The findings and recommendations outlined herein will be considered in planning future programs relating to engine fuel control development.

Project 1G162203D144
Contract DAA JO2-68-C-0041
USAAVLABS Technical Report 69-41
June 1969

STUDY OF AN ADVANCED CONTROL SYSTEM FOR SMALL FREE-TURBINE ENGINES

Final Report

Hamilton Standard Engineering Report 5300

By
Thomas L. Soule
Donald E. Anschutz
Melvin L. Perkins

Prepared by
Hamilton Standard
Division of United Aircraft Corporation
Windsor Locks, Connecticut

for

U.S. ARMY AVIATION MATERIEL LABORATORIES
FORT EUSTIS, VIRGINIA

ABSTRACT

Advanced small free-turbine engines in the 2-to-5-pound-per-second airflow class currently envisioned for both helicopter and turboprop applications have undergone vast improvements in performance and efficiency which have led to large reductions in overall size. Effort is required at performance optimization and miniaturization of the engine control system to keep pace with these improvements.

This study program was undertaken to conceptually design an advanced engine control system for this class of engine, providing gas generator and power turbine control with torque, temperature, load sharing and overspeed limiting functions. The control system was to be designed to accommodate, with minimum hardware changes, such variants as regenerative cycle and/or variable geometry.

Efforts to determine the optimum control for the small engine of the mid-1970's fell into two major categories: mode of control selection and technology selection.

The overall system performance of ten modes of control was evaluated in detail. The selected mode consisted of a W_f/P_{T3} scheduling gas generator control and a proportional plus integral isochronous N_F governing control with turbine discharge temperature limiting.

Technology selection consisted of reviewing electronic, fluidic and hydromechanical technologies against a weighted set of evaluation criteria mutually established by Hamilton Standard and USAAVLABS for application to all portions of the proposed control system. This resulted in the selection of a hydromechanical gas generator control and an electronic N_F control with fluidic N_F overspeed sensing.

The resulting control is considered to be the optimum control for this class of engine based on the established criteria for production application in the mid-1970's.

FOREWORD

This is the final report on the Hamilton Standard project entitled "Advanced Control System for Application to Small Free-Turbine Engines". This study was conducted for the U.S. Army Aviation Materiel Laboratories (USAAVLABS) under Contract No. DAAJ02-68-C-0041, Project 1G162203D144, between July 1, 1968 and December 31, 1968.

USAAVLABS technical direction was provided by Mr. R. Furgurson, Propulsion Division. Mr. T.L. Soule served as the Hamilton Standard Program Manager and was supported by co-authors D.E. Anschutz, Design Project Engineer, and M.L. Perkins, Analytical Project Engineer. Mr. R.K. Rose of the General Electric Specialty Fluidics Operation supplied the fluidics technology contribution to the program.

TABLE OF CONTENTS

LIST OF ILLUSTRATIONS

LIST OF ILLUSTRATIONS (CONT)

LIST OF TABLES

LIST OF SYMBOLS

AC	alternating current
A/D	analog to digital
A_N	power turbine stator area
Btu	British thermal unit of heat
C	capacitance
°C	degree centigrade
C_D	coefficient of discharge
C_{HP}	horsepower correction factor
C_p	specific heat at constant pressure
C_P	propeller horsepower factor
C_{PC}	compressor specific heat
C_{PH}	turbine specific heat
C_Q	units correction factor
C_{PL}	burner pressure ratio
DC	direct current
D_D	helicopter rotor-drive damping coefficient - 12.4 ft-lb seconds/radian for 5 pps engine application*
$\frac{di}{dt}$	rate of change of current
DMFG	digital multivariate function generator
dN_E/dQ_E	torque limiting sensitivity - 0.08 rpm/ft-lb for 5 pps engine application

*item referred to 1720 rpm shaft speed

dN_E/dT_{5E}	temperature limiting sensitivity - 0.225 rpm/°R for 5 pps engine application
$d\Delta T/dFA$ or K_{TI}	burner temperature sensitivity
e	natural log base - 2.718
EMI	electromagnetic interference
f's	desired signal frequency
f/a	frequency to analog
FA	fuel-air ratio
°F	degrees Fahrenheit
FP_T	gas generator turbine flow parameter
f_r	reference signal frequency
f_s	signal frequency
FS	full scale
g	universal gravitational constant - 32.2 ft/second^2
G	general term for function gain
h	convection film heat transfer coefficient
hp	horsepower
HPDES	design horsepower
HPPT	power turbine horsepower
HP_R	parabolic power decrement
HP^x	peak horsepower ratio
HX_e	heat exchanger effectiveness

Hz	cycles per second
J_G	gas-generator-turbine inertia - 0.0121 ft-lb-seconds^2/ radian for 5 pps engine application*
J_{PROP}	propeller inertia - 7.5 ft-lbs second^2/ radian for 5 pps engine application*
J_{PT}	free-turbine inertia - 4.87 ft-lbs seconds^2/ radian for 5 pps engine application*
J_R	rotor inertia - 72.4 ft-lbs-seconds^2/radian for 5 pps engine application*
K	specific heat ratio
K_B	gain term of ratio units per second per degree Rankine - 0.1 pph/psi/°R for 5 pps engine application
K_D	helicopter rotor-drive spring rate - 3035 ft-lbs/radian for 5 pps engine application*
kHz	one thousand cycles per second
K_I	integral gain
K_{IP}	propeller control integral sensitivity
K_{IT}	trim control integral sensitivity
K_{NG}	N_G negative feedback gain to ratio units - 6.55×10^{-5} pph/psi/rpm for 5 pps engine application
K_P	gain term of proportional path
L	inductance
LVDT	linear variable differential transducer
M	mass
mils	thousandths of an inch
MOS	metal oxide semiconductor
MTBF	mean time between failures

*items referred to 1720 rpm shaft speed

MV	millivolt
NDRO	nondestructive read only
N_F	free-turbine speed
N_F REF	free-turbine set speed
N_G or N_E or N	gas generator speed
N_{GE}	gas generator speed error
N_{Gs}	gas generator sensed speed
$N_{Gs'}$	gas generator sensed speed biased by T_{T2}
N_G REF	gas generator set speed reference
N_P	propeller speed
N_R	rotor speed
n/r	nonregenerator
N^x	parabolic base speed
P_a or P_{AMB}	ambient pressure
PLA	gas generator power lever
pph	pounds per hour
pps	pounds per second
P_r	reference pressure
PR	pressure ratio
P_S	supply pressure
P_s	output pressure
PRV	pressure regulating valve

P_{S3}	compressor discharge static pressure
psia	pounds per square inch absolute
psig	pounds per square inch gage pressure
P_{T2}	compressor inlet total pressure
P_{T3}	compressor discharge total pressure
P_{T4}	turbine inlet total pressure
PTS	power turbine stator system
Q	fluidic term for ratio of reactance to resistance in a circuit
Q_{PT}	power turbine torque
Q_R	helicopter rotor torque
Q_s	shaft torque
Q_{SHAFT}	torque in free-turbine shaft
r	regenerator
R_o	gas constant - 53.35 ft-lbs/°R
R'	reference signal
R	resistance
°R	degrees Rankine
RF	radio frequency
rpm	revolutions per minute
RSS	square root of sum of the squares technique for error analysis
RU	gas generator ratio units

s	Laplace operator
SV	stator vane
t	time
T	absolute temperature
T_{T2}	compressor inlet total temperature
T_{T3}	compressor discharge temperature
$T_{T3.5}$	regenerator discharge total temperature, cold side
T_{T4}	turbine inlet total temperature
T_{T5}	turbine discharge total temperature
T_{T6}	free-turbine discharge total temperature
TV	throttle valve or main metering valve
V	volts
VCO	voltage-controlled oscillator
VG	compressor variable-geometry function
W_a	engine airflow
W_f or W_{fe}	engine fuel flow
W_f/P_{T2}	ratio of engine fuel flow to compressor inlet total pressure
W_f/P_{T3}	ratio of engine fuel flow to burner pressure
W_G	regenerator airflow
Z	general regenerative scheduling parameter
Z_2	$W_f/P_{T2}\ (1 - T_{T3.5}/T_{T4})$
Z_3	$W_f/P_{T3}\ (1 - T_{T3.5}/T_{T4})$

α_{NF}	lead/lag ratio of N_F compensator
β'	collective pitch signal to engine control
β_H	helicopter blade collective pitch
β_P	propeller blade angle
$\partial(W_f/P_{T3})/\partial N_{GE}$	partial derivative of gas generator ratio units with respect to speed error -6.55×10^{-5} pph/psi/rpm for 5 pps engine application
Δ	symbol indicating increment in a particular parameter
ΔP	regulated pressure drop across control metering valve
$\Delta P/P$	$P_{T3} - P_{S3}/P_{T3}$
$\Delta P/\Delta P$	$P_{T3} - P_{S3}/P_{T3} - P_{T2}$
η_{PT}	power turbine efficiency - 0.9
γ	ratio of specific heats
ω	frequency
ϕ	phase angle
τ	time constant
τ_2	lag time constant of N_F compensator
τ_5	turbine temperature lag time constant
τ_β	time constant of β reset mechanism - 0.01 second
τ_c	lead time constant of temperature compensator - 1.0 second
τ_D	time constant of torque motor servo - 0.0143 second
τ_{N_F}	time constant of power turbine speed sensor

τ_p	propeller control lead time constant - 0.3 second
τ_{PR}	time constant of control pressure-regulating valve - 0.02 second
τ_Q	time constant of torque sensor - 0.02 second
$\tau_{T_{T5}}$	time constant of T_{T5} temperature sensor
Θ or Θ_{T2}	ratio of ambient temperature to standard day condition

INTRODUCTION

This program was directed at the conceptual design and analytical study of an advanced engine control system for a small (2-to-5-pound-per-second airflow) free-turbine engine. Program technical objectives included the following:

1. Maintenance of a high degree of flexibility and commonality in the control system for this range of engine size
2. Elimination of the need for gear reduction to drive the control
3. Decreased contamination sensitivity
4. Ability to operate with various fuel grades
5. Efficient integration with other accessories
6. Increased reliability
7. Decreased maintenance
8. Provision for engine analyzer inputs
9. Adaptability for control of a regenerative mode engine
10. Improved vulnerability resistance
11. Lower cost potential

Specific design features of the control included the following:

1. Control of starting, acceleration and deceleration fuel flow
2. Automatic start sequencing
3. Full-range governing of gas generator speed
4. Free-turbine power control with speed selection
5. Closed-loop turbine temperature limiting
6. Torque limiting
7. Load sharing

8. Provision for compressor and turbine variable geometry

9. Backup redundancy for single component failure

10. Satisfactory performance over the range of environment defined in MIL-E-5007C

11. Provision to allow operation from sea level to 35,000 feet at ambient temperatures of -65°F to 130°F

The program was accomplished in two phases: Phase I, Preliminary Design Phase; and Phase II, Final Design Phase. The tasks accomplished under Phase I included the following:

1. Definition of the characteristics of the engine

2. Finalization of the requirements and functions required by the control system

3. Analysis of proposed control modes

4. Technology review and selection

5. Optimized packaging studies

Phase II tasks accomplished included the following:

1. Modifications to the preliminary design

2. Finalization of the control system design

3. Analysis and simulation of the final system

4. Identification of high-risk components

5. Definition of the system design configuration

A flow diagram showing how the study program developed, significant milestones along the way and their interrelationship, as well as results and conclusions arising from the program are shown in Figure 1.

Subsequent sections of this report will explain how the program was conducted and will discuss the results in detail.

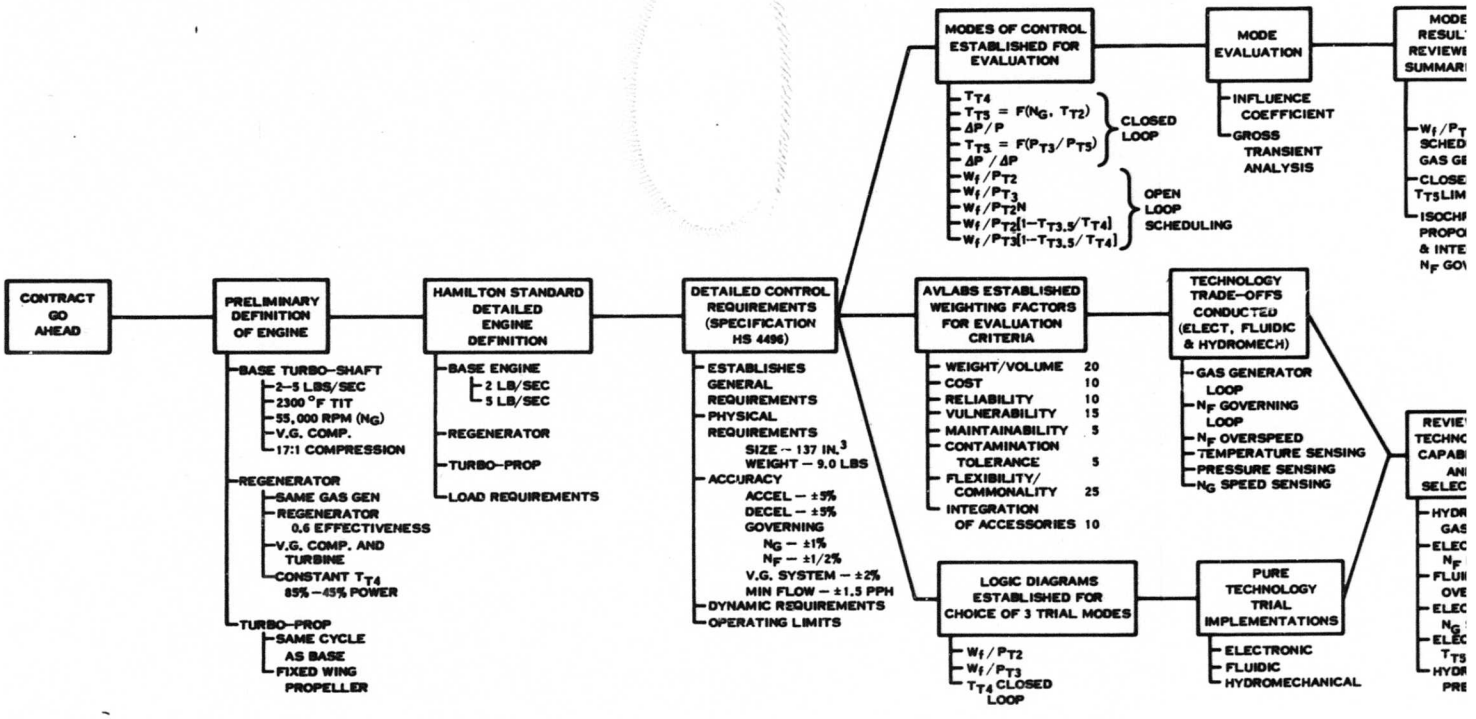

Figure 1. Development of Advanced Control Program.

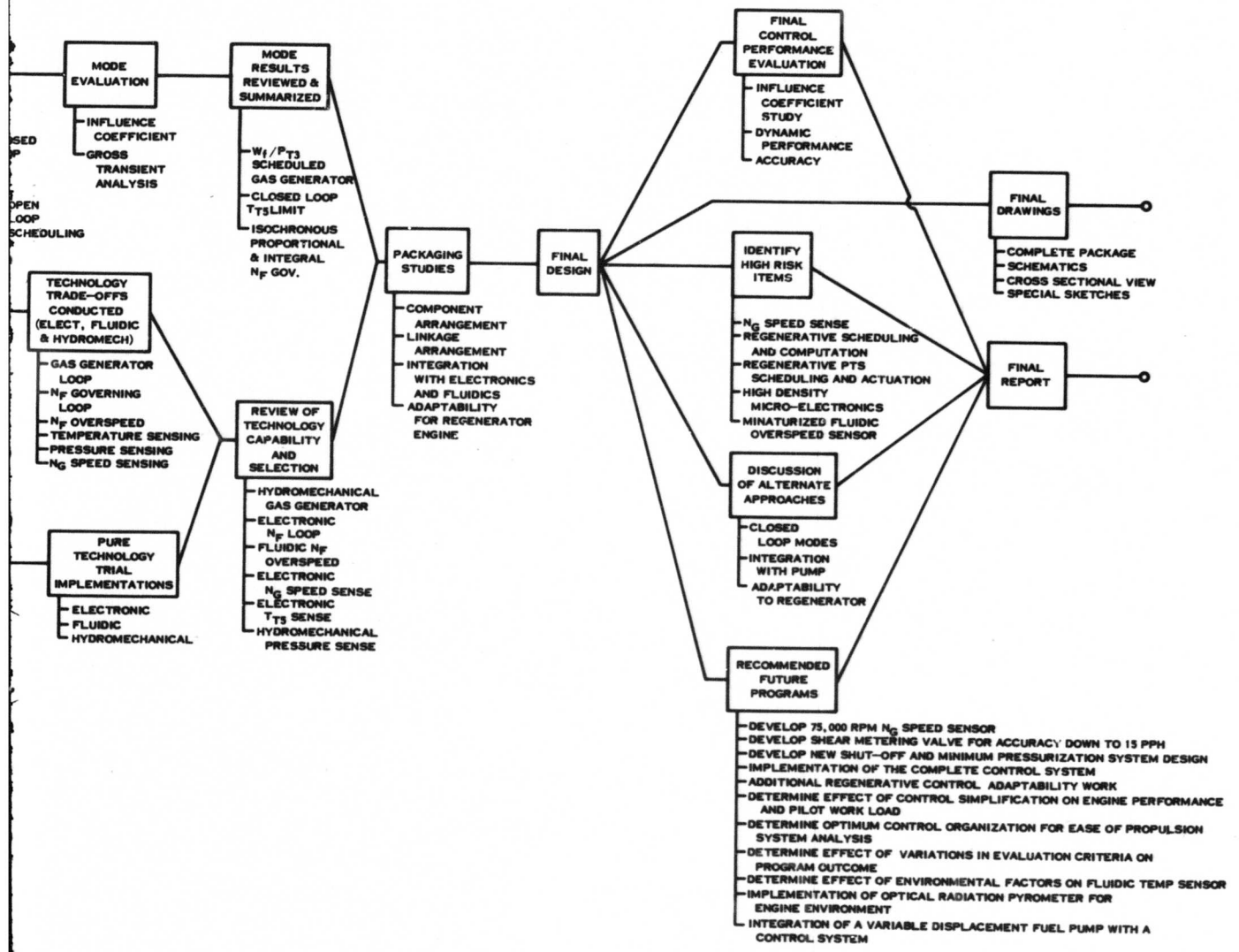
MODE EVALUATION
INFLUENCE COEFFICIENT
GROSS TRANSIENT ANALYSIS
MODE RESULTS REVIEWED & SUMMARIZED
W_f/P_{T3} SCHEDULED GAS GENERATOR
CLOSED LOOP T_{TS} LIMIT
ISOCHRONOUS PROPORTIONAL & INTEGRAL N_F GOV.
TECHNOLOGY TRADE-OFFS CONDUCTED (ELECT, FLUIDIC & HYDROMECH)
GAS GENERATOR LOOP
N_F GOVERNING LOOP
N_F OVERSPEED
TEMPERATURE SENSING
PRESSURE SENSING
N_G SPEED SENSING
PURE TECHNOLOGY TRIAL IMPLEMENTATIONS
ELECTRONIC
FLUIDIC
HYDROMECHANICAL
REVIEW OF TECHNOLOGY CAPABILITY AND SELECTION
HYDROMECHANICAL GAS GENERATOR
ELECTRONIC N_F LOOP
FLUIDIC N_F OVERSPEED
ELECTRONIC N_G SPEED SENSE
ELECTRONIC T_{TS} SENSE
HYDROMECHANICAL PRESSURE SENSE
PACKAGING STUDIES
COMPONENT ARRANGEMENT
LINKAGE ARRANGEMENT
INTEGRATION WITH ELECTRONICS AND FLUIDICS
ADAPTABILITY FOR REGENERATOR ENGINE
FINAL DESIGN
FINAL CONTROL PERFORMANCE EVALUATION
INFLUENCE COEFFICIENT STUDY
DYNAMIC PERFORMANCE ACCURACY
IDENTIFY HIGH RISK ITEMS
N_G SPEED SENSE
REGENERATIVE SCHEDULING AND COMPUTATION
REGENERATIVE PTS SCHEDULING AND ACTUATION
HIGH DENSITY MICRO-ELECTRONICS
MINATURIZED FLUIDIC OVERSPEED SENSOR
DISCUSSION OF ALTERNATE APPROACHES
CLOSED LOOP MODES
INTEGRATION WITH PUMP
ADAPTABILITY TO REGENERATOR
RECOMMENDED FUTURE PROGRAMS
DEVELOP 75,000 RPM N_G SPEED SENSOR
DEVELOP SHEAR METERING VALVE FOR ACCURACY DOWN TO 15 PPH
DEVELOP NEW SHUT-OFF AND MINIMUM PRESSURIZATION SYSTEM DESIGN
IMPLEMENTATION OF THE COMPLETE CONTROL SYSTEM
ADDITIONAL REGENERATIVE CONTROL ADAPTABILITY WORK
DETERMINE EFFECT OF CONTROL SIMPLIFICATION ON ENGINE PERFORMANCE AND PILOT WORK LOAD
DETERMINE OPTIMUM CONTROL ORGANIZATION FOR EASE OF PROPULSION SYSTEM ANALYSIS
DETERMINE EFFECT OF VARIATIONS IN EVALUATION CRITERIA ON PROGRAM OUTCOME
DETERMINE EFFECT OF ENVIRONMENTAL FACTORS ON FLUIDIC TEMP SENSOR
IMPLEMENTATION OF OPTICAL RADIATION PYROMETER FOR ENGINE ENVIRONMENT
INTEGRATION OF A VARIABLE DISPLACEMENT FUEL PUMP WITH A CONTROL SYSTEM
FINAL DRAWINGS
COMPLETE PACKAGE
SCHEMATICS
CROSS SECTIONAL VIEW
SPECIAL SKETCHES
FINAL REPORT

B

DISCUSSION

DEFINITION OF ENGINE AND LOAD CHARACTERISTICS

An appropriate engine definition is essential in evaluating the performance of one control mode versus another. To this extent the engine definition must be sufficiently sophisticated that all control modes are evaluated fairly on a realistic, rather than an idealistic, model. A balance must be reached in which the engine model does not become overly intricate, or study time and attention will be diverted from the primary object of comparing and selecting means of control. A deliberate attempt has been made in selecting the following engine to delete second-order effects that would not likely alter the choice between modes while retaining the features that lend realism to the study. To this end, a single-spool gas generator, rather than a twin spool, was studied; component efficiencies have been held constant, and the variable-geometry compressor is represented as a fixed, ideal compressor.

The basic engine cycle considered in this report is a single-spool gas generator with variable compressor stators supplying hot gas to a fixed-geometry, free turbine driving the power output shaft. A second engine cycle is considered in lesser detail to explore the growth possibilities of the base control mode. This cycle adds a regenerator and variable power turbine stators to the basic cycle. Simple schematics of both engines are shown in Figures 2 and 3.

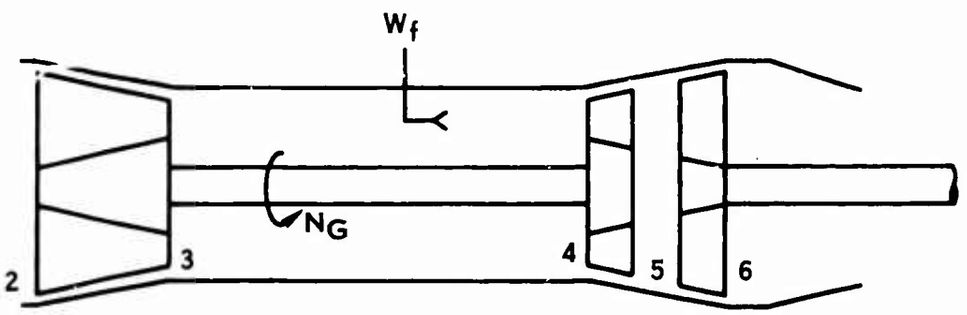

Figure 2. Schematic of Base Engine.

The block diagram of the engines (and loads) is presented in Figure 4. The thermodynamic engine equations are conventional in most respects. Additional dynamic features are incorporated in the block diagram on the basis of simulation experience to more nearly reproduce the transient behavior of an engine. These features include an exponential lag and delay time to approximate the burner dynamics, lag and lead/lag transfer functions for a first-order regenerator

simulation, and the metal thermal storage dynamic effects. A selector switch is shown, indicating burner inlet temperature, and is either T_{T3} for the base engine or $T_{T3.5}$ for the regenerative engine.

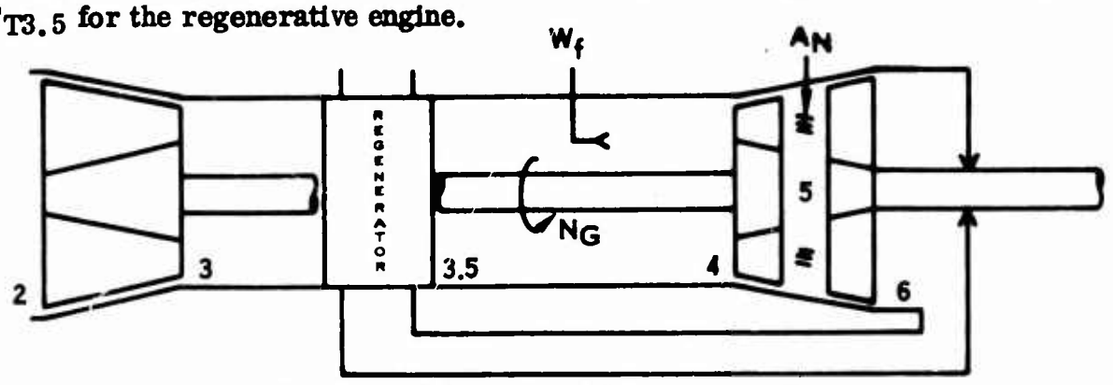

Figure 3. Schematic of Regenerator Engine.

Input signals to the engine (and loads) are fuel flow (W_f), power turbine stator area (A_N), collective pitch (β_H), and propeller blade angle (β_P). The specific parameter supplied to the load by the engine is optimum power turbine horsepower (HPPT). A parabolic decrement of power as a function of load speed is included before evaluation of the specific load equations. The load speed, which is used to define power turbine torque (Q_{PT}), is either power turbine speed or propeller speed, depending on the application. The propeller and helicopter load simulations are also shown on Figure 4, although only one would be used in a given study. Gear ratios are not shown, and all output shaft parameters are referred to propeller shaft speed.

Parametric values assigned to the engine cycles are presented in Figures 5 and 6 for the base engine and in Figures 7 and 8 for the regenerative engine. These values are a prognosis of the advance in engine design techniques anticipated in the near future. The base engine is assumed to have a design point pressure ratio of 17:1 and a steady-state turbine inlet temperature of 2760°R. This is typical of what will likely be available with advances in materials and cooling techniques of engines designed in the early 1970's. It is further assumed that the base engine efficiencies will permit the delivery of 1285 optimum horsepower from an airflow of 5 pounds per second and a fuel flow of 458 pounds per hour. Figures 5 and 6 show steady-state engine parameter values throughout the useful power range and also show the acceleration limiting condition assumed for proper surge and temperature protection of the engine. A plot of W_f/P_{T3} ratio is also included for steady-state and acceleration limiting.

The gas generator rotor time constant given in Figure 5 has conventional values ranging from 0.36 second to 2.0 seconds. Other engine dynamics of vital importance are a 0.01-second burner lag, a 0.035-second burner delay time, and a thermal storage lag time constant of 1 second accompanied by a 0.95-second

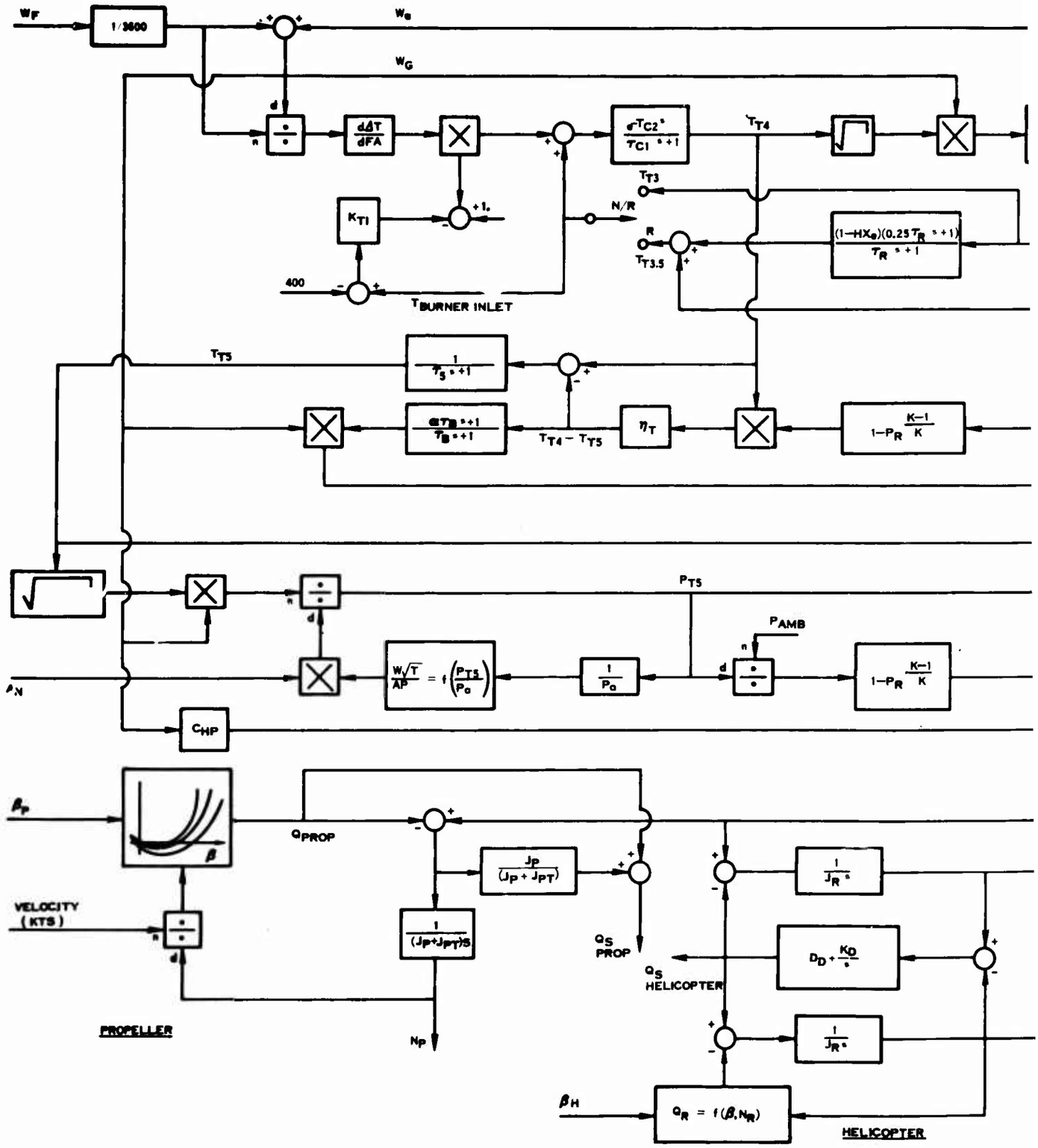

Figure 4. Block Diagram of Engine Simulation With Helicopter or Propeller Loads

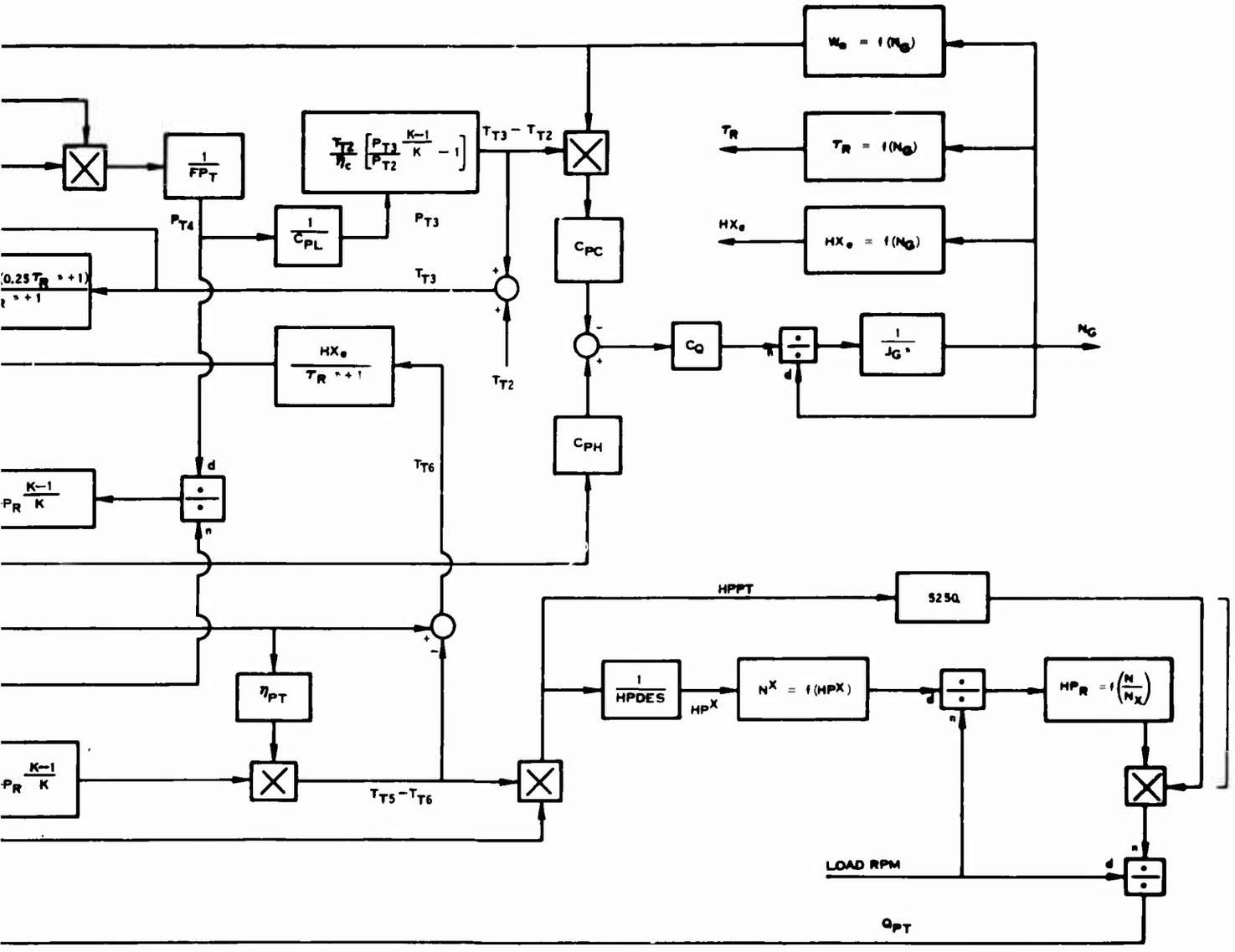
$W_e = f(N_G)$
T_R
$T_R = f(N_G)$
HX_e
$HX_e = f(N_G)$
$\frac{1}{FP_T}$
$\frac{T_{T2}}{\eta_c}\left[\frac{P_{T3}}{P_{T2}}^{\frac{K-1}{K}} - 1\right]$
$T_{T3} - T_{T2}$
P_{T4}
$\frac{1}{C_{PL}}$
P_{T3}
C_{PC}
T_{T3}
T_{T2}
C_Q
$\frac{1}{J_G s}$
N_G
$\frac{HX_e}{T_R s + 1}$
C_{PH}
T_{T6}
HPPT
S250
$\frac{1}{HPDES}$
HP^X
$N^X = f(HPX)$
$HP_R = f\left(\frac{N}{N_X}\right)$
η_{PT}
$T_{T5} - T_{T6}$
LOAD RPM
Q_{PT}

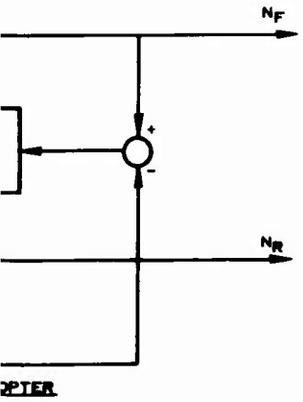
N_F
N_R

OPTER

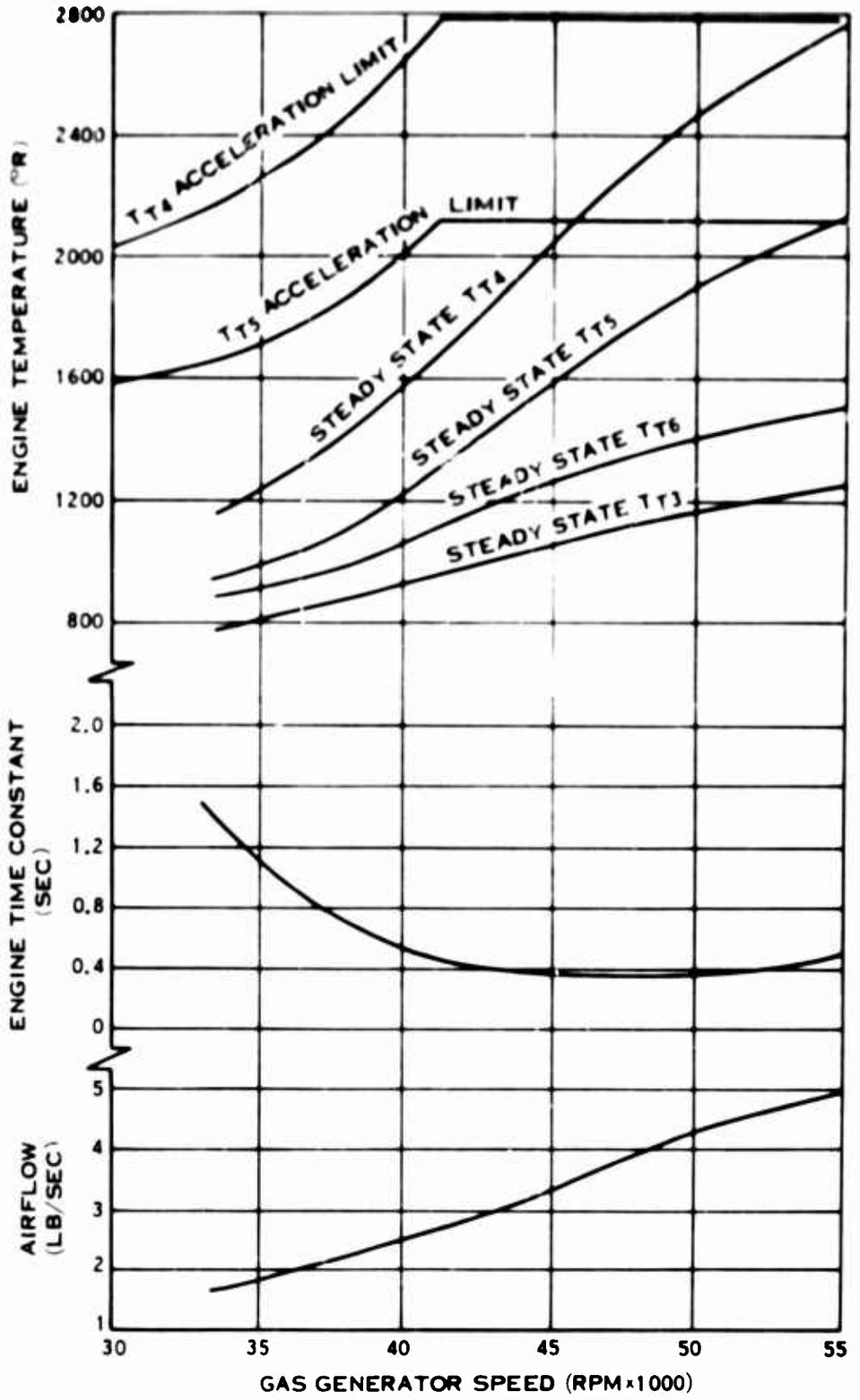

Figure 5. Base Engine Characteristics (Sea Level, Static, Standard Day).

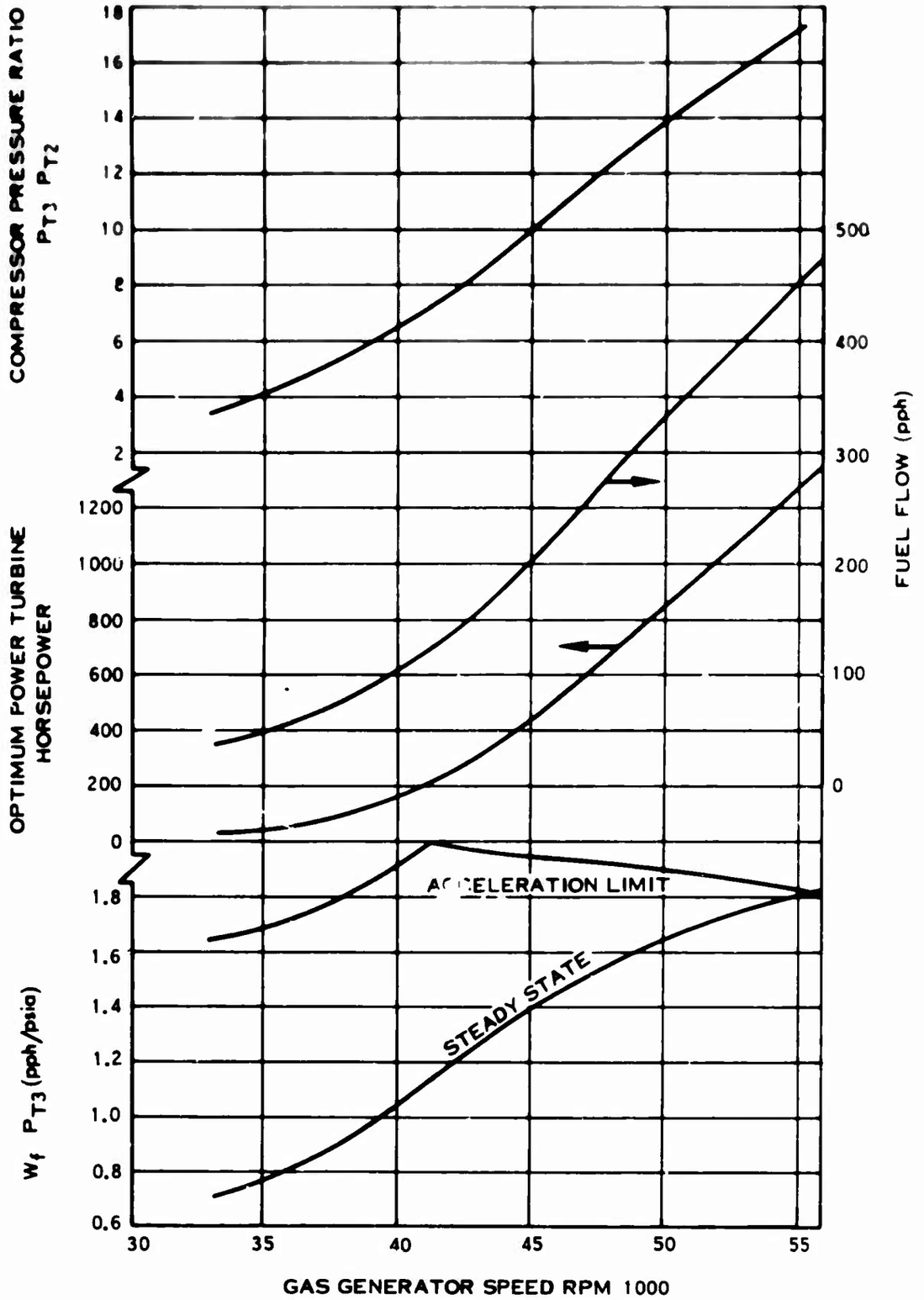

Figure 6. Base Engine Characteristics (Sea Level, Static, Standard Day).

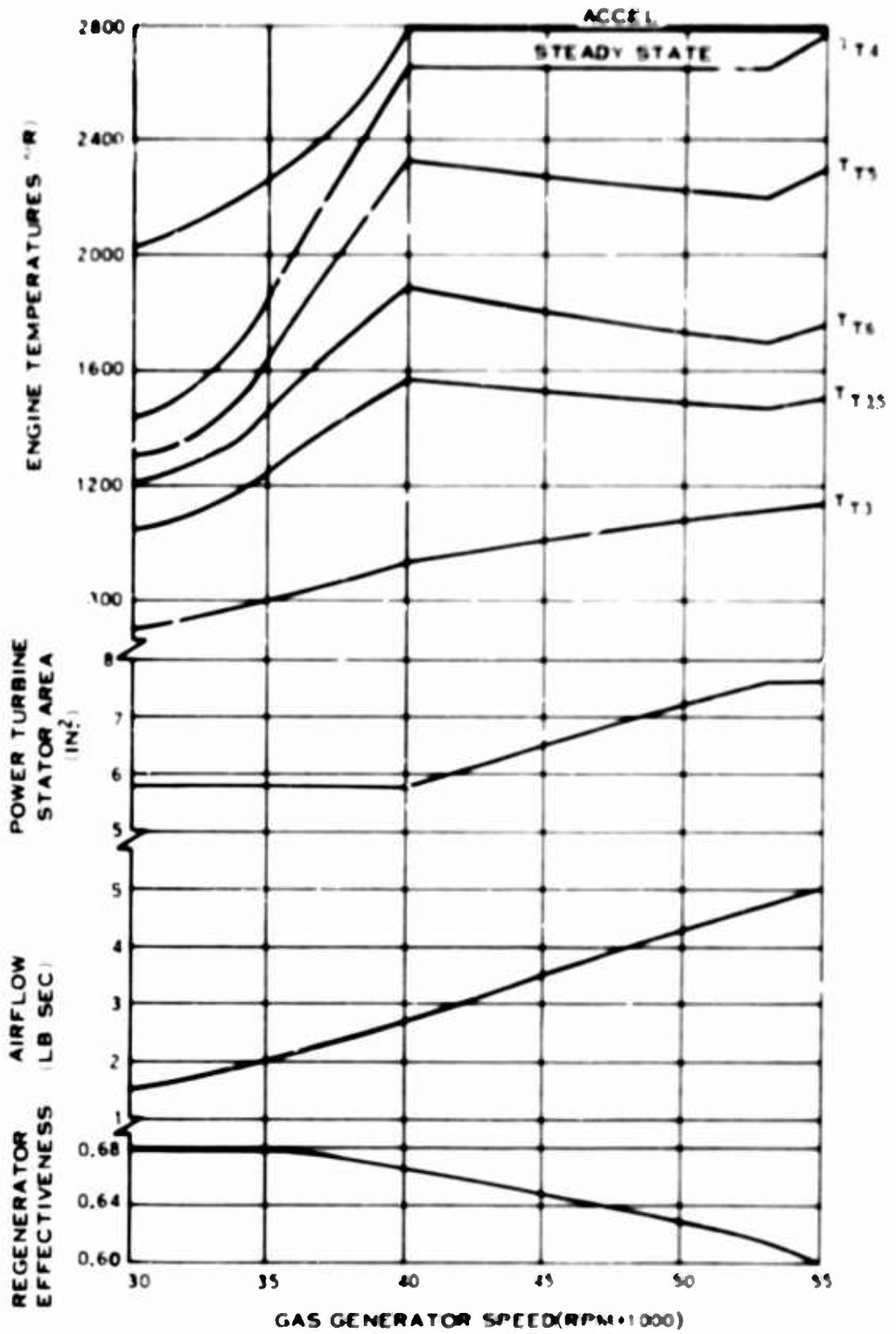

Figure 7. Regenerative Engine Characteristics (Sea Level, Static, Standard Day).

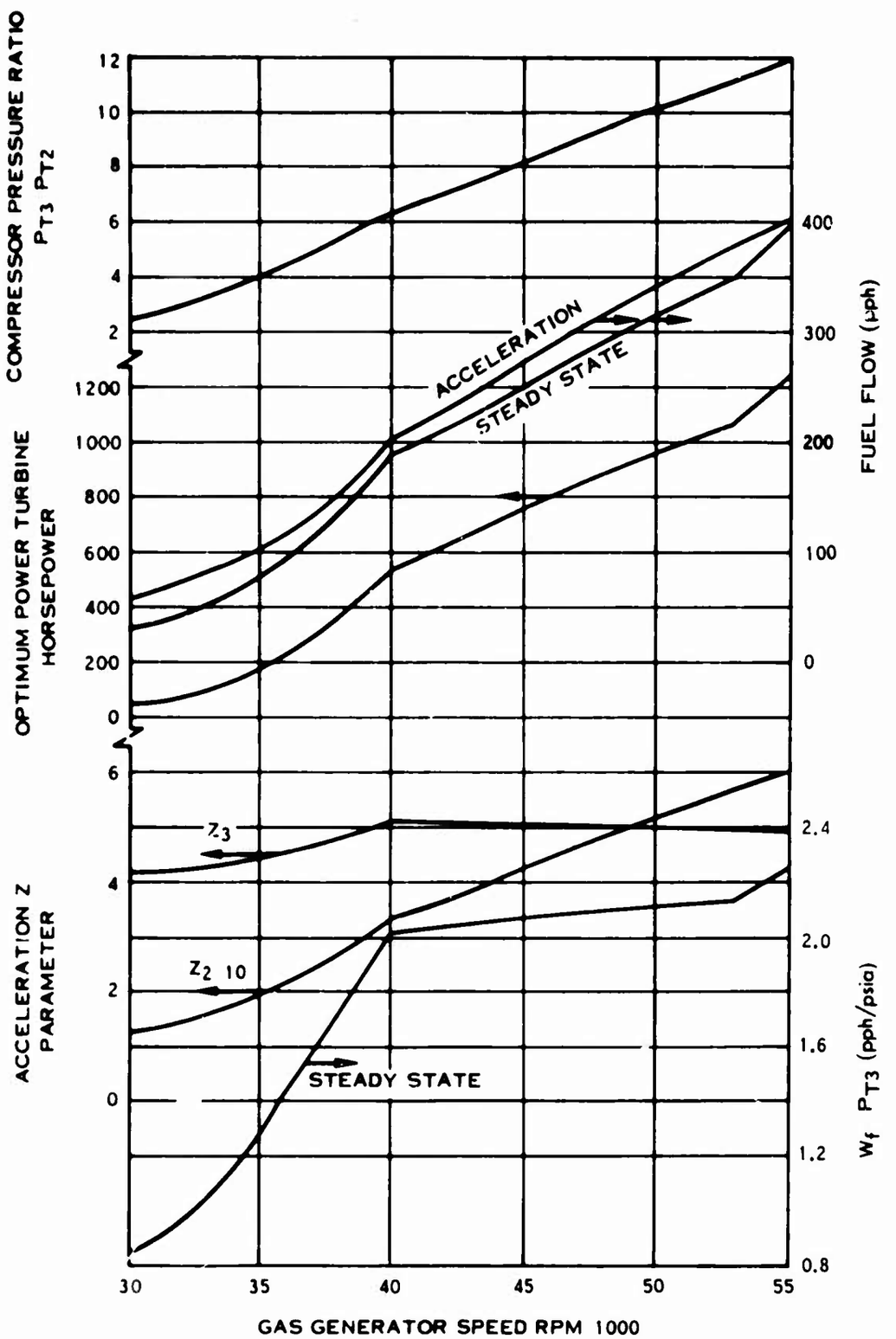

Figure 8. Regenerative Engine Characteristics (Sea Level, Static, Standard Day).

lead time constant. These dynamics were maintained at a constant value during the transients, although the effect of varying the values was determined for closed temperature loop control modes.

The regenerative engine is characterized at the design point by a pressure ratio of 12:1 and a turbine inlet temperature of 2760° R. The steady-state curves of Figures 7 and 8 illustrate the manner in which the power turbine stator area (A_N) must be scheduled to maintain an efficient operating temperature of 2650° R throughout the mid-power range. This temperature reduction provides longer engine life in the normally used power range while retaining a reserve of power for emergency or short-term use. Power turbine stator modulation is not employed for powers less than 45 percent to avoid the acceleration limit.

Also shown with the regenerator characteristics of Figures 7 and 8 is an interesting ratio of engine parameters designated as the Z parameters. These parameters are similar to the conventional W_f/P_{T2} ratio for Z_2 or the conventional W_f/P_{T3} ratio for Z_3; but both have been modified by the factor $T_{T3.5}/(T_{T4}-T_{T3.5})$. This factor is of value because it is a unique function of gas generator speed and inlet temperature for the acceleration limit. Hence it is possible to schedule a T_{T4} limit by measuring regenerator discharge temperature $T_{T3.5}$, N_G, and T_{T2}.

The dynamics for the regenerator engine are similar to those given for the base engine above plus a regenerator time constant that varies from 2.5 seconds at 5-pounds-per-second airflow to 7.5 seconds at 1-pound-per-second airflow. An increase of regenerator effectiveness from 60 percent to 68 percent was assumed for these same airflows.

LOAD DEFINITION

Helicopter

A schematic diagram of a simple, nonarticulated rotor without hydraulic damping is shown in Figure 9.

This type of rotor was selected because it offers the most severe test of control system stability. Coefficients, shown in the list of symbols, have been assigned to the components that represent a system having a resonant frequency of 25 radians per second with 10 percent of critical damping. In general, the control system that has the stability margin to control this rotor would have ample margin to control an articulated rotor with hydraulic damping.

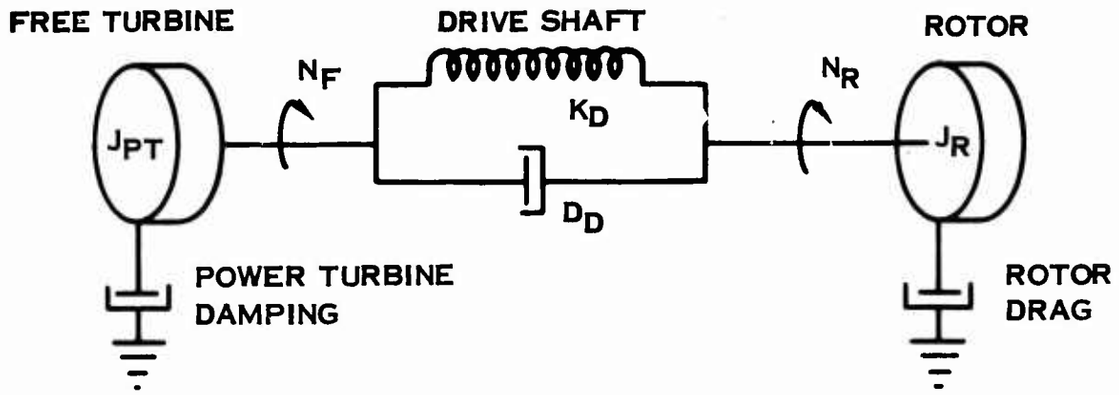

Figure 9. Schematic of Helicopter Load Representation.

The steady-state power requirements for a sea level, standard day hover condition are presented in Figure 10 as a function of rotor speed (referred to propeller shaft speed) and collective pitch angle. While this characteristic is typical, the power characteristics will, of course, change significantly throughout the flight envelope and preclude any precise scheduling of power with rotor speed and collective pitch. The combination of inexact schedule prediction and limited system gain for stability margin creates an absolute necessity for an isochronous rotor speed control to maintain ± 0.5 percent speed accuracy under all flight conditions. Hence, all control modes considered in this report have been evaluated on the basis of requiring an error-integrating speed governor.

Propeller

The propeller selected for this study is a lightweight, 10-foot-diameter propeller having a tip speed of 900 ft/sec at takeoff and a polar moment of inertia equal to 7.5 ft-lb-sec^2/rad. The propeller is designed with an integral speed control which can be overriden by a variable minimum pitch stop to gain manual control. A schematic of the propeller load representation is shown in Figure 11.

The fixed-wing propeller characteristics are shown on Figure 10 in a non-dimensional form. Further discussion on the control correlation is presented in the section entitled "Description of Proposed System for Regenerator Mode".

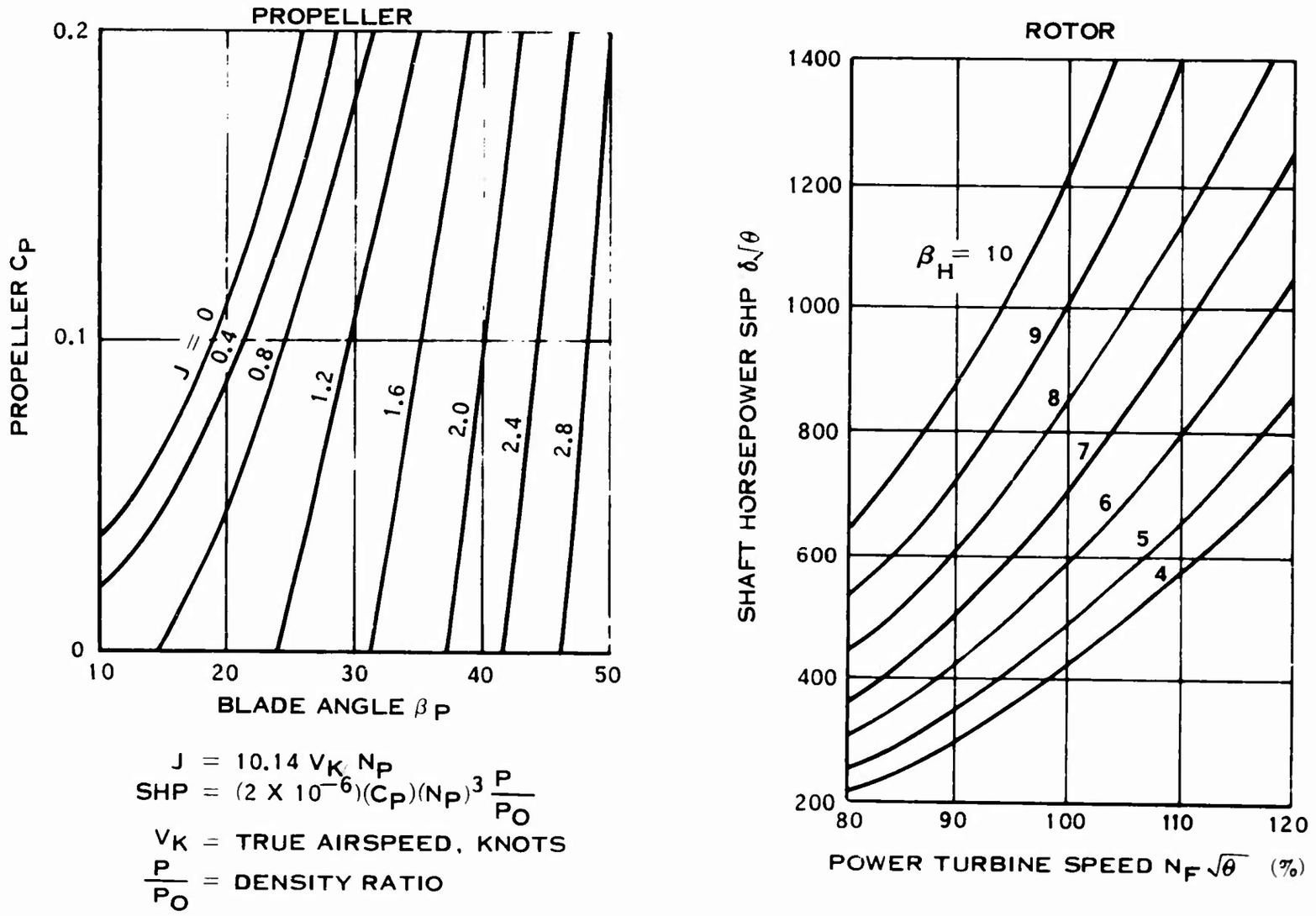

$$J = 10.14\, V_K / N_P$$

$$SHP = (2 \times 10^{-6})(C_P)(N_P)^3 \frac{P}{P_O}$$

V_K = TRUE AIRSPEED, KNOTS

$\frac{P}{P_O}$ = DENSITY RATIO

Figure 10. Typical Propeller and Helicopter Rotor Load Characteristics Referred to Propeller Shaft Speed.

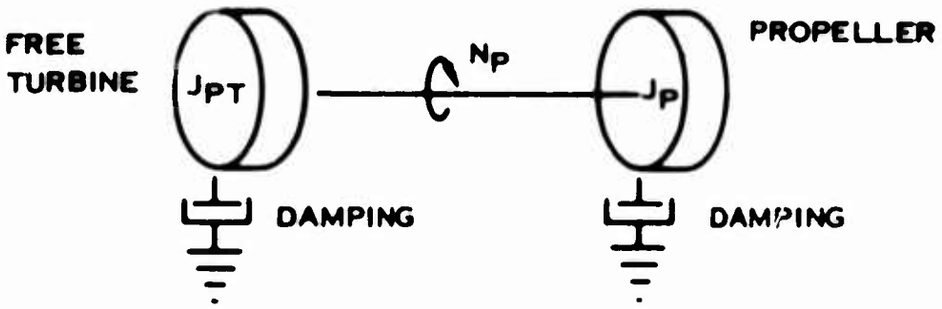

Figure 11. Schematic of Propeller Load Representation.

DEFINITION OF CONTROL REQUIREMENTS

Since the objective of this advanced engine control system program is to study various approaches to control design, including effects of both mode of control and various technologies available to perform the required functions, the results of an extensive study such as this depend considerably on the complexity of the basic control requirements that are needed to satisfy the engine. As can be seen in the previous section describing engine requirements, the engine is a complex high-performance machine requiring many control parameters and relatively good accuracies. It was therefore important to establish a realistic control specification as a solid, nonchanging set of ground rules to be used during the ensuing trade-off studies.

The specification was arrived at by summarizing the general requirements of several small advanced engines currently under development. These were then modified as required to meet the objectives of the basic study program. Control schedules were defined for both the base and the regenerator engines in general terms wherever possible to allow the schedules to be adapted to any mode of control or technology. Typical examples of these curves are shown at the end of the following condensed version of the control specification used as the base for this study program.

Condensed Control Specification

Scope

This specification describes the requirements for a main fuel control to be used on an aircraft gas turbine engine having a free-turbine power shaft. The control shall perform the following functions:

1. Control gas generator speed
2. Control power turbine speed
3. Schedule acceleration and deceleration fuel flows
4. Provide positive fuel flow shutoff in the power lever off position
5. Establish minimum fuel flow
6. Limit maximum gas generator speed
7. Limit maximum power turbine speed

8. Limit control inlet pressure during fuel shutoff conditions

9. Sequence automatic starting

10. Limit gas generator turbine inlet temperature

11. Limit power turbine torque

12. Provide for load sharing (torque) in multiengine installations

13. Control compressor variable stator vane position

14. Control power turbine variable stator vane position.

15. Provide compressor inlet temperature bias for schedules

Physical Characteristics

Weight (dry)	9.0 lb maximum
Size	See Figure 12
Electromagnetic Interference Resistance	Per MIL-STD-461 Class ID
Leakage (External)	1.5 cc/minute at overboard drain only
Drive (N_G and N_F)	Either capable of operating at engine speed (75,000 rpm maximum) or operating without mechanical drive
Flight Maneuver Forces	Withstand conditions per Figure 3 of MIL-E-8593 (ASG)
Flight Attitude Conditions	Withstand conditions per paragraph 3.3.8 of MIL-E-8593 (ASG)
Life Requirements	2000 hours minimum between overhauls

Service Conditions

Extreme range conditions will not be encountered during more than 2 percent of the control operating time.

Parameter	Normal Range	Extreme Range
Pressures		
Control Discharge (psia)	5 to 600	650
Bypass (psia)	40 to 145	5 to 150
Control Inlet (psia)	200 to 850	200 to 900
Ambient Air, P_{AMB} (psia)	0 to 15	0 to 15
Compressor Discharge Air, P_{T3} (psia)	5 to 250	5 to 275
Compressor Inlet, P_{T2} (psia)	3.5 to 22	3.5 to 22
Flows		
Control Discharge (lb/hr)	15 to 625	
Shutoff Leakage (cc/min)	1.0 max at 200 psi	1.0 max at 200 psi
Temperatures		
Ambient Air	-65°F to +180°F	-65°F to +250°F
Fuel (control inlet)	-65°F or 12 centistokes to +130°F	-65°F or 12 centistokes to +130°F
Fuel (control discharge)	200°F max	200°F max
Compressor Inlet, T_{T2}	-65°F to +200°F	-125°F to +210°F
Compressor Discharge, T_{T3}	1420°R	1600°
Turbine Inlet, T_{T4}	2780°R	2900°R to 1-2 sec bursts
Mechanical Inputs		
N_F Speed, Turbine (rpm)	0 to 34,400	36,000

N_R Speed, Gearbox (rpm)	0 to 1720	1806
Q_{PT} Torque (in.-lb)	45	63
N_F Acceleration (rpm/sec)	25%/sec	25%/sec
N_G Speed (rpm)	0 to 55,000	57,800
N_G Torque (in.-lb)	5	10
N_G Acceleration (rpm/sec)	16,500	
N_G Deceleration (rpm/sec)	25,000	
Power Lever Position, N_G		
Off	0° to 3°	
Ground Idle	23.5° to 26.5°	
Flight Idle	45° to 50°	
Military	98.5° to 101.5°	
Emergency	117° to 120°	
Power Lever Operating Torque		
Range (in.-lb)	0 to 25	
Variation (in.-lb)	10 max	

Vibration

See Figure 13

Electrical Power Available

Variable voltage/variable frequency alternator, 10 watts at 10 percent N_G

Operating Fluids and Fuel Specific Gravity Compensation

A design objective shall be the capability of operating the control with JP4, JP5, CITE, and calibration fluid without the use of a specific gravity adjustment.

Fuel Contamination and Filtration

The control shall function satisfactorily with fuel contaminated to the extent specified in paragraph 3.4.1.3 of MIL-E-5007C. Filters shall be capable of successfully passing the engine control qualification test without cleaning.

Schedules and Accuracies

All the specified accuracies in Tables I and II include repeatability, hysteresis, fuel temperature, and full altitude and temperature envelope effects. In addition, the accuracy of any remote sensors, such as torque sensors, temperature sensors, etc., shall be included in the maximum allowable band specified. Figures 14 through 20 referred to in Tables I and II indicate various scheduling requirements.

TABLE I. GAS GENERATOR ACCURACIES

Function	Steady State Requirements		Dynamic Requirements	
	Base Engine	Regenerative Engine	Base Engine	Regenerative Engine
Acceleration Scheduling*	W_f/P_{T3} Mode (Figure 4) Below 55% N_G: ±2 pph or ±7.5% W_f/P_{T3}, whichever is larger. Above 55% N_G: ±5% W_f/P_{T3} T_{T4} Mode ±50° T_{T4}	T_{T4} Mode (Figure 6) ±50° T_{T4}	W_f/P_{T3} Mode > 30,000 rpm ±8% W_f/P_{T3} within 0.1 sec after step input ±4% W_f/P_{T3} throughout acceleration transient. T_{T4} Mode > 30,000 rpm ±8% T_{T4} within 0.15 sec after step input ±4% T_{T4} throughout acceleration transient.	T_{T4} Mode > 30,000 rpm ±8% T_{T4} within 0.15 sec after step input ±4% T_{T4} throughout acceleration transient.
Deceleration Scheduling*	W_f/P_{T3} Mode 0.476 ± 5% W_f/P_{T3} T_{T4} Mode (Figure 7) ± 30° T_{T4}	Fuel Air Ratio 0.0035 ± 10%	W_f/P_{T3} Mode > 30,000 rpm ±8% W_f/P_{T3} within 0.2 sec after step input ±5% W_f/P_{T3} throughout deceleration transient. T_{T4} Mode > 30,000 rpm ± 8% T_{T4} within 0.3 sec after step input ± 5% T_{T4} throughout deceleration transient.	Fuel Air Ratio > 30,000 rpm ± 20% within 0.2 sec after step input ± 10% throughout deceleration transient.
Start Sequence	The gas generator shall be capable of automatic starting independent of power lever position within the confines of Figures 15, 16 and 17 in combination with minimum flow without discontinuities.			
Speed Governing	± 1% N_G See Figure 19	± 1% N_G See Figure 19	0.04 sec max between N_G and W_f	0.04 sec max between N_G and W_f
Limiting	Constant corrected horsepower: ±5% W_f/P_{T3} Constant speed: ±1% N_G (Figure 21) Constant T_{T4} ±2.0% T_{T4}		-	-
Min Flow	36 ± 1.5 pph	15 ± 1.5 pph	-	-
Variable Compressor Geometry	± 2% N_G See Figure 20	± 2% N_G See Figure 20	± 6% Actuator position	± 6% Actuator position

*Accuracies given are for modes originally considered for specification. Equivalent accuracies were calculated as new modes developed.

TABLE II. POWER TURBINE ACCURACIES

Function	Steady-State Requirements		Dynamic Requirements	
	Base Engine	Regenerative Engine	Base Engine	Regenerative Engine
Speed Governing	For 70% to 110% N_F: ± 0.5% N_F		±0.75% N_F	
Speed Governing Compensation	-	-	Integral and proportional control with series/lead/lag compensation Lag: 0.75 ± 0.1 sec Lead/lag ratio: 0.2 ± 0.04 Additional lag total: 0.04 sec	
Speed Governing Startup	-	-	The power turbine transient overspeed following a step power lever increase from a ground idle underspeed (including braked rotor) shall not exceed ±7% N_F.	
Torque Limiting	4280 ft-lbs ± 5%		± 12% after gross step increases in collective pitch. Sensor ≤ 0.02 sec	
N_F Overspeed	120% N_F ± 2%		-	-
Load Sharing	Match engine Loads within 5.0%		-	-
Stator Positioning	Not required	± 1% of max stroke. See Figure 14.	-	-

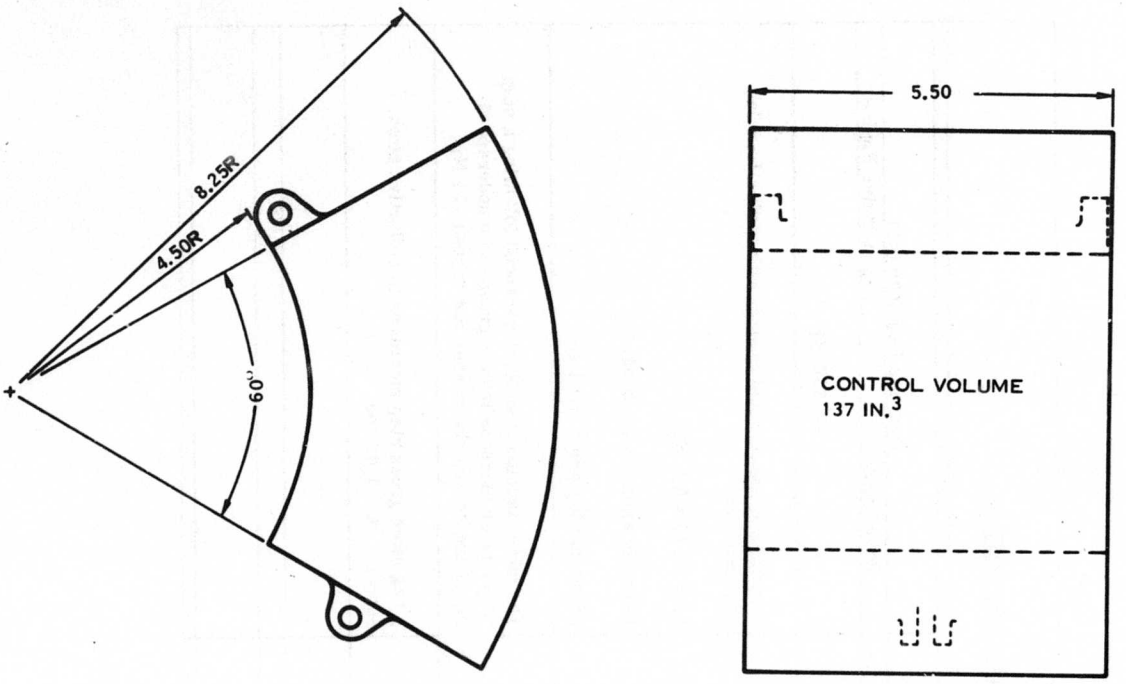

Figure 12. Fuel Control Envelope.

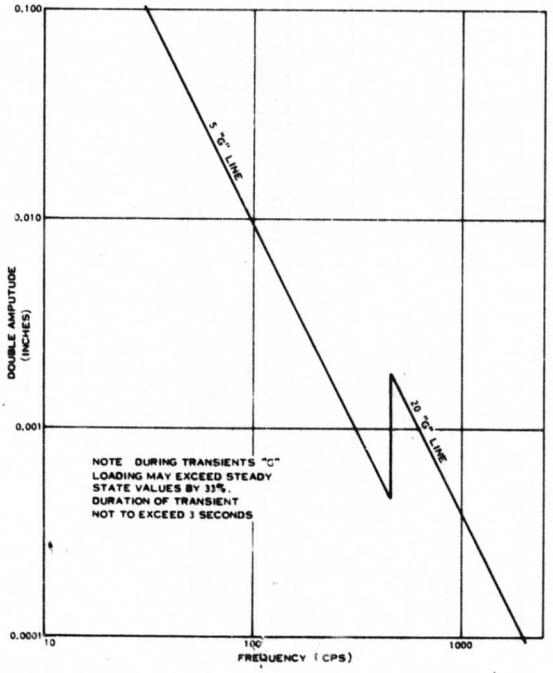

Figure 13. Steady-State Vibration Input at Control Mounting Pad.

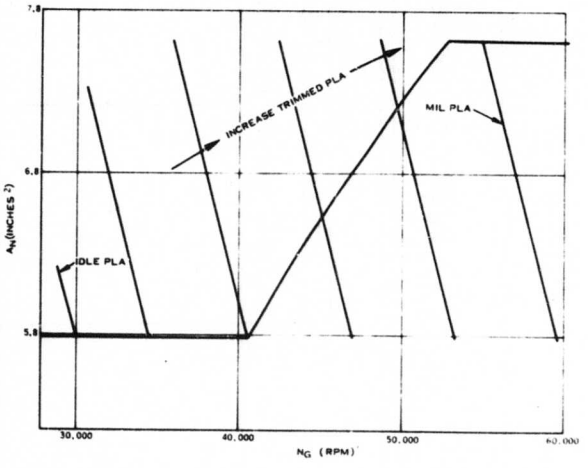

Figure 14. Power Turbine Stator Schedule.

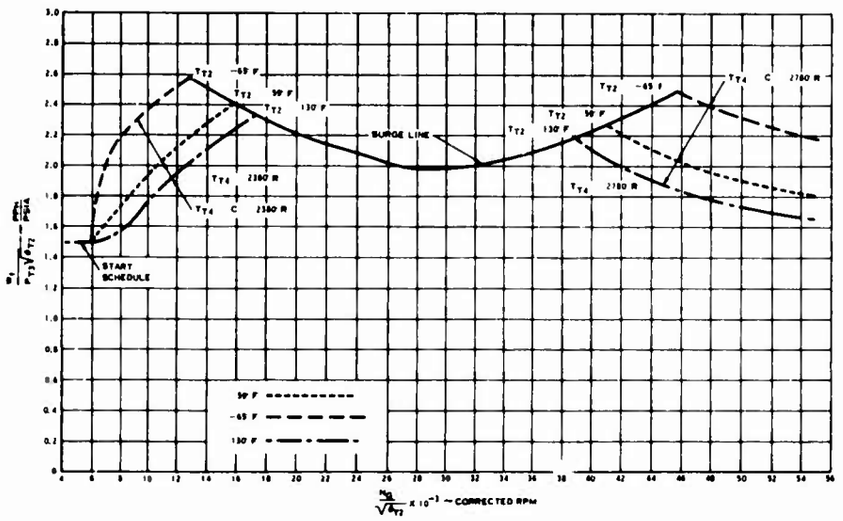

Figure 15. Acceleration Schedule - Base Engine W_f/P_{T3} Mode.

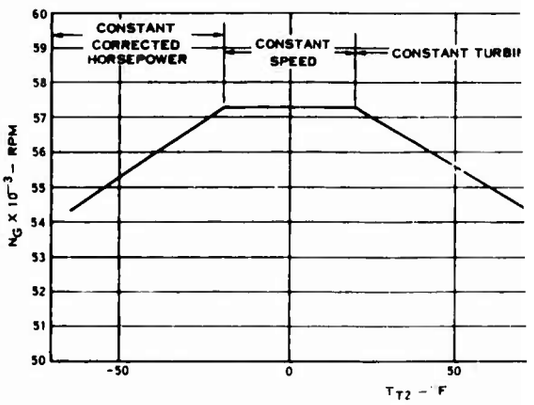

Figure 16. Gas Generator Ma Schedule - Base E

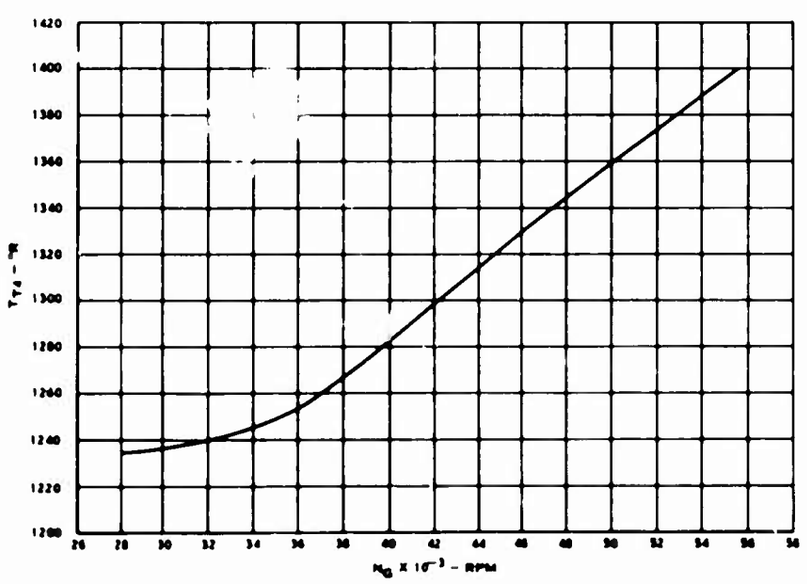

Figure 18. Deceleration Schedule - Base Engine.

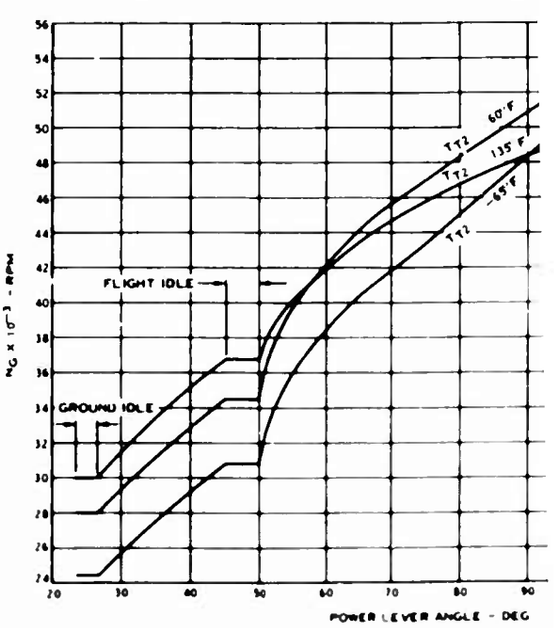

Figure 19. N_G vs Power Leve

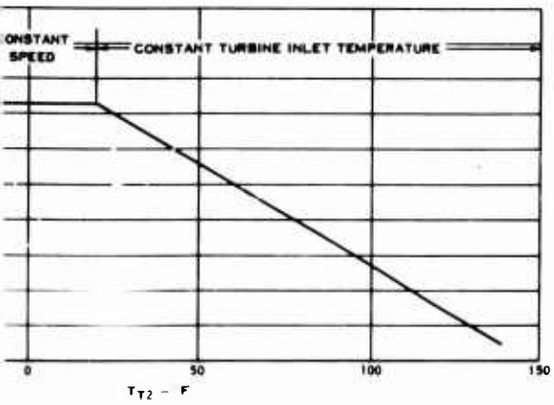

Gas Generator Maximum Power Schedule - Base Engine.

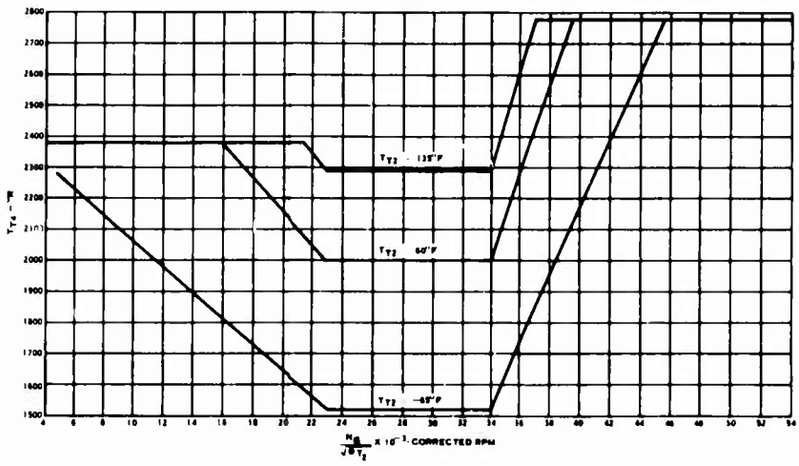

Figure 17. Acceleration Schedule - Regenerative Engine.

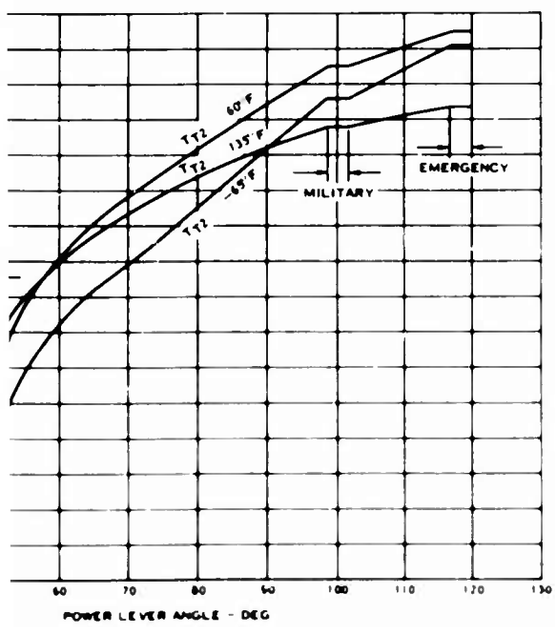

N_G vs Power Lever Angle.

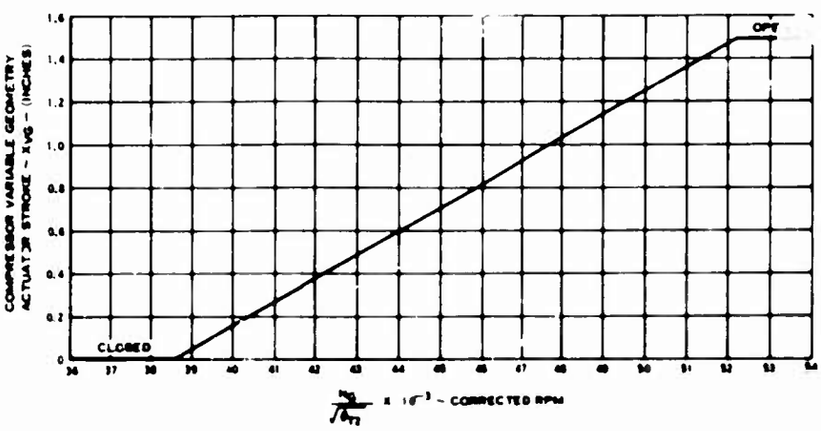

Figure 20. Compressor Variable - Geometry Schedule.

CONTROL MODE STUDIES

Introduction

The overall control function of a basic engine contains several regimes of operation such as turbine inlet temperature limiting and surge protection during accelerations, turbine inlet temperature scheduling during steady-state power turbine speed governing, gas generator speed governing, power limiting, etc. Each regime can be realized with significantly different computational logic and with significantly different sensed parameters. This section explores the relative advantages of several of the more prominent and practical control modes from the standpoint of the defined engine, in a transient and static accuracy performance evaluation.

Influence Coefficient Study

Considerable insight into the worth of any control mode can be determined from the influence that inherent engine, control and sensor variations have on the primary objective of each operating regime. An influence coefficient can be defined as the ratio of any dependent parameter to any independent parameter determined when the complete system of engine, control and load is in closed-loop operation. The influence coefficient is a closed-loop steady-state transfer function expressed in units of percent per percent of point. The amount of change occurring in a dependent parameter can be determined by multiplying the variation in any input amplitude by the influence coefficient. When the independent input is an error source, such as a sensor error, then knowledge of the influence coefficients permits a direct comparison of the capability of different control modes relative to the sensor accuracy, as a simple example. Influence coefficients for several modes of control were determined by employing vector algebra in a digital computer program to solve the equation set generated as follows:

1. Partial differential equations for the engine and helicopter rotor load were written in general terms and computation was provided to assign proper coefficients for any desired point of operation.

2. Partial differential equations were written for each mode of control such that operation in a particular regime would be ideal.

3. Error sources representing perturbations from the ideal system were assigned as independent inputs for sensing probe stations, sensor accuracy, control computation accuracy, engine deterioration factors and compressor air bleed extraction.

This set of equations was solved for the ratio of any engine or control dependent

parameter to any of the error sources at each of five possible operating regimes for a number of control modes. Figure 21 shows the general nature of the control modes considered in the following regimes:

1. Steady-state turbine inlet temperature limiting
2. Steady-state gas generator speed governing on a droop line
3. Steady-state shaft horsepower/inlet pressure limiting on a governor droop line
4. Acceleration turbine inlet temperature limiting
5. Acceleration surge bucket limiting

Engine inlet temperature effects were considered throughout the influence coefficient study but have been deleted in Figure 21 for clarity. The control modes shown in this figure represent a cross section of schemes ranging from those prominent in current use, some particularly adapted to direct temperature sensing, some readily adaptable to regenerator engine cycles, and to some of an outright speculative nature. Half of the control modes are characterized by scheduled fuel flow for limiting, while the remaining half determine fuel flow by integrating an error signal in a closed-loop control. No attempt was made in this particular portion of the study to assess dynamic errors or to assign dynamic compensation to the modes since this was covered in the following section on gross transient analysis performance.

The results of the influence coefficient study are tabulated for each operating regime in Tables III through VII. The first column in these tables is a reference to the source of error identified in the second column. The error sources are generally self-evident. The errors designated "sensor" include the sensor, reference, and amplification needed to do the actual computation, but do not include error due to location of the sensor relative to the true mean engine parameter. Such error is designated "probe" error. The fuel control computing errors apply to all other errors that occur in scheduling controls when ideal sensors and probes are assumed. The engine parameter variations are due to engine deterioration over a period of time. The final error source is compressor discharge bleed air extraction which is normally an independent variable with installation demands but which could be caused by compressor case battle damage.

The third column assigns an amplitude to the errors based on the trade-off made in the technology section of this report and represents a realistic error magnitude within the confines of weight, volume, cost and reliability setup for this program.

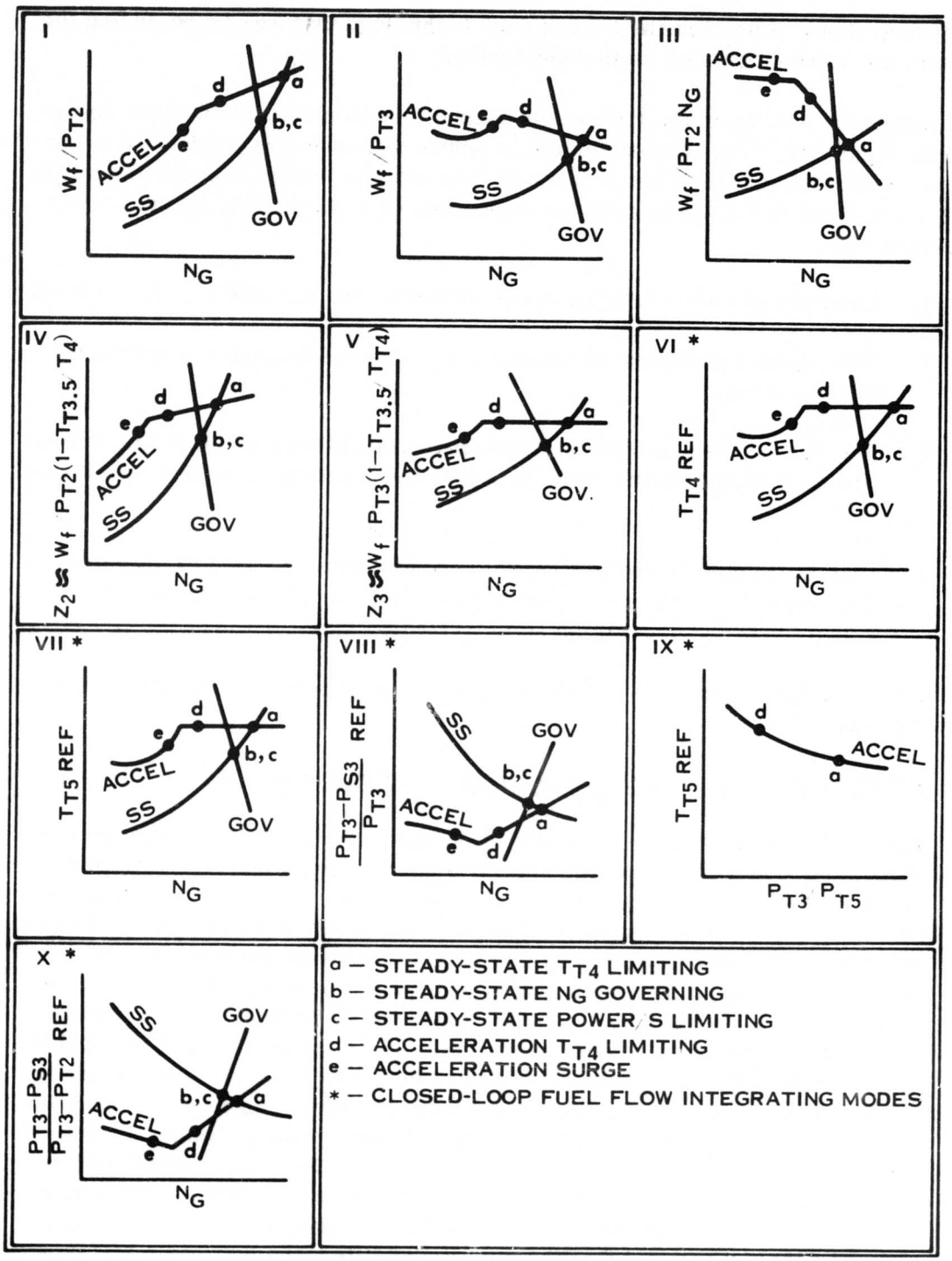

Figure 21. Influence Coefficient Study of Control Modes and Regimes.

The errors shown represent the best of each technology that was found during the program and were calculated on the RSS method.

Each remaining column in the tables represents a particular control mode designated on Figure 21. The numbers in the columns represent the product of the influence coefficient and the error amplitude. An attempt has been made to summarize the resulting individual errors for each mode of control, applying the following ground rules:

1. Control and sensor errors occur randomly and a ± RSS subtotal is made.

2. The engine parameter variations are simultaneous, and an algebraic subtotal is made.

3. The sum of the subtotals is presented with and without bleed air extraction to obtain the total error plus and minus potential noted in the bottom row.

4. Both the subtotals and total error potential must be used deliberately as they represent only one of several possible ways in which the individual error results can be summarized.

A discussion of each of the five operating regimes considered is provided in the following sections.

Steady-State Turbine Inlet Temperature Limiting (Table III)

Table III summarizes the influence of the system errors at the intersection of the control acceleration limiting line with the engine steady-state line. See point "a" in Figure 21. The errors are expressed in degrees Rankine difference between the actual turbine inlet temperature (T_{T4}) and the desired reference. It would be expected that a direct measurement of T_{T4} and a closed-loop integrating control would provide the best T_{T4} accuracy. However, the table shows such a control, Mode VI, to be inferior to a turbine discharge temperature sensing mode, VII, solely on the basis of obtainable sensor accuracy. It is judged that thermocouples can be used successfully at T_{T5} temperature levels, while some form of fluidic sensor would have to be used at the T_{T4} station. The next best control mode in terms of overtemperature and total error band is Z_3, Mode V. Z_3 offers better performance than the conventional W_f/P_{T3} Mode II, because bleed air extraction has no effect on turbine inlet temperature with a properly biased Z_3 schedule. The table points out that the significant difference between a W_f/P_{T3} control, Mode II, and a W_f/P_{T2} control, Mode I, is the bleed air extraction

TABLE III. STEADY-STATE TURBINE INLET TEMPERATUR INFLUENCE COEFFICIENT SUMMARY

Errors	Source Description	Amplitude % of Point	I W_f/P_{T2} °F	II W_f/P_{T3} °F	III W_f/P_{T2N_G} °F	IV Z_2 °F	V Z_3 °F	VI $T_{T4} = C$ °F	T_{T5}
			Steady-State Turbine Inlet Temperature Limi						
Control and Sensor Errors	Compressor SV Schedule	±5.12	± 61.184	± 32.51	±103.936	± 77.824	-	-	
	T_{T2} Sensor	±2.00	± 56.4	± 24.4	-	± 36.2	-	-	
	T_{T2} Probe *	±1.00	± 28.2	± 12.2	-	± 18.1	-	-	
	T_{T3} Sensor	±1.50	-	-	-	± 18.9	± 26.0	-	
	T_{T3} Probe *	±2.00	-	-	-	± 25.2	± 34.7	-	
	T_{T4} Sensor	±3.16	-	-	-	-	-	± 87.3	
	T_{T4} Probe *	±2.50	-	-	-	-	-	± 69.0	
	T_{T5} Sensor	±1.20	-	-	-	-	-	-	± 3
	T_{T5} Probe *	±2.00	-	-	-	-	-	-	± 5
	P_{T2} Sensor	±0.51	± 8.4	-	± 11.3	± 7.8	-	-	
	P_{T2} Probe *	±2.00	± 33.6	-	± 44.4	± 30.5	-	-	
	P_{T3} Sensor	±0.35	-	± 3.2	-	-	± 7.3	-	
	P_{T3} Probe *	±2.20	-	± 51.4	-	-	± 46.1	-	
	P_{T3}/P_{T5} or P_{T3}/P_{T2} Ratio Sensor	±1.10	-	-	± 45.2	-	-	-	
	P_{T3}/P_{T5} or P_{T3}/P_{T2} Probe *	±3.00	-	-	±123.2	-	-	-	
	$(P_{T3}-P_{S3})/P_{T3}$ Ratio Sensor	±2.10	-	-	-	-	-	-	
	$(P_{T3}-P_{S3})/P_{T3}$ Probe *	±2.00	-	-	-	-	-	-	
	$(P_{T3}-P_{S3})/(P_{T3}-P_{T2})$ Ratio Sensor	±2.50	-	-	-	-	-	-	
	$(P_{T3}-P_{S3})/(P_{T3}-P_{T2})$ Probe *	±2.00	-	-	-	-	-	-	
	N_G Speed Sensor	±0.16	± 2.6	± 1.4	± 4.5	± 3.4	-	-	
	Fuel Control	±4.60	± 75.6	-	-	-	-	-	
	Computing Errors	±3.05	-	± 71.1	-	-	-	-	
	(With Ideal Sensors)	±4.65	-	-	±130.0	-	-	-	
		±4.30	-	-	-	± 73.1	-	-	
		±3.10	-	-	-	-	± 65.0	-	
	RSS Subtotal of Control and Sensor Errors		±121.001	+ 97.813	±216.895	+122.610	± 91.014	±111.276	± 6
Engine Parameter Variations	Compressor Efficiency	-3.00	+ 26.4	+ 37.5	+ 45.9	-	-	-	
	Burner Efficiency	-0.50	- 8.2	- 11.7	- 14.3	- 7.6	- 10.4	-	
	Gas Gen Turbine Efficiency	-3.00	-	-	-	-	-	-	- 3
	Gas Gen Turbine Nozzle Erosion	+2.00	- 9.0	- 59.4	- 97.6	-	- 41.8	-	- 1
	Power Turbine Nozzle Erosion	+1.00	-	-	-	-	-	-	+
	Burner Pressure Loss	+0.20	- 0.9	- 6.2	- 10.2	-	- 4.4	-	
	SHP Extraction/lb of Air**	+9.00	-	-	-	-	-	-	
	Algebraic Subtotal of Engine Variables		+ 7.3	- 39.8	- 76.2	- 7.6	- 56.6	-	- 3
	P_{T3} Bleed Air Extraction	+5.00	+ 59.6	- 31.9	-101.5	+ 76.2	-	-	
	Total Error Potential (°F)		+187.901 -121.001	+ 97.813 -169.513	+216.895 -394.595	+198.810 -130.210	_ 91.014 -147.614	±111.276	+ 6 -10

* All probe errors are defined as the difference between the true mean engine parameter value and the actual valve determined by averaging at the probe locations.

** Units are hp/lb/sec for SHP/W_a error amplitude.

DY-STATE TURBINE INLET TEMPERATURE LIMITING
LUENCE COEFFICIENT SUMMARY

Steady-State Turbine Inlet Temperature Limiting Regime

III	IV	V	VI	VII	VIII	IX	X
W_f/P_{T2N_G}	Z_2	Z_3	$T_{T4} = C$	$T_{T5} = f(N_G, T_{T2})$	$\frac{\Delta P}{P} = f(N_2, T_{T2})$	$P_{T3}/P_{T5} = f(T_{T5})$	$\frac{\Delta P}{\Delta P} = f(N_G, T_{T2})$
°F	°F	°F	°F	°F	°F	°F	°F
±103.936	± 77.824	-	-	-	± 56.320	-	± 44.032
-	± 36.2	-	-	-	± 42.0	-	± 45.2
-	± 18.1	-	-	-	± 21.0	-	± 22.6
-	± 18.9	± 26.0	-	-	-	-	-
-	± 25.2	± 34.7	-	-	-	-	-
-	-	-	± 87.3	-	-	-	-
-	-	-	± 69.0	-	-	-	-
-	-	-	-	± 33.4	-	± 33.4	-
-	-	-	-	± 55.6	-	± 55.6	-
± 11.3	± 7.8	-	-	-	-	-	± 1.0
± 44.4	± 30.5	-	-	-	-	-	± 4.0
-	-	± 7.3	-	-	-	-	-
-	-	± 46.1	-	-	-	-	-
± 45.2	-	-	-	-	-	± 61.2	-
±123.2	-	-	-	-	-	±168.0	-
-	-	-	-	-	± 69.9	-	-
-	-	-	-	-	± 65.5	-	-
-	-	-	-	-	-	-	± 80.0
-	-	-	-	-	-	-	± 64.0
± 4.5	± 3.4	-	-	-	± 2.4	-	± 1.9
-	-	-	-	-	-	-	-
-	-	-	-	-	-	-	-
±130.0	-	-	-	-	-	-	-
-	± 73.1	-	-	-	-	-	-
-	-	± 65.0	-	-	-	-	-
±216.895	+122.610	± 91.014	±111.276	± 64.861	±120.661	+190.201	+122.5
+ 45.9	-	-	-	-	+ 64.6	-	+ 62.2
- 14.3	- 7.6	- 10.4	-	-	-	-	-
-	-	-	-	- 30.1	-	-	-
- 97.6	-	- 41.8	-	- 14.5	+111.2	+111.2	+111.2
-	-	-	-	+ 7.3	-	- 56.6	-
- 10.2	-	- 4.4	-	-	+ 11.6	+ 11.6	+ 11.6
-	-	-	-	-	-	-	-
- 76.2	- 7.6	- 56.6	-	- 37.3	+187.4	+ 66.2	+285.0
-101.5	+ 76.2	-	-	-	+278.0	-	+278.0
+216.895	+198.810	_ 91.014	±111.276	+ 64.861	+586.061	÷256.401	+685.512
-394.595	-130.210	-147.614		-102.661	-120.661	-190.201	-122.512

he parameter value

B

TABLE IV. STEADY-STATE GAS GENERATOR SPEED GOVERNING

Errors	Source Description	Amplitude % of Point	I W_f/P_{T2}	II W_f/P_{T3}	III W_f/P_{T2} N_G	IV Z_2	V Z_3	T_{T4}
			Steady-State Gas Generator					
			$\%N_G$	$\%N_G$	$\%N_G$	$\%N_G$	$\%N_G$	
Control and Sensor Errors	Compressor SV Schedule	±5.12	±0.763	±0.302	±0.292	±1.337	±0.993	
	T_{T2} Sensor	±2.00	±0.142	±0.016	-	±0.074	±0.278	
	T_{T2} Probe *	±1.00	±0.071	±0.008	-	±0.037	±0.139	
	T_{T3} Sensor	±1.50	-	-	-	±0.145	±0.264	
	T_{T3} Probe *	±2.00	-	-	-	±0.194	±0.352	
	T_{T4} Sensor	±3.16	-	-	-	-	-	
	T_{T4} Probe *	±2.50	-	-	-	-	-	
	T_{T5} Sensor	±1.20	-	-	-	-	-	
	T_{T5} Probe *	±2.00	-	-	-	-	-	
	P_{T2} Sensor	±0.51	±0.040	-	±0.044	±0.059	-	
	P_{T2} Probe *	±2.00	±0.156	-	±0.174	±0.230	-	
	P_{T3} Sensor	±0.35	-	±0.037	-	-	±0.074	
	P_{T3} Probe *	±2.20	-	±0.234	-	-	±0.463	
	P_{T3}/P_{T5} or P_{T3}/P_{T2} Ratio Sensor	±1.10	-	-	±0.088	-	-	
	P_{T3}/P_{T5} or P_{T3}/P_{T2} Probe *	±3.00	-	-	±0.240	-	-	
	$(P_{T3} - P_{S3})/P_{T3}$ Ratio Sensor	±2.10	-	-	-	-	-	
	$(P_{T3} - P_{S3})/P_{T3}$ Probe *	±2.00	-	-	-	-	-	
	$(P_{T3} - P_{S3})/(P_{T3}-P_{T2})$ Ratio Sensor	±2.50	-	-	-	-	-	
	$(P_{T3} - P_{S3})/(P_{T3}-P_{T2})$ Probe *	±2.00	-	-	-	-	-	
	N_G Speed Sensor	±0.16	±0.125	±0.147	±0.147	±0.099	±0.114	±
		±4.60	±0.359	-	-	-	-	
	Fuel Control	±3.05	-	±0.322	-	-	-	
	Computing Errors	±4.65	-	-	±0.404	-	-	
	(With Ideal Sensors)	±4.80	-	-	-	±0.544	-	
		±3.10	-	-	-	-	+0.651	
	RSS Subtotal of Control and Sensor Errors		±0.882	±0.522	±0.606	±1.488	±1.390	±
Engine Parameter Variations	Compressor Efficiency	-3.00	-0.411	-0.345	-0.294	-0.855	-1.134	-
	Burner Efficiency	-0.50	-0.039	-0.053	-0.044	-0.058	-0.105	
	Gas Gen Turbine Efficiency	-3.00	-0.609	-0.585	-0.495	-0.972	-1.287	-
	Gas Gen Turbine Nozzle Erosion	+2.00	-0.152	-0.376	-0.296	-0.172	-0.648	-
	Power Turbine Nozzle Erosion	+1.00	+0.146	+0.140	+0.118	+0.233	+0.309	+
	Burner Pressure Loss	+0.20	+0.015	-0.010	-0.006	+0.030	-0.003	+
	SHP Extraction/Lb of Air **	+9.00	-0.090	-0.090	-0.006	-0.012	-0.016	-
	Algebraic Subtotal of Engine Variables		-1.140	-1.319	-0.823	-1.806	-2.884	-1
	P_{T3} Bleed Air Extraction	+5.00	-0.150	-0.565	-0.440	-0.115	-0.920	-
	Total Error Potential (Percent)		+0.882 -2.172	+0.522 -2.406	+0.606 -1.869	+1.488 -3.409	+1.390 -5.194	+ -2

* All probe errors are defined as the difference between the true mean engine parameter value and the actual value determined by averaging at the probe locations.

** Units are hp/Lb/sec for SHP/W_a error amplitude.

AS GENERATOR SPEED GOVERNING INFLUENCE COEFFICIENT SUMMARY

Steady-State Gas Generator Speed Governing Regime

3	III $W_f/P_{T2}\,N_G$	IV Z_2	V Z_3	VI $T_{T4}=f(N,T_{T2})$	VII $T_{T5}=f(N_G,T_{T2})$	VIII $\frac{\Delta P}{P}=f(N_G,T_{T2})$	IX $P_{T3}/P_{T5}=f(T_{T5})$	X $\frac{\Delta P}{\Delta P}=f(N_G,T_{T2})$
	$\%N_G$	$\%N_G$	$\%N_G$	$\%N_G$	$\%N_G$	$\%N_G$	$\%N_G$	$\%N_G$
	±0.292	±1.337	±0.993	±0.451	±0.364	±0.195		±0.251
	-	±0.074	±0.278	±0.126	±0.100	±0.062		±0.078
	-	±0.037	±0.139	±0.063	±0.050	±0.031		±0.039
	-	±0.145	±0.264	-	-	-		-
	-	±0.194	±0.352	-	-	-		-
	-	-	-	±0.404	-	-		-
	-	-	-	±0.320	-	-		-
	-	-	-	-	±0.122	-		-
	-	-	-	-	±0.204	-		-
	±0.044	±0.059	-	-	-	-		±0.004
	±0.174	±0.230	-	-	-	-		±0.018
	-	-	±0.074	-	-	-		-
	-	-	±0.463	-	-	-		-
	±0.088	-	-	-	-	-		-
	±0.240	-	-	-	-	-		-
	-	-	-	-	-	±0.264		-
	-	-	-	-	-	±0.252		-
	-	-	-	-	-	-		±0.303
	-	-	-	-	-	-		±0.242
	±0.147	±0.099	±0.114	±0.139	±0.143	±0.151		±0.147
	-	-	-	-	-	-		-
	-	-	-	-	-	-		-
	±0.404	-	-	-	-	-		-
	-	±0.544	-	-	-	-		-
	-	-	+0.651	-	-	-		-
	±0.606	±1.488	±1.390	±0.713	±0.471	±0.368	-	±0.493
	-0.294	-0.855	-1.134	-0.516	-0.414	-0.222	-	-0.231
	-0.044	-0.058	-0.105	-	-	-	-	-
	-0.495	-0.972	-1.287	-0.585	-0.585	-0.585	-	-0.585
	-0.296	-0.172	-0.648	-0.104	-0.140	+0.406	-	+0.406
	+0.118	+0.233	+0.309	+0.140	+0.140	+0.140	-	+0.140
	-0.006	+0.030	-0.003	+0.018	+0.015	+0.071	-	+0.071
	-0.006	-0.012	-0.016	-0.090	-0.090	-0.090		-0.090
	-0.823	-1.806	-2.884	-1.137	-1.074	-0.280	-	-0.289
	-0.440	-0.115	-0.920	-0.420	-0.335	+0.860	-	+0.860
	+0.606	+1.488	+1.390	+0.713	+0.471	+1.228	-	+1.353
	-1.869	-3.409	-5.194	-2.270	-1.880	-0.648	-	-0.782

Mode Not Capable of N_G Speed Governing Without N_G Speed Sensor

gine parameter value and the

B

TABLE V. STEADY-STATE SHAFT HORSEPOWER LIMITING INFLUENC

Errors			Steady-State Shaft Horsepower/P_{T2}				
	Source Description	Amplitude % of Point	I W_f/P_{T2} %HPPT/P_{T2}	II W_f/P_{T3} %HPPT/P_{T2}	III W_f/P_2N_G %HPPT/P_{T2}	IV Z_2 %HPPT/P_{T2}	V Z_3 %HPPT/P_{T2}
Control And Sensor Errors	Compressor SV Schedule	± 5.12	9.600	11.213	3.205	7.060	8.023
	T_{T2} Sensor	± 2.00	2.014	2.570	-	2.222	3.702
	T_{T2} Probe	± 1.00	1.007	1.285	-	1.111	1.851
	T_{T3} Sensor	± 1.50	-	-	-	0.564	1.128
	T_{T3} Probe	± 2.00	-	-	-	0.752	1.504
	T_{T4} Sensor	± 3.16	-	-	-	-	-
	T_{T4} Probe	± 2.50	-	-	-	-	-
	T_{T5} Sensor	± 1.20	-	-	-	-	-
	T_{T5} Probe	± 2.00	-	-	-	-	-
	P_{T2} Sensor	± 0 51	0.140	-	0.653	0.229	-
	P_{T2} Probe	± 2.00	0.550	-	2.562	0.898	-
	P_{T3} Sensor	± 0.35	-	0.131	-	-	0.314
	P_{T3} Probe	± 2.20	-	0.823	-	-	1.973
	P_{T3}/P_{T5} or P_{T3}/P_{T2} Ratio Sensor	± 1.10	-	-	1.313	-	-
	P_{T3}/P_{T5} or P_{T3}/P_{T2} Probe	± 3.00	-	-	3.582	-	-
	$(P_{T3}- P_{S3})/P_{T3}$ Ratio Sensor	± 2.10	-	-	-	-	-
	$(P_{T3}- P_{S3})/P_{T3}$ Probe	± 2.00	-	-	-	-	-
	$(P_{T3}- P_{S3})/(P_{T3}- P_{T2})$ Ratio Sensor	± 2.50	-	-	-	-	-
	$(P_{T3}- P_{S3})/(P_{T3}- P_{T2})$ Probe	± 2.00	-	-	-	-	-
	N_G Speed Sensor	± 0.16	0.440	0.514	0.147	0.323	0.367
	Fuel Control	± 4.60	1.265	-	-	-	-
	Computing Errors	± 3.05	-	1.141	-	-	-
	(With Ideal Sensors)	± 4.65	-	-	0.405	-	-
		± 4.80	-	-	-	2.155	-
		± 3.10	-	-	-	-	2.781
	RSS Subtotal of Control and Sensor Errors		± 9.967	± 11.673	± 5.657	± 7.906	± 9.843
Engine Parameter Variations	Compressor Efficiency	- 3.00	+ 3.651	+ 3.888	+ 2.229	+ 1.767	+ 0.249
	Burner Efficiency	- 0.50	- 1.375	- 0.187	- 0.044	- 0.220	- 0.449
	Gas Gen Turbine Efficiency	- 3.00	+ 5.085	+ 5.172	+ 3.813	+ 3.447	+ 1.719
	Gas Gen Turbine Nozzle Erosion	+ 2.00	+ 1.186	+ 0.400	+ 3.450	+ 1.046	- 1.056
	Power Turbine Nozzle Erosion	+ 1.00	- 1.743	- 1.764	- 1.438	- 1.350	- 0.937
	Burner Pressure Loss	+ 0.20	- 0.130	- 0.216	+ 0.169	- 0.063	- 0.196
	SHP Extraction/Lb of Air	+ 9.00	+ 0.046	+ 0.047	+ 0.030	+ 0.025	+ 0.004
	Algebraic Subtotal of Engine Variables		+ 6.72	+ 7.34	+ 8.209	+ 4.652	- 0.666
	P_{T3} Bleed Air Extraction	± 5.00	- 4.030	- 5.475	+ 0.355	- 3.950	- 7.425
	Total Error Potential (Percent)		+ 16.687 - 13.997	+ 19.013 - 17.148	+ 14.221 - 5.657	+ 12.558 - 11.856	+ 9.843 - 17.934

WER LIMITING INFLUENCE COEFFICIENT SUMMARY

y-State Shaft Horsepower/P_{T2} Limiting Regime

	IV Z_2	V Z_3	VI $T_{T4} = f(N, T_{T2})$	VII $T_{T5} = f(N_G, T_{T2})$	VIII $\frac{\Delta P}{P} = f(N_G, T_{T2})$	IX $\frac{P_{T3}}{P_{T5}} = f(T_{T5})$	X $\frac{\Delta P}{P} = f(N_G, T_{T2})$
T2	%HPPT/P_{T2}	%HPPT/P_{T2}	%HPPT/P_{T2}	%HPPT/P_{T2}	%HPPT/P_{T2}	%HPPT/P_{T2}	%HPPT/P_{T2}
	7.060	8.023	10.685	11.003	13.046		17.562
	2.222	3.702	-	2.87	2.758		4.056
	1.111	1.851	-	1.435	1.379		2.028
	0.564	1.128	-	-	-		-
	0.752	1.504	-	-	-		-
	-	-	1.419	-	-		-
	-	-	1.123	-	-		-
	-	-	-	0.431	-		-
	-	-	-	0.718	-		-
	0.229	-	-	-	-		0.325
	0.898	-	-	-	-		1.274
	-	0.314	-	-	-		-
	-	1.973	-	-	-		-
	-	-	-	-	-		-
	-	-	-	-	-		-
	-	-	-	-	1.272		-
	-	-	-	-	1.211		
	-	-	-	-	-		1.999
	-	-	-	-	-		1.599
	0.323	0.367	0.490	0.504	0.598		0.805
	-	-	-	-	-		-
	-	-	-	-	-		-
	-	-	-	-	-		-
	2.155	-	-	-	-		-
	-	2.781	-	-	-		-
	± 7.906	± 9.843	± 10.848	± 11.503	± 13.496	-	± 18.383
	+ 1.767	+ 0.249	+ 3.285	+ 3.645	+ 5.976	-	+ 7.455
	- 0.220	- 0.449	-	-	-	-	-
	+ 3.447	+ 1.719	+ 5.172	+ 5.172	+ 9.552	-	+11.553
	+ 1.046	- 1.056	+ 1.352	+ 1.230	+ 0.106	-	- 1.282
	- 1.350	- 0.937	- 1.764	- 1.764	- 2.813	-	- 3.292
	- 0.063	- 0.196	- 0.117	- 0.136	- 0.466	-	- 0.710
	+ 0.025	+ 0.004	+ 0.047	+ 0.052	+ 0.1024	-	+ 0.128
	+ 4.652	- 0.666	+ 7.975	+ 8.205	+12.457	-	+ 13.852
	- 3.950	- 7.425	- 4.96	- 4.67	- 6.90	-	- 9.83
	+ 12.558	+ 9.843	+ 18.823	+ 19.708	+ 25.953	-	+ 32.235
	- 11.856	- 17.934	- 15.808	- 16.173	- 20.396	-	- 28.213

Mode Not Capable of Power Limiting Without N_G Speed Sensor

B

TABLE VI. ACCELERATION TURBINE INLET INFLUENCE COEFFICIENT SUMM

Errors			Acceleration Turbine Inlet Temp								
			ΔWF Error in % Fuel Flow								
	Source Description	AMPLITUDE % OF POINT	I W_f/P_{T2}		II W_f/P_{T3}		III $W_f/P_{T2}\,N_G$		IV Z_2		
			$\pm\Delta W_f\%$	Δt sec	$\pm\Delta W_f\%$	Δt sec	$\pm\Delta W_f\%$	Δt sec	$\pm\Delta W_f\%$	Δt sec	$\pm\Delta W_f\%$
Control and Sensor Errors	Compressor SV Schedule	±5.12	-	-	5.622	1.024	1.203	0.230	0.701	0.128	3.807
	T_{T2} Sensor	±2.00	3.982	0.73	0.902	0.17	-	-	3.154	0.58	0
	T_{T2} Probe	±1.00	1.991	0.37	0.451	0.08	-	-	1.577	0.29	0
	T_{T3} Sensor	±1.60	-	-	-	-	-	-	0.323	0.06	1.330
	T_{T3} Probe	±2.00	-	-	-	-	-	-	0.404	0.07	1.662
	T_{T4} Sensor	±3.16	-	-	-	-	-	-	-	-	-
	T_{T4} Probe	±2.50	-	-	-	-	-	-	-	-	-
	T_{T5} Sensor	±1.20	-	-	-	-	-	-	-	-	-
	T_{T5} Probe	±2.00	-	-	-	-	-	-	-	-	-
	P_{T2} Sensor	±0.51	0.510	0.09	-	-	1.585	0.29	0.165	0.03	-
	P_{T2} Probe	±2.00	2.000	0.37	-	-	6.216	1.14	0.646	0.12	-
	P_{T3} Sensor	±0.40	-	-	0.598	0.11	-	-	-	-	0.544
	P_{T3} Probe	±2.20	-	-	3.289	0.61	-	-	-	-	2.994
	P_{T3}/P_{T5} or P_{T3}/P_{T2} Ratio Sensor	±1.20	-	-	-	-	2.305	0.42	-	-	-
	P_{T3}/P_{T5} or P_{T3}/P_{T2} Probe	±3.00	-	-	-	-	5.772	1.06	-	-	-
	$(P_{T3} - P_{S3})/P_{T3}$ Ratio Sensor	±1.66	-	-	-	-	-	-	-	-	-
	$(P_{T3} - P_{S3})/P_{T3}$ Probe	±2.00	-	-	-	-	-	-	-	-	-
	$(P_{T3} - P_{S3})/(P_{T3} - P_{T2})$ Ratio Sensor	±1.91	-	-	-	-	-	-	-	-	-
	$(P_{T3} - P_{S3})/(P_{T3} - P_{T2})$ Probe	±2.00	-	-	-	-	-	-	-	-	-
	N_G Speed Sensor	±0.19	0.036	0.01	0.133	0.02	0.273	0.05	0.231	0.04	-
	Fuel Control Computing Errors (With Ideal Sensors)	±3.79	3.525	0.65	-	-	-	-	-	-	-
		±2.85	-	-	4.261	0.78	-	-	-	-	-
		±4.01	-	-	-	-	6.548	1.21	-	-	-
		±4.35	-	-	-	-	-	-	4.276	0.79	-
		±2.98	-	-	-	-	-	-	-	-	4.055
	RSS Subtotal of Control and Sensor Errors		6.042	1.112	7.873	1.441	11.144	2.050	5.655	1.042	6.688
Engine Parameter Variations	Compressor Efficiency	-3.0	+1.00	0.09	+1.50	0.14	+1.64	0.15	-	-	-
	Burner Efficiency	-0.5	-0.50	0.05	-0.75	0.07	-0.81	0.07	-0.47	0.04	-0.68
	Gas Gen Turbine Efficiency	-3.0	-	-	-	-	-	-	-	-	-
	Gas Gen Turbine Nozzle Erosion	+2.0	-0.37	0.03	-3.56	0.33	-2.48	0.23	-	-	-2.70
	Power Turbine Nozzle Erosion	+1.0	-	-	-	-	-	-	-	-	-
	Burner Pressure Loss	+0.2	-0.04	0.00	-0.37	0.03	+0.39	0.04	-	-	-0.16
	SHP Extraction/Lb of Air	+9.0	-	-	-	-	-	-	-	-	-
	Algebraic Subtotal		+0.09	0.17	-3.18	0.57	-1.26	0.49	-0.47	0.04	-3.54
	P_{T3} Bleed Air Extraction	+5.0	+4.02	+0.37	-1.48	-0.14	-7.07	-0.65	+4.70	0.43	0
	Total Error Potential (Seconds)			1.652		2.011		2.540		1.512	

A

TION TURBINE INLET TEMPERATURE LIMITING
COEFFICIENT SUMMARY.

celeration Turbine Inlet Temperature Limiting Regime

ΔT Accel Time Error in Seconds

	IV Z_2		V Z_3		VI $T_{T4} = C$		VII $T_{T5} = (N_G, T_{T2})$		VIII $\frac{\Delta P}{P} = f(N_G, T_{T2})$		IX $\frac{P_{T3}}{P_{T5}} = f(T_{T5})$		X $\frac{\Delta P}{\Delta P} = f(N_G, T_{T2})$	
ec	$\pm\Delta W_f\%$	Δt sec	$\pm\Delta W_f\%$	Δt sec	$\pm\Delta W_f\%$	Δt sec	$\pm\Delta W_f\%$	Δt sec	$\pm\Delta W_f\%$	Δt sec	$\pm\Delta W_f\%$	Δt sec	$\pm\Delta W_f\%$	Δt sec
0	0.701	0.128	3.807	0.691	4.111	0.768	4.111	0.768	7.035	1.306	4.111	0.768	-	-
	3.154	0.58	0	-	0	-	0	-	1.758	0.32	-	-	2.316	0.43
	1.577	0.29	0	-	0	-	0	-	0.879	0.16	-	-	1.158	0.21
	0.323	0.06	1.330	0.24	-	-	-	-	-	-	-	-	-	-
	0.404	0.07	1.662	0.30	-	-	-	-	-	-	-	-	-	-
	-	-	-	-	4.751	0.88	-	-	-	-	-	-	-	-
	-	-	-	-	3.782	0.70	-	-	-	-	-	-	-	-
	-	-	-	-	-	-	1.816	0.33	-	-	1.816	0.33	-	-
	-	-	-	-	-	-	3.060	0.57	-	-	3.060	0.57	-	-
	0.165	0.03	-	-	-	-	-	-	-	-	-	-	0.097	0.02
	0.646	0.12	-	-	-	-	-	-	-	-	-	-	0.384	0.07
	-	-	0.544	0.10	-	-	-	-	-	-	-	-	-	-
	-	-	2.994	0.55	-	-	-	-	-	-	-	-	-	-
	-	-	-	-	-	-	-	-	-	-	3.600	0.66	-	-
	-	-	-	-	-	-	-	-	-	-	9.000	1.66	-	-
	-	-	-	-	-	-	-	-	3.046	0.56	-	-	-	-
	-	-	-	-	-	-	-	-	3.670	0.67	-	-	-	-
	-	-	-	-	-	-	-	-	-	-	-	-	1.277	0.23
	-	-	-	-	-	-	-	-	-	-	-	-	1.344	0.25
5	0.231	0.04	-	-	-	-	-	-	0.255	0.05	-	-	0.158	0.03
	-	-	-	-	-	-	-	-	-	-	-	-	-	-
	-	-	-	-	-	-	-	-	-	-	-	-	-	-
1	-	-	-	-	-	-	-	-	-	-	-	-	-	-
	4.276	0.79	-	-	-	-	-	-	-	-	-	-	-	-
	-	-	4.055	0.75	-	-	-	-	-	-	-	-	-	-
50	5.655	1.042	6.688	1.225	7.333	1.362	5.437	1.012	2.796	1.613	11.114	2.053	3.213	0.592
5	-	-	-	-	-	-	-	-	+2.91	0.27	-	-	+2.73	0.25
7	-0.47	0.04	-0.68	0.06	-	-	-	-	-	-	-	-	-	-
	-	-	-	-	-	-	-1.87	0.17	+0.13	0.01	-	-	+0.12	0.02
3	-	-	-2.70	0.25	-	-	-0.86	0.08	+6.16	0.57	+6.02	0.55	±6.15	0.57
	-	-	-	-	-	-	+0.44	0.04	+0.03	0.00	-3.0	0.28	+0.03	0.00
4	-	-	-0.16	0.01	-	-	+0.37	0.03	+0.55	0.06	+0.62	0.06	+0.65	0.06
	-	-	-	-	-	-	-	-	-	-	-	-	-	-
9	-0.47	0.04	-3.54	0.32	0	0	-1.93	0.32	+9.78	0.91	+3.65	0.89	+9.68	0.90
65	+4.70	0.43	0	0	0	0	0	0	+15.32	+1.41	0	0	+15.29	+1.41
40		1.512		1.545		1.362		1.332		3.933		2.943		2.902

B

TABLE VII. ACCELERATION SURGE LIMITING INFLUENCE C

Errors			Acceleration Surge Limiting										
	Source Description	Amplitude % of Point	I W_f/P_{T2}		II W_f/P_{T3}		III $W_f/P_{T2}-N_G$		IV Z_2		V Z_3		T_{T4}
			ΔW_f %	Δt sec	ΔW_f %	Δt sec	ΔW_f %	Δt sec	ΔW_f %	Δt sec	ΔW_f %	Δt sec	ΔW_f
Control and Sensor Errors	Compressor SV Schedule	+5.12	0.061	0.010	5.614	1.034	22.597	4.157	0.645	0.118	4.163	0.765	4.1
	T_{T2} Sensor	±2.00	12.370	2.276	9.285	1.708	-	-	11.546	2.125	8.394	1.545	8.3
	T_{T2} Probe	±1.00	6.185	1.138	4.643	0.854	-	-	5.773	1.062	4.197	0.772	4.1
	T_{T3} Sensor	±1.60	-	-	-	-	-	-	0.919	0.169	1.321	0.243	-
	T_{T3} Probe	±2.00	-	-	-	-	-	-	1.149	2.114	1.651	0.304	-
	T_{T4} Sensor	±3.16	-	-	-	-	-	-	-	-	-	-	4.74
	T_{T4} Probe	±2.50	-	-	-	-	-	-	-	-	-	-	3.75
	T_{T5} Sensor	±1.20	-	-	-	-	-	-	-	-	-	-	-
	T_{T5} Probe	±2.00	-	-	-	-	-	-	-	-	-	-	-
	P_{T2} Sensor	±0.51	0.515	0.095	-	-	1.529	0.281	0.479	0.088	-	-	-
	P_{T2} Probe	±2.00	2.019	0.372	-	-	5.998	1.104	1.880	0.346	-	-	-
	P_{T3} Sensor	±0.40	-	-	0.598	0.110	-	-	-	-	0.546	0.100	-
	P_{T3} Probe	±2.20	-	-	3.289	0.605	-	-	-	-	3.004	0.553	-
	P_{T3}/P_{T5} or P_{T3}/P_{T2} Ratio Sensor	±1.20	-	-	-	-	7.223	1.329	-	-	-	-	-
	P_{T3}/P_{T5} or P_{T3}/P_{T2} Probe	±3.00	-	-	-	-	18.059	3.323	-	-	-	-	-
	$(P_{T3}-P_{S3})/P_{T3}$ Ratio Sensor	±1.66											
	$(P_{T3}-P_{S3})/P_{T3}$ Probe	±2.00	-	-	-	-	-	-	-	-	-	-	-
	$(P_{T3}-P_{S3})/(P_{T3}-P_{T2})$ Ratio Sensor	±1.91	-	-	-	-	-	-	-	-	-	-	-
	$(P_{T3}-P_{S3})/(P_{T3}-P_{T2})$ Probe	±2.00	-	-	-	-	-	-	-	-	-	-	-
	N_G Speed Sensor	±0.19	2.537	0.467	2.042	0.376	0.552	0.102	2.590	0.477	2.169	0.399	2.16
	Fuel Control Computing Errors (With Ideal Sensors)	±3.79	3.825	0.704	-	-	-	-	-	-	-	-	-
		±2.85	-	-	4.261	0.784	-	-	-	-	-	-	-
		±4.01	-	-	-	-	12.025	2.213	-	-	-	-	-
		±4.35	-	-	-	-	-	-	4.089	0.752	-	-	-
		±2.98	-	-	-	-	-	-	-	-	4.069	0.749	-
	RSS Subtotal of Control and Sensor Errors		±14.720	2.709	±13.267	2.419	±32.744	6.025	±14.015	3.328	±11.852	2.181	±12.10
Engine Parameter Variations	Compressor Efficiency	-3.0	+0.895	+0.082	-1.366	+0.126	+2.767	+0.255	-9.850	+0.906	-	-	-
	Burner Efficiency	-0.5	-0.505	+0.046	-0.748	+0.069	-1.450	+0.133	-0.470	+0.043	-0.683	+0.064	-
	Gas Generator Turbine Efficiency	-3.0	-0.043	+0.004	-0.026	+0.002	-0.031	+0.003	+0.005	+0.001	-0.032	+0.003	-
	Gas Gen Turbine Nozzle Erosion	+2.0	-0.394	0.036	-3.581	+0.329	-13.195	+1.214	+0.001	-	-2.730	+0.251	-
	Power Turbine Nozzle Erosion	+1.0	+0.013	+0.001	+0.013	+0.001	+0.012	+0.001	+0.012	+0.001	-0.008	+0.001	-
	Burner Pressure Loss	+0.2	-0.034	+0.003	-0.370	+0.034	-1.377	+0.127	+0.003	-	-0.282	+0.026	-
	SHP Extraction/Lb of air	+9.0	-	-	-	-	-	-	-	-	-	-	-
	Algebraic Subtotal		-0.068	+0.172	-3.346	+0.561	-13.274	1.733	-10.299	+0.951	-3.735	+0.345	-
	P_{T3} Bleed Air Extraction	+5.0	+3.988	+0.367	-1.482	+0.136	-18.063	+1.662	+4.701	+0.433	-	-	-
	Total Error Potential (Seconds)		-	+3.248	-	+3.116	-	+9.420	-	+4.712	-	+2.526	-

A

SURGE LIMITING INFLUENCE COEFFICIENT SUMMARY

Acceleration Surge Limiting Regime

N_G sec	IV Z_2		V Z_3		VI $T_{T4} = f(N_G, T_{T2})$		VII $T_{T5} = f(N_G, T_{T2})$		VIII $\frac{\Delta P}{P} = f(N_{G1}, T_{T2})$		IX $\frac{P_{T3}}{P_{T5}} = f(T_{T5})$		X $\frac{\Delta P}{\Delta P} = f(N_G, T_{T2})$	
	ΔW_f %	Δt sec	ΔW_f %	Δt sec	ΔW_f %	Δt sec	ΔW_f %	Δt sec	ΔW_f %	Δt sec	ΔW_f %	Δt sec	ΔW_f %	Δt sec
57	0.645	0.118	4.163	0.765	4.160	0.765	4.091	0.753	7.112	1.308	-	-	3.781	0.696
-	11.546	2.125	8.394	1.545	8.386	1.543	8.407	1.547	10.055	1.850	-	-	15.077	2.774
-	5.773	1.062	4.197	0.772	4.193	0.7715	4.204	0.774	5.027	0.925	-	-	7.538	1.387
-	0.919	0.169	1.321	0.243	-	-	-	-	-	-	-	-	-	-
-	1.149	2.114	1.651	0.304	-	-	-	-	-	-	-	-	-	-
-	-	-	-	-	4.745	0.873	-	-	-	-	-	-	-	-
-	-	-	-	-	3.754	0.691	-	-	-	-	-	-	-	-
-	-	-	-	-	-	-	1.818	0.335	-	-	-	-	-	-
-	-	-	-	-	-	-	3.030	0.558	-	-	-	-	-	-
81	0.479	0.088	-	-	-	-	-	-	-	-	-	-	0.906	0.167
04	1.880	0.346	-	-	-	-	-	-	-	-	-	-	3.552	0.065
-	-	-	0.546	0.100	-	-	-	-	-	-	-	-	-	-
-	-	-	3.004	0.553	-	-	-	-	-	-	-	-	-	-
29	-	-	-	-	-	-	-	-	-	-	-	-	-	-
23	-	-	-	-	-	-	-	-	-	-	-	-	-	-
									2.981	0.549				
-	-	-	-	-	-	-	-	-	3.592	0.661	-	-	-	-
-	-	-	-	-	-	-	-	-	-	-	-	-	1.613	0.297
-	-	-	-	-	-	-	-	-	-	-	-	-	1.689	0.311
02	2.590	0.477	2.169	0.399	2.166	0.399	2.174	0.400	1.889	0.348	-	-	2.855	0.525
-	-	-	-	-	-	-	-	-	-	-	-	-	-	-
-	-	-	-	-	-	-	-	-	-	-	-	-	-	-
13	-	-	-	-	-	-	-	-	-	-	-	-	-	-
-	4.089	0.752	-	-	-	-	-	-	-	-	-	-	-	-
-	-	-	4.069	0.749	-	-	-	-	-	-	-	-	-	-
25	±14.015	3.328	±11.852	2.181	±12.104	2.227	±11.059	2.035	±14.224	2.617			±18.041	3.255
55	-9.850	+0.906	-	-	-	-	-0.094	+0.009	+ 2.713	+0.250	-	-	+1.075	+0.099
33	-0.470	+0.043	-0.683	+0.064	-	-	-	-	-	-	-	-	-	-
03	+0.005	+0.001	-0.032	+0.003	-	-	-1.757	+0.162	-0.019	+0.002	-	-	-0.026	+0.002
14	+0.001	-	-2.730	+0.251	-	-	-0.841	0.077	+6.041	+0.566	-	-	+6.048	+0.556
01	+0.012	+0.001	-0.008	+0.001	-	-	+0.420	+0.039	+0.009	+0.001	-	-	+0.017	+0.002
27	+0.003	-	-0.282	+0.026	-	-	+0.003	-	+0.629	+0.058	-	-	+0.632	+0.058
-	-	-	-	-	-	-	-	-	-	-	-	-	-	-
33	-10.299	+0.951	-3.735	+0.345	-	-	-2.269	+0.287	+9.373	+0.867	-	-	+7.746	+0.717
62	+4.701	+0.433	-	-	-	-	-	-	+15.083	1.388	-	-	+5.123	+0.471
20	-	+4.712	-	+2.526	-	2.227	-	+2.322	-	+4.872	-	-	-	+4.443

B

effect. Bleeding air increases the temperature on a W_f/P_{T2} control schedule while lowering the temperature on a W_f/P_{T3} control schedule. It can be seen that the control modes that use pressure ratios have a rather significant penalty in both sensing error and engine parameter variation errors that effectively eliminates them from consideration.

It is concluded that steady-state turbine inlet temperature is most accurately controlled from a T_{T5} integrating closed-loop control with the sensor accuracies that are to exist in the foreseeable future.

Steady-State Gas Generator Speed Governing (Table IV)

Table IV summarizes the influence of system errors at the intersection of a control droop line and the engine steady-state line. See point "b" in Figure 21. This intersection has been biased to maintain a constant mechanical speed throughout the ideal flight envelope for all control modes applicable. (Note that Mode IX can be used only in temperature limiting.) Table IV enumerates the errors in terms of percent of gas generator topping speed. Since the influence depends significantly on the droop slope, it is essential that an equitable adjustment be made between droops expressed in different units for each mode. The droop slopes used in Table IV were assigned on the basis that each would yield the same change in turbine inlet temperature per percent speed (6.8 percent T_{T4} per 1.0 percent N_G).

The total error potential summary shows the T_{T5} Mode VII and the two pressure ratio Modes VIII and X to have the smallest error band. However, Modes VIII and X show the greatest likelihood of permitting an overspeed to occur, especially while extracting air flow. A W_f/P_{T2} Mode I control has accuracy potential nearly equal to the T_{T5} Mode VI control and, as is shown later, has significant transient advantage. W_f/P_{T3} Mode II is similar to W_f/P_{T2} Mode I but tends to decrease speed more when air is extracted. Mode III has essentially the same accuracy as a W_f/P_{T2} control.

The Z_2 and Z_3 control Modes IV and V are poor governors, having the worst error bands of all modes considered.

The conclusion is that a W_f/P_{T2} control droop line offers the simplest and nearly the most accurate means of maintaining constant mechanical speed topping governor.

Steady-State Shaft Horsepower Limiting (Table V)

Table V summarizes the influence of the various system errors at the intersection of the engine steady-state line and a droop line biased in such a

manner as to hold shaft horsepower over inlet pressure to a constant limited ratio. See point "c" in Figure 21. The table error values are expressed in percentage of shaft horsepower. The droop slope employed is the same as that used in the N_G governing discussion in the preceding section.

Power limiting schedules are extremely dependent on the accuracy of the compressor stator vane schedule, as can be seen for all modes in the first row. The best limiting accuracy is maintained in Mode III, where W_f/P_{T2} N_G is biased as a function of P_{T3}/P_{T2} and N_G. This mode would be outstanding if the inaccuracy in obtaining a measured P_{T3}/P_{T2} ratio was not so large. The mode is virtually immune to bleed air extraction compared with significant power losses for every other control mode. Gas generator compressor and turbine deterioration makes significant inroads on all modes except Z_3. The pressure ratio Modes VIII and X are particularly subject to engine errors.

It must be concluded that none of the modes offer very precise power limit with the steep droop employed for N_G speed governing. Significant changes could be realized with a smaller droop slope at the expense of additional control complexity.

Additional control modes such as P_{T3} limiting would have to be explored if the engine or load required a more precise power limit than the values shown.

Acceleration Turbine Inlet Temperature Limiting Regime (Table VI)

Table VI shows the influence of errors on the system at a point where acceleration is limited by turbine inlet temperature (see point "d" in Figure 21).

The table values have been modified and the units are not in T_{T4} degrees, but in units of percentage of fuel flow error that exists at a given N_G speed between the ideal acceleration and the actual acceleration. Accompanying the ΔW_f is another column labeled Δt that estimates the change in total acceleration time that the error would cause if it persisted in the same amount throughout the acceleration. The Δt penalty has been assessed on the basis that the temperature must never exceed its limit; thus, if an error tends to increase the temperature, the nominal value must be decreased, which is a penalty in acceleration time. The engine parameter variation errors are charged with only that portion of the gross error that is due to the control mode; the unavoidable acceleration time change that would occur with deterioration even if a true T_{T4} temperature were maintained has not been charged as penalty.

Table VI shows the direct temperature sensing schemes, VI and VII, to offer the least penalty in acceleration time. But as shown in a following section, the transient errors are intolerable for such a control mode. The best scheduling control errors are found in the Z_3 and Z_2 modes, which are only slightly better than the conventional W_f/P_{T3} and W_f/P_{T2} modes. A large portion of all scheduling control mode error can be attributed to pressure sensing and metering accuracy, as would be expected. With the exception of the pressure ratio modes, the control and sensor errors are the dominant errors, with only about one-third of the total due to the combined effects of engine deterioration and bleed air extraction.

Acceleration Surge Limiting Regime (Table VII)

Table VII shows the influence that the various system errors have on acceleration limiting in a surge bucket such as that shown at point "e" in Figure 21.

The table values were computed using the same rules explained in the Table VI discussion. Surge lines were assigned to all modes on the basis of having identical T_{T4} vs N_G speed characteristics.

Direct sensing of T_{T4} or T_{T5} and comparing with a reference temperature biased by speed and inlet temperature have the best accuracy potential and would be a clear choice if they were not handicapped by the dynamic inaccuracy illustrated in the following section covering gross transient performance. The scheduling control modes which rank in best error potential are Z_3, W_f/P_{T3} and W_f/P_{T2}. Control- and sensor-originated errors are dominant in acceleration surge limiting, as was noted in the acceleration temperature limiting regime.

Gross Transient Analysis Program

The dynamic response of the engine driving a helicopter rotor is an essential means of comparing different control modes. The transient accuracy and stability for the same flight maneuver demonstrated by the different controls when operating in various control regimes such as power turbine speed governing, torque limiting, or temperature limiting are presented in this section of the report.

A digital computer model of the engine, helicopter rotor, and several control possibilities has been written using MIMIC simulation language. The engine and rotor model contains the equations represented in Figure 4 introduced in the section on engine and load characteristics. Block diagrams containing equations for the following control modes are presented with the discussion of each mode:

1. W_f/P_{T3} scheduling control with electronic trimmer

2. T_{T5} closed-loop control with electronic trimmer

3. T_{T4} closed-loop control with electronic trimmer

For the system operating on power turbine speed governing, torque limiting, or T_{T5} limiting, the transient responses are determined by making a step increase in collective pitch (β_H) from 4 degrees to 8 degrees. This transient is referred to as a beta acceleration transient. For the system operating on gas generator speed governing, transient responses are determined by making a step change in N_G reference from a steady-state condition defined by N_G = 60 percent to a steady-state operating condition defined by N_G = 95 percent. This is equivalent to making a step increase in power level position.

W_f/P_{T3} Control Mode

Figure 22 shows the nonlinear block diagram of the W_f/P_{T3} control. There are seven inputs to the control: the power lever position (N_G PLA), the power turbine speed-setting lever position (N_F REF), the collective pitch position, and four engine parameters. These parameters are gas generator speed (N_G), power turbine speed (N_F), compressor discharge total pressure (P_{T3}), and compressor inlet total temperature (T_{T2}). All transient responses were determined for sea level standard day condition; therefore, T_{T2} was held constant at 59° F. The primary manipulated variable used to control engine output power is the ratio of engine fuel flow to compressor discharge total pressure (W_f/P_{T3}) and is referred to as ratio units. The link between the electronic and hydromechanical portions of the control is provided by the torque motor servo, which is represented in Figure 22 by a simple lag with time constant τ_D.

The position of the main fuel flow metering valve is established by multiplying two variables representing W_f/P_{T3} and P_{T3}. Fuel flow is made proportional to metering valve stroke by making the area proportional to the metering valve stroke and by maintaining a constant pressure drop across the metering valve area. This differential pressure is maintained constant by the pressure-regulating valve, which is represented by a simple lag with time constant τ_{PR}.

The gas generator speed signal to the control is biased by T_{T2} and is represented by the three-dimensional function N_GS'. Whenever this value exceeds the value set by the power lever position, the control will limit ratio units inversely proportional to gas generator speed through a droop-type governor

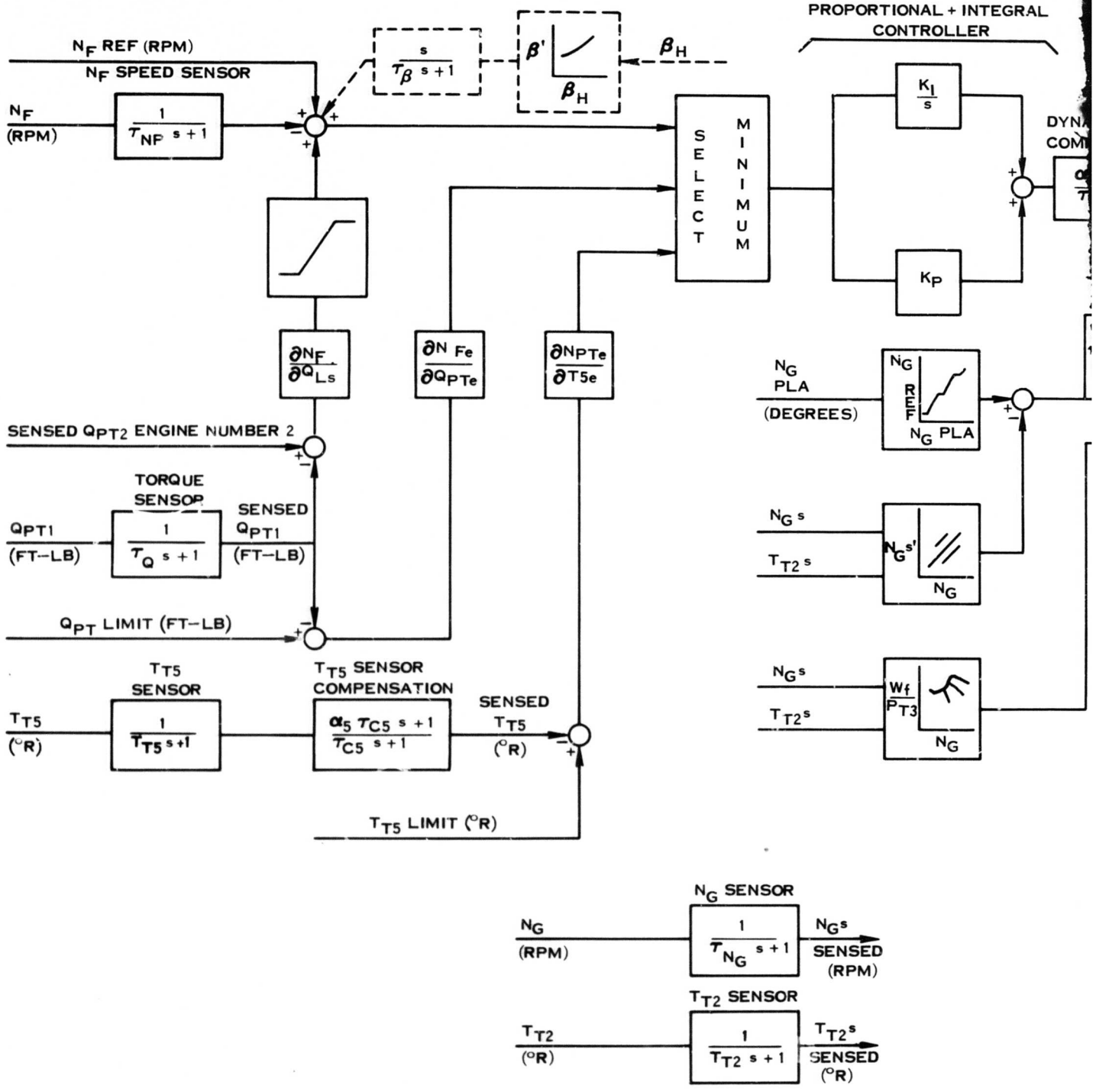

Figure 22. Nonlinear Block Diagram of W_f/P_{T3} Control for Base Engine.

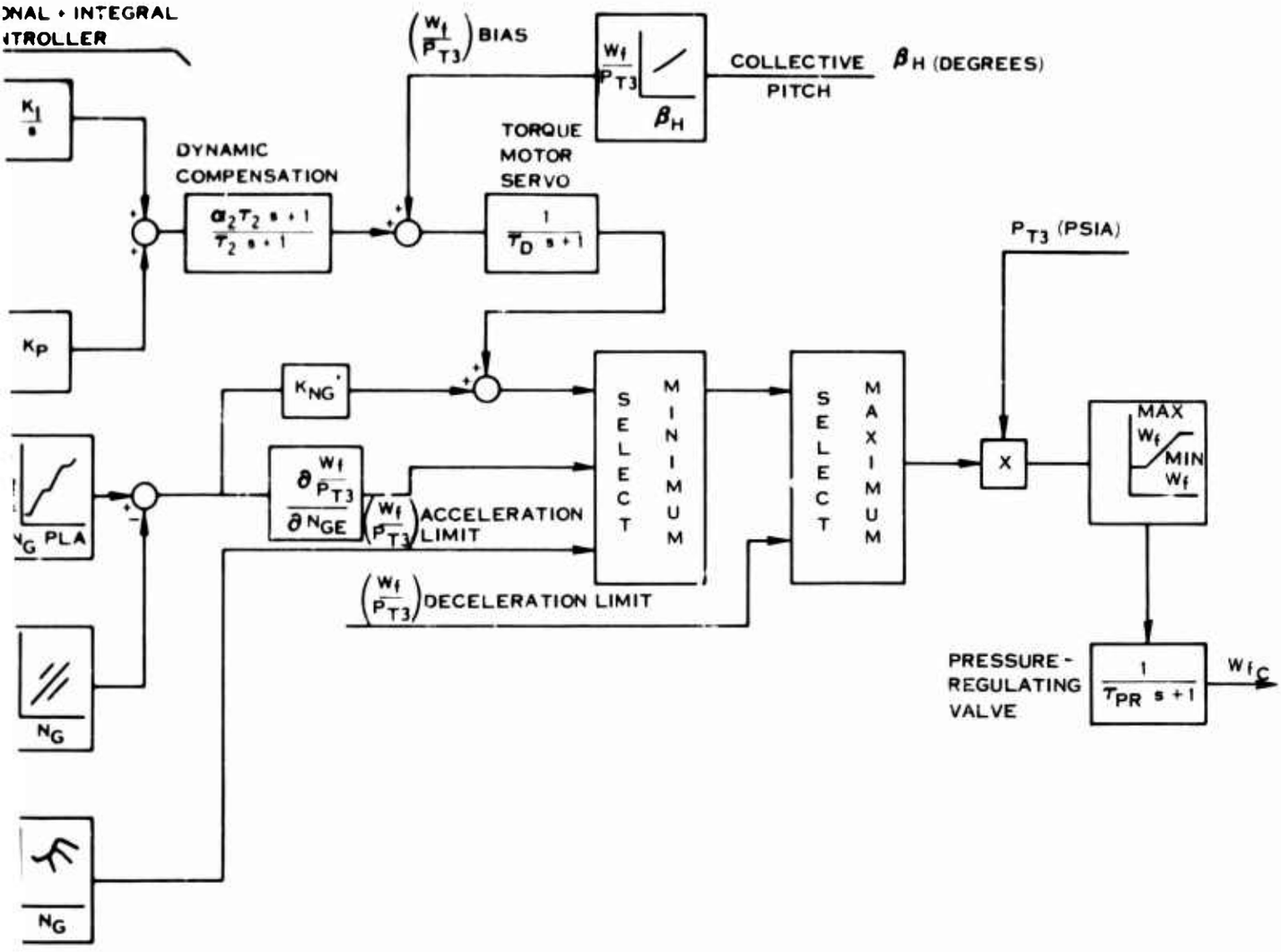
ONAL + INTEGRAL
NTROLLER
$\left(\frac{W_f}{P_{T3}}\right)$ BIAS
$\frac{W_f}{P_{T3}}$
β_H
COLLECTIVE PITCH
β_H (DEGREES)
$\frac{K_I}{s}$
DYNAMIC COMPENSATION
$\frac{\alpha_2 T_2 s + 1}{T_2 s + 1}$
TORQUE MOTOR SERVO
$\frac{1}{T_D s + 1}$
P_{T3} (PSIA)
K_P
K_{NG}
SELECT MINIMUM
SELECT MAXIMUM
X
MAX W_f
MIN W_f
$\frac{\partial \frac{W_f}{P_{T3}}}{\partial N_{GE}}$
$\left(\frac{W_f}{P_{T3}}\right)$ ACCELERATION LIMIT
$\left(\frac{W_f}{P_{T3}}\right)$ DECELERATION LIMIT
N_G PLA
N_G
N_G
PRESSURE-REGULATING VALVE
$\frac{1}{T_{PR} s + 1}$
W_{f_C}

B

represented by the gain ($\partial W_f/P_{T3}/\partial N_{GE}$). In other controlling regimes, the control provides negative N_G feedback through the gain K_{NG}.

To protect the engine from compressor surge and turbine overtemperature during accelerations, the control provides a schedule of maximum W_f/P_{T3}. This schedule is biased by T_{T2} and is represented by the three-dimensional function (W_f/P_{T3}) acceleration limit. Since there is no closed-loop control over this value, the W_f/P_{T3} control is referred to as an open-loop or scheduling type control.

Protection against engine flameout during deceleration is provided by a minimum Wf/P_{T_3} limit which is held constant at 0.560 pph/psia. Absolute maximum and minimum fuel flow limits are also provided and represent maximum and minimum stops for the metering valve.

The desired power turbine speed (N_F) is established by the power turbine speed-setting lever position and is represented in Figure 22 by N_F REF. Actual power turbine speed is fed back to the control through the power turbine speed sensor, represented by a simple lag with time constant τ_{N_F}. As shown in Figure 22, the control provides a W_f/P_{T3} bias signal which is scheduled as a function of β_H. Since the power required of the power turbine is determined by the collective pitch position (β_H), this signal anticipates changes in power demand and enables the engine to accelerate or decelerate more rapidly than would be possible if the control had to depend only on the N_F error signal. This significantly reduces transient power turbine speed errors. An alternative to this scheme was also investigated. This scheme, represented by the dotted portion of Figure 22, adds to N_F reference a signal proportional to the derivative of β_H. For the reasons given below, this scheme was judged unacceptable and the scheduling scheme was chosen in preference to the beta derivative scheme. When operating in the power turbine governing regime as determined by the minimum selector on the left of Figure 22, the control will maintain power turbine speed equal to the reference speed through the proportional-plus-integral controller. This same controller is used in the torque-limiting and T_{T5}-limiting regimes. Torque-limiting operation occurs when power turbine shaft torque exceeds the torque limit. This torque limit is provided to protect the engine from mechanical damage due to excessive torque. T_{T5}-limiting operation occurs when power turbine discharge temperature exceeds the T_{T5} limit. This limit provides further protection against turbine overtemperature. The W_f/P_{T3} control also provides for torque-sharing control for twin-engine applications; however, this feature was not investigated in the gross transient analysis.

N_F Governing With W_f/P_{T3} Control

In order to make the system operate on N_F governing, the torque limit and the T_{T5} limit were made arbitrarily high to ensure that the minimum selector always selected the N_F governing path. For this reason, beta acceleration transients for both the β_H schedule and β_H derivative schemes are almost identical. In actual practice, however, the torque limit and the T_{T5} limit would have finite, realistic values. In this instance, the beta acceleration transient response for the beta derivative scheme would be slower and would have a larger underspeed error. The reason for this is that the large β_H signal which results from a step change in β_H would cause the minimum selector to select either the torque limiting path or the T_{T5} limiting path. In either case, the full benefit of the β_H signal is lost, and a longer time is required to accelerate the engine. Figure 23 shows beta acceleration transient responses of % N_G, % N_F, P_{T3}, metered fuel flow, T_{T4} and shaft torque as a function of time. As shown on the % N_F trace, during the first 1.1 second of the transient, the system is operating open-loop on the W_f/P_{T3} acceleration limit. The high-frequency oscillations evident in this time interval are due to the lightly damped rotor resonance and in no way do these oscillations reflect closed-loop instability. For time > 1.1 second, the system is operating closed-loop on N_F governing. As is evident from the transient responses, the system has good closed-loop stability.

Torque Limiting With W_f/P_{T3} Control

To demonstrate the torque-limiting capabilities of the control, the torque limit was set at 2500 ft-lb. This value was adequate to ensure that, for a beta acceleration transient, the system would end up controlling to the torque limit. Figure 24 shows beta acceleration transient responses for both the beta schedule and beta derivative schemes. As is evident from the traces of Figure 24, the β_H derivative scheme has a much slower response than the β_H schedule system. Referring to the block diagram of Figure 22, it is seen that for the beta derivative scheme, a step increase in β_H causes a large N_F error signal to appear at the input to the minimum selector. This causes the minimum selector to select either the torque-limiting or the T_{T5}-limiting paths. In this instance, the torque-limiting path is selected. By switching to the torque-limiting path, the whole purpose behind the β_H reset mechanism is thereby defeated. The large β_H signal does not become integrated and at no time does the system reach the acceleration limit. The β_H schedule scheme circumvents this problem by adding a W_f/P_{T3} bias signal as a function of β_H downstream of the minimum selector and integrator, thereby enabling the system to reach the acceleration limit. For the first 0.5 second of the transient, the W_f/P_{T3} control with the β_H schedule is operating open-loop on the acceleration limit. For t > 0.5 second, the

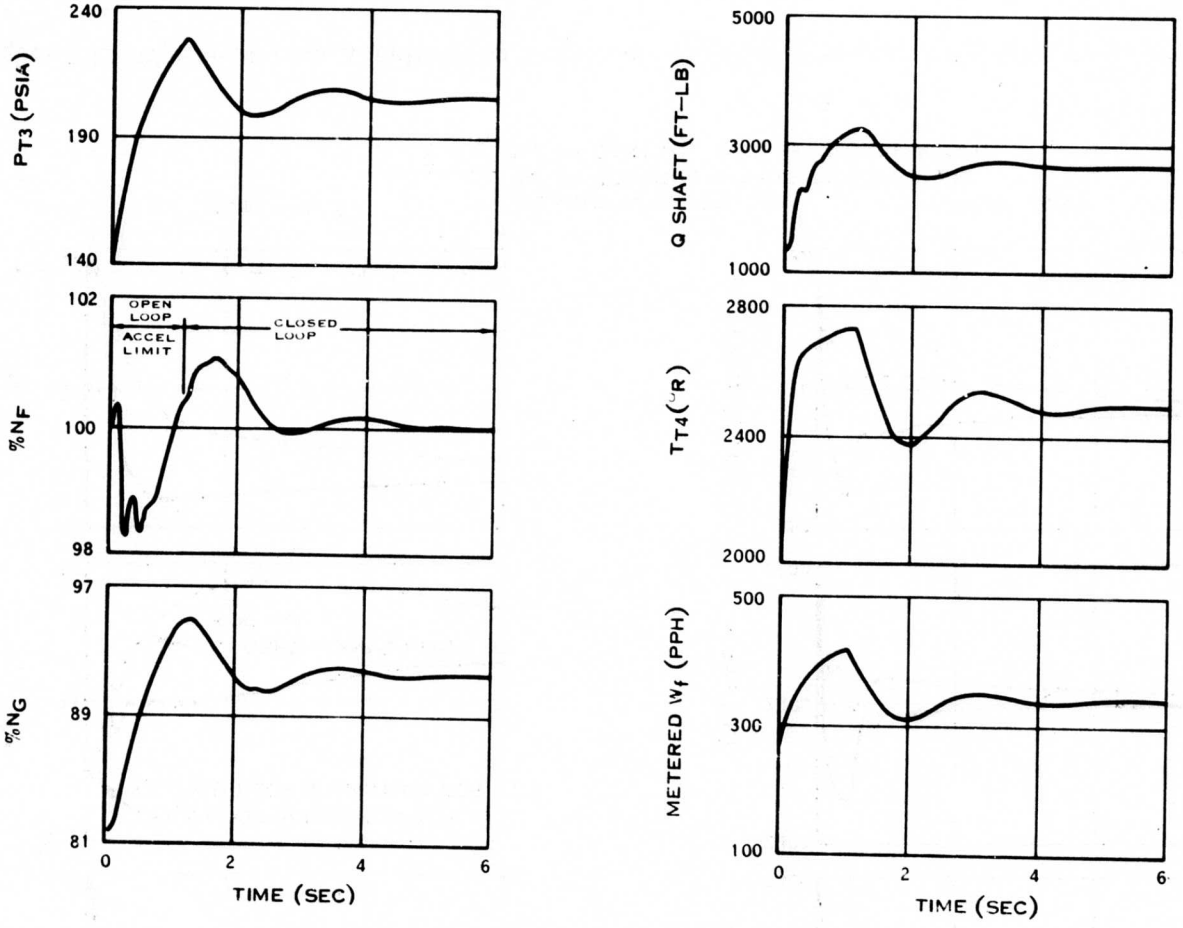

Figure 23. W_f/P_{T3} Gross Acceleration Transient - N_F Governing - β_H Step From 4° to 8°.

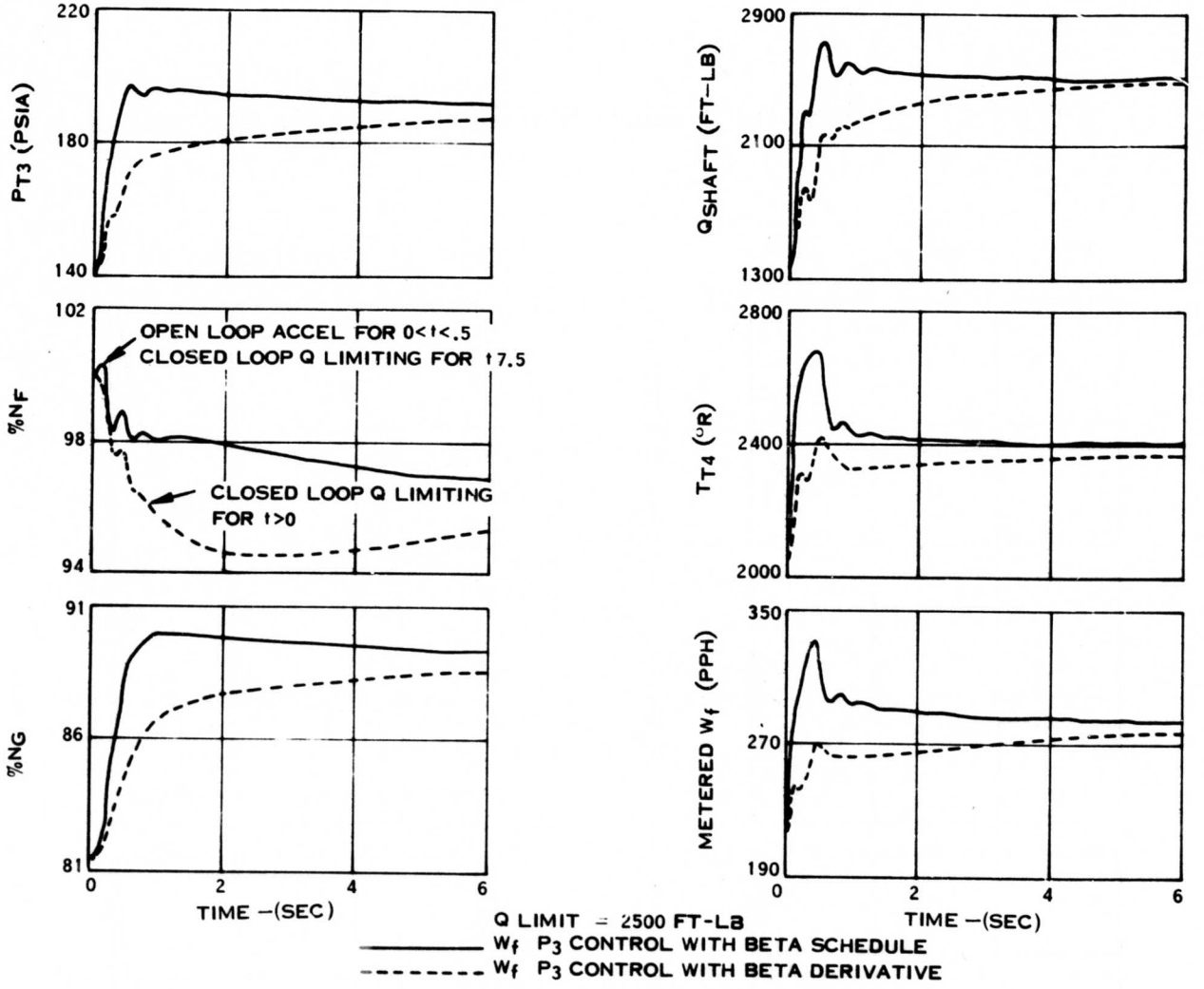

Figure 24. W_f/P_{T3} Gross Acceleration Transient - Torque Limiting - β_H Step From 4° to 8°.

system is operating closed-loop on torque limiting. The traces of Figure 24 exhibit acceptable closed-loop stability.

T_{T5} Limiting With W_f/P_{T3} Control

In order to demonstrate the temperature-limiting capabilities of the control, the T_{T5} limit was set at 1900°R and the torque limit was set arbitrarily high to ensure that the minimum selector would not select the torque-limiting path. Figure 25 shows beta acceleration transient responses for both the beta schedule and beta derivative schemes. For the beta derivative scheme, the responses are significantly slower and the N_F underspeed is larger than for the beta schedule scheme. As in the torque-limiting regime, the minimum selector prevents the large beta derivative signal from being selected, thereby preventing a rapid acceleration. At no time during the entire transient is the acceleration limit reached. For the beta schedule scheme, however, the system is operating open-loop on the W_f/P_{T3} acceleration limit for approximately the first 0.2 second of the transient. This result is a considerably more rapid acceleration.

To summarize, both schemes exhibit acceptable closed-loop stability. For large beta acceleration transients, however, the beta derivative scheme is judged unacceptable because the logic of the control prevents the collective pitch input from influencing control action. This problem does not occur with the scheduling scheme. The W_f/P_{T3} bias signal immediately begins to influence control action.

As a result, the scheduling scheme responds faster and also has better transient accuracy than the beta derivative scheme.

T_{T5} Control Mode

Figure 26 shows the nonlinear block diagram used in the MIMIC simulation of the T_{T5} control. For the T_{T5} control, fuel flow is established by the product of W_f/P_{T2} and P_{T2} where P_{T2} is compressor inlet total pressure. Since all transients were run at standard day sea level conditions, T_{T2} and P_{T2} were maintained constant at 59°F and 14.7 psia, respectively. By comparing the block diagrams for the W_f/P_{T3} control and the T_{T5} control as shown in Figures 22 and 26, respectively, the following observations are made. During power turbine speed governing, and torque limiting, the W_f/P_{T3} control has negative N_G feedback, whereas the T_{T5} control does not. To protect the engine from compressor surge and turbine overtemperature during gross accelerations, the T_{T5} control provides closed-loop control of turbine inlet temperature by scheduling T_{T5} acceleration limit as a reference biased with T_{T2}. Sensed T_{T5} is compared to this reference value and the

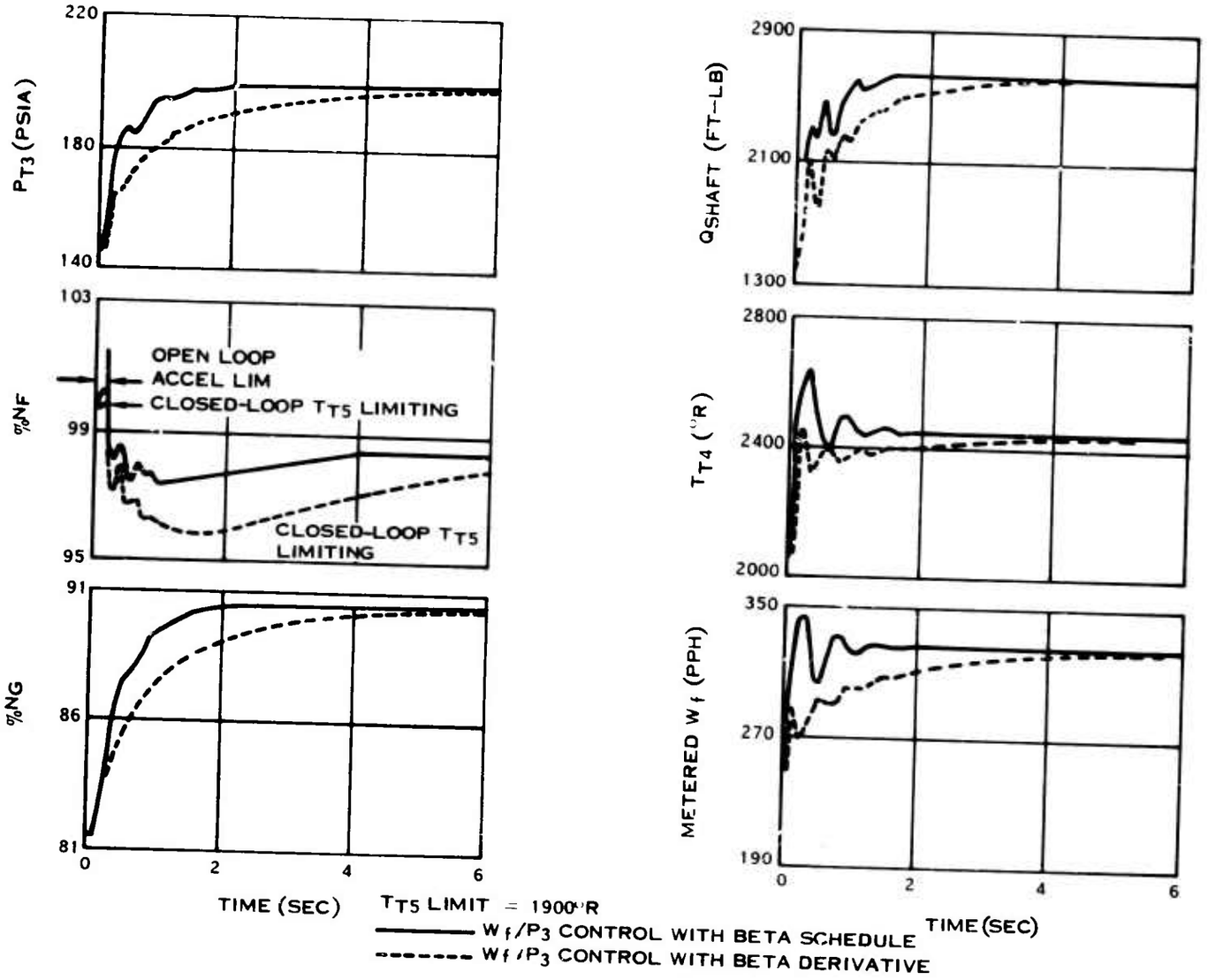

Figure 25. W_f/P_{T3} Gross Acceleration Transient - T_{T5} Limiting - β_H Step From 4° to 8°.

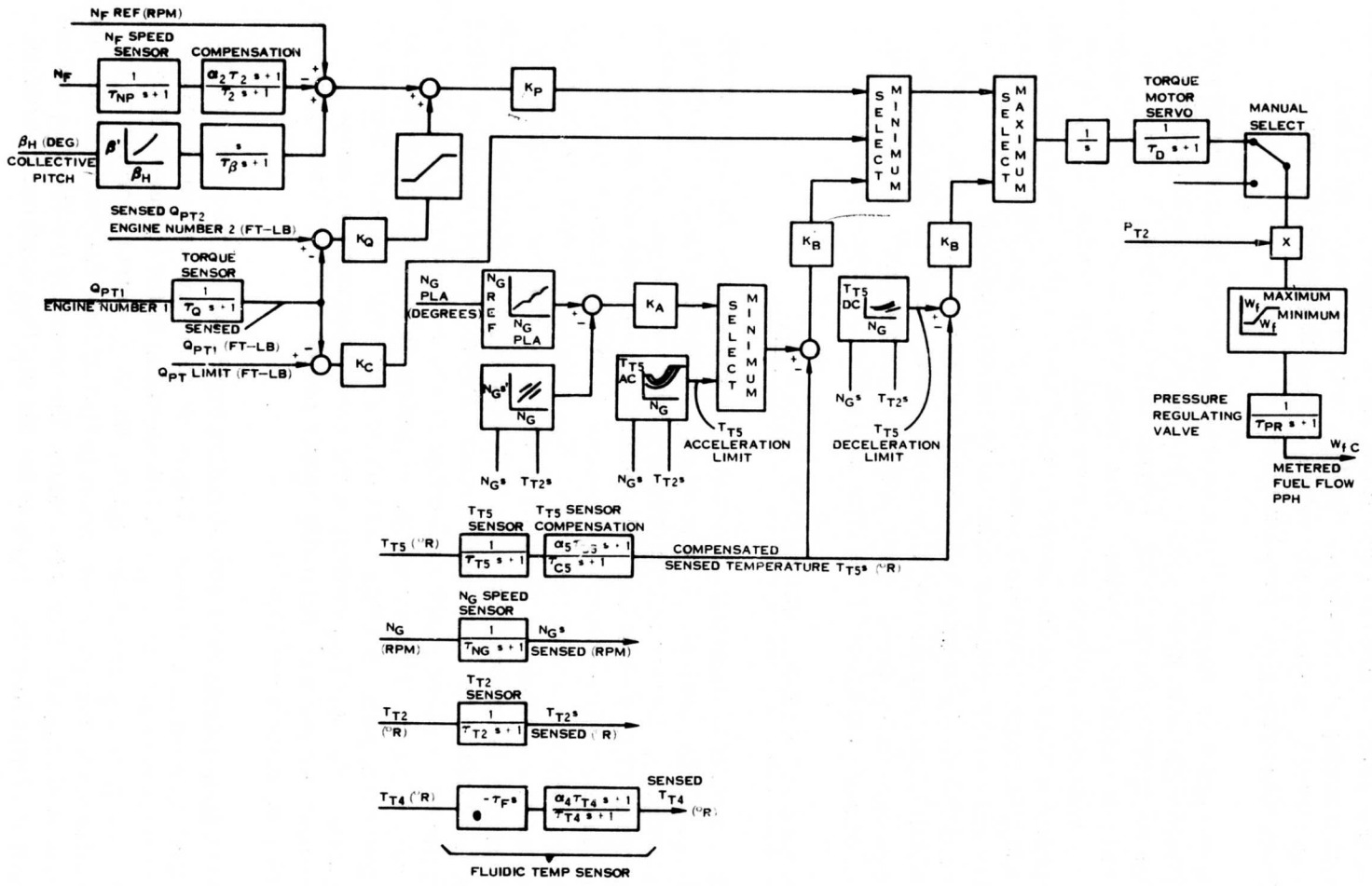

Figure 26. Nonlinear Block Diagram of T_{T5} Control for Base Engine.

integral of this error is used to control the engine. Because of this feedback control action during accelerations, the T_{T5} control is referred to as a closed-loop control. A similar procedure is used to protect the engine against flameout during gross decelerations.

As shown in Figure 26, the lead/lag compensation in the N_F governing loop is placed before the beta reset signal. An alternative to this arrangement was examined in which the lead/lag compensation was placed between the gain K_P and the minimum selector. This latter scheme was rejected because of large N_F underspeed errors on N_F governing. The reason for the large N_F underspeed errors with the second arrangement is that, for a step change in beta, the beta reset signal when passed through the lead/lag compensation causes the input to the minimum selector to become negative for an interval of time even though N_F sensed speed is below the reference. The negative portion of this signal causes fuel flow to decrease, which in turn causes a further decrease in N_F speed. This problem will not occur so long as the beta reset signal is not part of the input to the lead/lag compensator.

N_F Governing and Torque Limiting With T_{T5} Control

Figure 27 shows beta acceleration transient responses for the T_{T5} control in the N_F governing regime. To ensure that the system operates in the N_F governing regime, the torque limit was set arbitrarily high. By comparing Figures 23 and 27, it is seen that both controls exhibit good closed-loop stability, but the W_f/P_{T3} control is superior to the T_{T5} control in that it has a faster response and yields a lower N_F underspeed error for the same beta acceleration transient. The reason for this is that, at the instant the beta step change is applied, the large beta reset signal causes the minimum selector to switch to the acceleration limit. However, because of the short time constant of the beta reset mechanism (τ_β), the beta reset signal decays to zero very rapidly. This causes the minimum selector to switch back to the N_F governing path. All this takes place within the first 0.06 second of the transient. The W_f/P_{T3} control, on the other hand, remains on the acceleration limit for a considerably longer period of time. This causes the engine to accelerate more rapidly.

In order to demonstrate the torque-limiting capabilities of the control, the torque limit was set at 2500 ft-lb. Figure 28 shows the beta acceleration transient responses for the T_{T5} control operating in the torque-limiting regime. As in the N_F governing regime, the T_{T5} control operates on the acceleration limit only for a very short period of time due to the rapid decay of the beta reset signal. For this reason, the response for the T_{T5} control is somewhat slower than the response for the W_f/P_{T3} control as shown in Figure 24. Closed-loop stability, however, is acceptable.

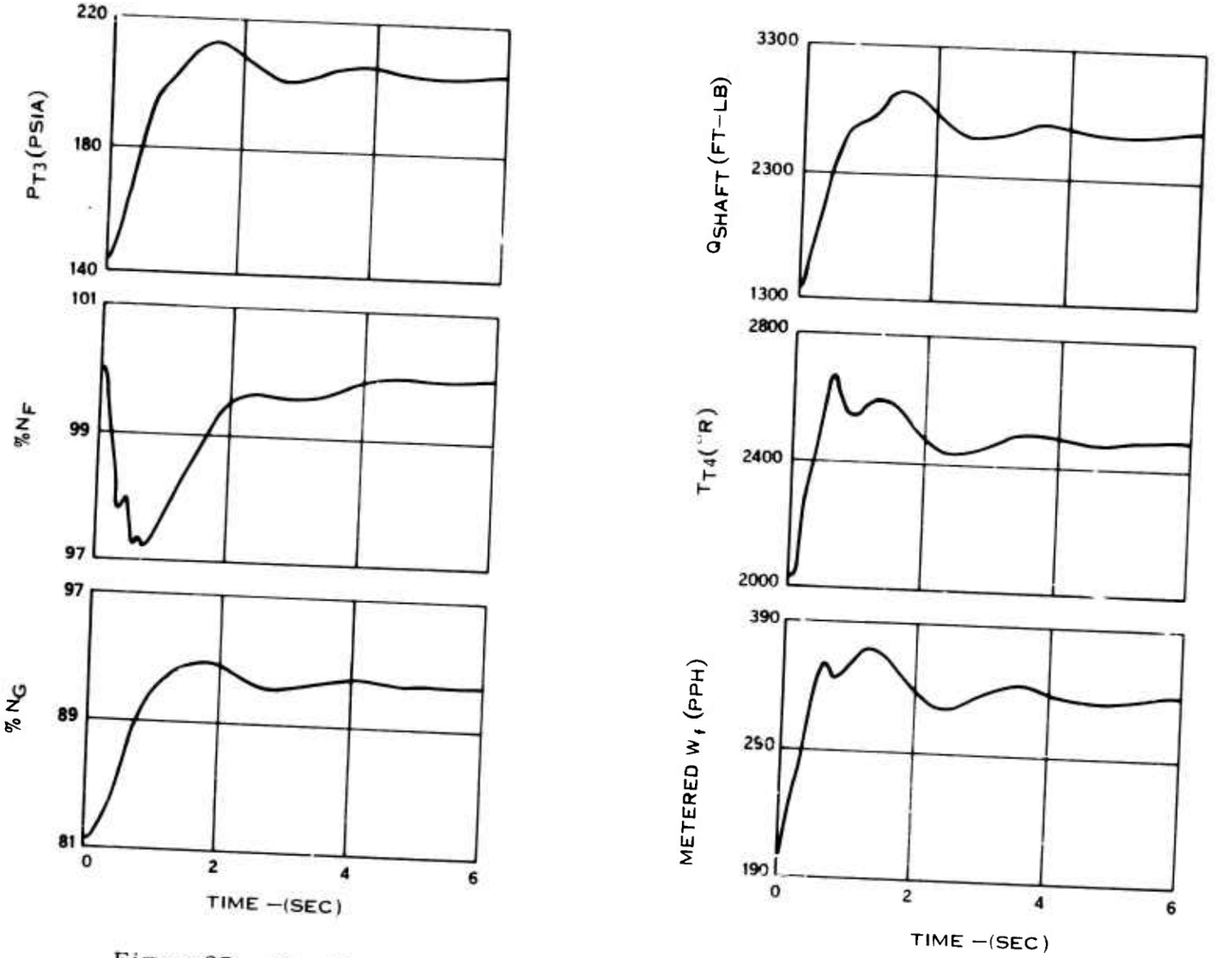

Figure 27. T_{T5} Gross Acceleration Transient - N_F Governing - β_H Step From 4° to 8°.

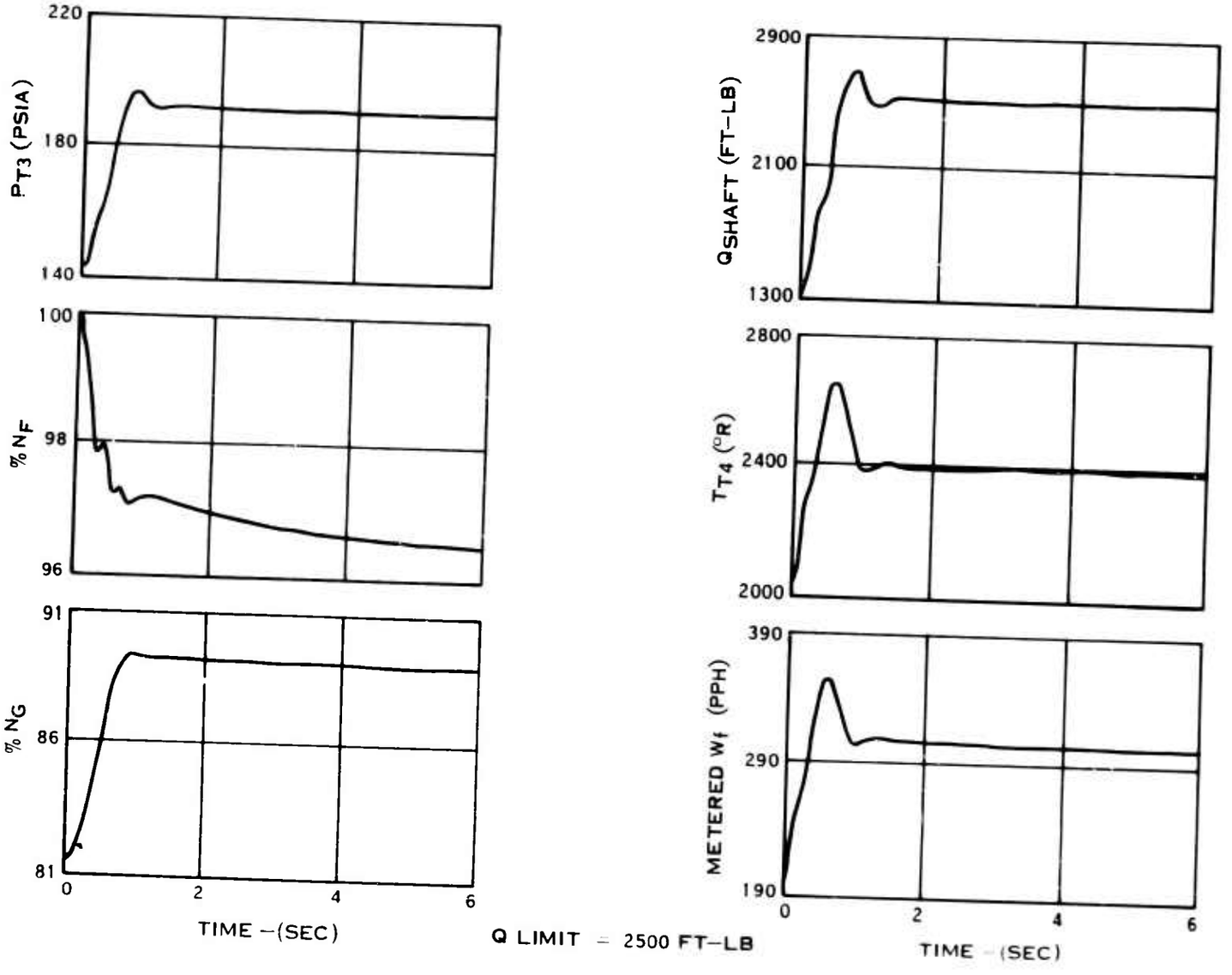

Figure 28. T_{T5} Gross Acceleration Transient - Torque Limiting - β_H Step From 4° to 8°

N_G Governing - T_{T4} Acceleration Control

To demonstrate the N_G governing capabilities of the W_f/P_{T3} and the T_{T5} controls, gross acceleration transients were made by making a step change in N_G reference from a steady-state operating condition defined by N_G = 60% to a steady-state operating condition defined by N_G = 95%. This disturbance will be referred to as a 60-95 N_G REF step input. These transients were also made to compare the W_f/P_{T3}, T_{T5} and the T_{T4} controls in their ability to keep turbine inlet temperature (T_{T4}) from exceeding its acceleration limiting value in both the surge and constant T_{T4} regions. For reasons given below, a closed-loop temperature acceleration control represented by the T_{T5} and the T_{T4} control modes is rejected in favor of a scheduled acceleration limiting control exemplified by the W_f/P_{T3} control.

The T_{T5} and T_{T4} controls were rejected in favor of the W_f/P_{T3} control because for a 60-95 N_G REF step, the closed-loop controls yielded turbine inlet temperature as high as 650°F above the surge limit. The closed-loop controls do not accurately control turbine inlet temperature to the acceleration limit because: the various control and engine time lags (such as sensors, servos and burner delays) severely limit the amount of loop gain that can be put into the system and still have stable operation; and a closed-loop control which is accurate during a transient would have to have a high loop gain. To demonstrate this, an ideal system was simulated. The ideal system consists of the T_{T5} control whose only dynamic element is the integrator, and the base engine having only the engine time constant. For the ideal system the velocity constant of the open-loop transfer function from T_{T5} error to T_{T5} can, theoretically, be made as high as necessary to achieve a very accurate system, since there are no secondary lags to create a stability problem. Curve 1 of Figure 29 shows T_{T4} vs percent N_G for the ideal system for K_B = 25 RU/sec °F and for a 60-95 N_G REF step. For K_B = 25 RU/sec °F, the velocity constant is approximately 1000 radians per second at the low power condition. Because of the very large loop gain, curve 1 of Figure 29 coincides with the ideal T_{T4} acceleration schedule.

Curve 2 of Figure 29 shows T_{T4} vs % N_G for the ideal system having a 0.01 sec burner dead time. For this case, it is necessary to reduce K_B to 0.6 RU/sec °F in order to maintain good system stability. Even with this slight departure from the ideal, it is seen that the performance of the system is beginning to deteriorate. Curve 3 of Figure 29 shows the transient response for the ideal system but with a 0.035 sec burner dead time. This is the value of burner delay time that has been assumed throughout this study. For this case, K_B must be decreased to 0.2 RU/sec °F in order to

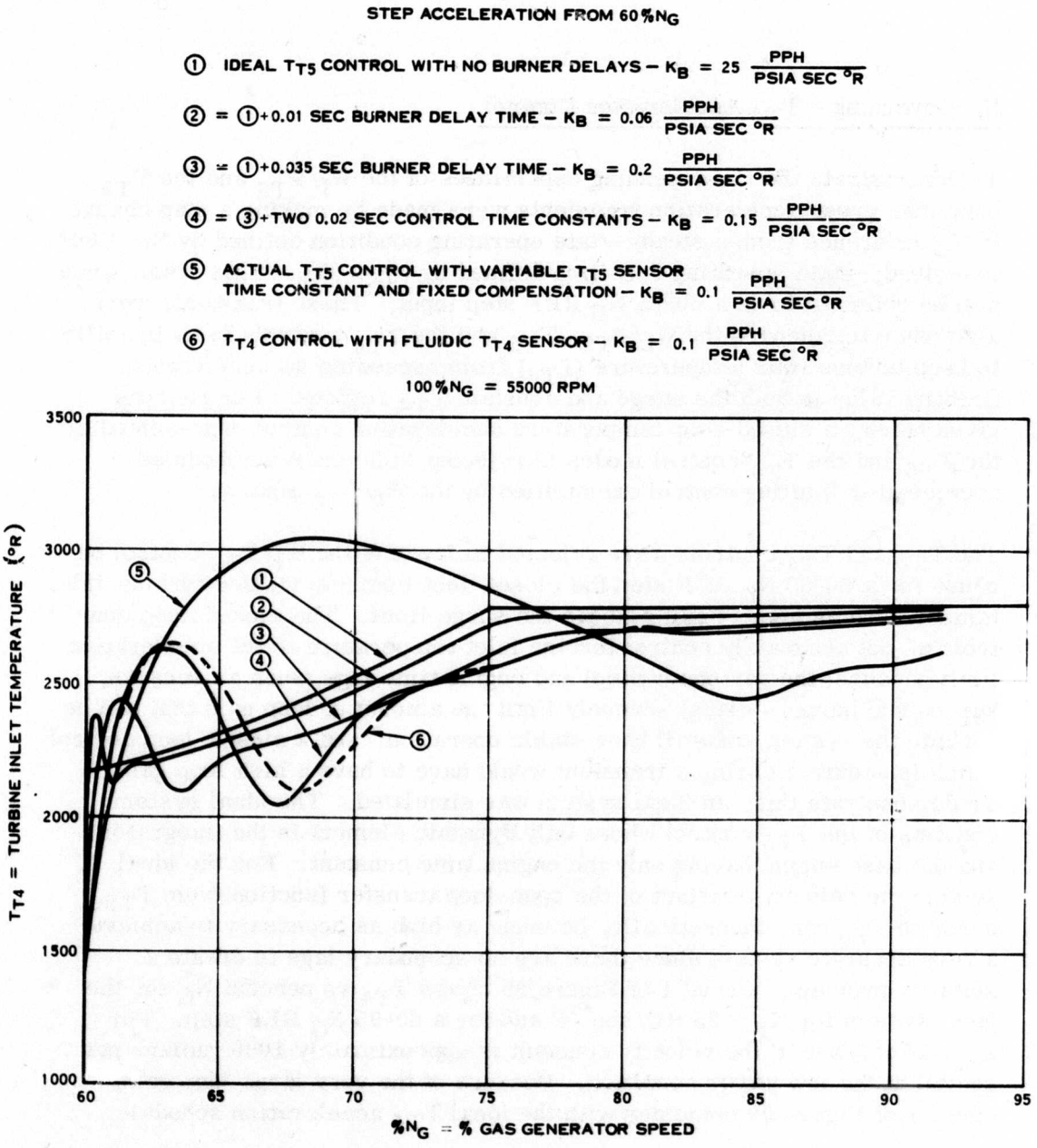

Figure 29. Deterioration of Closed-Loop Temperature Acceleration Control With Inherent System Secondary Time Constants.

maintain essentially the same stability margin. Curve 3 represents the best performance that can be achieved with a real engine and an ideal T_{T5} control which is a control with a perfect T_{T5} sensor and no dynamics other than the integrator. To show the effect of a departure from the ideal control, two 0.02-second simple lags were inserted into the loop. In particular, the torque motor servo and the pressure regulating valve were each given 0.02 second time constants. For this case, curve 4 of Figure 29 shows the results of a 60-95 N_G REF step input. To maintain good stability, the value of K_B had to be reduced to 0.15 RU/sec °F. Referring to curve 4, there is approximately a 400°F peak transient T_{T4} overtemperature error and a 350°F peak transient T_{T4} undertemperature error. Curve 5 of Figure 29 gives the response for a realistic T_{T5} control; the block diagram is given in Figure 26. To make the system more realistic, the T_{T5} sensor time constant was made to vary with N_G speed to reflect the variations in the temperature sensor time constant that would be expected due to changes in airflow rate. The T_{T5} sensor compensation, however, remains fixed. Referring to curve 5, it is seen that the T_{T5} control will have a T_{T4} maximum overtemperature error of approximately 650°F, which is completely unacceptable.

A 60-95 N_G REF step transient was also determined for the T_{T4} control. The block diagram of the T_{T4} control is completely analogous to the T_{T5} control, as shown in Figure 26. The only exception is in the temperature sensor. The T_{T4} sensor in the T_{T4} control is of the fluidic type and is represented by an ideal time delay and a lead/lag network as shown in Figure 26. The delay time represents the transport delay from the hot air to the resonant cavity of the fluidic sensor, and the lead/lag represents thermal loss to the sensor walls.

Curve 6 of Figure 29 shows the result of a 60-95 N_G REF step transient for this control. As can be seen by comparing curves 4 and 6, there is no significant difference between the results of the T_{T5} control with an ideal T_{T5} sensor and the T_{T4} control with the fluidic type sensor. Both control modes give very poor T_{T4} temperature control during gross accelerations.

The 60-95 N_G REF step transient was also determined for the W_f/P_{T3} control mode. Figure 30 depicts a comparison of the scheduled (W_f/P_{T3}) and the closed-loop (T_{T5} and T_{T4}) controls and their ability to control turbine inlet temperature during accelerations. Also shown in Figure 30 is the ideal T_{T4} schedule. Referring to Figure 30, it is seen that the W_f/P_{T3} has a T_{T4} undertemperature error of approximately 300°F. As a function of time, Figure 31 shows % N_G, T_{T4}, P_{T3} and metered fuel flow as a result of a 60-95 N_G REF step for both the W_f/P_{T3} and the T_{T5} controls.

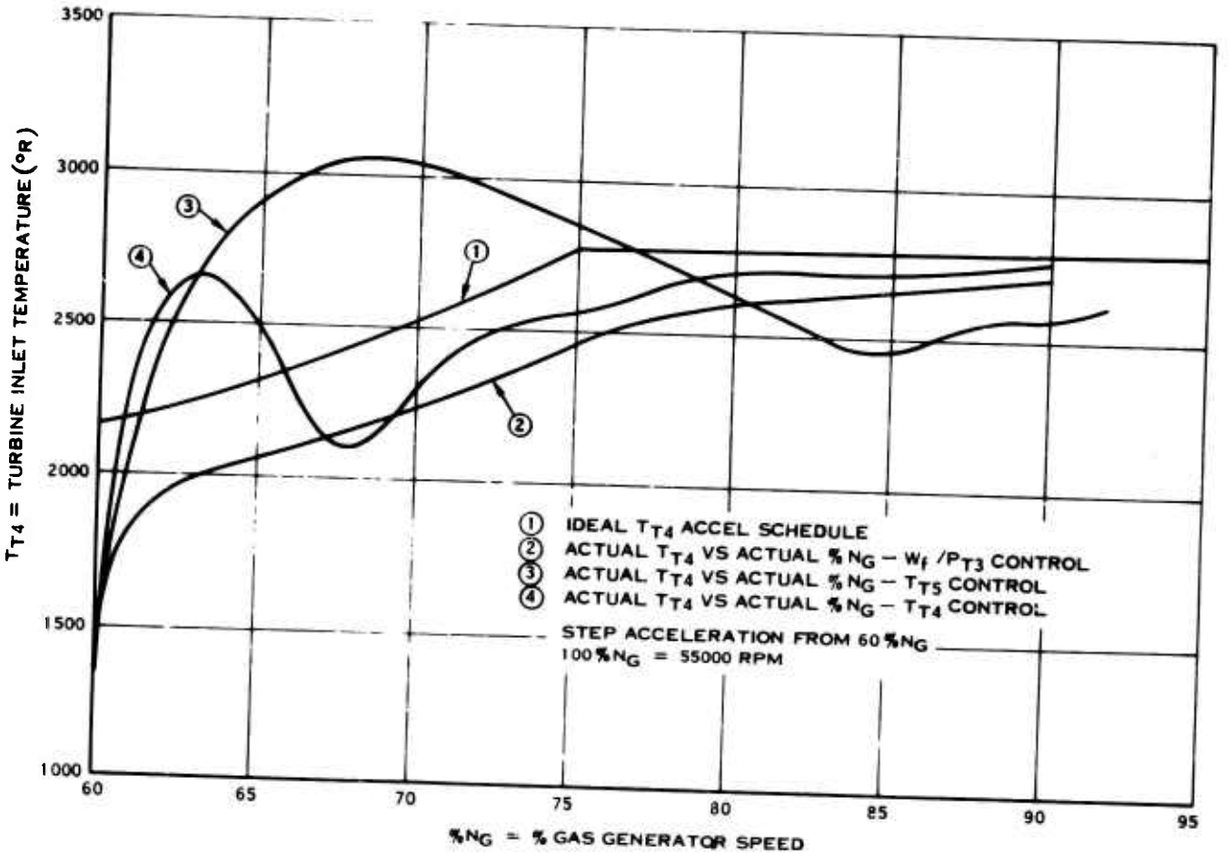

Figure 30. Comparison of Scheduling vs Closed-Loop Acceleration Limiting Controls.

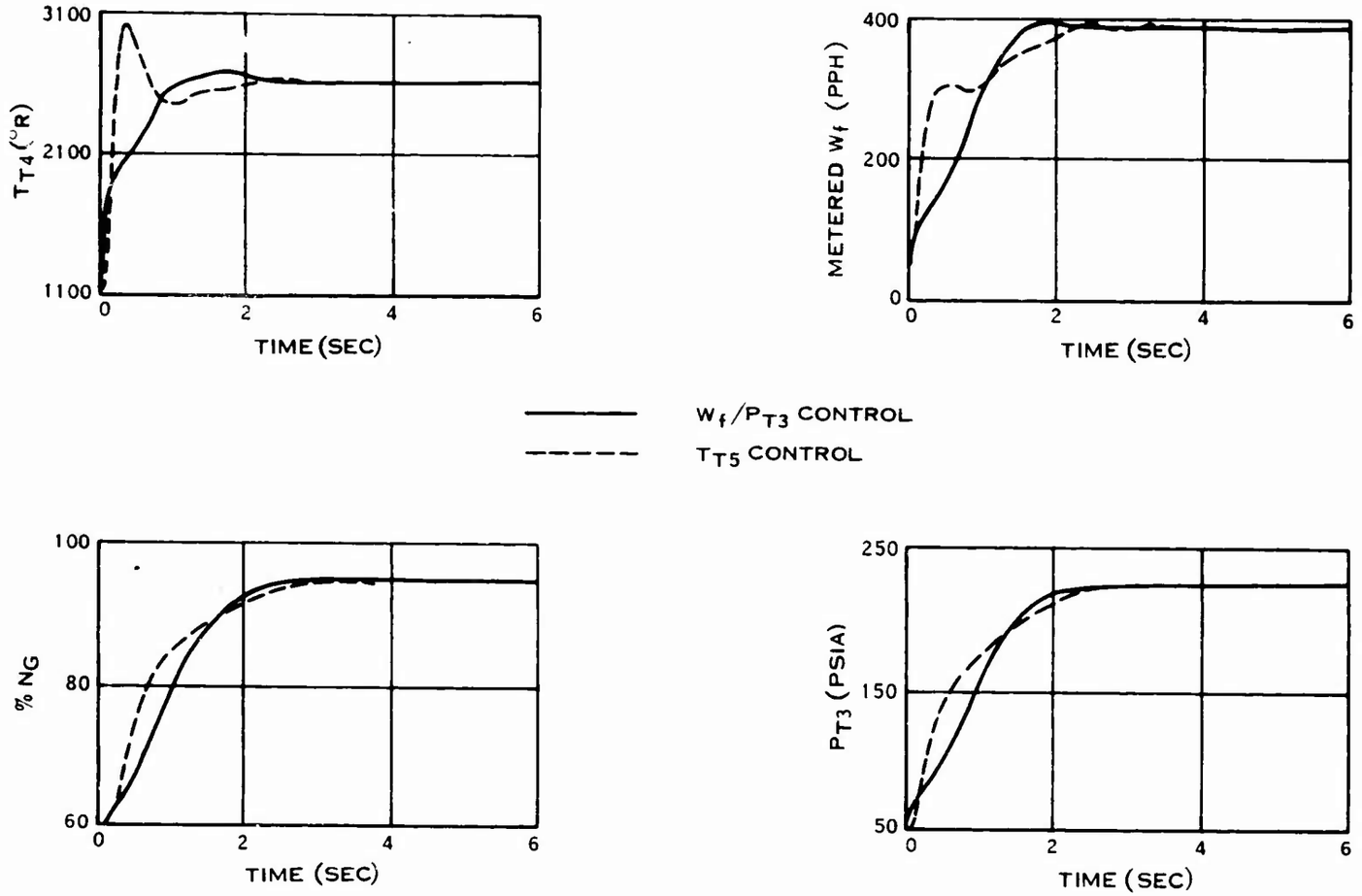

Figure 31. Comparison of Gross Acceleration Transients Between W_f/P_{T3} and T_{T5} Controls in N_G Governing Regime - 60-95% Step Increase in N_G REF.

Figure 29 makes evident the fact that the closed-loop temperature control permits excessive overshoots during an acceleration. In order to maintain T_{T4} below the surge limit, it would be necessary to bias the limiting value downward; however, any method considered results in longer acceleration times and increased power turbine underspeeds. Reduction of the temperature limit by the amount of the worst conceivable overshoot would result in a reduction of the temperature limit at all values of N_G resulting in a situation where high power steady-state operating conditions may be affected. It has been determined from the MIMIC computer simulation that a reduction of the T_{T4} limit by 100°F results in a 48% increase in acceleration time. The T_{T4} limit reduction for the overshoot shown in Figure 29 would be approximately 400°F. Other approaches considered include a transient reduction in the T_{T4} limit whereby the T_{T4} limit would be reset downward as a function of some transient signal such as rate of change of N_G or Q_{PT} and secondly lead overcompensation of the temperature sensor (i.e., the lead compensation is greater than the lag time constant) under all operating conditions. It is questionable whether either of the above approaches could be accomplished with the required accuracy and/or simplicity consistent with the goals established for this program.

Other Control Mode Considerations

Consideration has been given to other aspects of the control mode logic in addition to the above studies. Some of these are discussed below:

1. Multiple Control Integrators or Not?

The accuracy required in power turbine speed governing as well as in turbine inlet temperature limiting dictates that the control be integral in nature. Should there be a separate integral device in each regime? Do other operating regimes which are normally proportional benefit by using the integrator as long as it is a necessary control component? To answer these, frequency response studies were conducted on each regime control loop to determine the allowable gains, crossover frequency and compensation necessities. From these it was determined that a single-valued, integral-plus-proportional component could become common to each regime, except gas generator speed governing and acceleration/deceleration limiting. This is highly desirable, for it means that transferring operation from one regime to another would have to take place at the integrator input and will keep the integrator actively employed. The alternative of inserting an integrator in both the power turbine speed-governing and the temperature-limiting loops would require regime transfer at the integrator output, creating a situation where one integrator is unemployed and must saturate in the

maximum fuel flow direction. Important design advantages can be realized if a single integrator is selected.

2. Load Sharing

Load sharing on a multiengine installation must become a part of the control logic when each engine control has an individual isochronous governor. The best parameter to measure and the logic the control employs is a subject nearly equal in scope to that of this entire study. Shaft torque was arbitrarily chosen as the load share signal simply to provide an example on which to base the design.

The torque share control logic selected depends on the nature of the power turbine speed reference, speed sensor, and integrator. If individual, analog-type power turbine speed sensors and integrators are used for each control, the load share control must bias the speed error in steady-state as well as transient conditions. Where a common digital speed reference and speed sensor is designed to provide a common error signal to each engine control integrator, the load share control need only make up transient mismatch. It was determined that this could best be accomplished by pulling the low engine up while setting the high engine down to permit net power to remain constant. The makeup could be accomplished either in a proportional manner or with an on-off deadband type of control. Saturation limits must be provided for relief in case of engine or sensor failure.

3. Overspeed Protection

In a single-spool gas generator, N_G overspeed protection is provided by the N_G governor max PLA droop line in normal operation, with a topping function designed into the acceleration schedule for a backup.

A dual-rotor gas generator can be protected by this basic mode, given favorable dynamic matching of engine components. However, if the match permits the low-pressure spool to overspeed without overspeeding the high spool, additional protection must be given to the low rotor. Such protection would be in the form of a low rotor speed limit whose error would be applied to the minimum selector ahead of the integral-plus-proportional component in the hybrid control.

Power turbine overspeed protection is provided with the fluidic governor described in the design description of the control.

4. Surge Protection

Some control modes schedule or reference surge protection with parameters that tend to pull an engine out of surge, if it occurs, while other control modes tend to perpetuate the surge by increasing fuel flow. Table VIII shows the type of action taken by the control mode candidate of this study.

TABLE VIII. SURGE RECOVERY CHARACTERISTICS

Mode	Surge Limit	Resists Surge	Perpetuates Surge
I	$W_f/P_{T2} = f(N_G, T_{T2})$	-	x
II	$W_f/P_{T3} = f(N_G, T_{T2})$	x	-
III	$W_f/P_{T2}\ N = f(N_G, P_{T3}/P_{T2})$	x	-
IV	$Z_2 = f(N_G, T_{T2})$	-	x
V	$Z_3 = f(N_G, T_{T2})$	x	-
VI	$T_{T4}\ REF = f(N_G, T_{T2})$	x	-
VII	$T_{T5}\ REF = f(N_G, T_{T2})$	x	-
VIII	$P_{T3}\text{-}P_{S3}/P_{T3}\ REF = f(N_G, T_{T2})$	x	-
X	$P_{T3}\text{-}P_{S3}/P_{T3}\text{-}P_{T2}\ REF = f(N_G, T_{T2})$	x	-

The control modes referenced with P_{T2} generally tend to perpetuate the surge, whereas the remaining control modes resist further surge by reducing fuel flow in response to such signals as increasing T_{T4} or T_{T5} temperatures, decreasing pressure ratio, decreasing airflow, or a decrease in P_{T3} pressure.

5. Battle Damage

Battle damage of a nature that leaves the engine operative but leaking compressor discharge airflow causes performance loss that is to a large extent dependent on control mode. Table IX indicates the

nature of such performance loss. The actual value would be dependent on the extent of the damage.

TABLE IX. EFFECT OF COMPRESSOR DISCHARGE AIR LOSS DUE TO BATTLE DAMAGE

Mode	Identity	T_{T4} Temperature Increases	Surge Margin Decreases	N_G Topping Speed Increases	Max Power Increases Beyond Limit
I	W_f/P_{T2}	x	x	-	-
II	W_f/P_{T3}	-	-	-	-
III	W_f/P_{T2} N	-	-	-	x
IV	Z_2	x	x	-	-
V	Z_3	-	-	-	-
VI	T_{T4}	-	-	-	-
VII	T_{T5}	-	-	-	-
VIII	$\Delta P/P$	x	x	x	-
X	$\Delta P/\Delta P$	x	x	x	-

The W_f/P_{T3} and Z_3 scheduling modes and the T_{T4} and T_{T5} closed-loop modes are the only controls studied that resist battle damage.

Control Mode Study Summary

Tables III through VII show the manner in which each system error influences system performance for various control modes throughout several regimes of operation. In each table an attempt has been made to summarize the effect of the individual errors and to gain some overall insight as to the absolute value of the control mode. As would be expected, each mode can perform the objective of some operating regime better than in other regimes. The degree of emphasis that one regime receives as compared with another is completely arbitrary; one installation may well place a premium on acceleration time, while another

may prefer to place the emphasis on temperature limiting. In order to determine some type of overall performance score relative to this mode analysis, a penalty factor scoring system was established wherein each mode was analyzed in each operating regime against an established performance scale as shown in Figure 32. Values were assigned to this scale from one to five inversely proportional to performance, thus resulting in a scoring system with the lowest overall value indicating best performance. Table X summarizes this penalty factor scoring system for each of the ten modes in accordance with the performance scale established in Figure 32. It would be up to the individual reader to assess this penalty function in each regime in a manner consistent with his individual requirements, perhaps resulting in a different overall score.

The decision reached from the influence coefficient study must be tempered by the conclusions reached in the transient analysis study. Closed-loop temperature control, which looks outstanding on the penalty factor summation, has unacceptable transient error performance on gross accelerations. The error is the result of a conflict between a large-loop velocity requirement and a realistic assumption of the secondary lags in the system: combustion delay, metering valve dynamics, and secondary dynamics in the sensor and computer.

Other factors may also be important in determining the correct control mode selection. For example, it has been shown that a W_f/P_{T3} acceleration schedule tends to resist surge propagation and battle damage airflow leakage better than a W_f/P_{T2} schedule.

It is concluded that a hybrid of modes as summarized below would best satisfy the requirements for the engine defined by this program:

1. A W_f/P_{T3} acceleration schedule on the basis of best transient performance and resistance to surge propagation and battle damage

2. A T_{T5} closed-loop temperature control to limit steady-state turbine inlet temperature more accurately than is possible with a W_f/P_{T3} schedule

3. A W_f/P_{T3} gas generator speed droop line to provide accurate topping for mechanical speed limiting

4. An integral-plus-proportional power turbine speed governor with load sharing capabilities to provide the necessary speed of response and steady-state accuracy for this important function

5. Collective pitch proportional load anticipation on the basis of superior transient performance, rather than a rate of pitch schedule

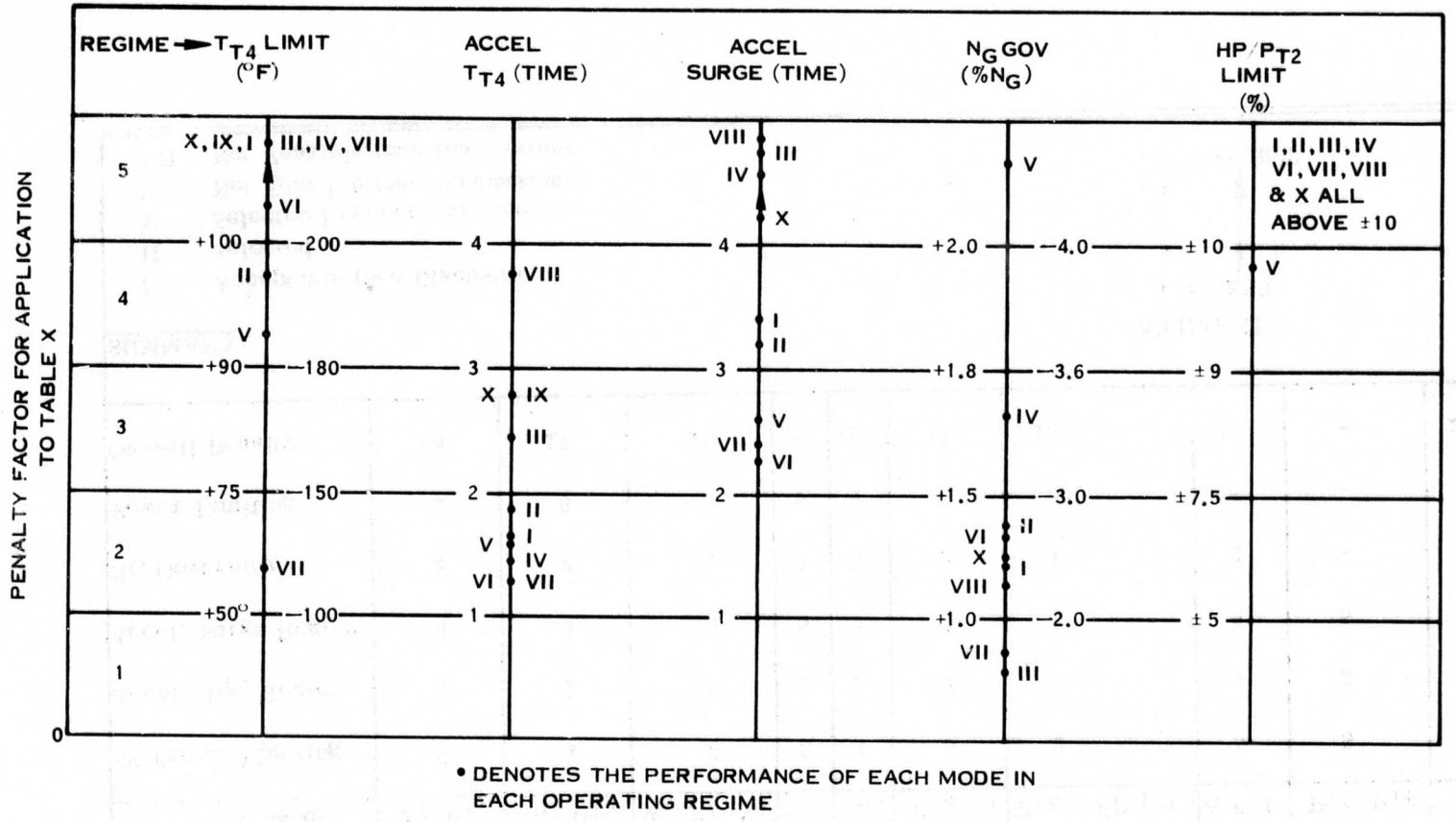

Figure 32. Penalty Factor vs Operating Regime.

TABLE X. CONTROL MODE PENALTY FACTOR SUMMARY

Regime \ Control Mode	I W_f/P_{T2}	II W_f/P_{T3}	III $W_f/P_{T2}N_6$	IV $\cdot Z_2$	V Z_3	VI $T_{T4} = C$	VII $T_{T5} = F(N_1\ \Theta)$	VIII $\Delta P/P$	IX P_{T3}/P_{T5}	X $\Delta P/\Delta P$
SS Temp. Limiting	5	4	5	5	4	5	2	5	5	5
Accel. T_{T4} Regime	2	2	3	2	2	2	2	4	3	3
Accel. Surge Regime	4	4	5	5	3	3	3	5	5	5
N_G Governing	2	2	1	3	5	2	1	2	-	2
Power Limiting	5	5	5	5	4	5	5	5	-	5
Overall Penalty	18	17	19	20	18	17	13	21	-	20

SUMMARY:

- I Acceptable (See Discussion)
- II Selected
- V Selected Regenerator Mode
- VI Not Feasible (See Discussion)
- VII Not Feasible (See Discussion)

RATING KEY

1 = BEST
2
3
4
5 = WORST

TECHNOLOGY APPLICATION STUDIES

Approach

An evaluation of the technologies and concepts that are possible in the makeup of an engine control must be based on criteria that are realistic from the standpoint of performance as well as many other factors. As discussed in the previous section, a specification for the control was written defining the basic system design requirements. In addition to this, a list of evaluation criteria and their weighting factors was established in conjunction with U.S. Army AVLABS and is described as follows:

Criteria	Weighting Factor	Comments
Size/Weight	20	The size and weight for each component or subsystem, as estimated by the appropriate technology, was assigned a weighting factor of 20.
Cost	10	Cost based on a relative production selling price of 1000 units at 100 per month was assigned a weighting factor of 10.
Reliability	10	Reliability as defined by mean time between failure (MTBF) was assigned a weighting factor of 10.
Contamination Resistance	5	A judgement score was assigned to each technology based on a weighting factor of 5. Contamination resistance is considered to be the ability of the technology to function in the face of expected contamination without failure or unacceptable degradation of performance.
Vulnerability	15	This factor has a weighting value of 15: 5 points for the relative size of the component; 5 points based on component failure which might contribute to failures external to the control, such as rupture of external fuel lines; and 5 points based on susceptibility of any portion of the system outside the basic package, the loss of which would result in rapid engine malfunction.
Maintainability	5	Maintainability was assigned a weighting value of 5 points: 3 points for estimated ease of maintenance in the field, and 2 points for maintenance at an overhaul facility.

Flexibility/ Commonality	25	Although assigned a weighting factor of 25, these criteria do not appear in the detailed technology trade-off charts since these criteria are more a function of basic design, rather than of technology.
Integration With Other Components	10	This criterion does not appear in the detailed technology trade-off charts for the same reason as given for flexibility/commonality. However, in both cases these criteria did receive overall design consideration.
Accuracy	0	Since accuracy is an absolute specification requirement, this criterion was not assigned a weighting factor; however, it is included in the chart to indicate the ability of the technologies to meet control requirements.

The above factors were utilized in the trade-off studies by assigning the highest number of points to the best technology in each category and a ratio of this to the others based on relative performance. The summation of points for each system then gives an indication of which functions each technology can do best. This knowledge, in combination with factors such as flexibility and ease of interfacing, aids in the selection of the best technology. Two other evaluation criteria, flexibility/commonality and integration of accessories, were not used in the technology trade-off studies since they are a function of basic design rather than selected technology. As a result, the maximum total score in the trade-off charts is 65 rather than 100.

A dual approach was taken in the evaluation process. First, a pure implementation approach to the complete control as defined by the specification was accomplished in each of the hydromechanical, fluidic and electronic technologies. The output for each included schematics, arrangement, cost, weight, accuracy and reliability within the constraints of the specification. The second aspect of this technology review consisted of specific implementation of those components or subsystems within the control that each technology could do best. These answers were then used to formulate the trade-off charts used in establishing the optimum technology or combination of technologies to be used in the final control.

Each response was reviewed for consistency of ground rules with respect to methods of calculating accuracy, reliability, cost, etc., and were revised frequently to maintain consistency of results.

Pure Technology Studies

As discussed in the preceding section, a control system in accordance with the specification was implemented in each of the three technology areas in as pure a fashion as technology limitations would permit. This approach allowed for any one of three modes of control: two open-loop schedule type, W_f/P_{T2} and W_f/P_{T3}, and one closed-loop control, T_{T4}. Estimated schedules were supplied for each mode for the base engine.

In addition to these schedules, considerable time was spent investigating ways to simplify the three-dimensional schedules into two-dimensional functions. However, this effort only solidified the need for complex three-dimensional schedules in a high-performance engine-fuel control combination. Therefore, each group was directed to supply three-dimensional scheduling as initially required. Due to the lack of a T_{T4} sensor that could meet the accuracy and response requirements, all three technologies chose the open-loop scheduling mode of control.

Figure 33 depicts the pure hydromechanical control approach. The control was sized and arranged using the latest miniaturized hardware developed in a current U. S. Army demonstration engine program in conjunction with new designs where improvements were possible. Because of the time available for this study program, the amount of effort which could be directed at further miniaturization was limited.

The control utilizes a hydromechanical speed governor with an oil-lubricated gear reduction box (described in detail in a later section of this report), three-dimensional cam scheduling, and a liquid-filled direct-acting T_{T2} sensor in the gas generator section.

In the N_F control section, a remote flyweight pressure generating type governor was incorporated after carefully considering a complete remote N_F governing and scheduling control configuration and a main control-mounted N_F system with an N_F flexible drive. It also was assumed that for torque sharing and torque limiting, the engine would supply a schedule of oil pressure relative to torque that could be utilized. This assumption was made to allow the hydromechanical technology to remain pure, i.e., without the need for electromechanical interface.

Figure 34 depicts the pure fluidic implementation of the W_f/P_{T3} mode. The control utilizes the latest standard fluidic block technology developed by the General Electric Specialty Fluidics Operation. Each block consists of multiple stainless steel laminates for the various circuits mounted on a central aluminum center body.

The main input parameters of N_G and N_F speed are basically frequency inputs from engine mounted choppers. Most major scheduling is accomplished by three-dimensional cams through the use of a mechanical-motion-to-fluidic-pressure-force-balance device which produces a differential pressure proportional to cam motion. This system is used for collective pitch bias, acceleration limiting, deceleration limiting and variable-geometry scheduling.

Four fluidic pressure-to-hydromechanical transducers are utilized for the T_{T2}, N_G, VG and throttle valve servos. These devices convert the low-level fluidic differential pressure to a high-level hydraulic pressure through the use of a diaphragm, feedback linkage, first-stage flapper valve and second stage pilot valve to obtain the high force level and slew rates required for these servos.

The torque-sharing and torque-limiting functions are produced through the use of an electromagnetic-torque-motor-to-fluidic-signal transducer similar to the mechanical input motion transducer. A detailed description of the operation, rough sizing and accuracy study of these components is included in Appendix V of this report.

The summing of two or more signals is done resistively through a proportional amplifier, analogous to electronic signal summing. Selection is performed by comparing two signals in a summing amplifier and allowing either the higher or lower value to continue. All signals have local loop feedback on them to eliminate any inaccuracies. The selection of three or more signals requires more circuitry as explained in Appendix V.

The overall system uses 1.2 lb/min of compressor discharge air extracted preferably from the inner annulus to reduce the level of contamination. The control incorporates a centrifugal filter and an in-line regulator to condition the air for the system. Additional hydromechanical components such as the fuel flow filter, pressurizing valve, shutoff valve, ΔP regulating valve and metering valve are the same as shown in Figure 33.

The pure electronic schematic is shown in Figure 35, and the arrangement drawing, in Figure 36. The system is implemented by hybrid digital-analog-pulse rate technique. The schedules are generated by a time-shared digital multivariate function generator, described in Appendix IV. The variable stator vanes are positioned by an electro-hydraulic actuator to take full advantage of the power density of these devices. The rest of the system is implemented by pulse rate modulation described in Appendix IV with the fuel valve being driven by a stepping motor through a rack-and-pinion coupling.

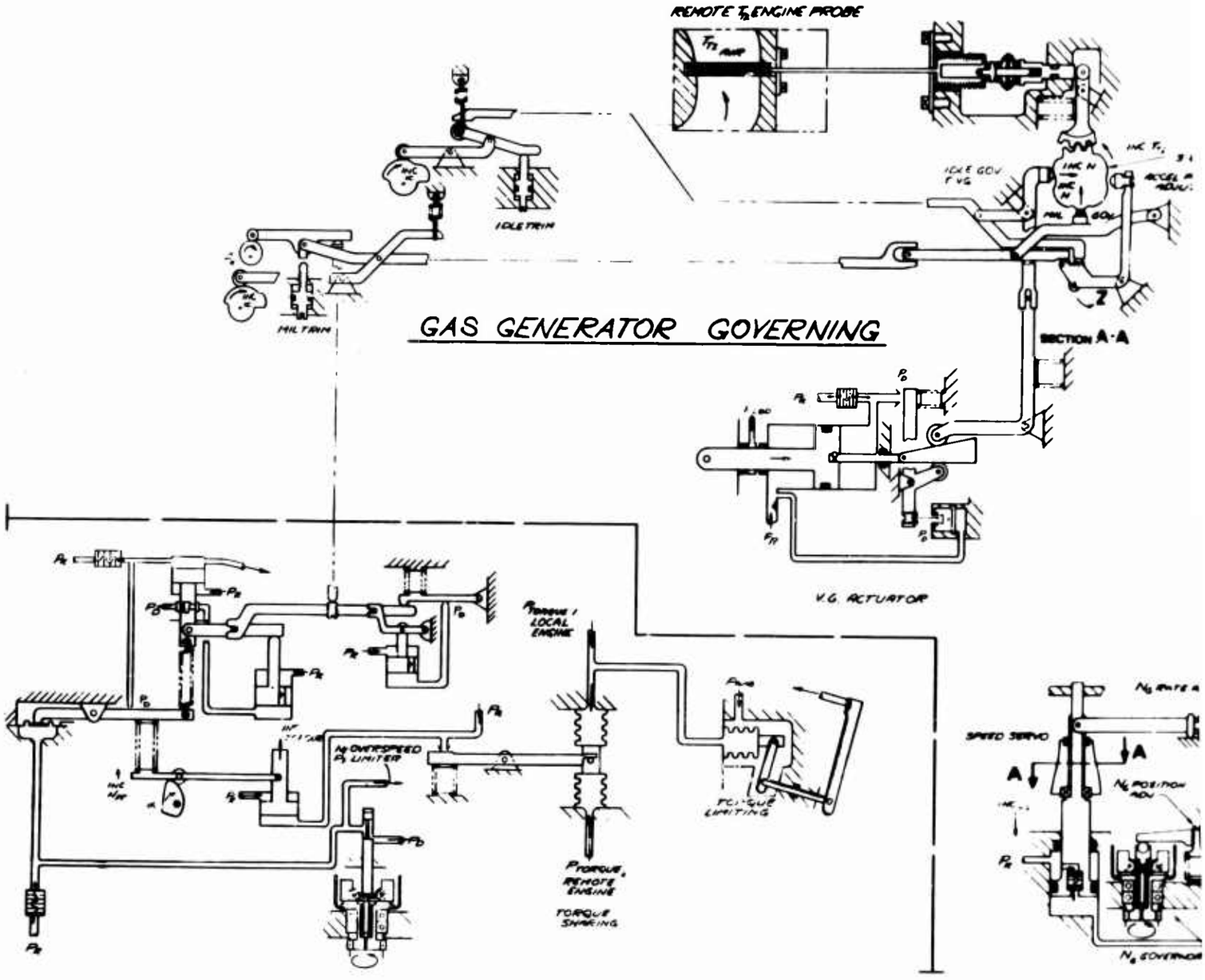

Figure 33. Schematic of Pure Hydromechanical Control Implementation.

A

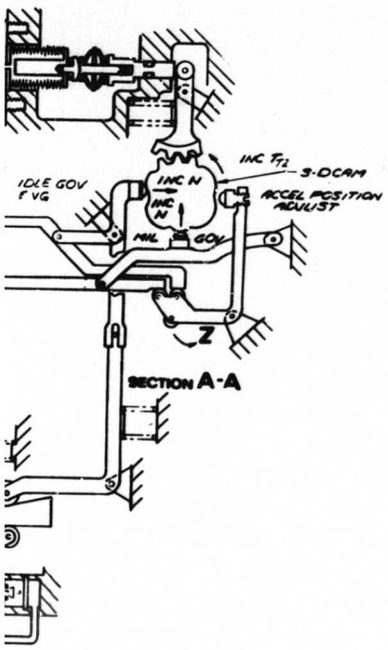

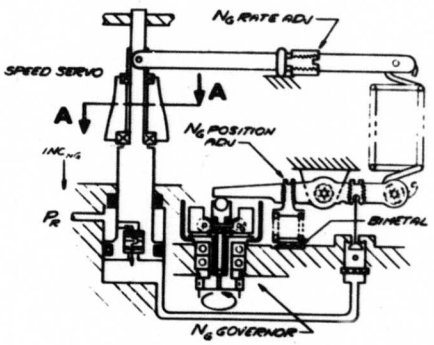

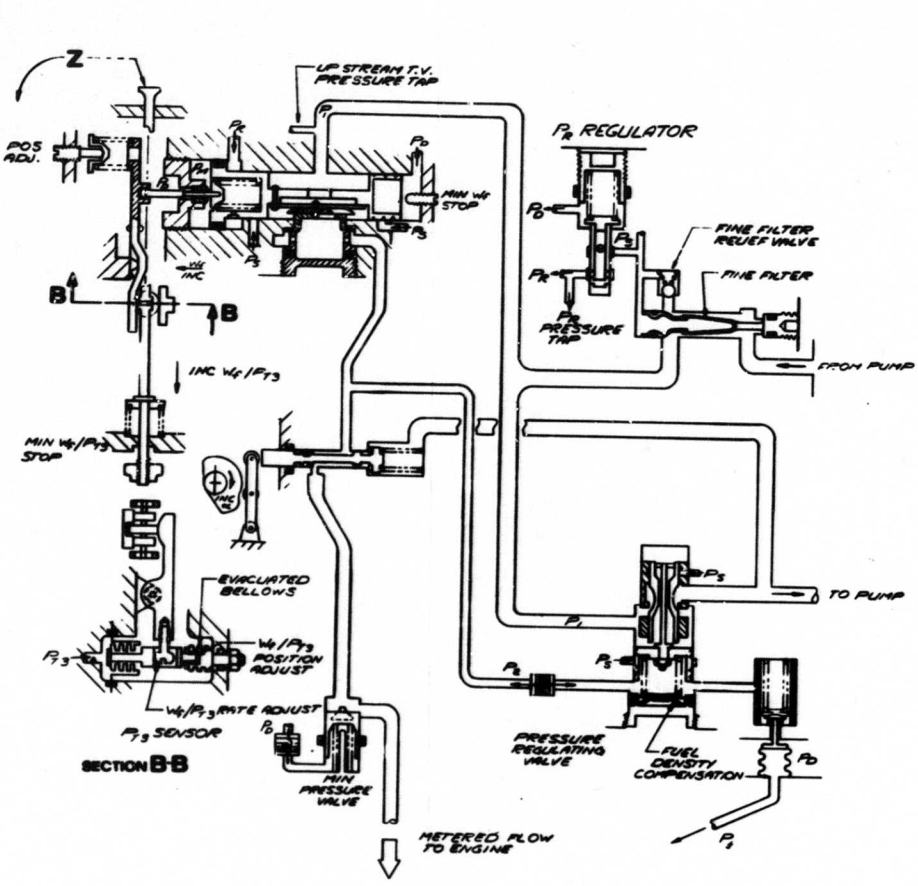

FUEL METERING

LEGEND
- P_D - CONTROL BODY PRESSURE
- P_R - REGULATED SERVO SUPPLY
- P_3 - SUPPLY PRESSURE (FINE FILTERED)
- P_{T3} - COMPRESSOR DISCHARGE PRESS.
- P_1 - T.V. INLET PRESSURE
- P_2 - T.V. OUTLET PRESSURE
- α - POWER LEVER
- P_M - METERED PRESSURE
- P_T - N_G OVERSPEED SIGNAL
- — ELECTRICAL CONNECTIONS

B

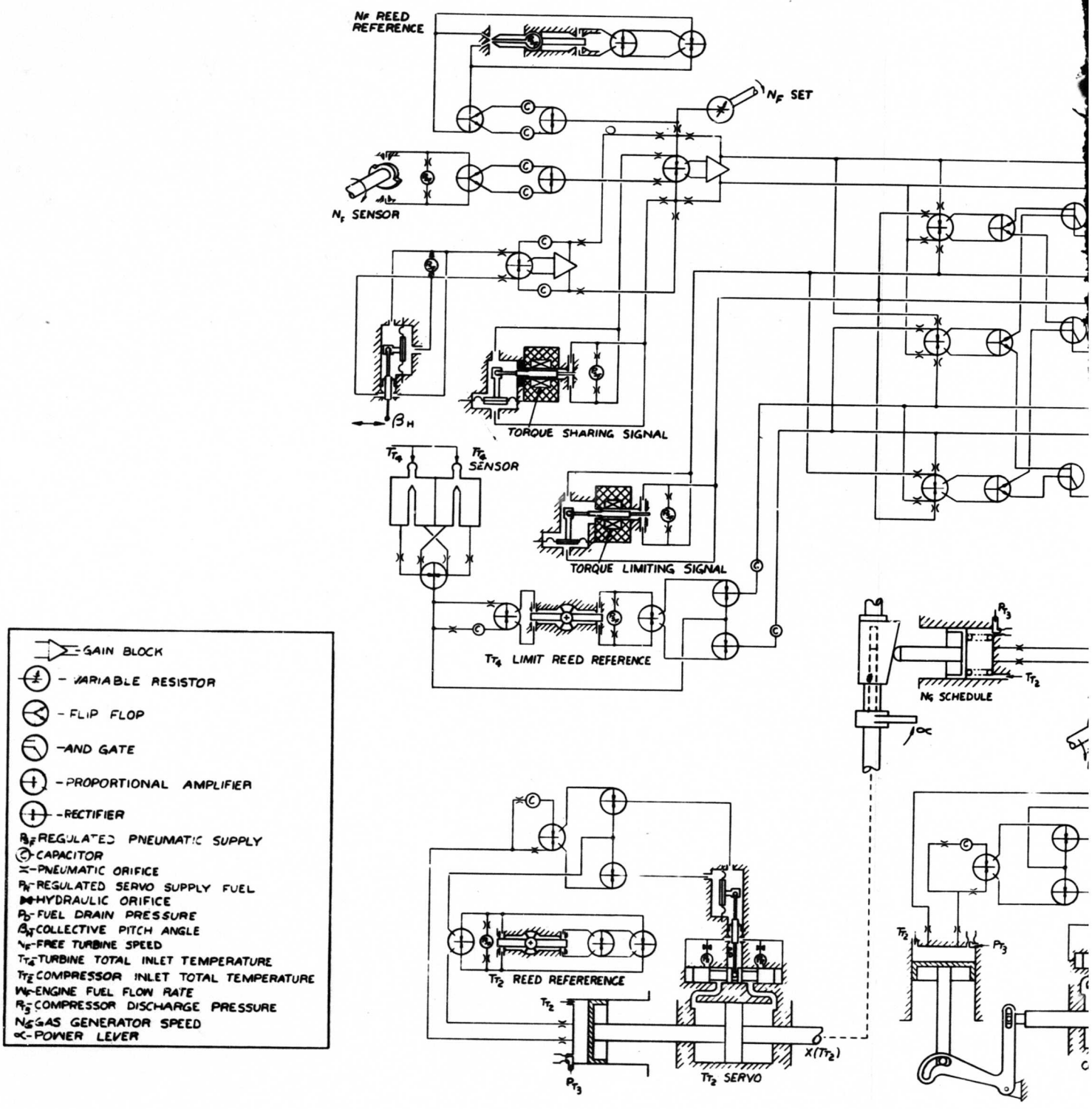

Figure 34. Schematic of Pure Fluidic Control Implementation.

A

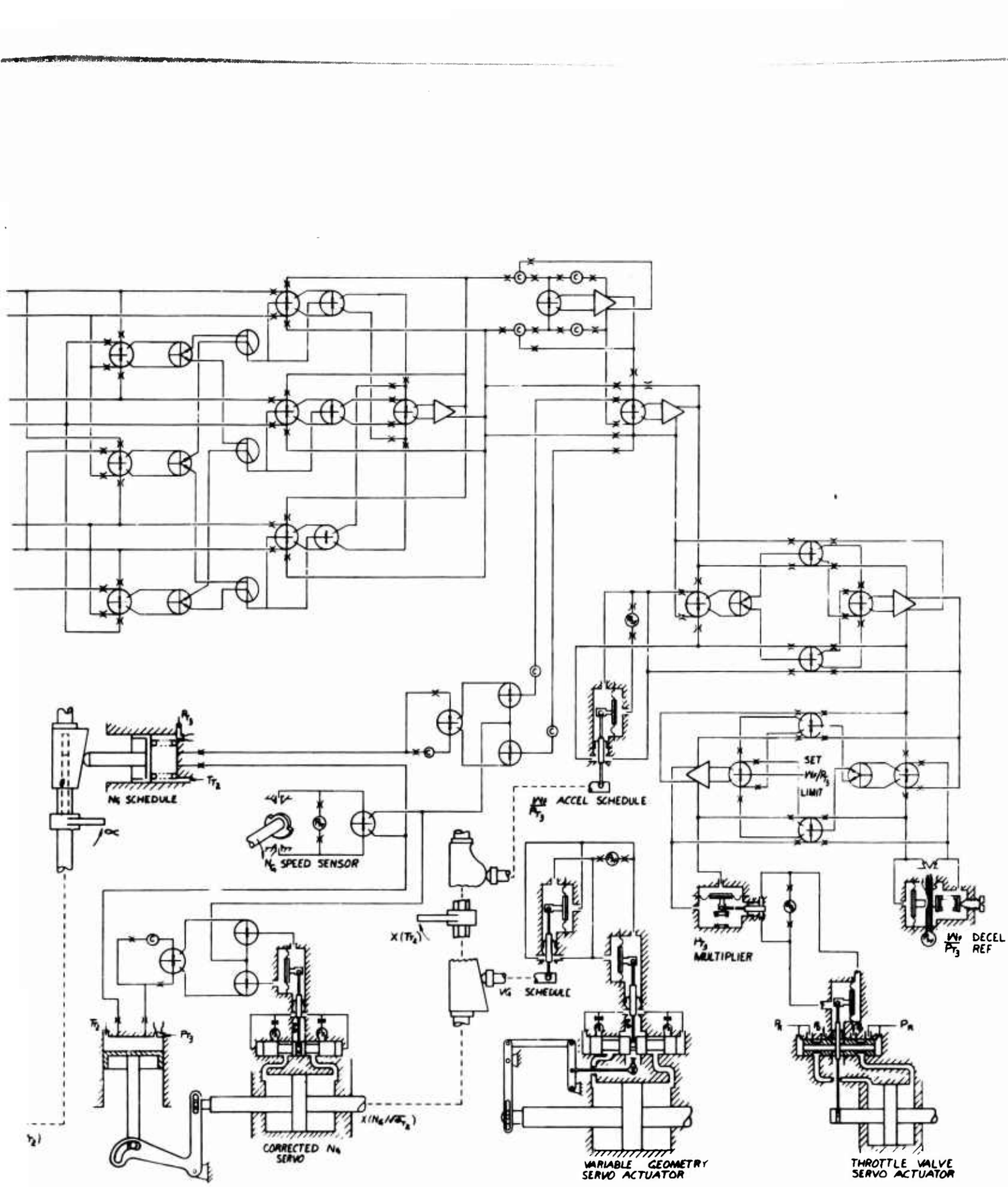
N_H SCHEDULE
N_H SPEED SENSOR
ACCEL SCHEDULE
SET LIMIT
MULTIPLIER
DECEL REF
$X(T_{T_2})$
V_G SCHEDULE
CORRECTED N_H SERVO
VARIABLE GEOMETRY SERVO ACTUATOR
THROTTLE VALVE SERVO ACTUATOR

B

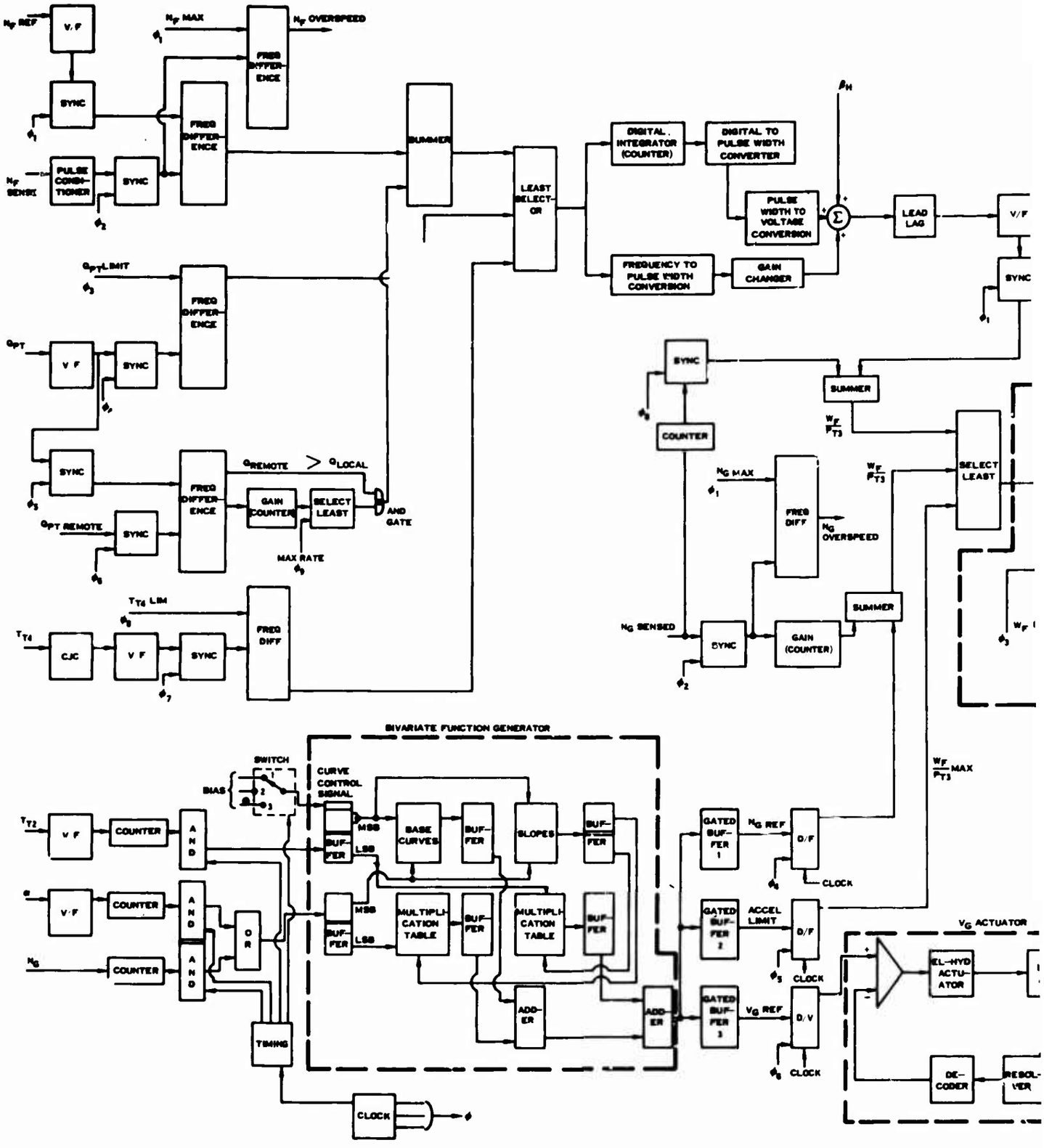

Figure 35. Schematic of Pure Electronic Control Implementation.

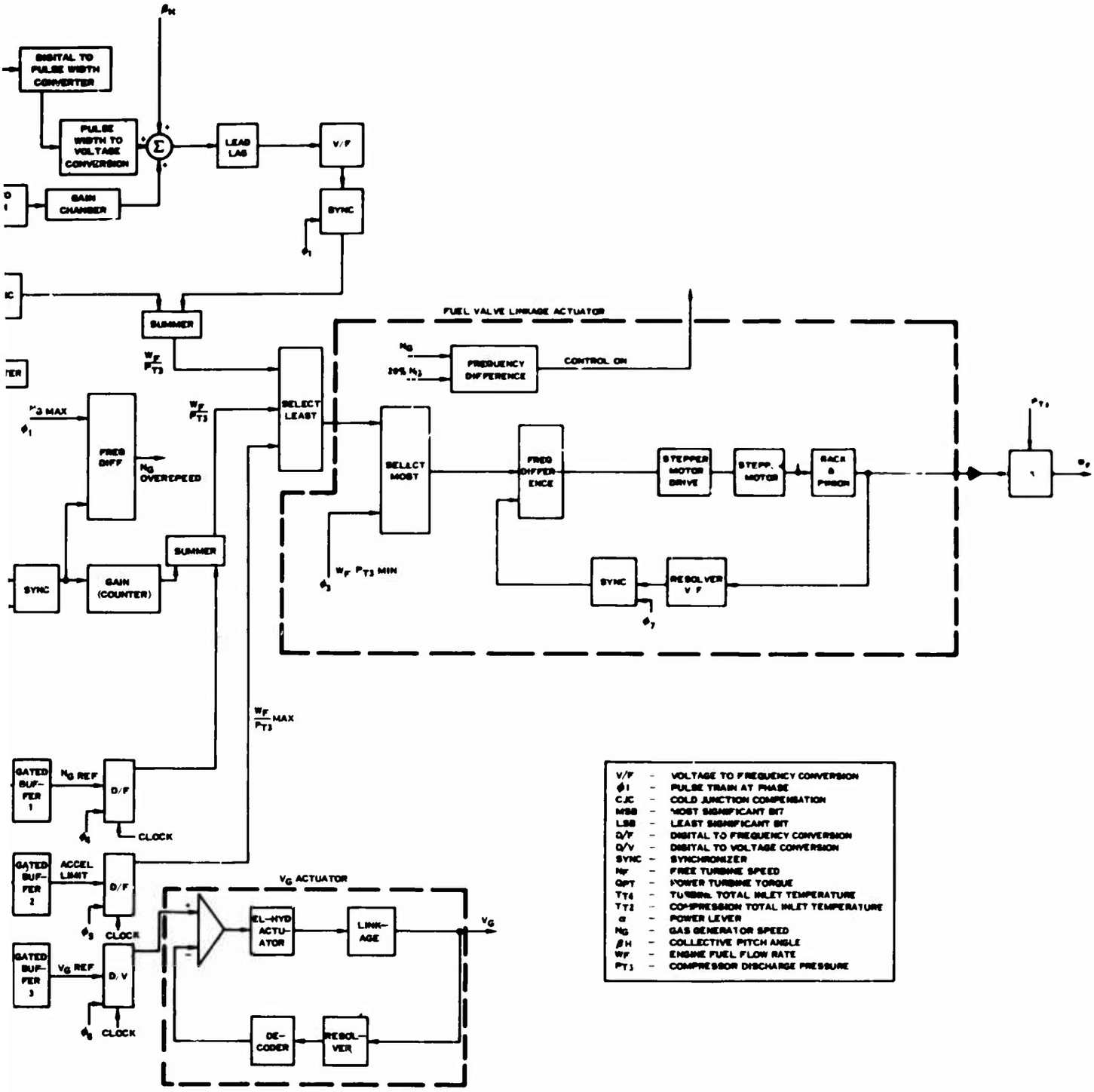

V/F	–	VOLTAGE TO FREQUENCY CONVERSION
ϕ1	–	PULSE TRAIN AT PHASE
CJC	–	COLD JUNCTION COMPENSATION
MSB	–	MOST SIGNIFICANT BIT
LSB	–	LEAST SIGNIFICANT BIT
D/F	–	DIGITAL TO FREQUENCY CONVERSION
D/V	–	DIGITAL TO VOLTAGE CONVERSION
SYNC	–	SYNCHRONIZER
N_F	–	FREE TURBINE SPEED
QPT	–	POWER TURBINE TORQUE
T_{T4}	–	TURBINE TOTAL INLET TEMPERATURE
T_{T2}	–	COMPRESSOR TOTAL INLET TEMPERATURE
α	–	POWER LEVER
N_G	–	GAS GENERATOR SPEED
β_H	–	COLLECTIVE PITCH ANGLE
W_F	–	ENGINE FUEL FLOW RATE
P_{T3}	–	COMPRESSOR DISCHARGE PRESSURE

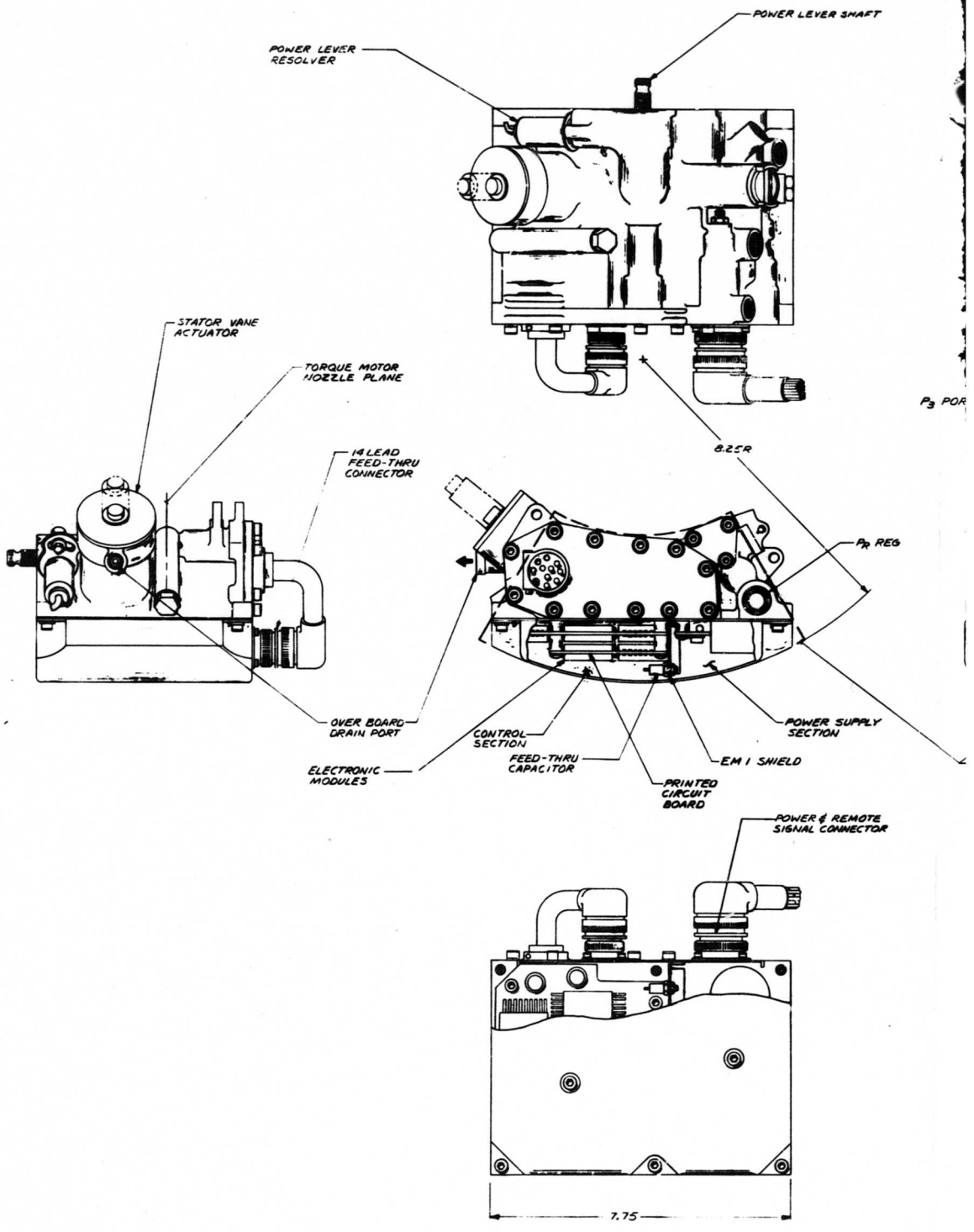

Figure 36. Arrangement Drawing of Pure Electronic Control Implementation.

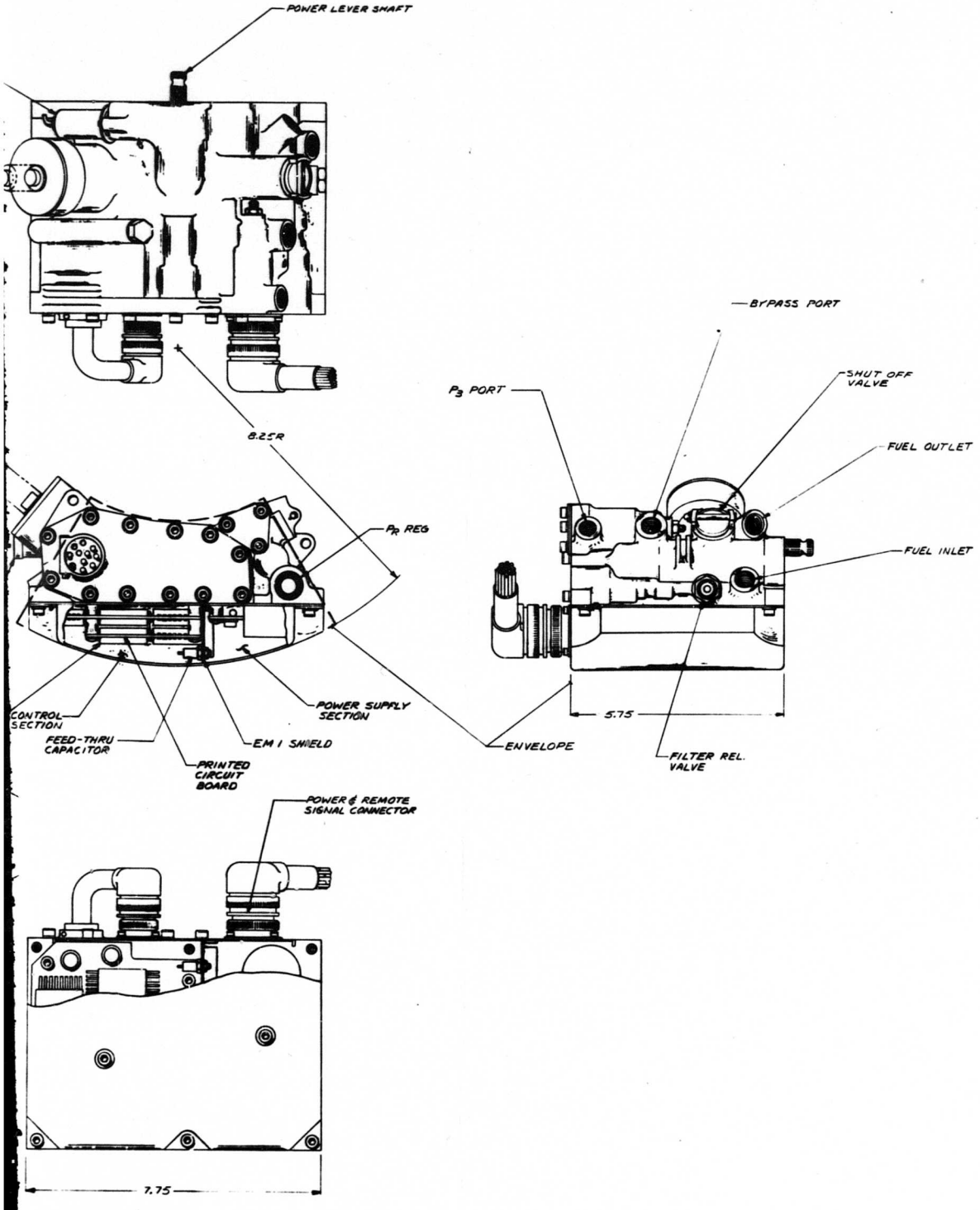

wing of Pure
ol Implementation.

B

The proposed digital multivariate function generator (DMFG) is unique in concept and, except for costly full-digital computer type approaches, it is the only general-purpose electronic device currently available for this purpose. It can closely approximate any multivariate function, whether discontinuous or analytic. The hardware requirements are influenced by the accuracy requirements of the application and by the characteristics of the function to be generated, but they are small compared with other methods of implementation of the same functions. The inputs and the outputs of the device are binary words, the length of which are determined by the accuracy requirements. In this design, the inputs are 9-bit words and the outputs are 8-bit words. The input words are obtained by counting the pulses of the pulse rate signals for a set period of time. The input buffers address a non-destructive read only (NDRO) memory which contains the points of the base curves and the associated slopes which are combined to provide the output of the DMFG. The same function generator is time-shared among the three schedules.

The outputs are fed into the appropriate buffers where they are converted into either pulse rate signals, for the acceleration and N_G schedules, or an analog voltage, for the VG schedule. The ambient temperature, input signal is converted into a pulse rate signal by a voltage-controlled oscillator (VCO). Alternately, if the conditions so demand, this signal could be converted by another method of analog-to-digital conversion.

Pulse rate modulation was selected as the basic implementation technique of the system because of its inherent accuracy and high reliability. The analog implementation suffers from low reliability when high accuracy is required. The complete digital computer approach entails prohibitive costs and excessive size.

Pulse rate components are also amenable to modern packaging techniques because of the standard sizes in which these components are manufactured. Only with such components could the high accuracy, high reliability and small size demanded from the control system be achieved. To attain these objectives, monolithic components which are common to all pulse rate systems will be used. The electronic components, except the power supply, will be metal oxide semiconductor (MOS) based. MOS devices are easier to build, are less expensive, require less power to run, and, consequently, are expected to be more reliable than bipolar-type devices. The chief drawback of MOS devices, the slower operating speeds, causes no problem in this application.

The W_f/P_{T3} signal drives a position loop with a stepping motor used as a power device. A stepping motor was selected primarily to allow the direct use of the pulse rate signal as input to the loop. The stepping motors currently available

can accept and follow the necessary slew rate, are sufficiently small, can survive the environment and are sufficiently reliable. The resolution achieved at the output is 1/2%, so that any limit cycle resulting from the output granularity will be of small amplitude and long period.

The proportional path and the subsequent summation of the trimmer section are implemented by analog technique. This approach has various advantages:

1. By converting from pulse rate to analog and later reconverting to pulse rate, the number of clock phases required by the entire system is reduced; hence, the allowable pulse width is increased.

2. Nonlinear gain characteristics are more easily implemented by analog than by pulse rate technique.

3. The analog lead/lag compensation is more trouble-free than the equivalent pulse rate compensation. Despite the added conversion hardware, the number of components, and hence reliability, remains virtually unchanged.

This approach is acceptable because the proportional path does not require high accuracy, and because errors added downstream of the integrator do not affect the steady-state accuracy.

The engine-mounted alternator provides unregulated AC power, the voltage of which is rectified, filtered and regulated to generate the precision voltages required within the control. The DC voltages are used to drive a sine wave generator which supplies power to the resolvers and/or LVDT's.

In addition to the power regulation, the control contains the necessary hydromechanical components including a P_{T3} bellows and output lever, a W_f/P_{T3} force balance multiplying system, a servo-operated throttle valve, fuel filter, pressurizing valve, shut-off valve, ΔP regulator and VG actuator (not shown in Figure 35). A more detailed description of the control is contained in Appendix IV.

Table XI summarizes the results from these pure technology studies.

TABLE XI. SUMMARY CHART - PURE TECHNOLOGY

		Hydromechanical	Fluidics	Electronics
Accuracy	Acceleration Limiting	±2.7%	±4.8%	±1.28%
	N_G Governing	±0.77%	±1.7%	±1.0%
	N_F Governing	±1.0%	±1.2%	±0.71%
	VG Actuator	±1.25%	±2.6% N_G	±1.94% N_G
Weight		15.53 lb	15.25 lb	10.65 lb
Volume		195 $in.^3$	180 $in.^3$	140 $in.^3$
MTBF		18,000 hr	14,500 hr	7,200 hr
Cost Ratio		1.0	1.6	1.6

Component and Subsystem Trade-Off for Technology Selection

In addition to the pure technology studies, individual studies were made of both component and subsystem areas where two or more of the technologies appeared to be competitive. The size of each subsystem for individual comparison varies and primarily relies on two basic facts. First, both electronics and fluidics require their own power supply and regulation that amount to a significant portion of their weight. This weight is required no matter how small a portion of the job they do. Second, each technology must be able to interface at the optimum point with another technology for maximum utilization of the hardware. Many of these interfaces are not available at the present time, without significant weight and size penalty, and therefore the interfaces used were limited to those which would be somewhat competitive.

The following section presents the major components and subsystems considered:

Gas Generator System Technology Selection

This system includes power lever scheduling, gas generator speed sensing, proportional droop governing, acceleration limiting, deceleration limiting and variable-geometry scheduling. A majority of the schedules are bivariate curves caused by compressor inlet temperature biasing. Each technology includes all input scheduling, computation and selection through to W_f/P_{T3} motion. The accuracies shown do not include P_{T3}, throttle valve and pressure-regulating valve errors.

The hydromechanical implementation of this system is the same as that shown in Figure 33, the pure hydromechanical control schematic, and includes the incorporation of the gear reduction box (discussed in the section on N_G speed sensor technology selection) to reduce the engine drive speed. All bivariate curve generation is accomplished on a standard three-dimensional cam translated by the N_G governor servo and rotated by the temperature sensor.

The weight of this gas generator computation system is 5.88 pounds, including 1 pound for the gear reduction box and its housing.

The following list summarizes the key facts about this system:

1. The three-dimensional cam concept is a low-cost, low-weight and accurate method to produce bivariate schedules.

2. The desired accuracy is obtainable.

3. The reliability of mechanical hardware is extremely high.

4. High force output actuators such as the VG servo can be reasonably small by using the high fuel pressures already available within the control.

5. To accept gas generator speeds at levels of 55,000 rpm severely punishes the hydromechanical governor.

The fluidic schematic of the gas generator system is the same as that shown in Figure 34 (the pure fluidic control schematic) and is described in detail in Appendix V. A summary of this system reveals that:

1. Extensive studies into possible methods of producing bivariate schedules resulted in the use of a three-dimensional cam in conjunction with a motion-to-fluidic-pressure transducer. This was the only approach that would meet the necessary accuracies.

2. The reliability of the system is acceptable on a speculative basis due to the relative newness of this technology.

3. The accuracy of the system is marginal due to temperature effects primarily in the large turndown ratio resonators, as discussed in the following section on N_G speed sensor technology selection.

4. The need for many fluidic-to-hydraulic interfaces (VG actuator, N_G governor, TV servo and T_{T2} servo) adds complexity and weight to the package.

5. The contamination tolerance of the system is expected to be low due to line and orifice sizes in the range of 0.020 inch diameter. This may be improved by the development of an effective centrifugal filter, but the degree of dirt, oil and water contained in engine P_{T3} air is very hard to guarantee, especially in hovering helicopter applications.

6. The amount of engine bleed air needed for this system is 0.01 lb/second at 20 psi. The effect of this level of air bleed becomes most severe on a 2-pound-per-second engine at low engine speeds, as shown in Table X. The prime method of reducing this air bleed is to reduce orifice sizing with the associated increase in contamination sensitivity.

The electronic gas generator system is the same as that shown in Figure 35 (the pure electronic control schematic) and described previously in this section. The bivariate schedules are generated in a digital multivariate function generator using a table look-up and interpolation process defined in Appendix IV. The estimate includes the necessary power conversion and regulation previously described, and the weight of the electronic gas generator computation system is 4.45 pounds. A summary of this system reveals that:

1. The accuracy requirements can be easily obtained.

2. The use of monolithic component technology and time-share processing of information results in a lightweight, small-volume package.

3. A reduction in the failure rate of semiconductors can be achieved by combining groups of them in one common monolithic device, thus reducing the number of soldered leads. However, the overall reliability of this electronic system is still only 40% of that of the hydromechanical version.

4. The digital multivariate function generator used for storage of all three dimensional schedules is expensive at the quantities set up in this program due to initial, nonrecurring costs.

5. High force output requirements such as for VG actuation are impractical to do with motors and are best accomplished with electrohydraulic devices.

6. High gas generator speeds are easily handled and actually preferred by electronic pulse pickups.

Assigning the appropriate weighting factors to the individual criteria as shown in Table XII, indicates that a hydromechanical implementation of the gas generator system appears to be the best. However, it should be noted that combining various portions of each technology into a form of hybrid may result in still better control, as will be discussed in the technology conclusions.

Power Turbine Governing Technology Selection

This subsystem includes torque sharing, torque limiting, collective pitch bias and proportional-plus-integral power turbine governing with lead/lag compensation. The accuracy requirements are quite stringent at ± 0.5% N_F speed. There is no requirement for bivariate curve generation with the schedules being either fixed-limit or two-dimensional. Each technology includes all input scheduling, computation and selection through to W_f/P_{T3} motion. The accuracies quoted do not include P_{T3}, throttle valve or regulating valve errors.

TABLE XII. GAS GENERATOR CONTROL TECHNOLOGY TRADE-OFF CHART

Criterion	Factor	Hydromechanical	Fluidic	Electronic
Schematic	-	Figure 33	Figure 34	Figure 35
Accuracy	Gov. Accel. VG	± 0.68% N_G ± 1.8% W/P ± 1.2% N_G	± 1.40% N_G ± 3.0% W/P ± 2.6% N_G	± 0.75% N_G ± 0.8% W/P ± 1.9% N_G
Size/Weight	20	15	14	20
Vulnerability	15	14	10	12
Cost	10	10	5	5
Reliability	10	10	8	4
Contamination Tolerance	5	4	2	5
Maintainability	5	4	5	4
Totals	65	57	44	50

The hydromechanical system schematic depicted in Figure 33 (the pure hydromechanical control schematic) utilizes a remote N_F governor requiring some form of mechanical speed mounting pad. This governor requires fuel pressure lines to and from the main control for operation. A summary of this system reveals that:

1. The system does not meet the accuracy primarily due to fuel temperature associated coefficient of discharge effects, regulated pressure effects and friction effects in the control-mounted components. More complex governing schemes were considered but added further weight and complexity.

2. The weight of the system (6.9 pounds) is high due to the amount of hardware required to get lead/lag compensation and torque sharing.

3. The vulnerability of the system is low due to its size and the fuel lines required between sensor and main control.

4. The engine weight is penalized for an N_F speed pad and for the hardware required to produce a hydraulic pressure as a function of absolute engine torque.

The fluidic schematic is shown in Figure 34 (the pure fluidic control schematic) and the operation is described in Appendix V. The following summarizes the highlights of this system:

1. The N_F governing accuracy does not meet the specification. The use of a Ni-span C reed resonator allows reasonable accuracies at maximum speed; however, part-speed settings have large temperature errors.

2. The reliability, contamination tolerance and air bleed conclusions discussed in the fluidic gas generator section also apply here.

3. The need for large-volume air capacitors in the lead/lag circuit results in a large-volume main package.

4. The selection circuitry required when more than two parameters are to be chosen is quite complex, requiring many selectors and amplifiers.

The electronic power turbine system is shown in Figure 50 (the final hybrid control schematic) and defined in the section on the definition of the evolved hybrid control. This N_F system differs from that shown in the pure electronic control in that it is primarily an analog control. The pure technology approach converted analog sensor inputs to digital because of the decision to use the digital memory technique in the gas generator section. Without this requirement, the pure analog approach was more compatible with analog sensors currently available. A summary of the system reveals that:

1. The accuracy requirements can be met.

2. Monolithic component technology results in a lightweight, improved reliability control, as previously discussed.

3. Interfacing with well-established electrical torque sensors requires a minimum of hardware.

4. Lead/lag compensation is accomplished with a minimum of weight and cost.

5. The cost of the unit more closely approaches the hydromechanical unit because of the extreme complexity required for the hydromechanical technology to meet the specification.

Table XIII, which summarizes the merits of the three technologies, indicates that the electronic system is the best overall way to execute these functions for the specification requirements. The only area of doubt is in reliability, which is expected to improve steadily in future years and which can also be backed up by a simple overspeed device discussed in a subsequent section of this report.

TABLE XIII. N_F GOVERNING CONTROL TECHNOLOGY TRADE-OFF CHART

Criterion	Factor	Hydromechanical	Fluidic	Electronic
Schematic	-	Figure 33	Figure 34	Figure 50
Accuracy	Gov.	± 1.0%	± 1.25%N	± 0.25%
	Sharing	± 5.0%	± 5.0%	± 2.1%
	Limiting	± 4.5%	± 3.5%	± 1.5%
Size/Weight	20	13	13	20
Vulnerability	15	5	11	13
Cost	10	10	7	7
Reliability	10	10	9	6
Contamination Tolerance	5	4	3	5
Maintainability	5	4	5	4
Totals	65	46	48	55

Turbine Inlet Temperature Sensing Technology Selection

Direct measurement of turbine inlet temperature (T_{T4}) for the purpose of closed-loop engine control on this parameter has been continually sought by engine and control manufacturers. Since the existence of an accurate, functional T_{T4} temperature sensor plays such an important role in the outcome of a study program of this type, much attention has been given to this area since the inception of the program. All known methods of temperature measurement were considered in terms of accuracy, reliability, flow-path obstruction response time, etc. Measurement methods demonstrating potential for this application have been tabulated in Table XIV. Although a few technologies show some promise, none could be recommended at this time due to accuracy, dynamic response or other limitations. The relative merits of the two best available at this time are shown in Table XV.

Immersion devices such as thermocouples and resistance probes, the most conventional devices for measurement of temperature in the range of interest, present several problems when subjected to a turbine inlet environment. Exposed thin-wire probes are unable to withstand the temperature, corrosive atmosphere, and gas velocity and present the problem of possible ingestion into the turbine in the event of service failure. Beefed-up, protected or shielded probes do not provide adequate time response and introduce problems of air flow restriction since several probes are required to provide some degree of averaging. The temperature measured is not the gas temperature but that of the device itself,which in practice has been shown to vary by 40°to 100°F from actual gas temperature. These devices, however, can be used for measurement of T_{T3} or T_{T5}, where they can be isolated from direct flame radiation and are in general subjected to a milder environment.

Pyrometric devices in general are impractical due to the requirement for complex electronics, motor-driven choppers and reference source lamps. One exception is the silicon-chip, photovoltaic-type pyrometer, which is a solid-state device with no moving parts and no requirement for input power. The silicon-chip pyrometer consists of a tubular housing with a sapphire window and quartz lens which focus radiant energy on a silicon cell. A voltage output on the order of 50 millivolts is produced at the upper temperature limit for which it is designed. The device can be made quite compact, possesses good accuracy at high temperature and excellent dynamic response. Although this device appears ideally suited to the application, considerable development is required before implementation. The gas temperature is not sensed directly, the pyrometer must be focused on a target within the gas stream. The lens must be kept clean to insure accuracy. Although some success in keeping the lens clean has been achieved by the use of purge air directed through a collimator mounted on the lens, this principle has not been proven for long periods of time or for a wide range of typical engine conditions, and routine maintenance at relatively short intervals for lens cleaning is anticipated.

The silicon chip pyrometer is sensitive to the ambient temperature at the sensor body which in addition is limited to a maximum of 250°F, necessitating provision for cooling and temperature compensation. A final problem with this device is severe loss of accuracy below 1600°F (see Figure 39), necessitating another means of temperature sensing be included to cover the lower temperature range or that a dual control mode be provided. Usefulness of this device at the present time appears to be limited to that of a temperature limit sensor in which application it could be focused on the first-stage turbine blades. Further development is required prior to application to closed-loop T_{T4} control.

The most attractive method of T_{T4} sensing at this time is the fluidic approach, since gas temperature can be measured directly over the full range of engine operation. Of several different methods of implementation of fluidic technology to this application, the dual-edge tone oscillator principle appears to represent the greatest progress in state-of-the-art development.

The time response of a single oscillator to a step change in temperature is characteristically a few milliseconds to reach 75% of the steady-state value (sensor purge time) followed by a long heat transfer time constant to reach steady state, which can be as great as 40 seconds. The dual-oscillator approach is based on a difference frequency, permitting compensation in the difference term. It has been shown that by carefully proportioning the flow rates through the high and low-frequency oscillators, considerable compensation is possible for steady-state environmental temperature changes, transient effects of the heat transfer characteristics of the two oscillators and transient effects of heat transfer in the inlet probe of the temperature sensor. With development, 67% compensation is considered a realistic design objective, resulting in an instantaneous transient error of approximately 10% of the step change in temperature, decreasing to zero transient error with a time constant on the order of 10 to 20 seconds (see Figure 38). Even for relatively large step increases in turbine inlet temperature, the transient error is not expected to exceed 4% of the final temperature on an absolute accuracy basis.

A major static error source existing with fluidic temperature sensors is the effect of humidity on the gas constant (R_o) and the ratio of specific heats (γ). The effect of humidity on these "constants" and the product (γR_o) is shown in Figure 37. Since the output frequency of an edge-tone oscillator is given by $K\sqrt{\gamma g R_o T}$, it can be readily seen that the resulting temperature measurement (T) is directly affected by any variation in the product γR_o. Over a complete range of operating conditions, the resulting temperature error due to humidity can be as great as ± 1.2%. The gas constant (R_o) is also affected by the fuel-air ratio and the hydrogen carbon ratio of the fuel used, but these effects are small in comparison to the effect of humidity.

TABLE XIV. SUMMARY OF POTEN TEMPERATURE SENS

Sensor	Type	Current State of the Art			
		Accuracy	Range	Response	
Thermoelectric	Bare - Wire Thermocouple (Platinum - Rhodium)	≈1.0%	3250°F	0.2-0.6 Second	Difficult to design sufficient reliability and durability for more rugged sacrifices response. Some drift due to oxid
	Multiple - Junction Thermocouple (Include Foil)	≈1.0%	3250°F	0.1-0.3 Second	Has improved response over single junction, but share the Attempt to make more rugged for turbine inlet service wo
	Shielded Thermocouple	0.75%	3250°F	Poor	Has increased reliability and ruggedness. Response very are difficult to fabricate. Improved accuracy due to reduc
Resistive	Platinum Probe	1.2%	2000°F	≈2 Seconds	Requires power supply. Above 2000°F, insulators cause e rial evaporation, strains that affect resistivity, and contac to 1900°F @ Hamilton Standard Electronics Department.
Pyrometric	Optical	—	—	—	Requires seeding of flame, elaborate equipment, reference
	Two-Color Ratio	2.5%	1800-3000°F	≈0.002	Requires motor driven iris and complex electronics.
	Lead Sulfide Detector	≈4.0%	550-7000°F	0.007	Multiscaling required to obtain range shown. Complicated
	Photomultiplier	—	—	0.180	Requires mechanical chopper and reference source lamp.
	Photoelectromagnetic	—	400-2900°F	<0.006	Requires multi-ranging, reference source lamp, motor dri
	Photovoltaic (Silicon Chip)	<1.0% above 2000°F	1400-3500°F	10 μ Seconds	Solid-state device with no moving parts. No power required remains clear. Ambient temperature at sensor limited to (response is adequate to use turbine blades.) Lens must be 50 mv output. Compact (approx. 1.5" x 0.75" diameter test Temperature limit of component must not be exceeded after
Fluidic	Edge - Tone Oscillator	>1.5%	1900°F	≈0.1 Second (75%)	Requires choked orifice in series, ejector at low ratio of P_T (90°/100 psi @ 550°F observed in Hamilton Standard tests). sensitive - operates on combustion products. Secondary tim regulation may be required for altitude conditions.
	Dual Edge - Tone Oscillator (Heterodyned)	>1.5%	1900°F	≈0.1 Second (90%)	Lower "beat" frequency output is in range of fluidic detector sensitivity and response, but amplifies static inaccuracies o two oscillators provides compensation for transient errors.
	Feedback Oscillator (Hamilton Standard Concept)	≈1.0%	1900°F	≈0.1 Second	Higher signal to noise ratio since oscillator completely switc feedback tubes. Operates on cleaner air since P_{T3} is used f Ratio of power jet pressure to exhaust pressure must be regu
	Delay Line Phase Discriminator	≈1.0%	1900°F	≈2 Seconds	Analog output signal would be sensitive to engine noise. Ejec reduce response. Contamination reduced, uses P_{T3} or exter combustion products.
Acoustic	Resonant Cavity	—	—	—	Difficulty in exciting and detecting resonance. Delay to deter
	Sonic Pulse Timing	≈6.0%	—	—	Attenuation at higher temperature reduces usefulness above 1 in accuracy shown). Low signal-to-noise ratio. Affected by p
Nuclear	Beta Radiation	—	—	—	Safety limitations on strength of isotope necessitates long cou
Pneumatic	Laminar Flow (Downstream Tube)	—	—	—	Poor repeatability, low sensitivity resulting in low accuracy.
Mechanical	Differential Expansion	—	—	0.4 to 0.8 Second	Sensor tested limited to 1200°F due to materials used (302 sta to manufacture, subject to creep and shifts.

A

MARY OF POTENTIAL TURBINE INLET PERATURE SENSORS

Comments	General Remarks
eliability and durability for use at turbine inlet. Response is function of wire diameter - attemps to make nse. Some drift due to oxidation, contamination by silicon or iron. (20°/100 hrs @ 2500°F)	Due to poor durability and need for averaging, several required per engine. ten probes in 2 pps engine cause 10% reduction (mass flow loss ≈ 5%). Electronic package required for averaging and amplification. Little recent progress in state of the art. No. 12 gage wire used for 1000 hours service at 1500°F (τ = 2 - 5 seconds)
single junction, but share the same durability problems. Tendency to overshoot (except for foil junction). for turbine inlet service would negate response advantage.	
ruggedness. Response very slow unless TC junction is grounded to sheath. TC bonded to sheath types proved accuracy due to reduction in sensivity to flame temperature variation.	
e 2000°F, insulators cause error, become nonlinear. Requires protective sheath to prevent: mate- affect resistivity, and contact of water vapor (causes probe to shunt @ T = 2000°F). Good experience d Electronics Department.	At Hamilton Standard Electronics Department: at 1900°F two have exceeded 2,000 hrs - five have exceeded 1,000 hrs. Several failures due to Q.C.
aborate equipment, reference source.	None appear practical for this application except for the silicon chip photovoltaic type.
d complex electronics.	
n range shown. Complicated construction Requires amplification	Considerable recent progress in the state of the art.
nd reference source lamp.	
ence source lamp, motor driven chopper.	
ng parts. No power required. Blue flame has no effect, yellow flame adds noise, but basic signal erature at sensor limited to 250°F (requires cooling). Must be focused on target in gas stream rbine blades.) Lens must be kept clear (successfully demonstrated with air-collimator lens.) x. 1.5" x 0.75" diameter tested.) Individual calibration required. Negligible flow restriction. it must not be exceeded after engine shutdown.	
es, ejector at low ratio of P_{T3} to exhaust pressure. Pressure sensitive at high temperature. in Hamilton Standard tests). Several sensors or input rake required for averaging. Dirt tion products. Secondary time constant is function of sensor heat transfer. Pressure altitude conditions.	Accuracies shown are those reported for ideal conditions. Accuracy in turbine inlet conditions requires determination and substantation. Humidity in inlet air (neglecting products of combustion) results in ≈ ± 1.2% error. Considerable recent progress in the state of the art.
is in range of fluidic detectors and more easily transmitted to remote detector. Has increased nplifies static inaccuracies of individual sensors. Uses twice the amount of airflow. Use of nsation for transient errors.	
ce oscillator completely switches during each cycle. Can provide averaging due to sampling in eaner air since P_{T3} is used for power jet. Feedback lines (2-10 feet) located at turbine inlet. xhaust pressure must be regulated to prevent gas mixing or distortion. No ejector required.	
nsitive to engine noise. Ejector may be required. Long delay line and preheat line seriously n reduced, uses P_{T3} or external air supply, but has more fluidic elements exposed to the	
ng resonance. Delay to determine resonant part.	
re reduces usefulness above 1500°F. Pulse generator is large. Sensitive to humidity (included -to-noise ratio. Affected by path length, gas swirl, gas velocity.	
isotope necessitates long counting times to obtain adequate resolution	
ity resulting in low accuracy. Considerable restriction to gas stream.	
due to materials used (302 stainless steel wire with quartz support). Low sensitivity, difficult and shifts.	

B

TABLE XV. TURBINE INLET TEMPERATURE SENSOR TECHNOLOGY TRADE-OFF CHART

Criterion	Factor	Hydro-mechanical	Fluidic	Electronic
Schematic		None Available	Dual Edge-Tone Oscillator	Silicon Chip Pyrometer
Accuracy		None Available	± 1.57%	1600°F ±4.5% 2500°F ± .7%
Size/Weight	20	None Available	18	20
Vulnerability	15	None Available	15	12
Cost	10	None Available	10	5
Reliability	10	None Available	10	8
Contamination Tolerance	5	None Available	3	5
Maintainability	5	None Available	5	2
Total		None Available	61	52

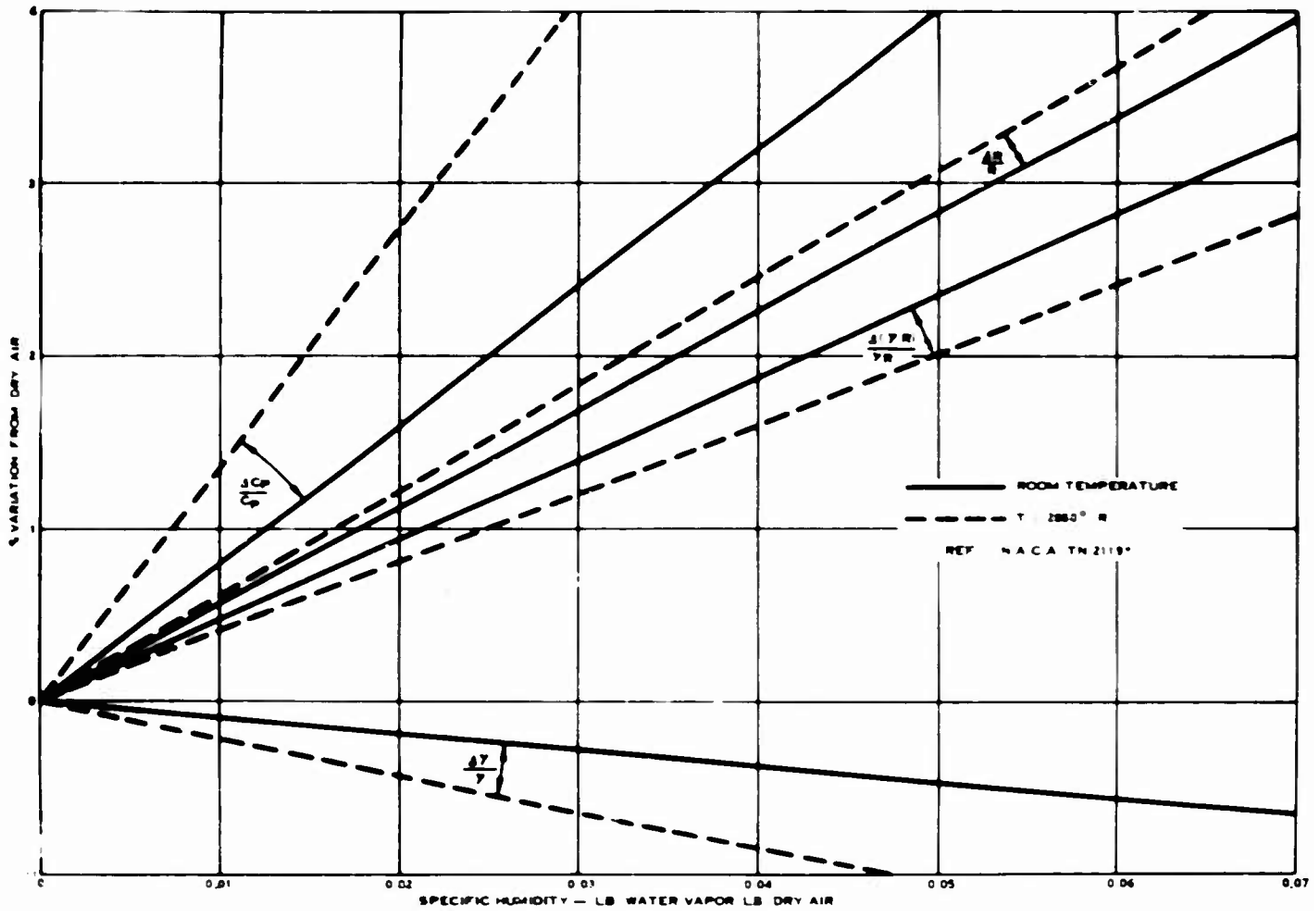

*SAMUELS J C AND GALE B M
EFFECT OF HUMIDITY ON PERFORMANCE OF
TURBO-JET ENGINES NATIONAL ADVISORY COMMITTEE
FOR AERONAUTICS JUNE 1950

Figure 37. Humidity Effects on Fluidic Turbine Inlet Temperature Sensor Accuracy.

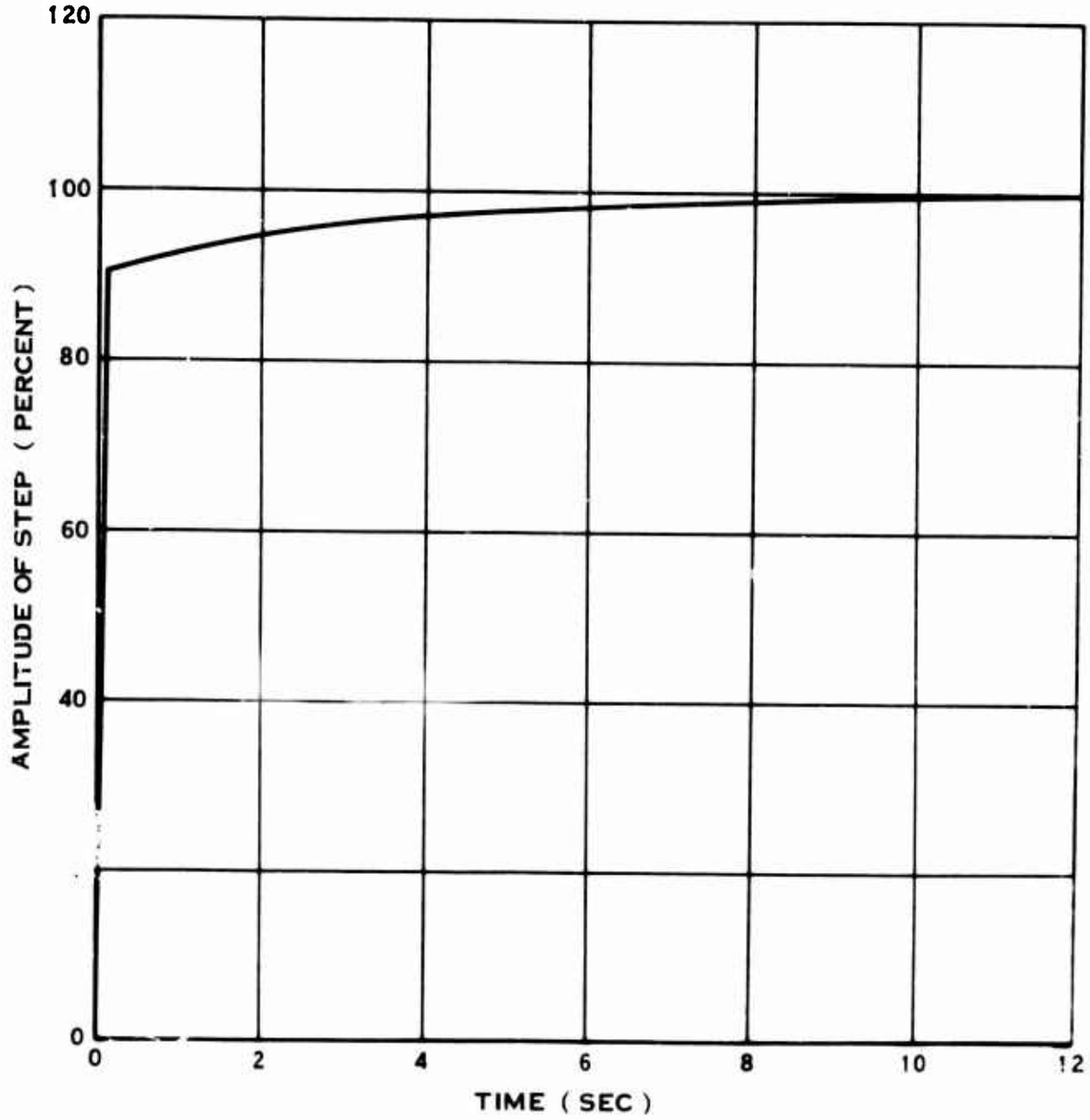

Figure 38. Time Response - Compensated Dual-Oscillator Fluidic Turbine Inlet Temperature Sensor.

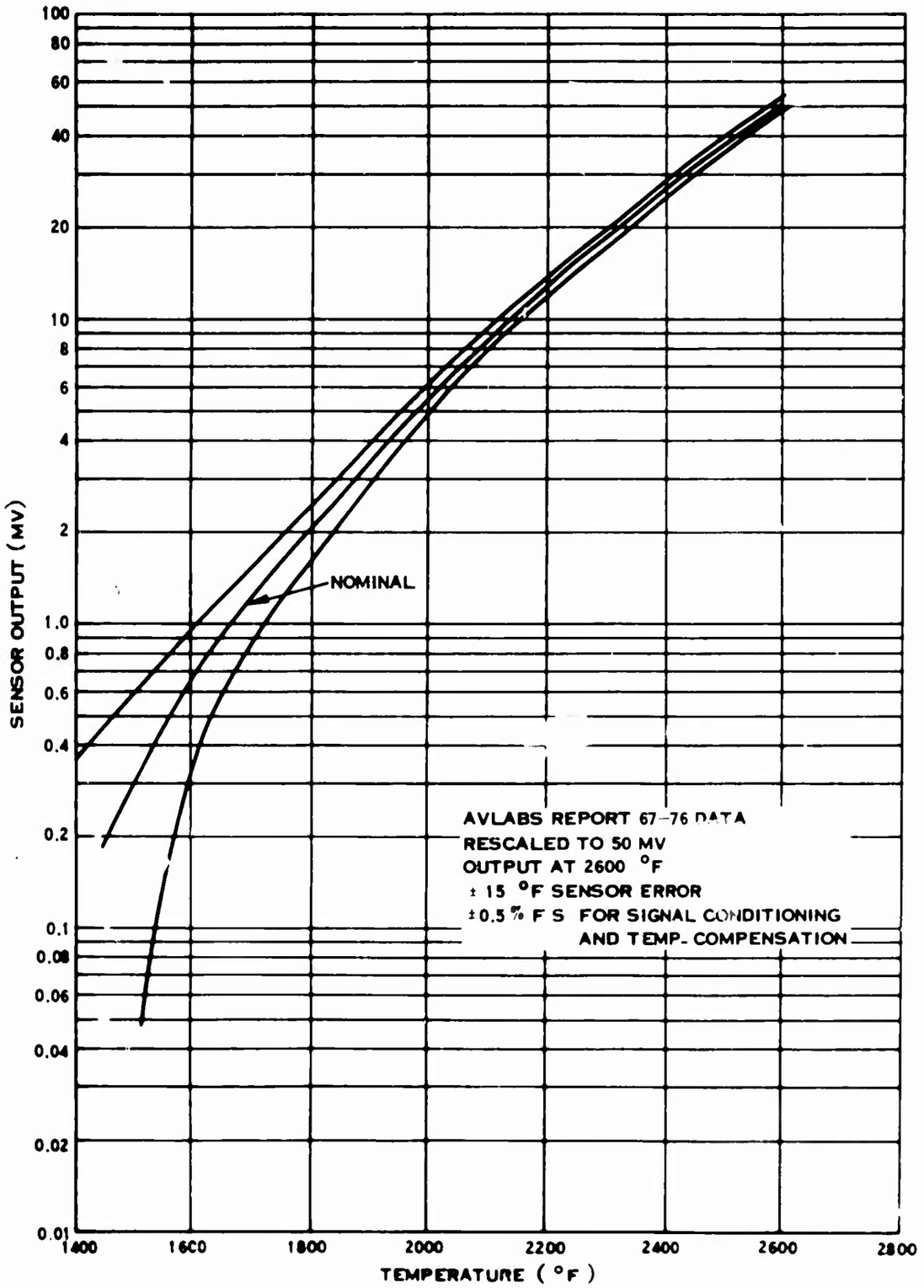

Figure 39. Definition of Error Band Optical Pyrometer Temperature Sensor.

Fluidic sensor development is also required in the area of materials capable of withstanding the environment of the turbine inlet and also in the area of contamination susceptibility, since the sensor operates on the products of combustion.

Both the silicon-chip pyrometer and the fluidic sensor present considerable potential for future turbine inlet temperature measurement applications. It is recommended that development and further refinement of these devices be actively encouraged.

Pressure-Sensing Technology Selection

The need for accurate pressure sensing in a scheduling control is important because of its effect on all performance. Most high-performance engines have a compressor pressure range of at least 50 to 1 and require accuracies of better than 1% over the full range. The following is a summary of the ability of the three technologies to handle this task.

Hydromechanical Pressure Sensing

The hydromechanical method used for the sensing of absolute pressure, such as P_{T3}, is a matched bellows set consisting of a motor bellows opposed by an evacuated bellows as shown in Figure 33 (the pure hydromechanical control implementation schematic). Since the output of the bellows set enters a force balanced system, the bellows set is operated continuously at constant geometry and is therefore less subject to modulus changes with temperature and time. Performance of this sensor type therefore approaches the theoretical maximum,where accuracy is determined essentially by the properties of the sensing element material.

Pressure ratio sensing can be accurately handled by the vector force balance-type sensor. This is a true pressure ratio sensor in that the displacement output signal from the force balance mechanism is a function of the ratio of the two forces involved and only a minor function of their individual magnitudes. The force vector mechanism also provides an inherent compensation of the pressure level effect on the sensor time constant, reducing this variation to provide a rapidly responsing sensor for a wide range of pressures.

Fluidic Pressure Sensing

In the fluidic consideration, P_{T3} is not sensed as such but is input directly to a multiplying circuit as shown in Figure 34 (the pure fluidic control implementation schematic). A differential pressure proportional to W_f/P_{T3} scheduled is applied to opposite sides of a diaphragm. Diaphragm motion is opposed by a spring, and the resulting displacement is transmitted to a

flapper lever. P_{T3} from a single source is diverted into two paths, each containing a restrictor and discharging through nozzles on opposite sides of the W_f/P_{T3} flapper lever. Output signals are picked off each leg between the respective restrictor and nozzle. The ratio of these output signals is a function of W_f/P_{T3}, their absolute pressure level is a function of P_{T3} and the resulting difference between the two output signals represents scheduled W_f.

Although the inherent simplicity of this system promises high accuracy, the restrictor-nozzle combination must be large enough to provide a usable signal at low P_{T3} pressure and to avoid choking at high pressure. Consequently, the resulting P_{T3} airflow through the system is considerably higher at high P_{T3} levels. This excessive bleed air flow not only inflicts a penalty on engine performance but increases susceptibility to contamination.

Electrical Pressure Sensing

A large variety of open-loop pressure-sensing devices of several basic types with various electrical outputs are commercially provided by numerous manufacturers. In general, open-loop sensors are a percentage of full-scale devices and although specifications in this form are often impressive, the turndown ratio of typical pressures sensed for engine control is such that sensor accuracy is inadequate in the low-pressure range. To permit measurement of a parameter such as burner pressure through a range of 5 to 250 psia and maintain 1% accuracy at the lowest point (5 psia), a sensor with an accuracy of 0.02% of full scale is required. Current technology does not approach this goal, and the use of multiple sensors to cover the range imposes a severe penalty in sensor duplication and necessary selection logic.

To maintain accuracy for large turndown ratios, a closed-loop device is required. Closed-loop transducers supplying electrical output typically involve hardware components which are basically electromechanical variants of fundamentally mechanical designs. The required conversion to provide electrical output results in accuracies that can only approach those of the basic mechanical device. Accuracies of two of the most promising electrical open loop transducers are compared to those of a closed-loop electromechanical transducer in Table XVI.

For similar reasons, a pressure ratio sensor must necessarily be a closed-loop device which combines the input pressure directly in order to maintain a usable degree of accuracy. Any attempt to compute pressure ratio from independent pressure signals results in gross inaccuracies since the errors are additive. In this case also, the conversion to provide electrical output can only approach that of the basic mechanical device. Pressure ratio sensors providing electrical output are shown in Table XVII.

TABLE XVI. SUMMARY OF POTENTIAL ABSOLUTE PRESSURE SENSORS

	Parameter	Range	(RSS) FS Accuracy	Equiv. Press.	% of Point	Comments	
Capacitive (Available)	P_{T3}	5-250 psia	± 0.675%	± 1.68 psi	± 33.7	Output:	Capacitive
						Wt.:	0.25 lb } Sensor
(Potential Sensor)			± 0.215%	± 0.538 psi	± 10.75	Vol.:	1.6 in.^{3} } Only
						Response:	0.005-0.030 sec
(Available)	P_{T2}	3.5-22 psia	± 0.675%	± 0.148 psi	± 4.23		
(Potential)			± 0.215%	± 0.0474 psi	± 1.35		
Variable Reluctance (Available)	P_{T3}	5-250 psia	± 0.2655%	± 0.665 psi	± 11.3	Output:	0-5 Volts
						Wt.:	1.6 lb } With
(Potential)			± 0.215%	± 0.375 psi	± 7.5	Vol.:	22 in.^{3} } Elec.
						Response:	0.01 sec
(Available)	P_{T2}	3.5-22 psia	± 0.2655%	± 0.0584 psi	± 1.17		
(Potential)			± 0.215%	± 0.033 psi	± 0.945		
Electromechanical Closed Loop (Voice Coil)	P_{T3}	5-250 psia	-	± 0.167 psi	± 3.35	Output:	0-5 Volts
						Wt.:	1-1.5 lb
	P_{T2}	3.5-22 psia	-	± 0.02 psi	± 0.575	Vol.:	12 in.^{3}
						Response:	0.01 sec

TABLE XVII. SUMMARY OF POTENTIAL PRESSURE RATIO SENSORS

Type	Output	Accuracy	Range	Response	Weight	Volume	Temp. Range	Comments
Force Balance-Closed-Loop	Digital (11 Bits) or Analog (0-5 Volts DC)	±0.1% F.S. for Temp. Shown	Probably Req'ts Design	< 1 sec	2 lb	50 in.^{3}	+20 to +180°F	1 Minute warm-up time req'd. Est: 1.2% P.R. pt. -65 to 250°F. Req'ts shock mount. High cost Electronics probably temp. limited.
Force Balance-Closed-Loop	AC (Synchro)	±1% P.R. Pt.	1-3 1-7	3 sec	4 lb	140 in.^{3}	400°F	Requires shock mount.
Modified AIC Lip Shock Sensor	Mechanical	±1.3% P.R. Pt.	Req'ts Design	≈ 0.2 sec	< 4 lb Est	< 50 in.^{3} Est	300°F	Est. wt. and vol. includes housing and servo.
Hydromechanical Vector Sensor	Mechanical	±1.2% P.R. Pt.	Req'ts Design	≈ 0.1 sec	3.5 lb	45 in.^{3}	300°F	Est. wt. and vol. includes housing and servo. For electrical output (0-5 Volts) add 1.8 lb
Electromech. Vector Sensor (With E-core)	0-5 Volts DC	±1% P.R. Pt.	Req'ts Design	≈ 0.05 sec	< 4 lb Est	< 50 in.^{3} Est	250°F	Est. wt. and vol. includes housing, servo and E-core (Sensor only 2.5 lb)
Two Open-Loop Transducers (P.R. Electronically Computed)	Capacitance	±24% P.R. Pt (Could be improved by matched temp. sens.)	Req'ts Design	≈ 0.02 sec Without electronics	1 lb Without electronics	5.4 in.^{3} Without electronics	-65 to 250°F	Requires electronic division. Electronics life marginal > 190°F. Prototype only, no production available. ±4.3% PR Pt. min. if temp. controlled.

Table XVIII compares the relative merits of each technology in the form of a technology trade-off chart. The table indicates that the hydromechanical pressure sensor is superior for this application.

TABLE XVIII. PRESSURE SENSOR TECHNOLOGY TRADE-OFF CHART

Criterion	Factor	Hydromechanical	Fluidic	Electronic
Schematic	—	Figure 33	Figure 34	—
Accuracy	250 psia 10 psia	0.5% 1.5%	0.43% 1.3%	0.215% 5.37%
Size/Weight	20	20	14	12
Vulnerability	15	15	10	10
Cost	10	8	10	6
Reliability	10	10	7	5
Contamination Tolerance	5	5	2	4
Maintainability	5	5	3	2
Total	65	63	46	Non-compliant

N_G Speed Sensor Technology Selection

The speed governing system for the proposed engine control design requires accurate speed sensing up to 75,000 rpm (2-pps base engine). Hamilton Standard's experience with speed-sensing devices does not include operation at speeds higher than 10,000 rpm. Consequently, there is little information available that exposes

the problems that would arise from operating speed sensors at significantly higher speeds. While some of the problems can be predicted, others are rather vague and would require a thorough testing program to determine their magnitude. Realizing this, it was decided that conclusions would be based on whatever information was available, and that future programs would be recommended to evaluate the questionable areas.

The speed-sensing device presently used in most controls is of the rotating flyball type. Operation up to 10, 000 rpm has presented some problems. Ultimately, however, satisfactory operation has been possible through development. With the new specification of 75, 000 rpm, problems that were only minor in the past become magnified significantly. Consequently, the first phase of the study program on the N_G speed system consisted of determining the problems associated with operating present flyball sensors at 75, 000 rpm.

In addition to studying the effects of high speed on the flyball sensors presently being used, an effort was made to develop a new concept for a mechanical sensor that would not be as sensitive to high-speed operation. Studies also were conducted on electrical and fluidic speed sensing devices. With a cross section of the three technologies of hydromechanics, electronics, and fluidics applied to speed-sensing devices, a comparison was made in terms of size, weight, accuracy and reliability. The result was the selection of an electrical system consisting of a torque motor controlled flapper valve interfaced to a speed servo and a resolver feedback.

The advantages and disadvantages of all the concepts studied are presented in the following paragraphs.

Flyball Speed Sensor

The flyball sensor, as shown in Figure 40, has speed-sensitive areas that would probably cause problems at 75, 000 rpm. Some of the more obvious problems are:

1. The centrifugal force acting on the flyweights becomes extremely large when operating at 75, 000 rpm. To reduce this force to more tolerable levels, smaller weights must be used. The cube size in steel required for the flyweight to produce a reasonable output force is 0. 066 inch. The accurate manufacture of parts this small is difficult and costly.

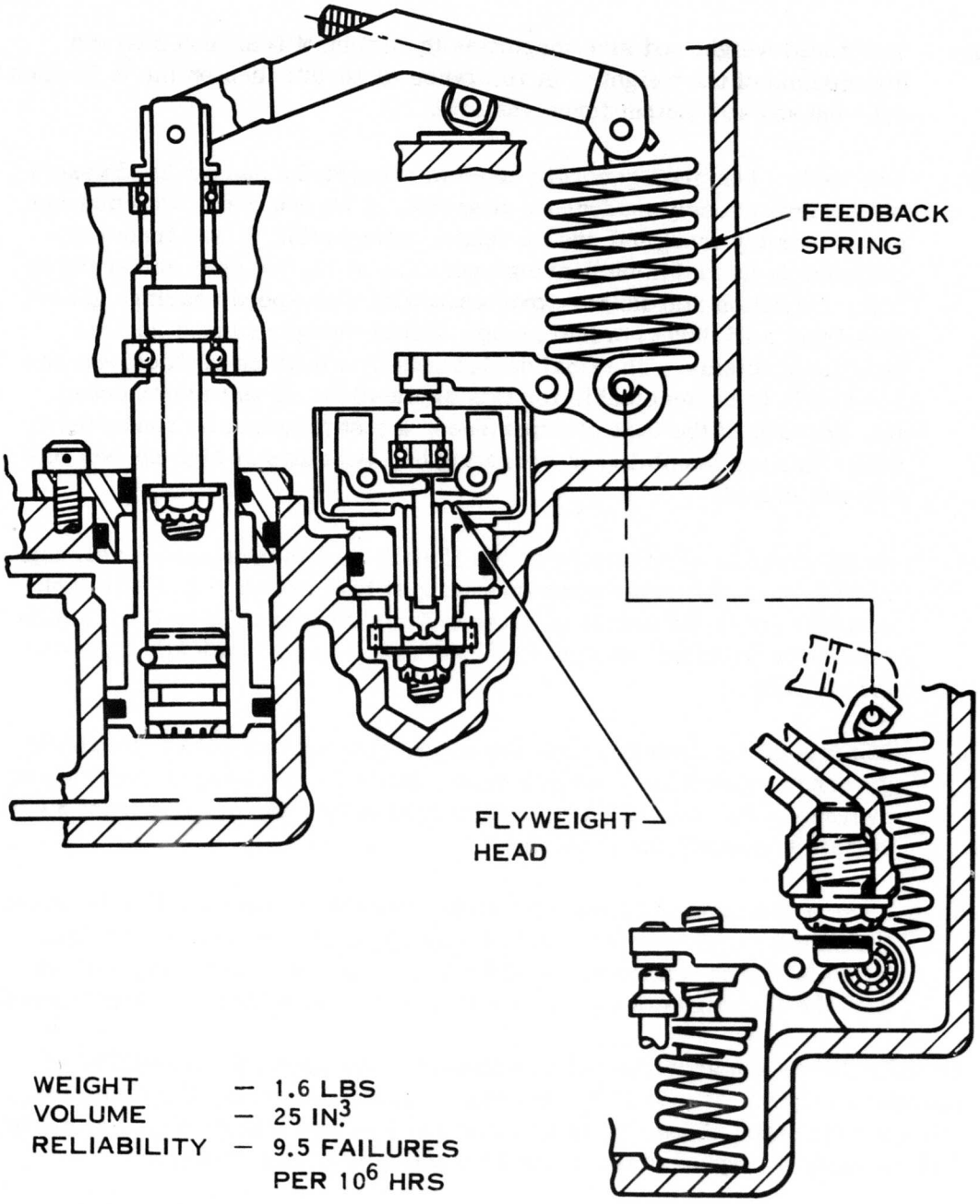

Figure 40. Implementation Sketch of Hydromechanical N_G Speed Governor.

2. The small weight and size magnifies the effect of tolerances on the dimensions of the weights. A tolerance of ±0.001 inch on the 0.66-inch cube causes ±9% output force variation.

3. The carbon bushings generally used to support the sensor head assembly become grossly inadequate at speeds of 75,000 rpm. Calculations are extremely marginal, and no vendor information gained from experience is available on bearing operation at 75,000 rpm immersed in fuel. Hamilton Standard's experience with high-speed bearings generates from a 35,000-rpm fuel pump. Initial designs caused serious bearing problems. The final design required bearing replacement too frequently to be acceptable for this application. It is recommended that because of the lack of experience, a test program be conducted to determine the feasibility of operating ball bearings at high speeds immersed in fuel.

4. Small amounts of unbalance of the flyball head causes excessively high loading of the bearings when operating at high speeds. A 0.001-inch eccentricity of the center of mass creates 20 pounds of load. To minimize this problem, each head would have to be dynamically balanced individually.

5. Scuffing of the flyweight toes due to inherent eccentricities in today's governor assemblies requires replacement (of the toes) at every major overhaul. Increasing the operating speeds by a factor of at least 8 will certainly magnify the problem.

6. Since a mechanical speed input to the control is required directly from the engine, a carbon face seal is also required. Face seal catalogs indicate that operation at 75,000 rpm is possible. However, just as with the bearings and the flyweight toes, no experience has been gained.

As indicated by the above list of potential problem areas, the feasibility of operating a flyball sensor at 75,000 rpm is poor. However, the exceptionally good accuracy obtainable from these devices in a small volume warrants further study if a speed drive is used for the fuel system pump.

Other Mechanical Speed Sensor

Some design effort was directed toward developing a new type of speed sensor that would not be as sensitive to high-speed operation as the flyball type. Different types of pressure-generating devices were studied. However, each concept had problems similar to the flyball-type sensor at high

speeds with additional problems concerning accuracy. Basically, a mechanical speed sensor better than the flyball type could not be developed in the time allotted for the program.

Gearbox for Flyball Sensor

Since the study of the flyball speed sensor indicated that high-speed operation was questionable, it was decided that a small, low-torque gearbox should be designed (shown in Figure 44) to reduce the speed input to more tolerable levels such as those that experience has shown to be practical (10,000 rpm). Experience at Hamilton Standard has shown that gears run with ball bearings and oil spray lubrication can perform properly with no significant wear for at least 500 hours. Based on this and other related experience, 2000 hours should also be possible, although reliability is questionable because of the lack of data.

The weight and volume penalty over the flyball sensor alone is severe, although necessary. In addition, the engine requires a tower shaft to provide speed input for the control. This shaft along with the associated hardware adds considerably to the weight penalty.

The questionable reliability and the engine tower shaft requirement makes the flyball-type sensor undesirable compared to the electronic systems that were studied, even though the mechanical governor came out with the higher point total.

Torque Motor-Controlled Servo With LVDT Feedback

The torque motor LVDT system, as shown in Figure 41, operates on a voltage amplitude principle. A magnetic speed pickup on the engine converts engine speed (N_G) through the proper electronic circuitry into a voltage. The voltage, through an amplifier, controls the displacement output of a torque motor. The displacement of the torque motor acting on a flapper valve controls the position of the N_G servo. Feedback is accomplished with an LVDT. Voltage output from the LVDT is controlled by the N_G servo position. The voltage from the LVDT nulls the magnetic pickup voltage and returns the torque motor to null.

The part of the total system error contributed by the torque motor and LVDT is relatively small compared to the error contributed by the voltage regulator. Voltage can be regulated to only ±3%. Since the system operates on voltage amplitude, the ±3% of voltage is directly a speed error. Improving this results in an exorbitant increase in cost. Therefore, this system is also not suited for the proposed control.

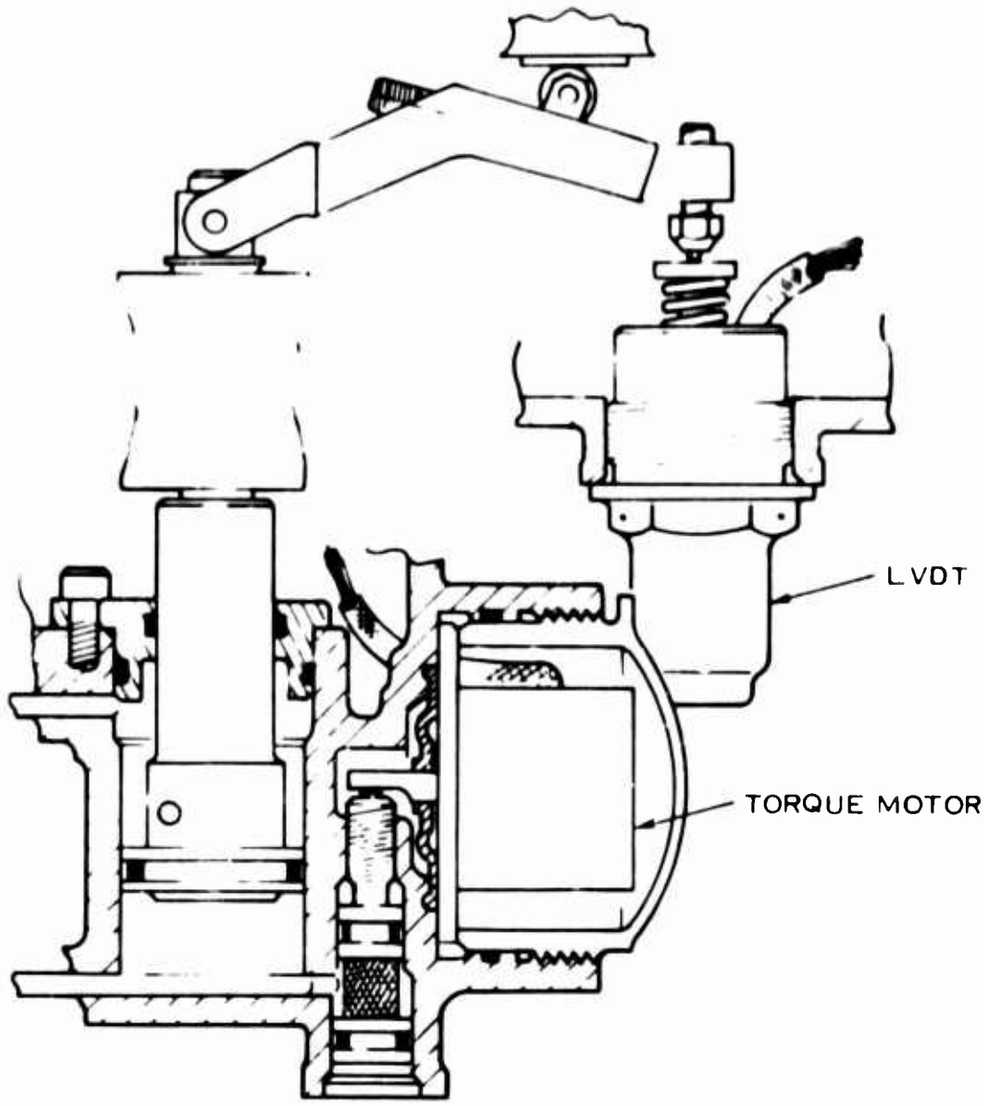

WEIGHT – 1.6 LB
VOLUME – 20.6 IN^3

Figure 11. Implementation Sketch of Electronic LVDT-Type N_G Speed Governor.

Torque Motor Controlled Servo With Resolver Feedback

The torque motor resolver system, as shown in Figure 42, operates on a voltage phase shift principle. A magnetic speed pickup on the engine converts speed into a pulse width signal. Through the necessary electronics, the pulse width signal displaces the torque motor and translates the N_G servo. Feedback is accomplished with a resolver. Output from the resolver is a phase shift width. This width nulls the pulse width speed input signal and returns the torque motor to null.

Using this phase shift principle eliminates the voltage amplitude error of ±3% caused by the voltage regulator. Therefore, the resolver system accuracy is greatly improved over that of the LVDT system. This system, due to its accuracy and simplicity was selected for the control application over all the other systems. The only drawback with this system seems to be the reliability that is associated with electronics operating in flight conditions. However, the electronic components necessary for the N_G system are common and have service experience. Electronics experience has shown poor reliability of the leads between the components. However, advanced electronic technology is showing that this reliability can be greatly improved by using metal oxide semiconductors combining many functions in one common chip, thus significantly reducing the number of leads.

Voice Coil-Spring Feedback

A new type of servo control system studied is the voice coil-spring feedback system as shown in Figure 43. The voice coil is comprised of a permanent magnet and an electrically excited coil. A magnetic pickup on the engine through appropriate electronic circuitry converts engine speed into voltage. The voltage excites the voice coil and causes an increased force output from the coil. The force output acts on the same type of servo system that the flyball sensor force acts upon. The problem is that for a reasonable size, the output force from the coil is very small. Small system input force presents serious problems with the system spring rate and stability that cannot be solved without increasing the operating force. Consequently, this system could not be made to work without increasing the weight considerably; i.e., voice coil weight had to be increased for more output force.

Fluidic N_G System

The fluidic speed system positions a servo piston and three-dimensional cam as a function of $N_G/\sqrt{\theta_{T2}}$, as shown in Figure 45. Pressure pulses from

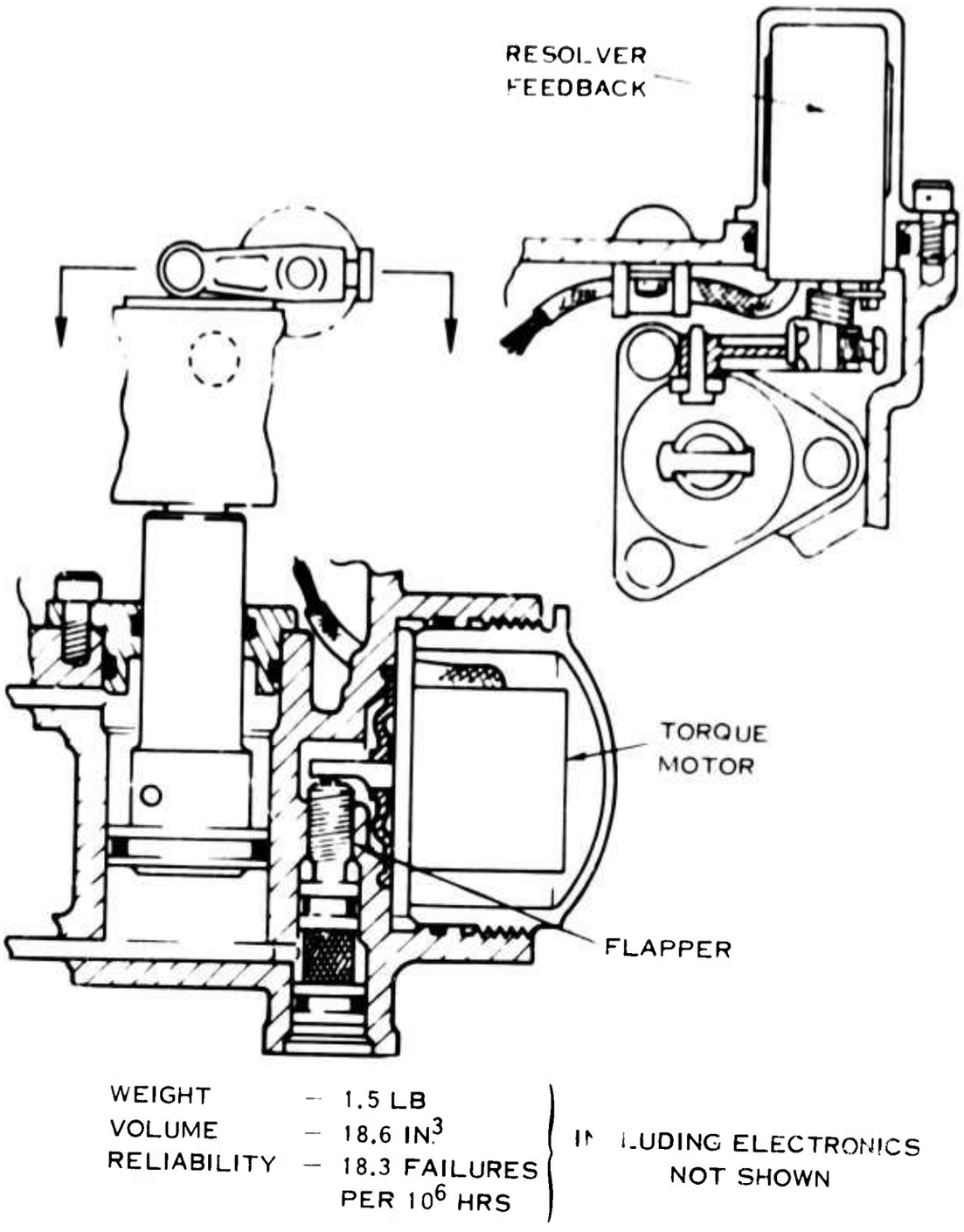

Figure 42. Implementation Sketch of Electronic Resolver-Type N_G Speed Governor.

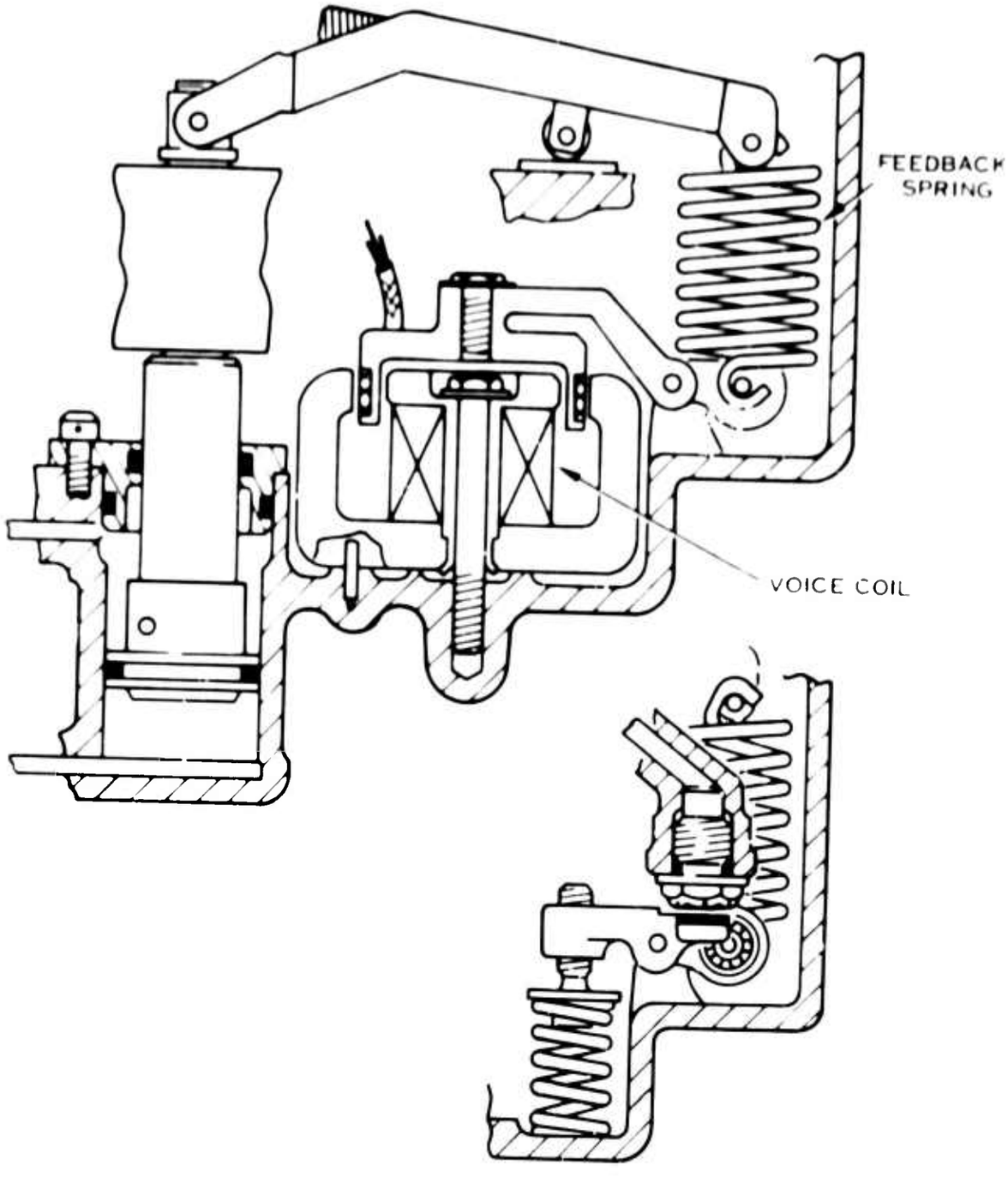

Figure 13. Implementation Sketch of Electronic Voice Coil-Type NG Speed Governor.

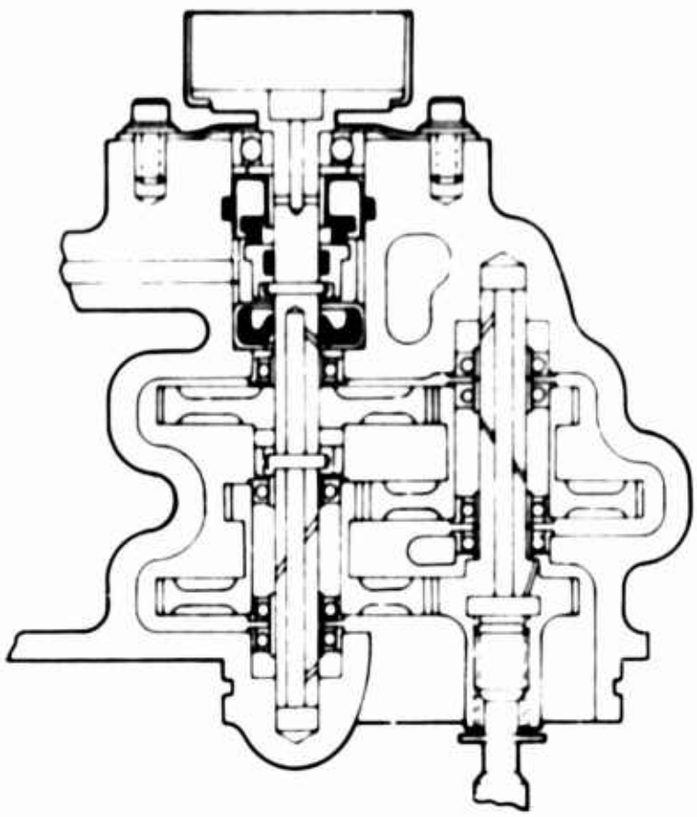

Figure 44. Implementation Sketch of Hydromechanical N_G Speed Governor Gearbox.

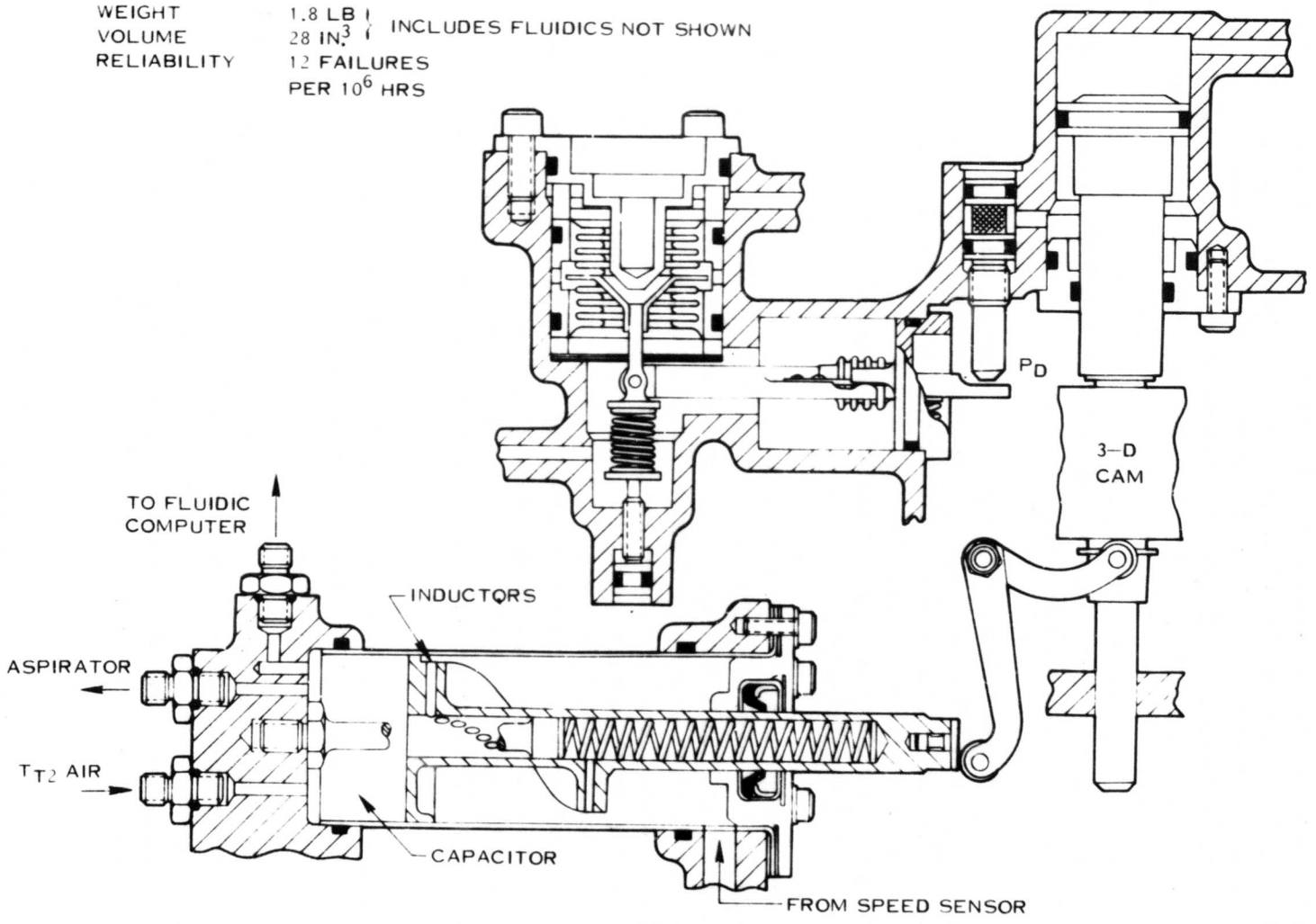

Figure 45. Implementation Sketch of Fluidic N_G Speed Governor.

a shaft-mounted chopper are applied to a Helmholtz resonator which is purged with T_{T2}. A phase discriminator circuit compares the chopper input to the natural frequency of the Helmholtz resonator and, from these AC fluidic signals, produces a differential pressure proportional to the frequency difference. The differential pressure is sensed by a bellows which in turn actuates a hydraulic flapper valve to position the servo piston. Feedback is accomplished by varying the volume (capacitance) and inductance of the Helmholtz resonator. System null is achieved when the natural frequency of the resonator equals the chopper input frequency.

A major problem encountered in the fluidic N_G system results from the need to vary the resonator frequency over a 10:1 speed range, requiring a 100:1 change in resonator volume. Some relief is obtained by simultaneously varying the inductance as accomplished in the proposed system, however, system gains at high speed remain considerably less than desired resulting in poor high-speed accuracy.

The basic requirement for accuracy of this governor is ±0.5% at 100% speed. This system was sized to reasonable dimensions and found to be at best a ±1.1% governor. A close review of the error contributors indicates that temperature effects within the resonator chamber (varying the resonant frequency and hence the set frequency) are the most significant. These errors are caused by three factors: first, the temperature variation caused by the driver gas which is basically compressor discharge air; second, the effects of ambient air or fuel around the chamber; and third, temperature effects on the fluidic circuitry causing extraneous errors. These errors can be reduced by using large amounts of T_{T2} purge air in the chamber at the expense of bleed air from the engine as summarized in Appendix III of this report

In addition to the basic accuracy problems, it was found that due to limited P_{T3} pressure available at low speeds from the compressor, operation of the governor could be limited at altitude to a 50 to 100% range.

Although the fluidic speed governor cannot be justified for selection at this time, if the requirement to eliminate the speed drive proves to be reasonable, the system does show promise. One major advantage to the use of fluidics in this loop is the inherent redundancy that is gained in a hybrid control with an electronic N_F governor in the event of an electrical power failure.

Considerable effort was put into the fluidic governor study, and, while preliminary solutions to some of the problems are shown in this report,

it is believed that the surface of a new technology has just been scratched and that further effort in this area would prove fruitful.

N_G Speed Governing Conclusion

As the trade-off chart (Table XIX) indicates, the hydromechanical sensor with the gearbox is the best overall system of those studied. However, the electronic system incorporating the resolver was the one chosen for the proposed advanced control system because of

1. The desire to eliminate the mechanical speed input to the control and the engine tower shaft

2. The desire not to draw off lubrication from the engine to supply the gearbox for the hydromechanical control

3. The lack of experience necessary to predict the reliability of a high-speed gearbox

4. The belief that development within the next few years will greatly improve the reliability of electronic components

An interesting fact is that at speeds of less than 10,000 rpm, there would be no question regarding which sensor was the most suitable. The hydromechanical flyball type far exceeds both the electrical and the fluidic in terms of cost, reliability, and accuracy at lower speeds.

It is evident from this study that extremely high speed operation of the mechanical components in today's fuel controls is not feasible. Since the trend of increasing maximum speed in future engine design continues, it is strongly recommended that programs be initiated to study the effects of operating mechanical components in fuel at high speeds and that further work be done on electronic and fluidic speed-sensing techniques.

N_F Overspeed Technology Selection

The desired characteristics of an overspeed sensor which were pertinent in selecting the technology approach for this application are:

1. Accuracy - generally better than ±1% of set point

TABLE XIX. N_G SPEED SYSTEM TRADE-OFF CHART

Criterion	Factor	Hydro-mechanical	Fluidic	Electronic
Schematic	-	Figure 33	Figure 34	Figure 50
Accuracy 35% N_G	-	± 0.82% N_G	± 1.65% N_G	± 1.75% N_G
100% N_G		± 0.24% N_G	± 1.10% N_G	± 0.615% N_G
Size/Weight	20	17.5	16	20
Vulnerability	15	14.4	12	12.6
Cost	10	10	6	7.3
Reliability	10	10	8	7.2
Contamination Tolerance	5	5	3	5
Maintainability	5	4	5	4
TOTAL	65	60.9	50	56.1

2. Temperature characteristics - must maintain accuracy over a range of temperatures

3. Shock and vibration capabilities - function properly with 20g shock and 20g peak acceleration up to frequencies of 1000 Hz

4. Low-speed checkout capability - all components must be checked in low-speed setting (85 to 95% rated speed). Should be adaptable to normal pre-flight checkout procedures

5. Speed sensing - the speed signal should be derived directly at the shaft where overspeed protection is required. Shaft mounted portions of sensor should be passive and simple in construction to be compatible with rotational speed

6. Time response - generally better than 50 milliseconds.

7. Speed range - sensor must retain proper discrimination from zero speed to speeds 30% greater than set point.

8. Power supply - the prime power supply for the overspeed sensor should be independent of the prime supply for the main fuel control system.

9. Weight and cost - protective or backup systems in general must have significantly lower cost and weight than the prime system.

The hydromechanical implementation of N_F overspeed consists of a remote N_F governor which produces a metered pressure proportional to speed as shown in Figure 33, the pure hydromechanical control implementation schematic. This pressure is supplied to a bellows and spring assembly in the main control which dumps the pressure behind the regulating valve, thus reducing fuel flow to zero. This system weighs 1.2 pounds.

The fluidic schematic is shown in Figure 50, the final hybrid control schematic, and utilizes a high speed fluidic pulse pickup directly on the shaft to measure N_F frequency. This frequency is compared with a reed resonator frequency to establish an error signal as described in Appendix I of this report. This system weighs 0.4 pound.

The electrical overspeed system consists of a two-position solenoid which would be placed in the N_F servo line between the N_F torque motor and the N_F servo. The overspeed electrical on-off signal from the electronic N_F sensor would open the metered pressure side of the N_F servo to drain, driving the control to idle power. This system would weigh 0.6 pound.

A review of the technology trade-off chart for N_F overspeed selection (Table XX) indicates that the fluidic and electrical versions are close in relative totals. However, the decision as to which to use should be made in favor of the fluidics with the use of an electrical N_F power turbine control. This allows for complete redundancy within the control for this function.

Metering Valve Study

The control specification requires that fuel be metered down to 15 pph. This is unique in that previous fuel control designs have never been required to meter fuel at such low levels. The specification also requires a reasonable degree of accuracy for metered fuel flow at different engine operating conditions. The most

TABLE XX. N_F OVERSPEED TECHNOLOGY TRADE-OFF CHART

Criterion	Factor	Hydro-mechanical	Fluidic	Electronic
Schematic	-	Figure 33	Figure 50	
Accuracy	-	± 1.2%	± 1.0%	± 0.6%
Size/Weight	20	7	20	15
Vulnerability	15	5	11	13
Cost	10	7	8	10
Reliability	10	10	8	6
Contamination Tolerance	5	4	3	5
Maintainability	5	5	5	4
Totals	65	38	55	53

stringent accuracy requirement occurs when the control is on deceleration limiting at low flows (near 15 pph for regenerative engine and 36 pph for base engine). The maximum error allowed at this condition is ± 1.0 pph for both base and regenerative engines. This error must include throttle valve positioning, throttle valve leakage, P_{T3} sensing, ΔP regulation, cam tolerances, and linkage friction.

Present-day throttle valve accuracies were found to be intolerable for this application. The main contributor to this relatively poor accuracy was fuel leakage across the metering windows. A design objective for this metering valve was then to either minimize or eliminate this leakage error. Also, because the specification noted the desire to eliminate the mechanical speed input for the control, the throttle valve had to be servo operated rather than rotated.

Of the throttle valve concepts studied, one exhibited a definite possibility for meeting these requirements. This concept was the shear-plate-type throttle valve. This concept not only eliminated the troublesome leakage error but also resulted in a low volume and very low weight valve configuration.

The shear plate concept and the other valve concepts studied are explained in the following discussion.

Nonrotating Spool Type

The spool valve is the type that has been most widely used in low-flow throttle valve applications to date. The most significant cause of error associated with this type of valve is the fuel leakage through the diametral clearance between the piston and the sleeve. If the fuel leakage would remain relatively constant, as it does at constant temperature, the error could be adjusted out. However, due to the temperature range that the control has to operate within, the fuel viscosity varies enough to cause varying leakage through the constant clearance. For a typical spool valve configuration, as shown in Figure 46, the fuel leakage is more than $\pm$ 1 pph for a $\pm$ 130^{o}F temperature variation. A diametral clearance of 0.0002 to 0.0006 inch is about the best that can be expected using present manufacturing techniques without an exorbitant increase in cost.

The leakage error combined with the other errors at the deceleration limiting condition results in a total error that does not meet the control specification of $\pm$ 1.0 pph even with the most optimistic assumptions.

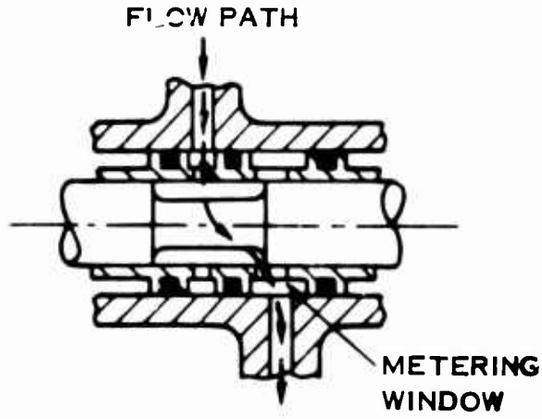

Figure 46. Spool Valve Type Metering Valve.

Rotating Spool Type

The rotating-type valve has the same metering configuration as the non-rotating valve. The fact that the rotating piston tends to center itself in the sleeve allows us to assume for accuracy considerations that the piston is concentric to the sleeve. This assumption reduces the theoretical leakage by a factor of 2.5. However, even with this reduction, the leakage error is a significant contributor to the total error, making the valve unsuitable for this application.

Another drawback associated with the rotating spool valve is the necessity for steel parts for wear resistance. Also, a mechanical speed input is required to rotate the piston, resulting in a significant amount of added weight and volume.

Flapper Valve Type

Flapper valves have been used by Hamilton Standard for many years to control a metered hydraulic pressure for the operation of servo operated systems. In recent applications, however, the flapper valve has been used as a fuel flow metering device. In this application the flapper valve, as shown in Figure 47, is part of a closed-loop system with the engine. Gross nonlinearities associated with the flapper valve are automatically corrected for in a closed-loop system. If the flapper valve were used in a scheduling system, however, the nonlinearities would result in metered flow error, and consequently the system would have very poor accuracy.

Another reason the flapper valve type throttle valve is not suited for this control is that at minimum flows the flapper gap becomes extremely small (less than 0.001 inch). This presents a severe problem when contaminated fuel is used.

Plug Type

The plug-type throttle valve minimizes the nonlinearity error associated with the flapper valve. It does this by providing a conical surface that can be contoured to compensate for the nonlinearity. However, this contoured plug leaves something to be desired for a production piece of hardware.

The small gap that occurs with the flapper valve at minimum flow also occurs with the plug valve, causing a fuel contamination problem.

Figure 47. Flapper Valve Type Metering Valve

C_D variations also tend to cause more error with the plug type valve than with other valves. The flow tends to remain laminar through the valve, a condition that causes large C_D variations. This configuration is shown in Figure 48.

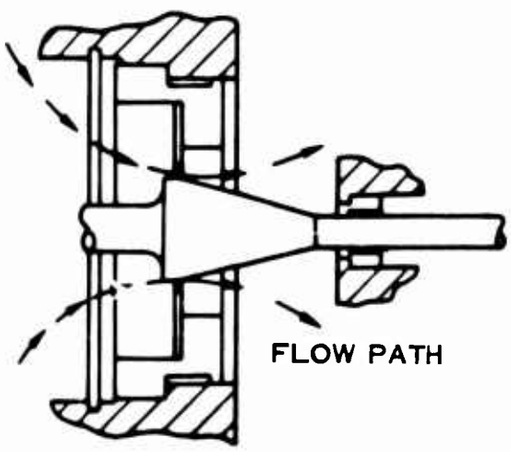

Figure 48. Plug Valve Type Metering Valve.

Shear Plate Type

Of all the throttle valve concepts studied, the shear plate type showed the most promise for metering to the established control requirements. The basic concept is described in Figure 49. Two relatively smooth plates (development is required to determine the optimum surface finish) are held in contact with one another by a normal force supplied by the flexure spring. Since the plates are in contact, fuel will flow only through the slot in one of the plates and not between the plates, thereby reducing the clearance of the leakage path to the microfinish of the contacting surfaces. The resulting leakage error is negligible. The flow is controlled by positioning one plate over the other, varying the length of the slot.

C_D variation can be held to a minimum by controlling the edge configuration on both plates.

The weight of the valve can be significantly reduced by manufacturing only the plates out of steel to resist wear and by manufacturing the piston and servo out of aluminum.

This throttle valve concept has been incorporated in the final hybrid control arrangement drawing shown in Figure 51.

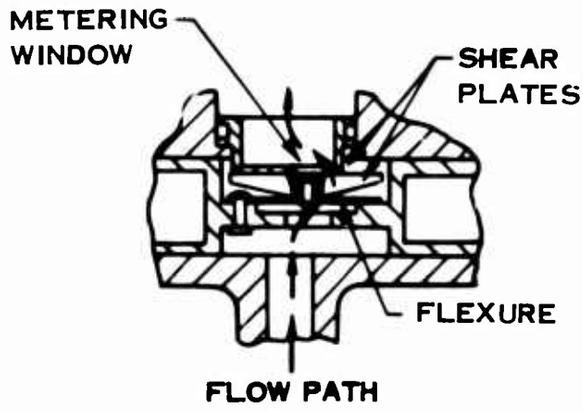

Figure 49. Shear Plate Type Metering Valve.

Technology Review Conclusions

It is apparent from the previous sections on subsystem and component trade-offs, in addition to the pure technology trade-offs, that each technology can do certain aspects of the total control system job better than others. This leads to the conclusion that a form of hybrid control, combining the best portions of each technology, should result in a better overall control. Therefore, a summary of the positive attributes of each should outline the basic type of hybrid to be constructed. The following is the list of key conclusions from the trade-off studies:

1. The three-dimensional cam is the most efficient and accurate way to schedule bivariate functions.

2. The reliability of a hydromechanical control is the best of the technologies.

3. High load actuators (variable geometry and power turbine stator) are best executed hydromechanically.

4. High speed sensing (55,000 to 75,000 rpm) should be done electrically.

5. Power turbine governing with accuracy requirements of ±0.5% speed should be done electrically.

6. Dynamic compensation (lead/lag) is easily accomplished electrically with a minimum weight penalty.

7. Power turbine torque limiting and torque sharing should be accomplished electrically due to significantly better accuracies and ease of interfacing with present-day state-of-the-art torque sensors.

8. Absolute pressure sensing should be done hydromechanically.

9. Turbine inlet temperature sensing can be accomplished, but accuracy and time response limitations with available sensors restrict their use to maximum limit devices.

10. N_F overspeed sensing should be accomplished by fluidics for small size and redundancy advantages.

A hybrid control with all of these features results in a better overall control than any of the pure technology approaches, as shown in Table XXI. However, it can be seen that the hybrid control does not always exceed a specific technology in all areas.

TABLE XXI. TECHNOLOGY TRADE-OFF CHART FOR COMPLETE CONTROL SYSTEM INCLUDING HYBRID

Criterion	Factor	Hydromechanical	Fluidic	Electronic	Hybrid
Schematic	-	Figure 33	Figure 34	Figure 35	Figure 50
Accuracy	-	Table XI	Table XI	Table XI	Table XXII
Size/Weight	20	13.5	14	20	17.5
Vulnerability	15	9.5	10.5	12.5	13.5
Cost	10	10	6	6	8
Reliability	10	10	8	4	8
Contamination Tolerance	5	4	2	5	5
Maintainability	5	4	5	4	4
Totals	65	51.0	45.5	51.5	56.(

DEFINITION OF THE EVOLVED HYBRID CONTROL SYSTEM

The results of the mode and technology studies discussed in the preceding sections indicate the reasons why a hybrid technology control with a multiple or hybrid mode is the optimum combination for the specific objectives set up in this program. However, to be sure that such a control could be packaged effeciently without being burdened with too many complicated interfaces, the control recommended was completely concept designed and arranged. This resulted in schematics, packaging drawings, accuracy studies and influence coefficient studies - all of which are summarized in the following section.

Functional Description of Base Engine Control

The following section describes the operation of the proposed hybrid advanced control system. Reference is directed to Figure 50, the hybrid control schematic, to assist in understanding the description.

Fuel Flow Controlling Elements

These components directly affect the major fuel flow path.

Filter

Fuel entering the control from the pump first encounters the filter assembly. Fine filtered flow passes through the cone-shaped 40-micron filter, while the main bulk of the fuel flow passes alongside the filter walls. The flow annulus is controlled to create a high-velocity wash action of the filter, resulting in approximately 20-micron effective filtration in the servo supply. In case of filter clog-up, a ball-relief valve is provided to maintain flow to the servo supplies.

Servo Supply Regulator (P_R Regulator)

This regulator provides a constant servo supply pressure to maintain adequate control accuracy and dynamic response. The valve has drain pressure plus a spring force acting on one end and the regulated pressure acting on the other end. Regulated pressure reaches the end of the piston through a lapped fit which provides the necessary damping for stability. The metering window in the center of the valve is arranged such that whenever the regulated pressure is in error, valve stroke will remove the error.

Throttle Valve

The throttle valve is the engine fuel flow metering element. Rate of fuel flow is controlled by varying the size of an orifice while maintaining a constant pressure drop across the orifice. A rectangular window is cut into a stationary block, while a spring-loaded plate guided in the valve body slides against the block and changes the area exposed to fuel flow. The throttle valve servo is a half-area servo with metered pressure acting on the spring end of the valve and servo supply pressure on the half-area. Pressure in the main fuel flow path is balanced inside the valve. A fixed orifice and flapper nozzle in the valve body modulates servo pressure to position the valve, and this position is fed back to the multiplying system by the spring. An adjustable minimum fuel flow stop is also provided.

Pressure-Regulating Valve

The pressure drop across the throttle valve is maintained at a constant 40 psi by the pressure-regulating valve. It accomplishes this function by sensing the pressure drop across the throttle valve metering window and bypassing flow as required to hold this value essentially constant. The mass rate of fuel flow is temperature-compensated by the bimetallic disc which trims the loading spring height. The regulating valve is positioned by upstream throttle valve pressure acting on one end, a spring force and downstream pressure acting on the other end, and a hydraulic flow force acting on the valve buckets. The flow buckets are designed such that the flow force nominally compensates for spring load changes as the valve takes different positions.

Windmill Bypass and Shutoff Valve

This valve effects a positive metered fuel flow shutoff and recirculates the flow that the control continues to meter while the engine windmills. When the control is on, a spring drives the valve open to allow flow to pass to the engine. During shutoff, a lever driven by the power lever cam strokes the valve against the spring load. A radial seal on the valve then passes over the outlet port and effects shutoff, while a face-type poppet seal opens to achieve bypass.

Minimum Pressurizing Valve

Fuel pressure is maintained at a minimum of 200 psi above drain pressure by the pressurizing valve in order to atomize fuel properly in the engine burner nozzles and to provide power to operate the control

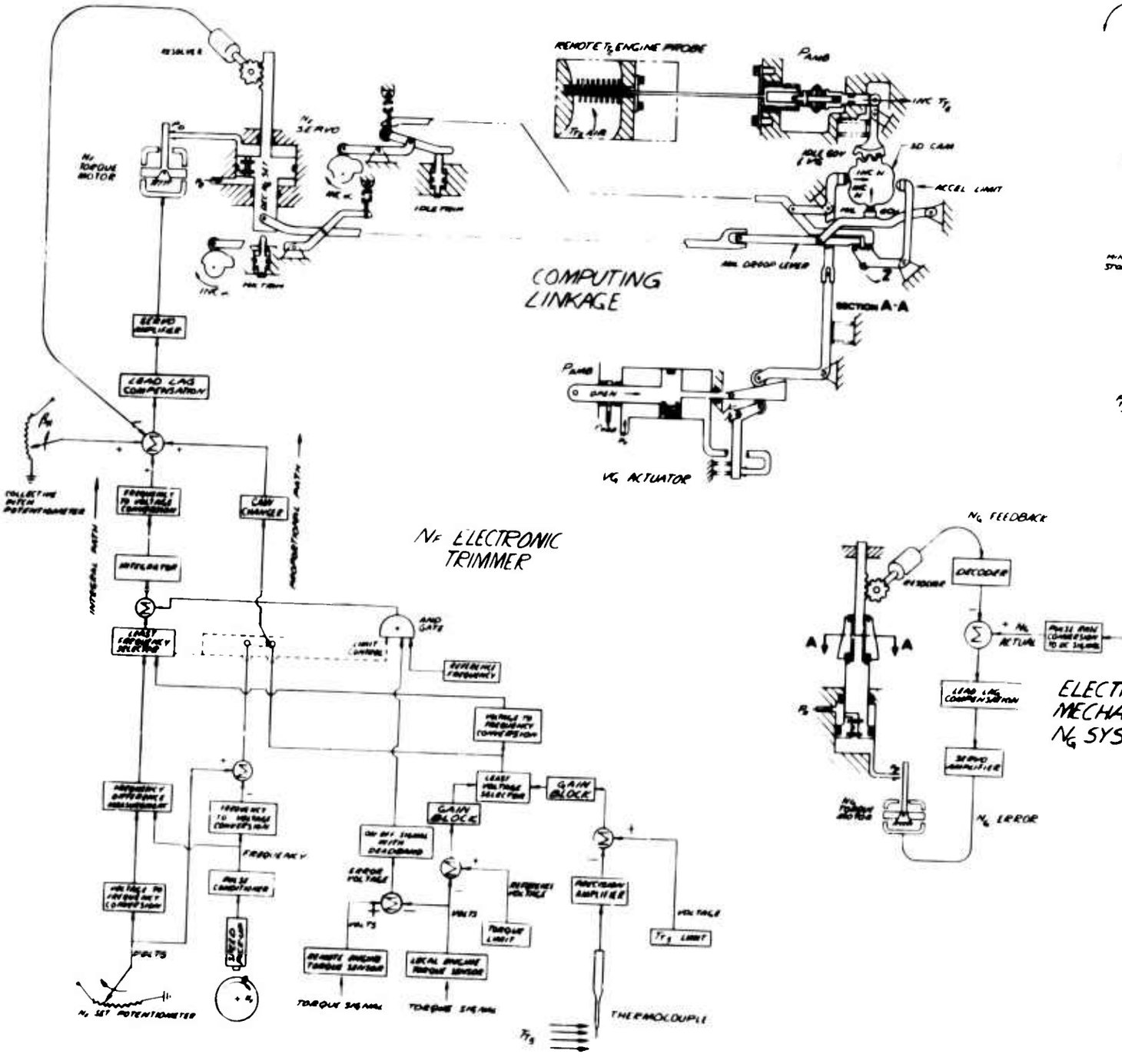

Figure 50. Final Hybrid Control Schematic.

MAIN FUEL FLOW CONTROLLING ELEMENTS

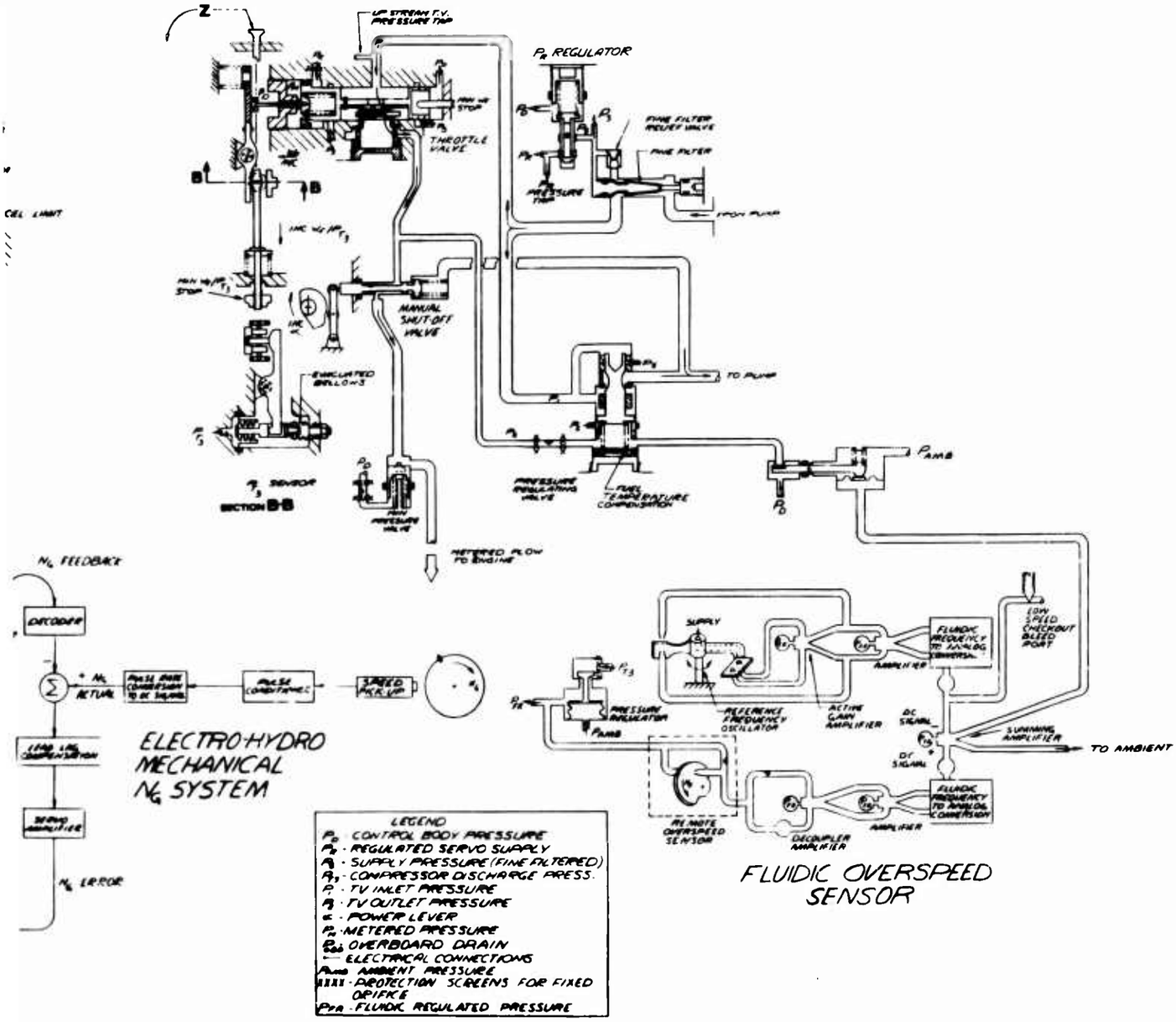

ELECTRO-HYDRO MECHANICAL N_G SYSTEM

FLUIDIC OVERSPEED SENSOR

LEGEND

- P_D CONTROL BODY PRESSURE
- P_R - REGULATED SERVO SUPPLY
- P_1 - SUPPLY PRESSURE (FINE FILTERED)
- P_{T_3} - COMPRESSOR DISCHARGE PRESS.
- P_1 - TV INLET PRESSURE
- P_2 - TV OUTLET PRESSURE
- α - POWER LEVER
- P_M - METERED PRESSURE
- P_{OB} OVERBOARD DRAIN
- ELECTRICAL CONNECTIONS
- P_{AMB} AMBIENT PRESSURE
- XXXX - PROTECTION SCREENS FOR FIXED ORIFICE
- P_{FR} - FLUIDIC REGULATED PRESSURE

B

servos. As back pressure from the engine nozzles increases, the valve opens completely and affords no restriction to flow. An orifice in the line on the reference side of the valve stabilizes this system.

N_G Servo System

This system provides the control with an indication of engine gas generator speed. It consists of a speed sensor, electronic system and electrohydraulic servo.

N_G Sensor

A magnetic N_G speed sensor is located adjacent to a rotating engine element. Once per rotation, a pulse is produced in the reluctance pickup and transmitted to the electronic system.

Electronic System

In the electronic system, the train of pulses from the pickup is converted into a digital number, then into a pulse-width modulated signal and finally into a DC signal. The pulse rate to digital conversion is accomplished by a counter that is activated for a constant time interval during every measuring cycle. To obtain the digital-to-pulse width conversion, the contents of the counter are transferred to a buffer. After the transfer, a new counting cycle starts. The buffer is interrogated during every output pulse of the digital-to-pulse-width converter, and its contents are loaded into a second counter. The output binary element is activated during the down count of the second counter. The pulse-width-to-DC conversion is accomplished by using the pulse-width modulated signal to chop a precision reference voltage signal, then filtering the chopped signal.

Electrohydraulic N_G Speed Servo

The DC signal obtained in the electronic section is used to drive a servo loop and position the N_G servo proportional to gas generator speed. The drive signal is compared with the servo position signal; the difference is passed through a lead/lag compensation to filter out high-frequency noise signals, then through a power amplification stage whose output drives a torque motor. The torque motor drives the flapper amplifier, which meters flow to the servo piston. Translation of the servo piston is sensed by a resolver whose output, converted to a DC signal, becomes the servo position signal in the feedback path. A three-dimensional cam is mounted on the N_G servo. This cam is translated by the

speed servo and rotated by the T_{T2} system through a gear on the cam. Computing signals, extracting from the three-dimensional cam, are: acceleration W_f/P_{T3} schedule, military and idle droop governing bias, and variable geometry actuator schedule.

T_{T2} Sensing System

This system provides the fuel control with an indication of compressor inlet temperature. A liquid-filled bulb is located at the engine inlet, and, as inlet air temperature varies, the specific volume of the enclosed liquid changes. Since the bulb is rigid, volume changes are transferred to the control-mounted bellows via the capillary tube. Fins and thin-wall construction of the bulb are utilized to provide rapid response to temperature changes. As liquid is transferred to or from the bulb, the bellows changes length and causes the linkage to rotate the three-dimensional cam. A spring is utilized to load the system into the bellows.

P_{T3} Sensor and Multiplication System

This system performs the computation of desired fuel flow using inputs of W_f/P_{T3} and P_{T3}.

P_{T3} Sensor

The P_{T3} sensor consists of a motor bellows and evacuated bellows set connected by a pushrod. Both bellows are referenced to drain pressure and use of the evacuated bellows allows measurement of absolute engine burner pressure. The net force produced by the bellows is transferred to the multiplying linkage by the bellows output lever.

Multiplying System

The multiplying system accomplishes the computation $W_f = W_f/P_{T3} \times P_{T3}$. The system functions by balancing torques on both sides of the multiplying lever. On one side roller position, proportional to desired W_f/P_{T3}, establishes a distance from the fixed pivot. Force, proportional to P_{T3}, is applied to the rollers at that point. This creates a torque proportional to desired fuel flow. On the other side of the multiplying lever a spring force, proportional to actual fuel flow, is entered at a fixed-moment arm. The flapper-nozzle opening is modulated by the force-balance linkage and the system is set

up such that a unique throttle valve position results for every combination of W_f/P_{T3} x P_{T3}. A minimum W_f/P_{T3} stop is included on the roller pushrod.

N_F Electronic Trimmer

There are three loops incorporated in the trimmer section: the power turbine governing loop biased by the torque sharing error signal, the temperature-limiting loop and the torque-limiting loop. Of these three, only one is active at a time, the one demanding the lowest N_G speed. The selected error signal is passed through a proportional and an integral path to provide both speed of response and steady-state accuracy. The outputs of the two paths are filtered and summed with the collective pitch anticipating signal. The result is proportional to the desired N_G required by the trimmer. It is converted into a mechanical displacement by an electrohydraulic servo.

Power Turbine Governing Loop

The speed of the power turbine is compared with a reference signal, and the difference between the two is the error of the power turbine governing loop. The actual turbine speed is sensed by a reluctance pickup, which provides a pulse train with a frequency proportional to the turbine speed. The reference signal, also a pulse train, is obtained from a potentiometer and voltage controlled oscillator (VCO) unit mounted in the cockpit. The power turbine loop provides optional control authority; i.e., it cannot obtain a gas generator speed higher than that requested by the power lever. When the speed control loop is active, the control will integrate until it eliminates the N_F speed error. Therefore, isochronous power turbine governing is provided within the physical limits of the components of the loop.

Exhaust Gas Temperature Limiting (T_{T5})

T_{T5} is sensed by a set of thermocouples located in the engine gas stream. The thermocouple output voltage is amplified and compared with the limit reference in an analog differential amplifier, and the resulting difference signal is passed to the analog-least selector.

Torque Limiting

Overtorque protection is provided by the torque-limiting loop. The torque signal is compared with the torque-limit reference signal in

an analog differential amplifier, and the resulting error signal is passed to the analog-least selector.

Torque Sharing

Load sharing is provided for dual-engine applications. The torque signals of the local and of the remote engines are compared and the resulting error is passed through a nonlinear element to provide on-off characteristics with dead band, which is necessary for stability. When the error exceeds the dead band it enables a pulse train to be added into the integrator, provided the trimmer is not in the limit mode. The torque sharing is inhibited in the limit mode to prevent impairment of the limiting action.

Collective Pitch Anticipation

The collective pitch anticipatory signal is obtained from a nonlinear potentiometer mounted on the collective pitch lever in the cockpit. The nonlinearity is designed according to the desired collective pitch schedule. The output of the potentiometer is added to the output of the proportional-plus-integral signal, with the resulting change in fuel flow helping to reduce the magnitude of the speed transients due to changes of turbine loading. The effect of the anticipatory signal is eventually eliminated by the integral action. Thus, the trimmer control prevents large speed fluctuations.

Electrohydraulic Servo

The DC signal, obtained in the electronic section, is used to drive a servo loop to generate a displacement proportional to the desired N_G speed. The drive signal is compared with the servo-piston signal, and the difference is passed through a lead/lag compensation to filter out high-frequency noise signals, then through a power amplification stage which drives the torque motor. The torque motor drives the flapper amplifier, which drives the servo piston. The position of the piston is sensed by a resolver and the output, converted to a DC signal, becomes the servo position signal in the feedback path.

Power Supply

The power supply generates four DC voltages, utilizing a constant current alternator as the power source. The alternator provides

unregulated AC power, which is rectified, filtered, and regulated to generate DC power as the first step in the regulation. This voltage is applied to a static inverter with secondary coils which yield the four regulated and constant-frequency AC voltages; these are then rectified, filtered, and further regulated to generate the precision voltages required by the control system. A constant-current alternator was chosen as the power source primarily because of its small size. A problem with this type of alternator is that the high source reactance results in voltage spikes when the load is suddenly reduced. Special protective measures are added to provide for this condition.

Pilot Inputs

Potentiometers are mounted in the aircraft cockpit to transmit electrical signals of collective pitch and desired N_F to the fuel control. The N_G desired and shutoff signals are transmitted mechanically to the fuel control power lever. For turboprop applications, a separate shutoff shaft will be required to separate the shutoff and N_G set linkage. For this condition, the shutoff shaft would be arranged concentric to the N_G shaft in the fuel control.

Variable-Geometry System

Variable-geometry actuator position is scheduled from the three-dimensional cam as a function of T_{T2} and N_G. A linkage system compares the input from the three-dimensional cam with actuator position using the actuator feedback cam. Any difference between scheduled and actual position deflects the flapper lever to port the flow to the actuator, correcting its position.

Acceleration-Limiting System

For the base engine, acceleration-limiting W_f/P_{T3} is scheduled from the three-dimensional cam as a function of T_{T2} and N_G. During accelerations, the military and idle governing links are able to increase ratio units only until the acceleration-limit lever contacts the three-dimensional cam.

N_G Governing System

N_G speed is controlled by the N_G governing system using inputs of power lever speed set, N_F trimmer demand, actual N_G and

T_{T2}. The military N_G power lever cam sets a maximum droop line which can be trimmed downward by the N_F trimmer. Set speed is compared with T_{T2}-biased actual speed on the military droop lever and the output applied to the acceleration limit lever. When the acceleration limit is reached, the tension spring is extended to absorb the excess linkage motion. In a similar manner, the idle-governing linkage sets N_G speed up to flight-idle speed. Externally adjustable military-speed and idle-speed trims are incorporated.

N_F Overspeed System

A fluidic N_F overspeed system is provided on the hybrid fuel controls. N_F speed is sensed and compared with a reference frequency. When N_F speed reaches the overspeed limit, a pressure signal is generated fluidically, which causes a drop in fuel flow. The system consists of a reference frequency circuit, an N_F sensed frequency circuit, a summing amplifier and a ΔP reset system.

Reference-Frequency Circuit

The reference-frequency oscillator consists of a torsional reed, which is excited by feedback from the active gain fluidic amplifier. A jet pipe mounted on the torsional reed directs its output at two receivers, which communicate with the control ports of the amplifier. The amplified signal is fed back as an exciting torque on the reed to sustain oscillation. The output of the oscillator is raised to the level required to drive the frequency-to-analog converter circuit by the next amplifier. Frequency-to-analog conversion is accomplished by first passing the flow through a fluidic flip-flop to convert the sinusoidal signal to a square wave, and then through two more amplifiers and capacitances to achieve pulse forming. The pulses are then filtered to give a DC signal, which is applied to the control port of the summing amplifier. A low-speed fluidic system checkout port is provided. By opening an orifice to vent, thus reducing the pressure, the reference DC signal can be made to simulate overspeed protection while at some safe operating speed.

A gas pressure regulator supplies regulated pressure to operate the fluidic system. P_{T3} air is bled off through an in-line regulator which maintains a constant supply pressure of 20 psig. A bellows has ambient pressure plus the bellows compressive spring force

acting on one side and the regulated pressure on the other side. Any force unbalance on the bellows, indicative of regulated pressure error, will change the poppet valve opening and remove the error.

N_F Sensed Frequency Circuit

The speed signal generator is a disc or drum mounted on a rotating shaft. The disc interrupts a jet of air, between a supply nozzle and receiver, once per revolution of the shaft. The resultant signal is a frequency equal to the shaft rotational frequency. The decoupler amplifier amplifies the AC signal and removes undesirable DC or extraneous, slowly varying, pressure signals that appear on the signal lines. The signal line is also pressurized through a dropping orifice from the supply to prevent ingestion of contaminants. The output of the decoupler amplifier is processed by a frequency-to-analog circuit and applied to the other control port of the summing amplifier in a manner similar to the reference circuit.

Summing Amplifier

The outputs of the two circuits are compared in a summing amplifier. The output of the summing amplifier is proportional to the difference between the reference frequency and the signal frequency. When the reference frequency is greater than the N_F speed frequency the output is vented. When the N_F speed frequency is greater than the reference frequency the polarity is changed and the output is applied to the diaphragm.

The fluidic operation of this amplifier is typical of the other amplifiers in this system in that a supply nozzle has its jet deflected proportionally to one or the other receivers by the relative magnitudes of the pressure in the control ports.

ΔP Reset System

The signal from the summing amplifier is applied to one side of a diaphragm. The other side of the diaphragm has a preload spring and ambient pressure applied to it. During overspeed conditions, the pressure signal from the fluidic computer strokes the diaphragm and linkage to open the flapper valve. Bleeding off the flow in the pressure regulating valve downstream sensing line creates a false throttle valve ΔP signal in a direction to reduce fuel flow. During nonoverspeed operation, the fixed orifice in the downstream sensing line serves to dampen the pressure regulating valve.

Physical Description of the Hybrid Engine Control System

The arrangement of the base engine hybrid fuel control, shown in Figure 51, consists of the following major components:

1. A main housing containing the hydromechanical elements and acting as the primary structure

2. An electronic computer package, which mounts on the side of the main housing and contains the electronic hardware and also supports the torque motors and resolvers

3. A fluidic computation package for the N_F overspeed system which mounts on the other side of the main housing

4. A linkage access cover

Cross-sectional views of important components are shown in Figure 52. These views show in detail how the control has been packaged, the density of packaging, and the interrelationship of some of the components.

The control is mounted on the engine by three pins. On one side, two concentric pins are connected to flanges on the engine case; on the other side, a drag link arrangement is planned. This system significantly reduces the overhung moment of the control and reduces the structure needed for mounting. Connections to the control include: fuel inlet, fuel outlet, fuel bypass, power lever, variable geometry and power turbine stator actuator outputs, electrical power supply lines, and the N_F overspeed signal.

One section of the main housing contains those elements directly concerned with the major fuel flow paths. These include: the filter, throttle valve, pressure-regulating valve, windmill bypass valve, minimum pressurizing valve, and servo supply regulator. Another section, surrounding the power lever and the N_G servo, comprises the linkage cavity. On one side, the linkage cavity is bounded by the electronic housing and affords a convenient region for electronic interfaces with the torque motors and resolvers. On the adjacent side, an access cover provides access to the linkage cavity.

The electronics package is contained in a housing that mounts the printed circuit support frames and electronic components and provides the required structural, radiation and thermal environments. Heat generated by the electronic circuits is transferred to the fuel in the drain cavity by conduction through the housings.

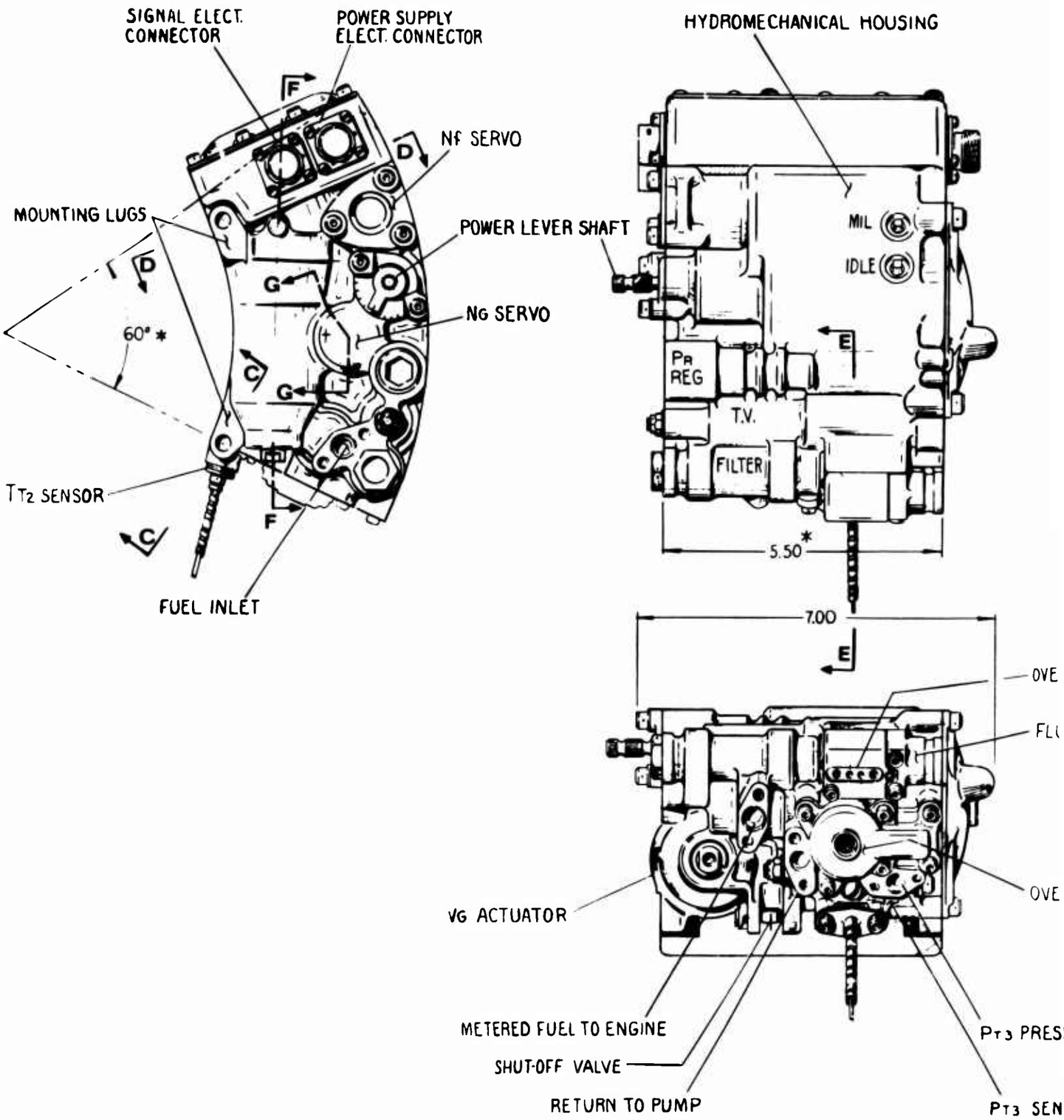

Figure 51. Final Hybrid Control Arrangement Drawing.

A

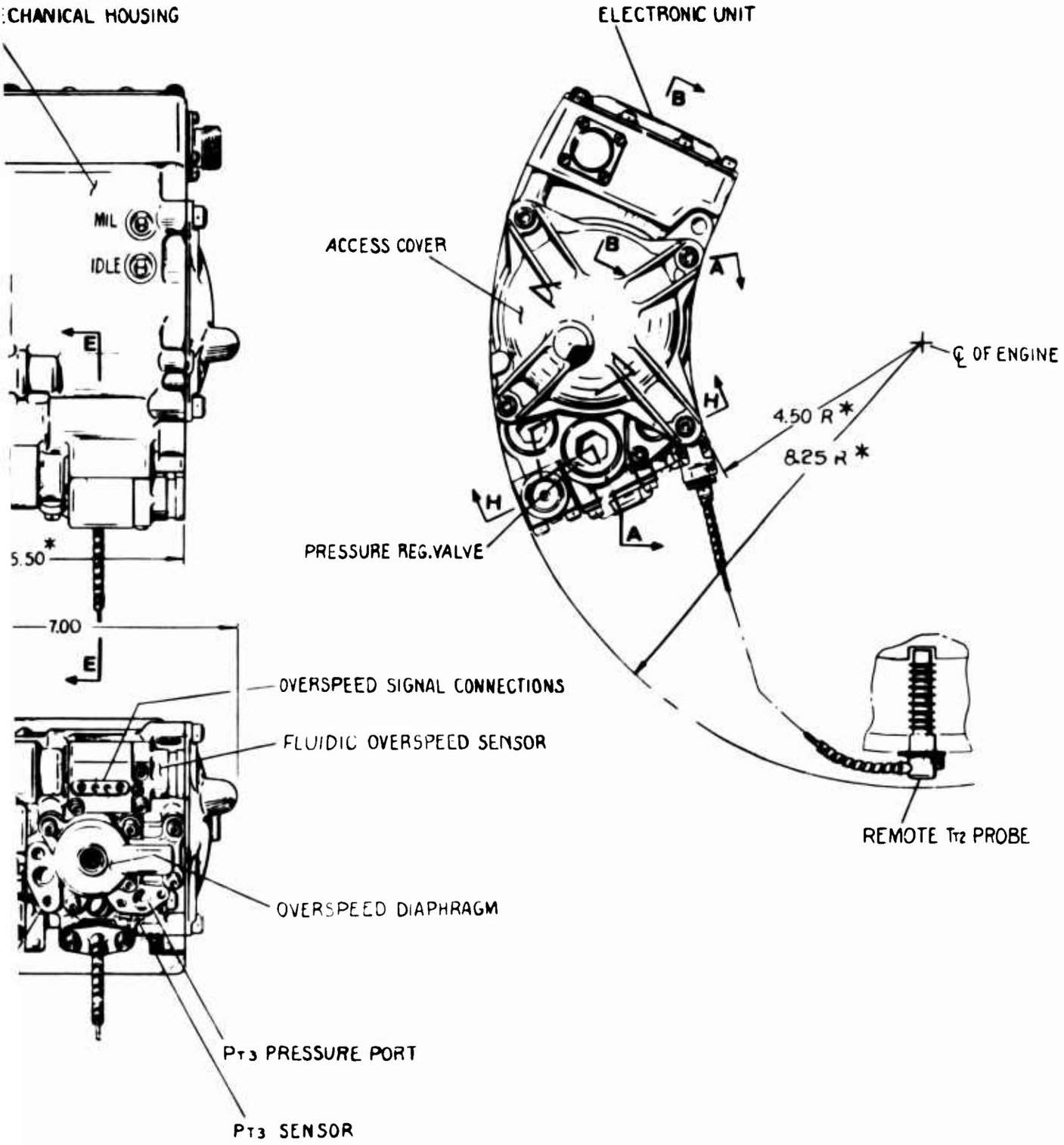
CHANICAL HOUSING
ELECTRONIC UNIT
MIL
IDLE
E
5.50 *
7.00
E
ACCESS COVER
B
B
A
H
H
A
PRESSURE REG.VALVE
℄ OF ENGINE
4.50 R *
8.25 R *
OVERSPEED SIGNAL CONNECTIONS
FLUIDIC OVERSPEED SENSOR
OVERSPEED DIAPHRAGM
PT3 PRESSURE PORT
PT3 SENSOR
REMOTE Tt2 PROBE

B

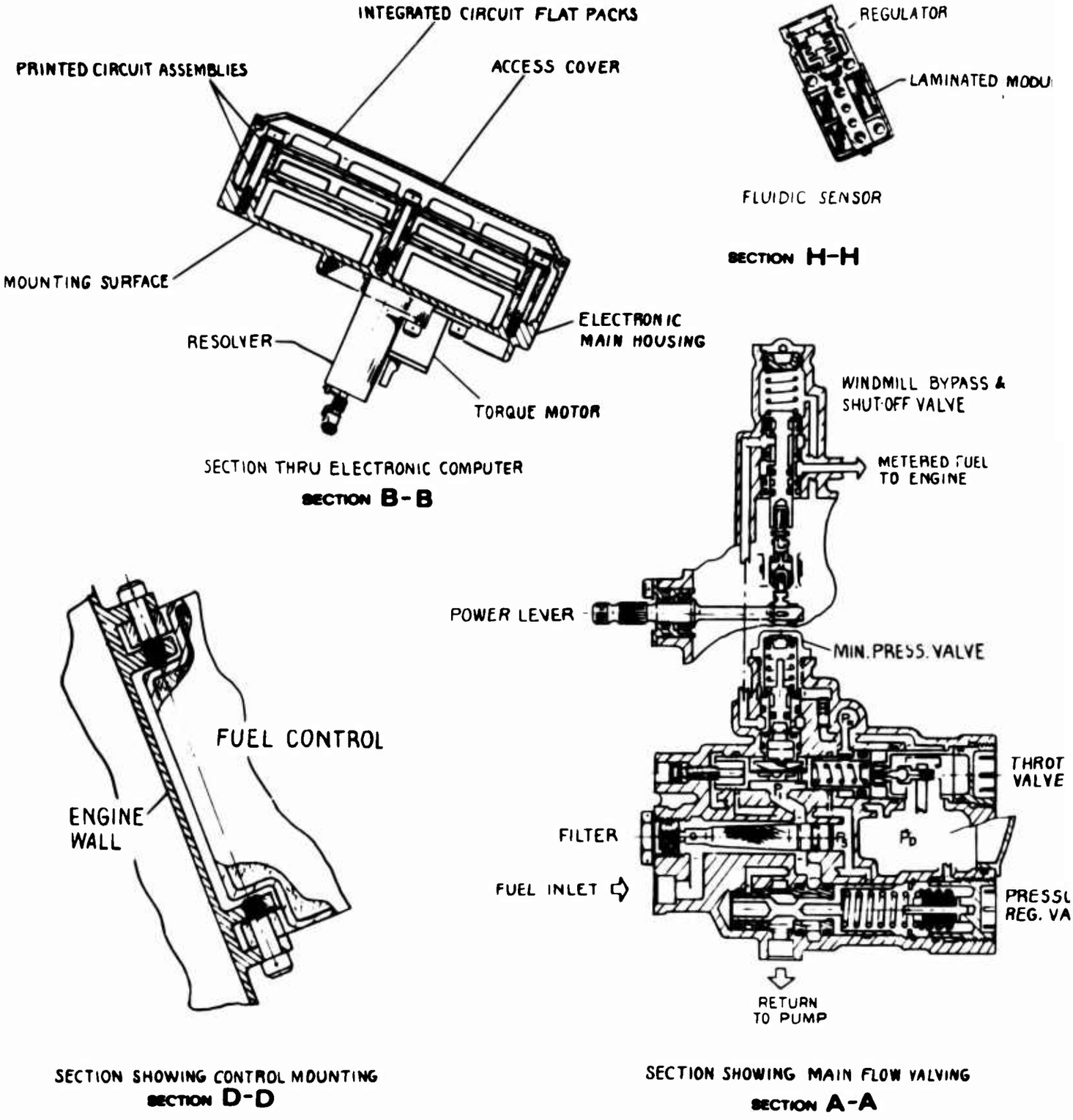

Figure 52. Final Hybrid Control Sectional Views.

A

EGULATOR

LAMINATED MODULES

R

MILL BYPASS &
OFF VALVE

METERED FUEL
TO ENGINE

RESS. VALVE

THROTTLE
VALVE

P_b

PRESSURE
REG. VALVE

VALVING

FUEL CONTROL

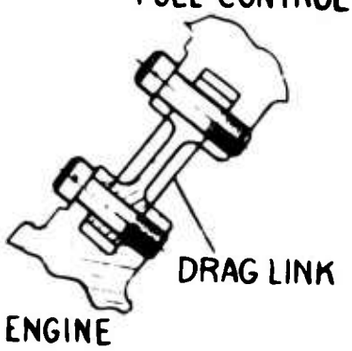

SECTION SHOWING CONTROL MOUNTING
SECTION **C-C**

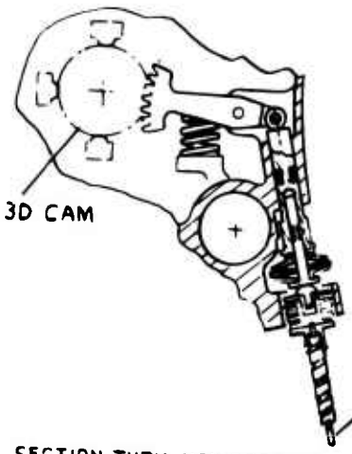

SECTION THRU NON-SERVOED T_{T2} SENSOR
SECTION **E-E**

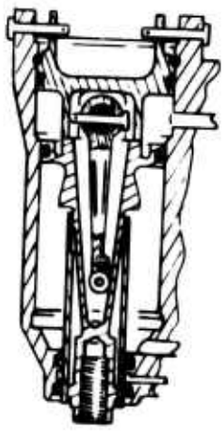

VG ACTUATOR

SECTION **F-F**

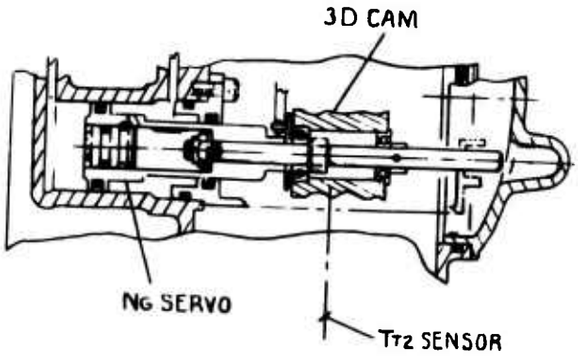

SECTION **G-G**

B

A sheet metal cover completes this assembly. All electrical interconnections are internal and include flexible circuitry to permit easy servicing while maintaining high reliability.

The N_T overspeed fluidic computer assembly consists of a main housing that contains the gas pressure regulator and mounts the laminated stainless steel fluidic modules. There are three modules: one each for the reference frequency circuit, the speed sensing circuit, and the summing amplifier circuit. A sheet metal cover protects this system.

Materials of construction include high-strength sand-cast aluminum for the large, complicated housings and the common wrought steel and aluminum alloys for smaller hardware items. Levers will generally be fabricated from precision investment castings or stamped sheet metal. Printed circuits are manufactured from multilayer fiberglass-epoxy copper laminates. Rubber O-rings and Teflon forms constitute the sealing elements.

It is estimated that the weight of the base engine control will be 12.0 pounds and its volume 150.0 cubic inches.

Final Hybrid Control Accuracy Summary

Accuracy analyses were made for the base and regenerative engine fuel controls. Table XXII summarizes the results and compares them with the specification requirements. Error estimates for any engine operating point were made by calculating the errors of the components involved, such as pressure regulating valve error or N_G servo error, then collecting and using the component errors to compute the system error.

Component errors were calculated as follows:

$$\text{Component error} = \sqrt{(\text{contributing error 1})^2 + (\text{contributing error 2})^2 + \ldots}$$

Operating point errors were calculated as follows:

$$\text{Operating point error} = \sqrt{\left[(\text{component error 1})\ (\text{gain})\right]^2 + \left[(\text{component error 2})\ (\text{gain})\right]^2 + \ldots}$$

This method of calculating accuracy is somewhat optimistic; but, since it is widely used and accepted, it afforded a rapid means for comparing the various technologies.

TABLE XXII ACCURACY SUMMARY - BASE ENGINE CONTROL

Control Operating Point	Calculated RSS Error	Specification Requirement
Acceleration Temp Limiting	± 2.99% of point W_f/P_{T3}	± 5.00% of point W_f/P_{T3}
Acceleration Surge Limiting	± 3.15% of point W_f/P_{T3}	± 5.00% of point W_f/P_{T3}
Acceleration Start Schedule	± 3.94% of point W_f/P_{T3}	± 7.5% of point W_f/P_{T3}
N_G Governing At Military	± 1.08% of point N_G	± 1.0% of point N_G
VG Schedule at Low Speed	± 1.17% of range N_G	± 2.0% of range N_G
VG Schedule at High Speed	± 1.08% of range N_G	± 2.0% of range N_G
Deceleration Schedule	± 3.51% of point W_f/P_{T3}	± 5.0% of point W_f/P_{T3}
N_F Governing at High Speed	± 0.40% of point N_F	± 0.50% of point N_F
Min Fuel Flow Limit	± 1.58 pph	± 1.50 pph
Torque Limiting	± 1.17% of limit torque	± 5.0% of limit torque
Load-Sharing Match	± 1.48% of Torque Match	± 5.0% of torque match
T_{T5} Limiting	± .46% of T_{T5} Limit	± 0.72% of T_{T5} limit

Sample calculation of base engine acceleration temp limiting error:

$$\text{Error} = \pm\sqrt{\left(\text{3-D cam error}\right)^2 + \left[\left(\text{NG servo error}\right)\left(\frac{\partial W_f/P_{T3}}{\partial N_G}\right)\right]^2 + \left[\left(\text{T}_{T2}\text{ sensor error}\right)\left(\frac{\partial W_f/P_{T3}}{\partial T_{T2}}\right)\right] + \left(\text{1/2 PRV error}\right)^2 + (\text{TV error})^2 + \left(\text{P}_3\text{ sensor error}\right)^2}$$

$$= \pm\sqrt{0.24^2 + (0.61 \times 0.65)^2 + (10 \times 0.154)^2 + 1.9^2 + 1.61^2 + 0.40^2}$$

$$= \pm \sqrt{8.97}$$

$$= \pm \quad 2.99$$

Examination of the accuracy summaries, Tables XXII and XXIII, shows two areas where the calculated error significantly exceeds the specification requirement, namely, the regenerative surge limit and the regenerative PTS schedule. Both of these systems require additional design and analytical activity. A program to pursue this area is included in the section on recommended future programs.

Influence Coefficient Summary of Final System

The hybrid control design has been studied for control system accuracy using the influence coefficient method developed in the section on mode studies. Control errors that have been calculated for this particular design are stated in the second column of Table XXIV. The influence coefficients for five different regimes of operation have also been determined and used to calculate the system errors shown in Table XXIV.

The first regime considered is steady-state turbine inlet temperature limiting as controlled by a closed-loop T_{T5} control mode. The sensing inaccuracies contribute error on an RSS basis of ±57.1°F. The major portion of this error is charged to the probable difference between the thermocouple probe average and the true mean engine T_{T5} temperature. It has been assumed that no more than six probes could be inserted into the airstream; hence, an error in average temperature signal at the turbine discharge will be experienced due to a nonuniform temperature profile. Deterioration in engine efficiencies and erosion will cause a decrease in turbine discharge temperature. The overall error potential indicates an increase of 57°F or a decrease of 94°F could occur. This is in excess of the desired ±50°F specification value but is due largely to factors outside of the control proper.

The second regime explores the ability of the control to maintain constant mechanical speed topping governing. The control and sensors have an RSS potential of ±0.73%. This inaccuracy is due largely to the speed-sensing system accuracy. However, engine deterioration can contribute significantly to the inaccuracy and cause a further net shift of 1.32% downward in speed. The overall potential is a band from 0.73% overspeed to 2.61% underspeed.

Horsepower limiting on the W_f/P_{T3} droop governing line has the accuracy potential of 17% overpower to 15% underpower due to all system causes. The control, sensors, and probes contribute ±9.8%, and the remainder comes from engine variations and bleed air extraction. The major error source is caused by airflow variations due to compressor stator vane scheduling inaccuracies. It is very likely that the stator vane could be saturated against a precise stop under high-power limiting conditions and, thus, cut the inaccuracy potential nearly in half.

TABLE XXIII. ACCURACY SUMMARY - REGENERATIVE ENGINE CONTROL

Control Operating Point	Calculated RSS Error	Specification Error
Acceleration Temp Limiting	± 2.89 of point W_f/P_{T3}	± 5.0% of point W_f/P_{T3}
Acceleration Surge Limting	± 7.24 of point W_f/P_{T3}	± 5.0% of point W_f/P_{T3}
N_G Governing at Military	± 1.12% of point N_G	± 1.0% of point N_G
VG Schedule at Low Speed	± 1.07% of range N_G	± 2.0% of range N_G
VG Schedule at High Speed	± .86% of range N_G	± 2.0% of range N_G
Deceleration Schedule	± 3.51% of point W_f/P_{T3}	± 5.0% of point W_f/P_{T3}
N_F Governing at High Speed	± 0.40% of point N_F	± 0.50% of point N_F
Min Fuel Flow Limit	± 1.44 pph	± 1.5 pph
Torque Limiting	± 1.17% of limit torque	± 5.0% of limit torque
Load-Sharing Match	± 1.48% of torque match	± 5.0% of torque match
T_{T5} Limiting	± 0.46% of T_{T5}	± 0.72% of T_{T5}
PTS Schedule at High Speed	± 6.20% of max stroke	± 1.0% of max stroke

TABLE XXIV. INFLUENCE COEFFICIENT SUMMARY - FINAL HYBRID CONTROL SYSTEM

Errors			Control Regime						
	Source Description	% Of Point	Steady-State T_{T4} Limiting	Steady-State N_G Limiting	Steady-State HP/θ Limiting	Acceleration Surge Limiting		Acceleration T_{T4} Limiting	
			°F	%	%	ΔW_f	Δt_{sec}	ΔW_f	Δt_{sec}
Control and Sensor Errors	Compressor SV Schedule	± 5.12 + 4.15	- -	- ± 0.242	- + 9.06	5.614 -	1.034 -	5.622 -	1.024 -
	T_{T2} Sensor T_{T2} Probe	± 2.00 ± 1.00	- -	± 0.016 ± 0.008	± 2.57 ± 1.29	9.285 4.643	1.708 0.854	0.902 0.451	0.17 0.08
	T_{T5} Sensor T_{T5} Probe	± 0.46 ± 2.00	± 12.8 ± 55.6	- -	- -	- -	- -	- -	- -
	P_{T3} Sensor — Intermediate pressure — High pressure P_{T3} Probe	± 0.40 ± 0.35 ± 2.20	- - -	- ± 0.037 ± 0.234	- ± 0.13 ± 0.82	0.598 - 3.289	0.110 - 0.505	0.598 - 3.289	0.110 - 0.61
	N_G Speed Sensor	± 0.70 ± 0.61	- -	- ± 0.561	- ± 1.96	7.540 -	1.398 -	0.490 -	0.09 -
	Fuel Control Computing	± 2.85 ± 3.05	- -	- ± 0.322	- 1.14	4.261 -	0.784 -	4.261 -	0.78 -
RSS Subtotal of Control and Sensor Errors			± 57.1	± 0.730	± 9.80	-	2.77	-	1.44
Engine Variations	Compressor Efficiency	- 3.00	-	- 0.345	- 3.888	1.366	0.126	+ 1.50	0.14
	Burner Efficiency	- 0.50	-	- 0.053	- 0.187	- 0.748	0.069	- 0.75	0.07
	Gas Gen Turbine Efficiency	- 3.00	- 30.1	- 0.585	- 5.172	- 0.026	0.002	-	-
	Gas Gen Turbine Nozzle Erosion	- 2.00	- 14.5	- 0.376	- 0.400	- 3.581	0.329	- 3.56	0.33
	Power Turbine Nozzle Erosion	- 1.00	+ 7.3	- 0.140	- 1.764	- 0.013	0.001	-	-
	Burner Pressure Loss	- 0.2	-	- 0.010	- 0.216	- 0.370	0.034	- 0.37	0.03
	SHP Extraction/lb of Air	- 9.0*	-	- 0.090	- 9.047	-	-	-	-
Algebraic Subtotal of Engine Variables			- 37.3	- 1.319	- 7.34	- 3.346	0.561	- 3.18	0.57
P_{T3} Bleed Air Extraction		+ 5.00	-	- 0.565	- 5.48	- 1.482	0.136	- 1.48	- 0.14
Total Error Potential			- 57.1 - 94.4	- 0.730 - 2.614	+ 17.14 - 15.28	-	3.467	-	2.01

*Units are HP/lb/sec

Acceleration time errors are shown in Table XXIV for surge and temperature limiting under the ground rules explained in the section on control modes. The period of acceleration is largely dependent on the accuracy of the control, sensors and probes. Compressor stator vane scheduling accuracy is a large contributor to the inaccuracies, as is the speed sensor and T_{T2} sensor in the surge bucket where the cam slopes are large. The engine variation is expressed only for that portion of the acceleration time error that is avoidable; i.e., the time difference, which would still occur with an ideal T_{T4} system, has not been included. It can be seen that the engine variation on such a basis is small compared with that contributed by the control and sensors.

IDENTIFICATION OF HIGH-RISK COMPONENTS IN FINAL SYSTEM

The final hybrid system has been analyzed to determine those portions of the system for which insufficient experience exists, either in terms of engine running or bench development testing, to warrant consideration of that component as developed for this advanced control program. Several areas of the control system fall into this category. They are listed below, with a discussion following, including a suggested evaluation program to minimize the risk associated with the use of these concepts:

1. 75,000-rpm speed sensor
2. The regenerative scheduling and computation system
3. The regenerative power turbine stator scheduling and actuation system
4. The use of high-density microelectronics
5. Miniaturized fluidic overspeed sensor

A 75,000-rpm speed sensor is required for the 2-pound-per-second version of this engine. This requirement is made necessary by the program objective that either the mechanical drive to the control be eliminated or the control have the capability of being driven at direct engine speed. Currently no fuel control experience in speed sensing above 15,000 rpm exists; as a result, this concept must be categorized as a high-risk component. The concept selected for implementing this high-speed sensor in the proposed control system employed an electromagnetic-speed counter with appropriate filtering, amplification and feedback from the hydraulically driven servo. However, it is recommended that further studies be conducted, pursuing both a mechanical-speed sensor with integral stepdown gearbox and a fluidic-speed sensor, before actual evaluation testing of the selected approach is accomplished. A subsequent section on recommended future programs defines a suggested program for further study and evaluation of this high-speed sensor

The regenerator scheduling and computation system, proposed as a modification to the base engine control for regenerative engine applications, is a new concept that has not been reduced to practice. Required inputs to this system include outputs from two separate three-dimensional cam surfaces and an output from a $T_{T3.5}$ servo. A relatively complex linkage system is then employed to calculate the desired W_f/P_{T3} position output from these inputs. This system could be evaluated as a component employing a special test fixture to determine the capability of the system; however, a more meaningful evaluation of the system would be accomplished by implementing one of the complete control system options as discussed in the future program recommendations section of this report.

The regenerative power turbine stator scheduling and actuation system proposed for this control system is a new system. It is not currently employed in a

control system, although its identification as a high-risk item stems more from the demanding accuracy and dynamic response requirements imposed on it than it does from its concept. The concept differs from conventional variable inlet guide vane systems only in that scheduled position is summed with trimmed power lever input prior to inputing the power turbine stator pilot valve through a droop cam. Since the problems associated with the development of this component are for the most part propulsion system oriented (i.e., schedule matching to maintain constant turbine inlet temperature, proper matching with regenerator characteristics and proper fuel pump sizing to meet slew rate requirements without excessive pump flow) the development of this system is best accomplished in conjunction with the implementation of a complete regenerative system and subsequent evaluation on an engine which was given as one of the options under the recommended future programs section of this report.

The use of high-density engine-mounted microelectronics, although currently in the process of being implemented for some engine mounted control systems, is not yet a proven concept and thus must be classified as a high-risk item. Factors such as acceptable reliability rates have not yet been established. Failures which tend to occur by complete malfunction rather than by gradual deterioration, interaction with EMI, susceptibility to lightning strikes, adverse effects of spikes in power supply systems, and potential temperature limitations are areas where additional information and/or experience is required to eliminate this technique from the high risk item list. Programs to evaluate the above areas of concern are active and with the application of high-density microelectronics to engine mounted applications currently under way, it is felt that no additional programs to this end are required at this time.

The miniaturized fluidic overspeed sensor proposed for this control system represents an advanced technology step over fluidic circuitry and systems currently undergoing evaluation. This advance lies primarily in the area of miniaturization of fluidic components. With this miniaturization, which is characterized by the size reduction of the basic circuit block from one inch square to one-half inch square, the risk of contamination sensitivity in an engine air environment increases. An evaluation program for this component should include, as a minimum, the design and manufacture of a working prototype of this miniaturized fluidic sensor in conjunction with its fluidic-to-hydromechanical interface device. This should be followed by performance testing to establish the components functional capability, which would then be followed by relatively long term endurance testing in contaminated air to establish the capability of the component to perform adequately in this environment.

ALTERNATE ARRANGEMENT SCHEME INVOLVING INTEGRATION OF CONTROL SYSTEM WITH PUMP

In considering approaches to reduce the size and weight of small turboshaft engine systems, it was recognized that little effort to date had been devoted to the integration of the fuel pump and control as a system (as opposed to merely packaging in a common casting). In addition to possible reductions in size, weight, and pump horsepower, the presence of an electronic trimmer in the control package makes it desirable to minimize temperature rise across the pump, as far as possible, to allow the use of fuel for cooling purposes. Based on knowledge of engine parameters for the 5-pps engine configuration generated in the program, the following list of requirements is defined:

Max flow (including servo flow)	= 1,450 pph at 550 psi at 100% N_G
Min flow (including servo flow)	= 285 pph at 300 psi at 15% N_G
Bypass to pump inlet (control servo flow)	= 250 pph at 300 psi
Fuel temp. rise (goal)	= 50°F max
Contamination	= MIL-E-5007C
Fuel	= JP4, JP5, CITE
Fuel (inlet)	= -65°F to +130°F
Available power source (to avoid dependence on reduction gearbox)	= 1) 200 V, 400 Hz, 3 ϕ 2) 28 VDC 3) Shaft (55,000 rpm)
Pump inlet pressure	= 30 psig
Dry lift	= MIL-E-5007C

With these requirements as a starting point, several systems were considered in conjunction with the Hydro-Aire Division of the Crane Co., which also supplied the detailed pump data and sizing presented subsequently. A summary of the concepts considered is presented as follows:

Concept 1, shown in Figure 53, consists simply of the conventional fixed displacement fuel pump (gear or vane), with bypass return of pump flow that is in excess of that required for metering to the engine. Maximum allowable speed established

for this concept is currently 24,000 rpm, thus requiring speed reduction for mechanical drive or the use of a 400-Hz synchronous electric motor. No advantage in temperature rise is obtained since temperature can rise to approximately 200°F at minimum flow. Inherent durability must be considered low and costs high by virtue of the complex design and material processing necessary to assure the required level of durability under MIL specification contamination conditions.

Concept 2, shown in Figure 54, is based on the centrifugal/retractable vane design. This responds to the problem of satisfying the dry lift requirements of MIL-E-5007 by utilizing a vane pump for priming and low-speed operation. Once the centrifugal pump generates sufficient pressure to take over pumping, pump discharge pressure is used to retract the vanes, thus minimizing vane wear and allowing very high speed operation. The presence of the positive displacement stage, however, dictates the use of a bypass regulator, thus reverting to the 200°F temperature rise of concept 1 and effecting no reduction in control complexity. For this application, therefore, the prime advantages of concept 2 would be the use of the inherently high durability of the centrifugal stage together with the ability to accept full engine speed (55,000 rpm) without use of a reduction gearbox.

Concept 3, shown in Figure 55, is based on the use of a pump with delivery varied by the fuel control to maintain a constant differential pressure across the fuel metering valve.

Two approaches to obtaining the variable displacement feature have been suggested. First, the use of axial piston pumps with variable stroke (as widely used in British engines) or inlet throttling may be considered. However, the mechanical complexity of these devices and the measures necessary to obtain adequate resistance to contamination make these concepts most unattractive for this application. The second approach is based on the use of a vane pump whose vane guide ring may be displaced relative to the rotor. Displacement may be effected either by deformation of the ring itself or by displacement of the ring relative to the rotor. The deformable vane guide ring approach has the advantage of maintaining balanced rotor loading in contrast to the unbalance inherent in the displaceable ring concept. The more immediate availability of the displaceable ring type, combined with the low magnitude of the unbalanced forces due to the small pump size, makes this the most attractive candidate for a variable displacement pump for this application. Figure 56 illustrates a concept for this type of variable displacement vane pump in a cartridge-type configuration. Details of this pump's estimated performance are shown in Figure 57.

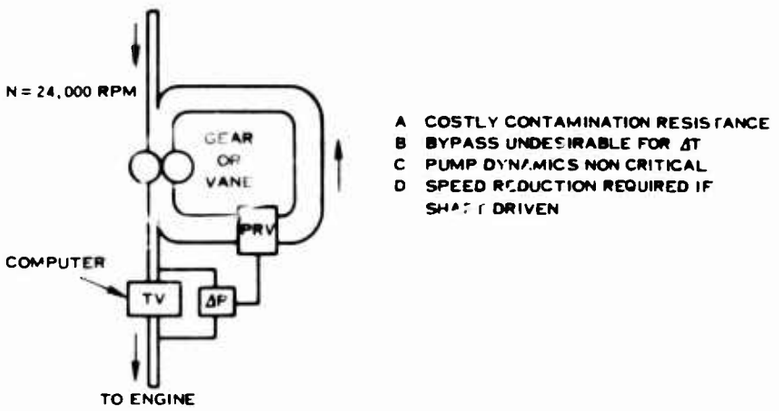

Figure 53. Schematic of Positive-Displacement Pumping System.

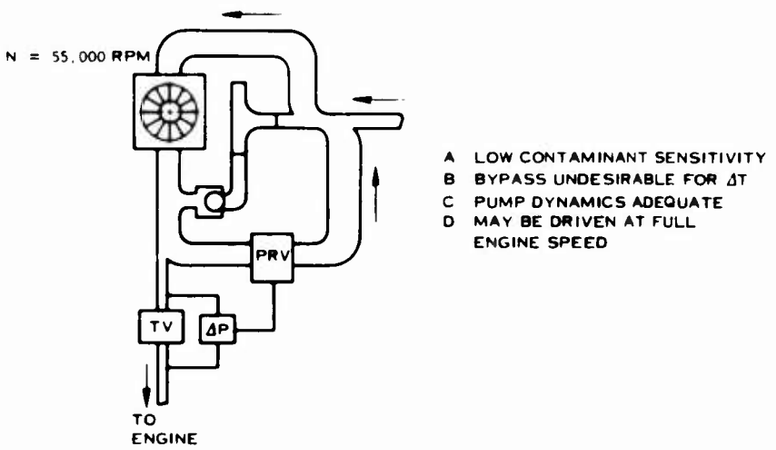

Figure 54. Schematic of a Centrifugal/Retractable Vane Pumping System.

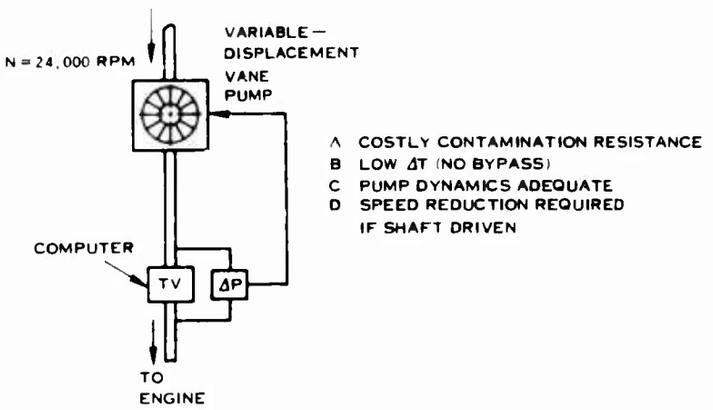

Figure 55. Schematic of Variable-Displacement Pumping System.

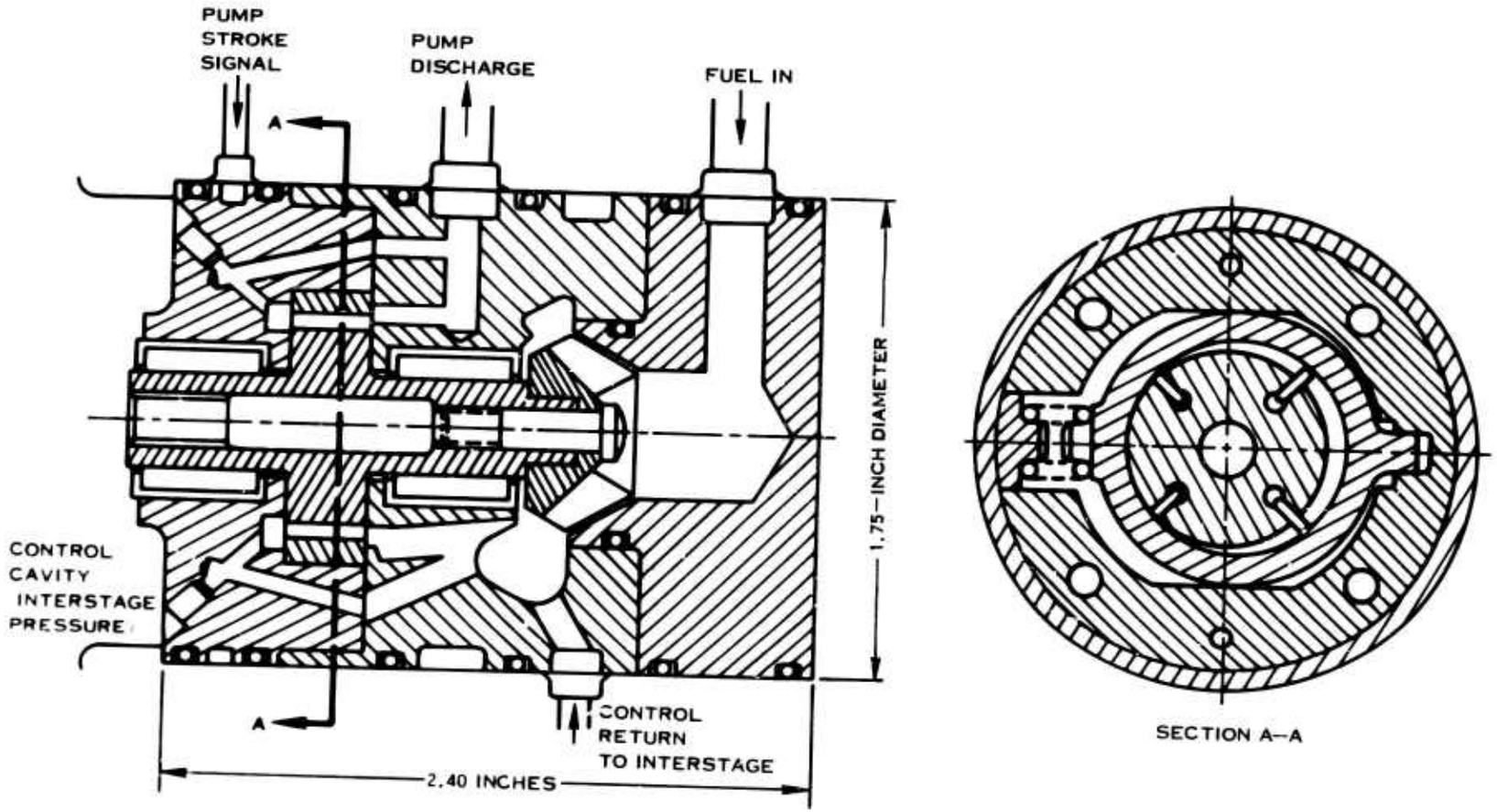

Figure 56. Variable-Displacement Vane Pump Cartridge Application.

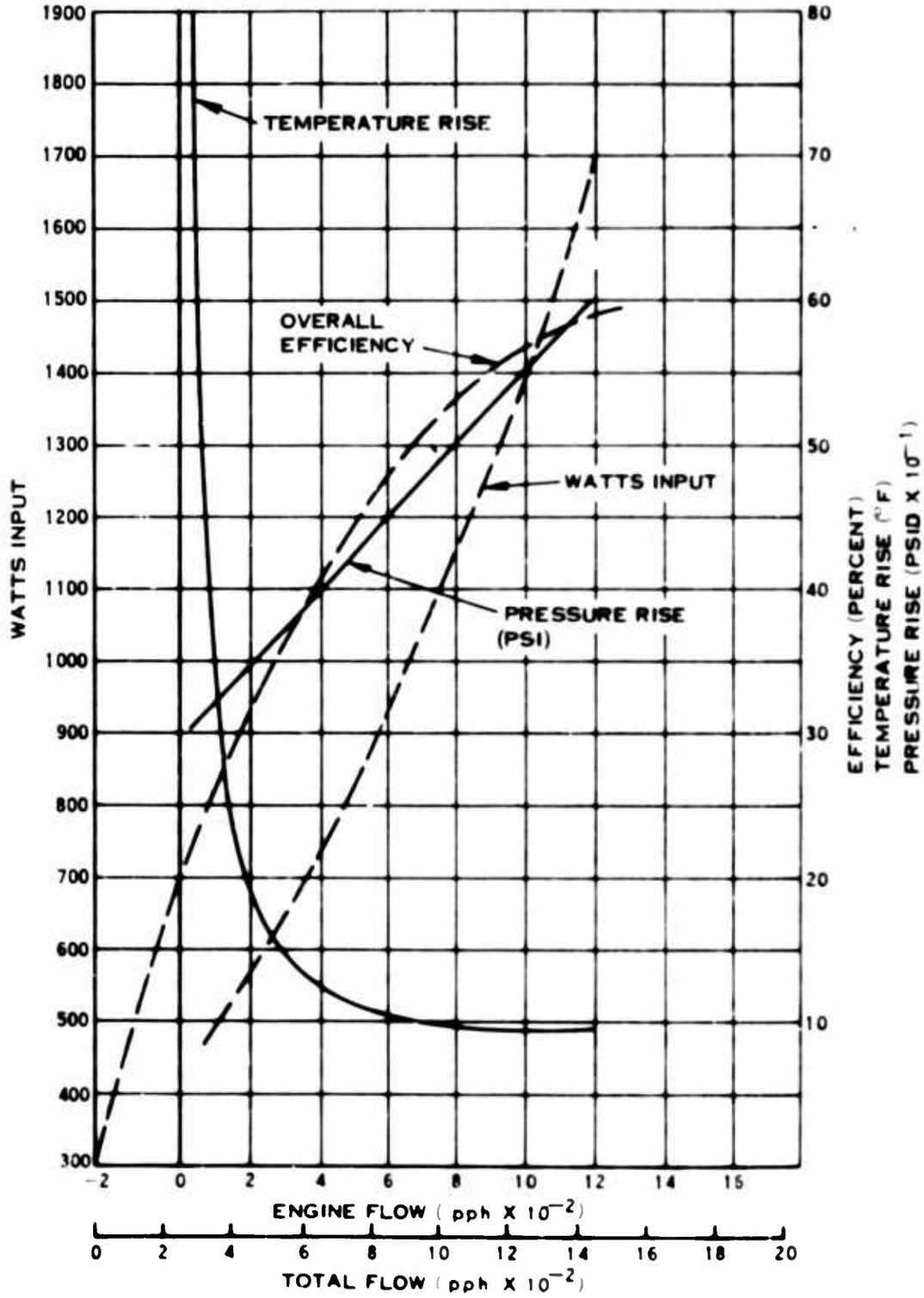

Figure 57. Estimated Performance of Variable-Displacement Vane Pump.

The outer periphery of the vane guide ring is closely fitted to the pump chamber so that a pressure differential can be imposed across the ring. The cam ring is spring loaded toward maximum flow so that an excess flow signal from the control would act to drive the ring to the left, compressing the spring and reducing pump delivery. The presence of the spring loading, together with friction, would indicate that the pressure differential existing across the control metering valve (40 psi) would be inadequate for direct actuation of the cam ring. Use of a servo pilot valve sensing metering valve head, therefore, would be necessary. The hydraulic servo output pressure of this valve could then be applied to the vane guide ring to maintain the fuel flow to the metering valve at the level necessary to hold a constant metering valve head. The requirements for variable geometry actuation make severe demands on the dynamic performance of this valve in order to maintain metering head during actuation transients. This may dictate the need for anticipatory signals to be transmitted from the variable geometry pilot valve to the metering head sensor valve. The complexity introduced into the fuel control by the necessity for such measures may offset the elimination of the bypass regulating valve resulting from the variable displacement pump. While the ultimate speed limit for this concept is considered to be in excess of 55,000 rpm, a suitable operating speed for initial use would be 24,000 rpm. Drive would be effected, therefore, by a synchronous 400 Hz electric motor or by engine shaft drive (although at the cost of the required speed reduction). The reduction in temperature rise which results from the elimination of the bypass recirculation flow (85°F versus 200°F for a bypass system) would make the concept attractive in systems where the high fuel flow turndown ratio would otherwise preclude taking advantage of the simplicity of fuel cooling for the electronic module. The concept shown reflects an advanced state of the art and would incorporate the new vane tip designs currently under development. These vane designs would allow the use of speeds of 24,000 rpm during the initial development period, with eventual growth capability to speeds in excess of 55,000 rpm. The potential for elimination of the reduction gearbox by use of high speed direct drive, together with its small size and low temperature rise properties, combine to make this concept the most attractive pumping system for the type of engine defined by this program. It is recommended, therefore, that development of a variable displacement pumping system be initiated, comprising the vane pump concept described above, together with the necessary fuel control sensing and actuation elements for total integration of pump and controls.

DESCRIPTION OF PROPOSED SYSTEM FOR REGENERATOR MODE

Mode Selection and Evaluation

Choice of a regenerative engine control was based on adaptability from the basic W_f/P_{T3} control and trimmer selected in the base engine study. The block diagrams of the engine and load controls are presented in Figure 58. These controls include the gas generator control system, a power turbine trim and topping control, and a propeller blade angle control. Ambient temperature biases have been deleted from these block diagrams for simplicity but are discussed in the static analysis and design sections of this report. The gas generator control modulates fuel flow and power turbine stator area in response to the trimmed power lever ($N_G REF$) and sensed engine parameters to establish the desired static and safe transient performance. The desired fuel flow acceleration schedule is actually a Z_3 parameter which is scheduled as a function of sensed speed and would be biased by engine inlet temperature, T_{T2}. This acceleration parameter, $W_f/P_{T3}(1-T_{T3.5}/T_{T4})$, defines safe limits and minimizes the effects of operating condition variations on the acceleration margin by examining both burner inlet pressure, P_{T3}, and regenerator discharge temperature, $T_{T3.5}$. The predicted acceleration turbine inlet temperature, T_{T4}, would be defined as a function of sensed speed and T_{T2} temperature. The use of this Z parameter then reduces fuel flow if the regenerator temperature is high and minimizes the undesirable turbine temperature variations which could occur if the temperature calculations were not included.

The trim control includes shaft torque and turbine discharge temperature limiting functions and a power turbine speed control. A load sharing function could also be included, as described in the base engine discussions, but is not shown on this block diagram. The power turbine speed control would be utilized as a conventional control mode for the helicopter application and as a topping governor on the turboprop installation. Helicopter collective pitch is a typical parameter utilized to minimize speed variations by anticipating the power requirements of the rotor as was described for the base engine.

The propeller control modulates blade angle to establish the desired propeller speed. This desired speed may be a function of power lever (PLA), and minimum blade angle schedules may also be established by PLA as shown. The gas generator engine then becomes a power supply, with safety limits, for the propeller. One portion of the propeller control system which is not shown on this block diagram includes the schedule coordination which is usually located in close proximity to the pilot. This management device would incorporate the equipment needed to provide pilot selection of options such as constant speed control, variable speed control, manual blade angle control or reverse thrust.

These options are relatively straightforward with the possible exception of reverse thrust. This mode would actually advance the fuel control power lever to a high-power condition when reversing is requested and the aircraft wheels are on the ground. Further discussion of all the propeller coordination options would become quite extensive and is beyond the scope of this study.

Deceleration and acceleration transients for this regenerative control mode are presented in Figures 59 and 60. The power turbine speed transient for the deceleration exhibits the high-frequency rotor and shaft resonance which is a primary factor involved in the definition of allowable control sensitivities. The lead/lag compensation shown in Figure 58 is used to improve the low frequency stability characteristics resulting from the power turbine and rotor inertias and damping. The acceleration transient illustrates the influence of the $T_{T3.5}$ temperature sensor dynamics on the turbine inlet temperature by showing performance with two different sensors: one with a time constant of 0.1 second, and a second with a time constant of 1.0 second. The slow responding sensor indicates a high indicated temperature during the final portion of the acceleration, which thus reduces fuel flow and T_{T4}. Thus the requirement for a fast temperature sensor is demonstrated by this acceleration.

Figures 61 and 62 illustrate typical accelerations into torque and temperature limiting modes of operation. The maximum limits for these runs have been lowered from the normal values to make certain that steady-state operation on the limiting mode would occur. This modification was required to demonstrate the relative stability of the mode. Torque limiting operation results in an underspeed condition as shown in the power turbine speed trace. The effect of speed on shaft horsepower significantly masks the torque oscillations, and the W_f/P_{T3} trace must be used to identify the control stability. Acceptable margins for a limiting control are demonstrated by this trace.

The effect of the T_{T5} sensor dynamics on the temperature-limiting control is presented in Figure 62. A short time constant is needed to provide reasonable stability as demonstrated by the separate T_{T4} and T_{T5} traces. Lengthening the time constant to 0.1 second produced a marked deterioration in the stability margin and would require a significant sensitivity reduction. A sensor time constant on the order of 1 to 3 seconds produced a very slow response with large transient errors, as demonstrated by the combined temperature transient. A power turbine underspeed condition similar to the torque-limiting transient occurred in this mode of operation also, but it was not included because it would add little additional information.

Both limiting modes resulted in limiting operation at some time after the actual limit was reached. This response resulted in large errors and was caused by the requirement to retract the trim integrator from the acceleration value

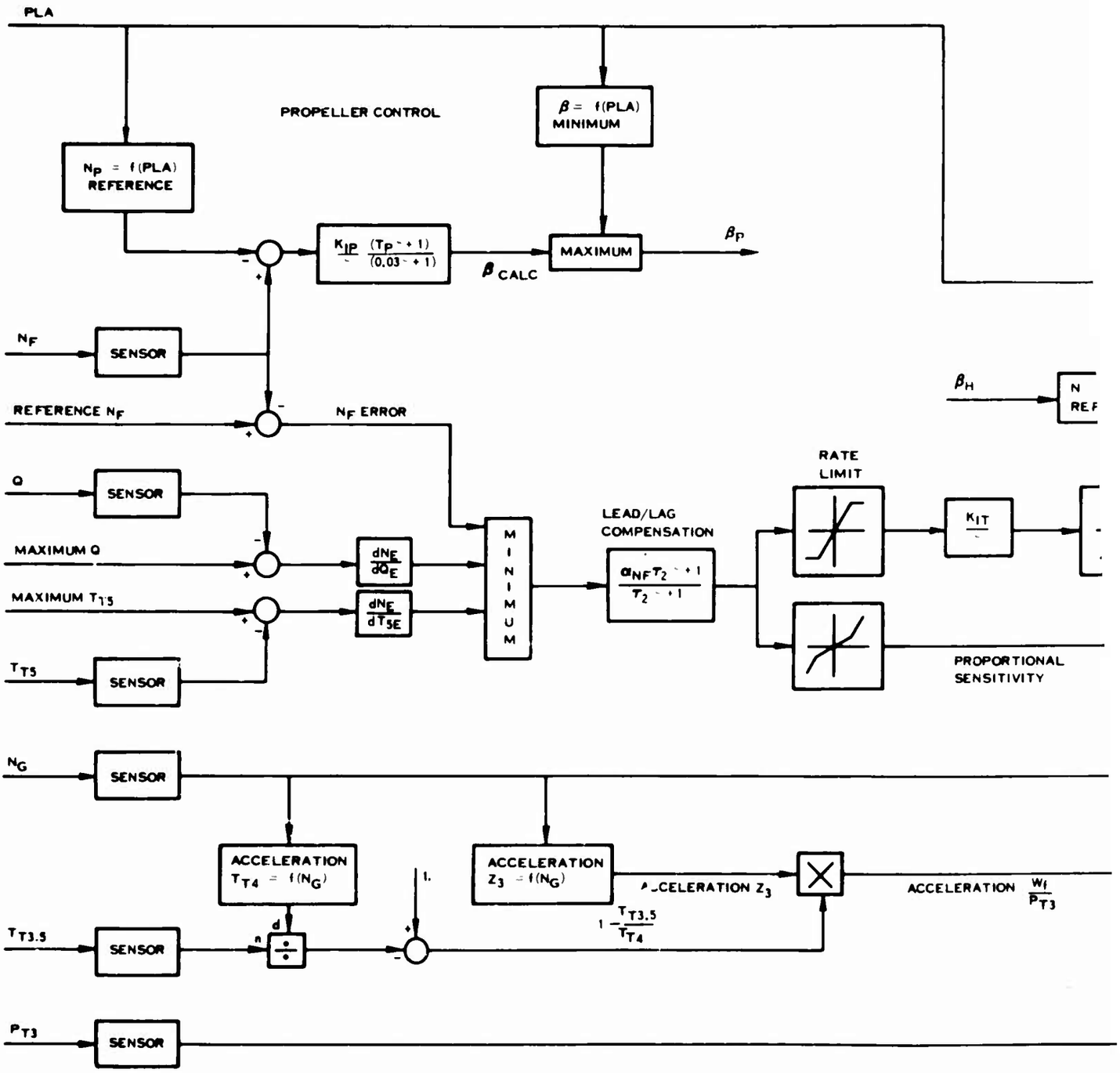

Figure 58. Engine and Load Control Block Diagram for the Regenerative Engine

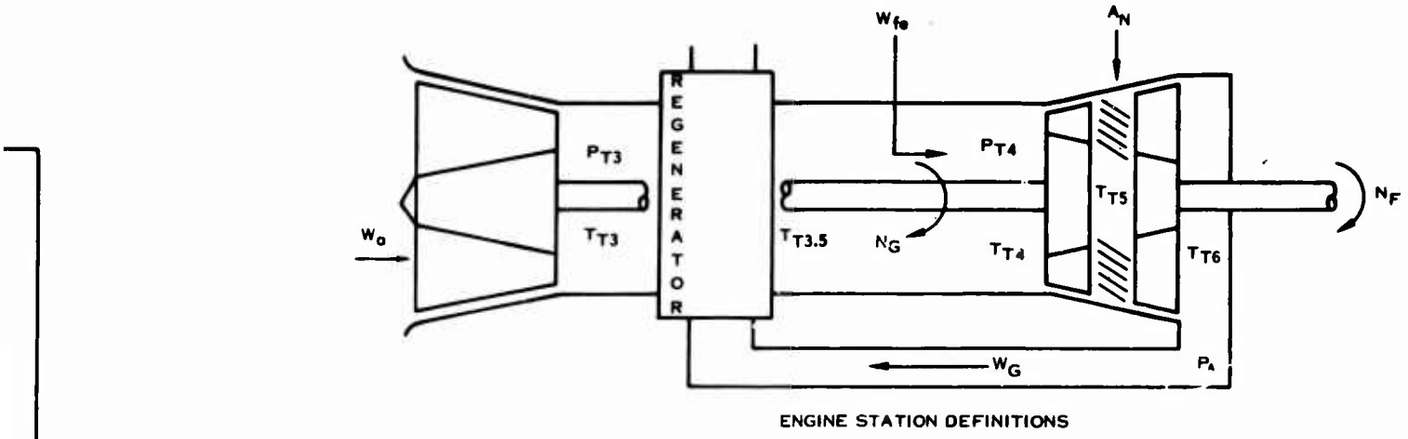

ENGINE STATION DEFINITIONS

B

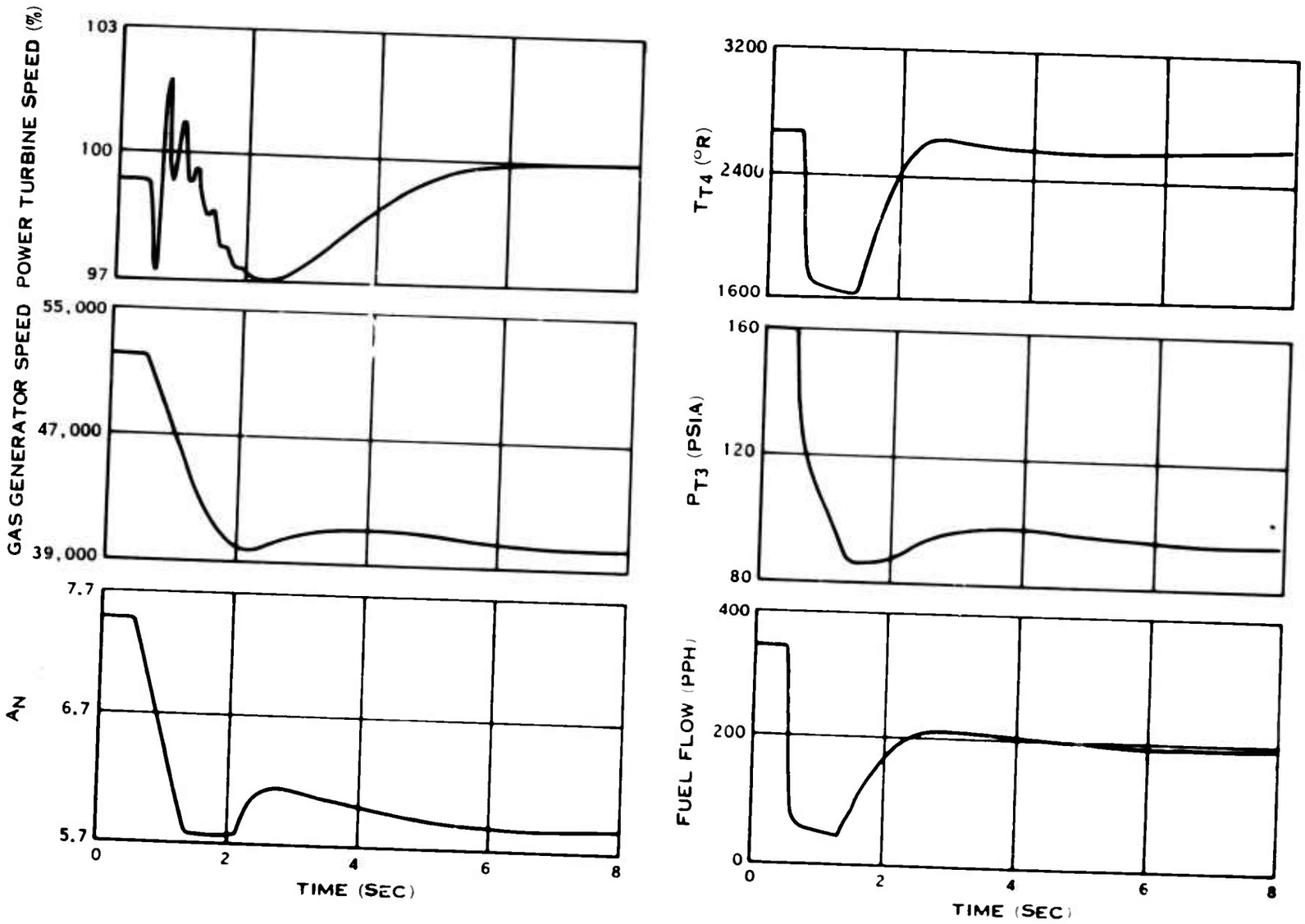

Figure 59. Normal Helicopter Deceleration - Regenerative Control.

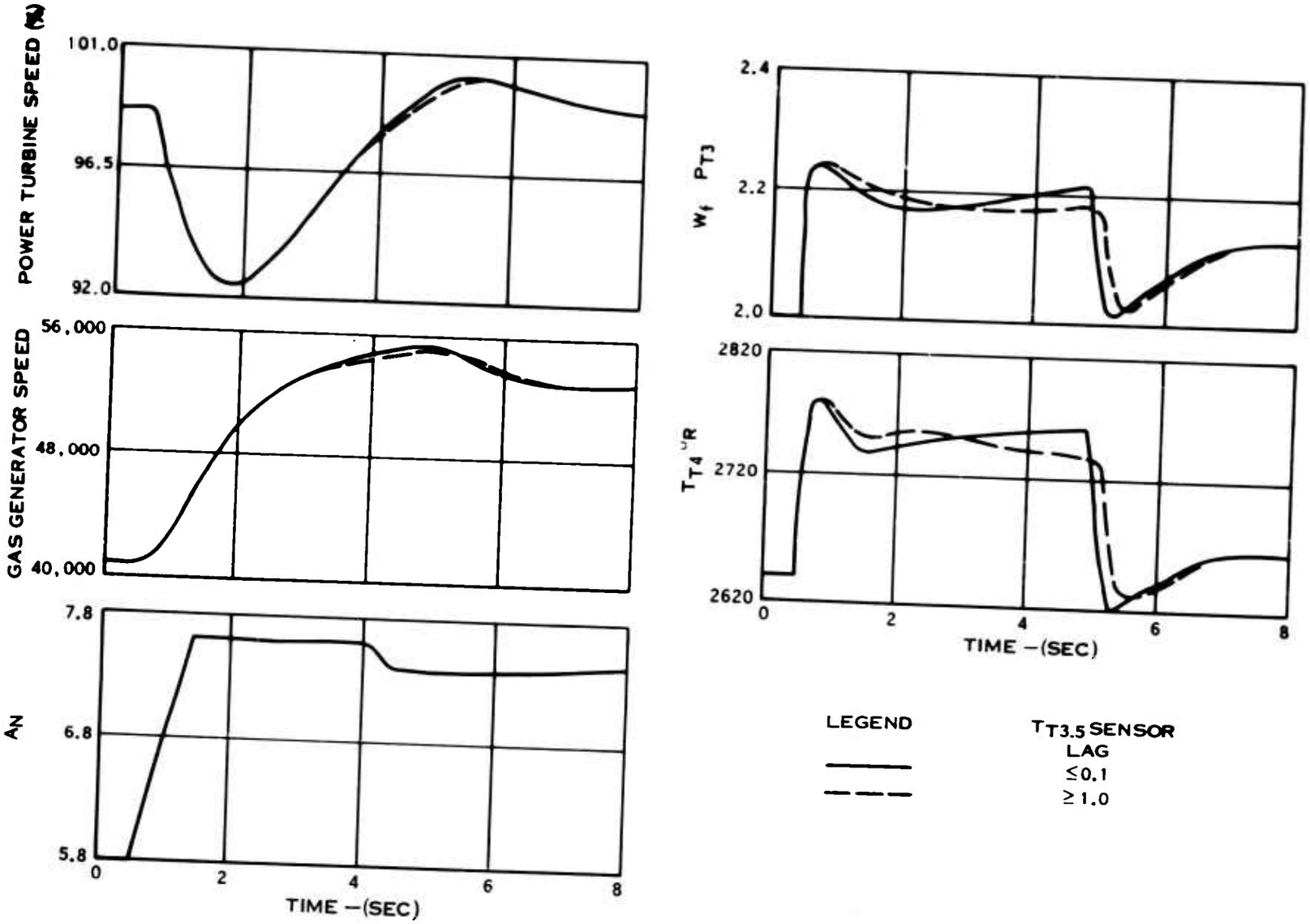

Figure 60. Normal Helicopter Acceleration - Regenerative Control.

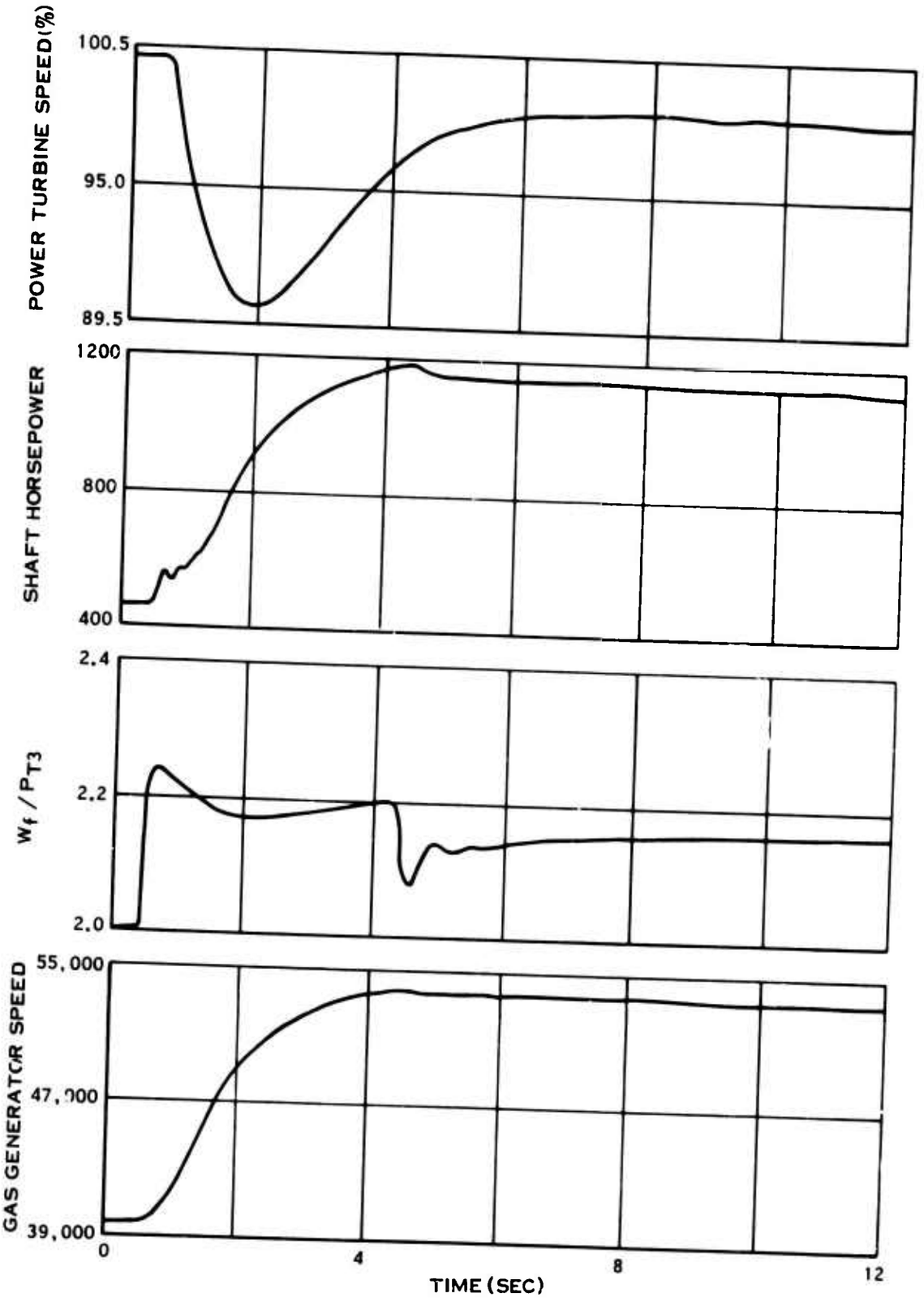

Figure 61. Acceleration Into Torque Limiting Mode - Regenerative Control.

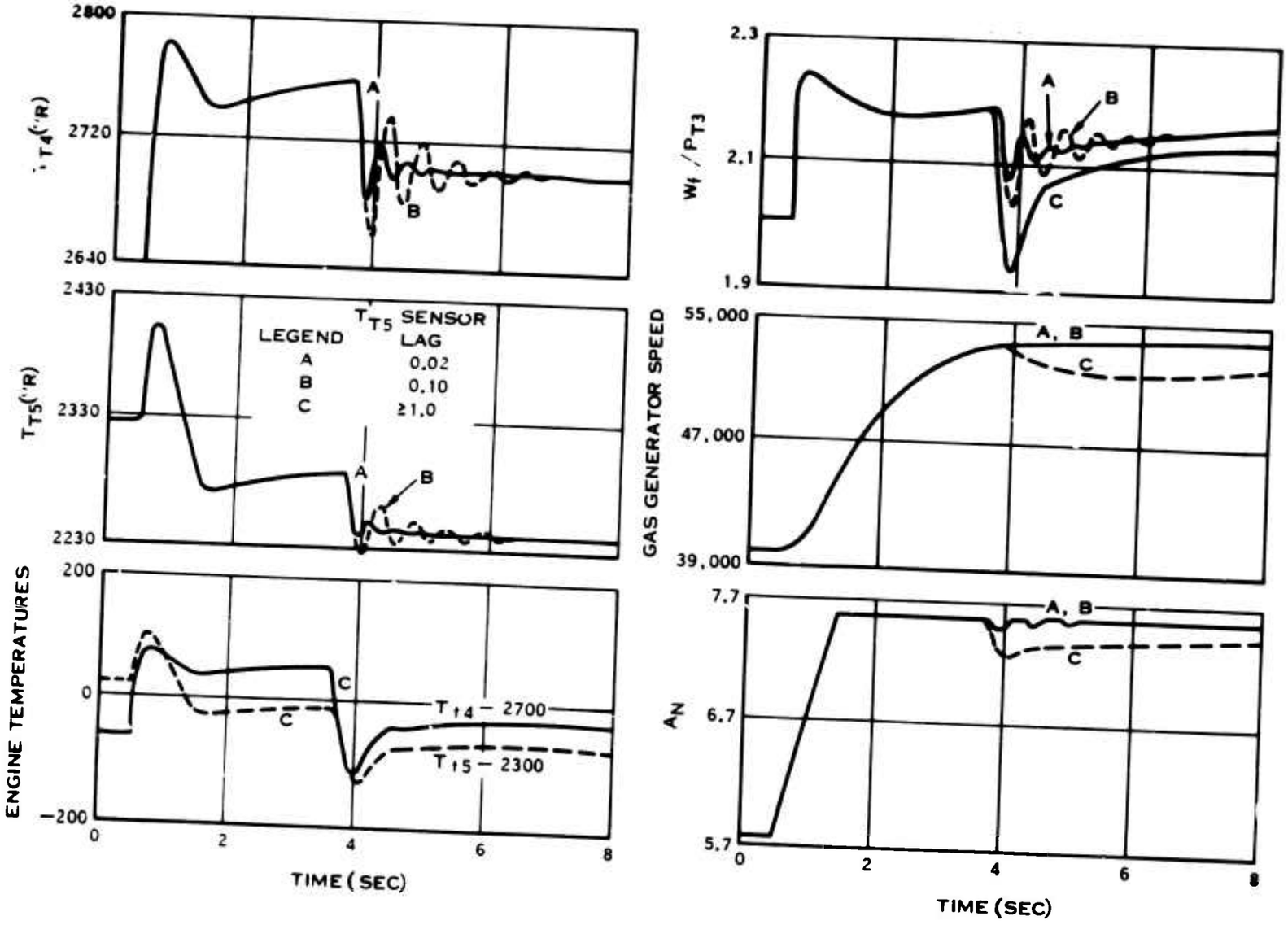

Figure 62. Acceleration Into T_{T5} Limiting Mode - Regenerative Control.

initially established by power turbine speed to levels required for the limiting mode. Thus some transient error should be anticipated for these controls.

One concern of this study was the use of a helicopter and turboprop installation. The controls for the helicopter and turboprop simulations were essentially identical. The collective pitch signal was locked at the maximum setting and the trim control reference speed was set higher for a propeller topping governor.

Typically large transients for operation in a propeller governing mode are presented in Figure 63. These transients include a full deceleration (shown by dotted traces), a full acceleration, and accelerations into topping governing and temperature-limiting modes of operation. All controls which were generated for the helicopter application performed satisfactorily on the turboprop. The temperature-limiting mode of operation produced a relatively small steady-state fuel flow and temperature reduction, and the resultant speed and thrust loss was also small. Topping governor operation produced a more pronounced effect. Propeller speed returned to the desired level in each case because the blade angle was modulated so as to reduce the load and match the power supplied by the engine.

Small transients to a partial power condition for a propeller control mode are presented in Figure 64. Comparison of the acceleration and deceleration traces (A and B) demonstrates the small signal stability of the gas generator controls and the influence of power turbine stator area on this stability margin. This area modulation results in a faster response for the gas generator at the expense of the thrust response. The third transient of this set of traces illustrates an acceleration with manual blade angle control. Large propeller speed excursions are experienced which will significantly reduce the thrust response from that normally expected from this mode of operation. Manual blade angle control must then be reserved for very slow power adjustments and is not a recommended power modulation means.

The major conclusion from this portion of the study is that the controls generated for a helicopter installation are also adequate for a turboprop application. A reasonably accurate gas generator control is desirable to minimize the variations of power supplied to the power turbine and to compensate for the uncertainties of the regenerator. A reasonably fast indication of the regenerator temperature is needed to provide satisfactory acceleration characteristics. A fast turbine discharge temperature sensor is also required to minimize excessive temperatures that would accelerate the turbine deterioration rate.

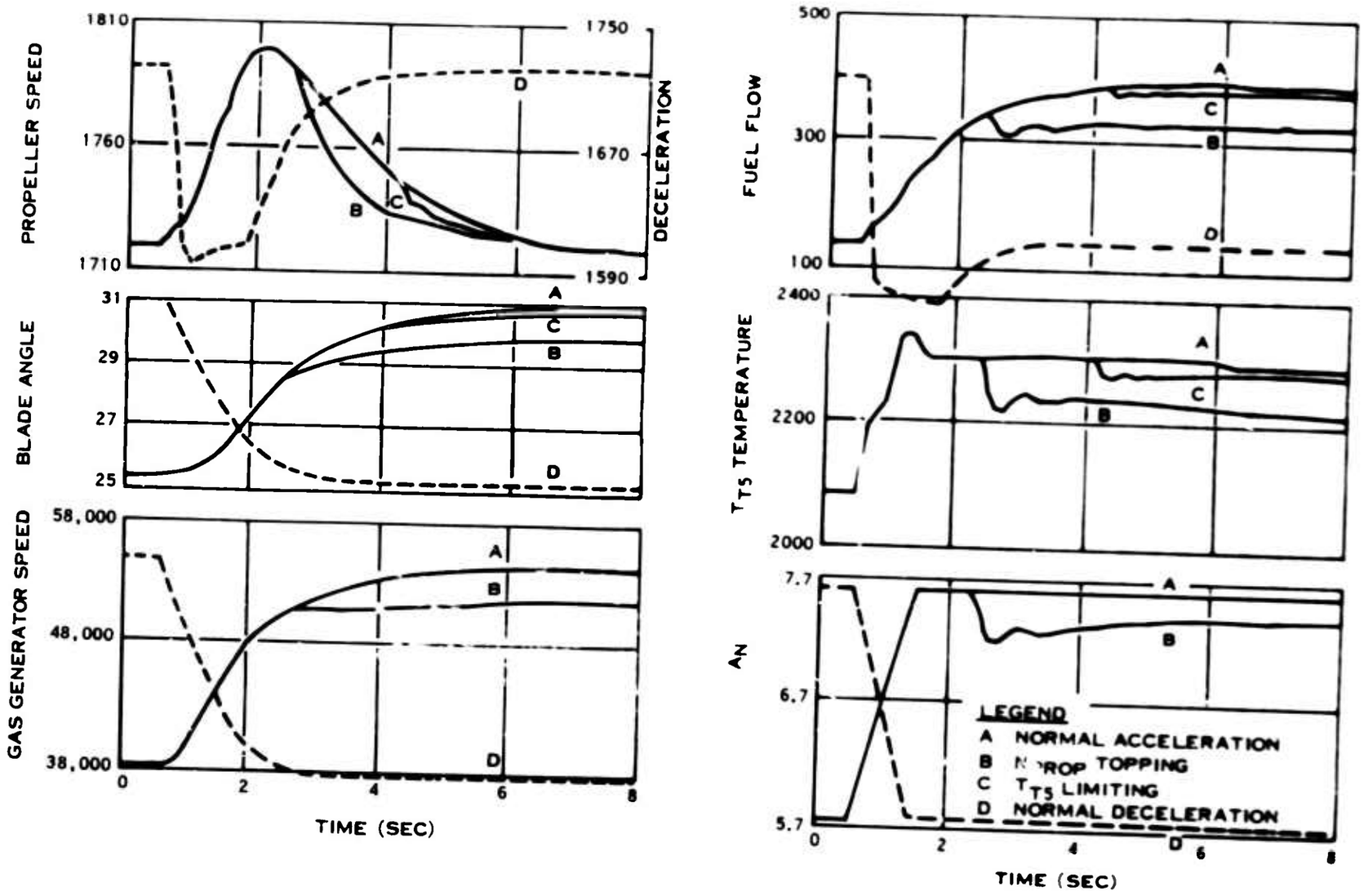

Figure 63. Typical Propeller Control Operation - Regenerative Control.

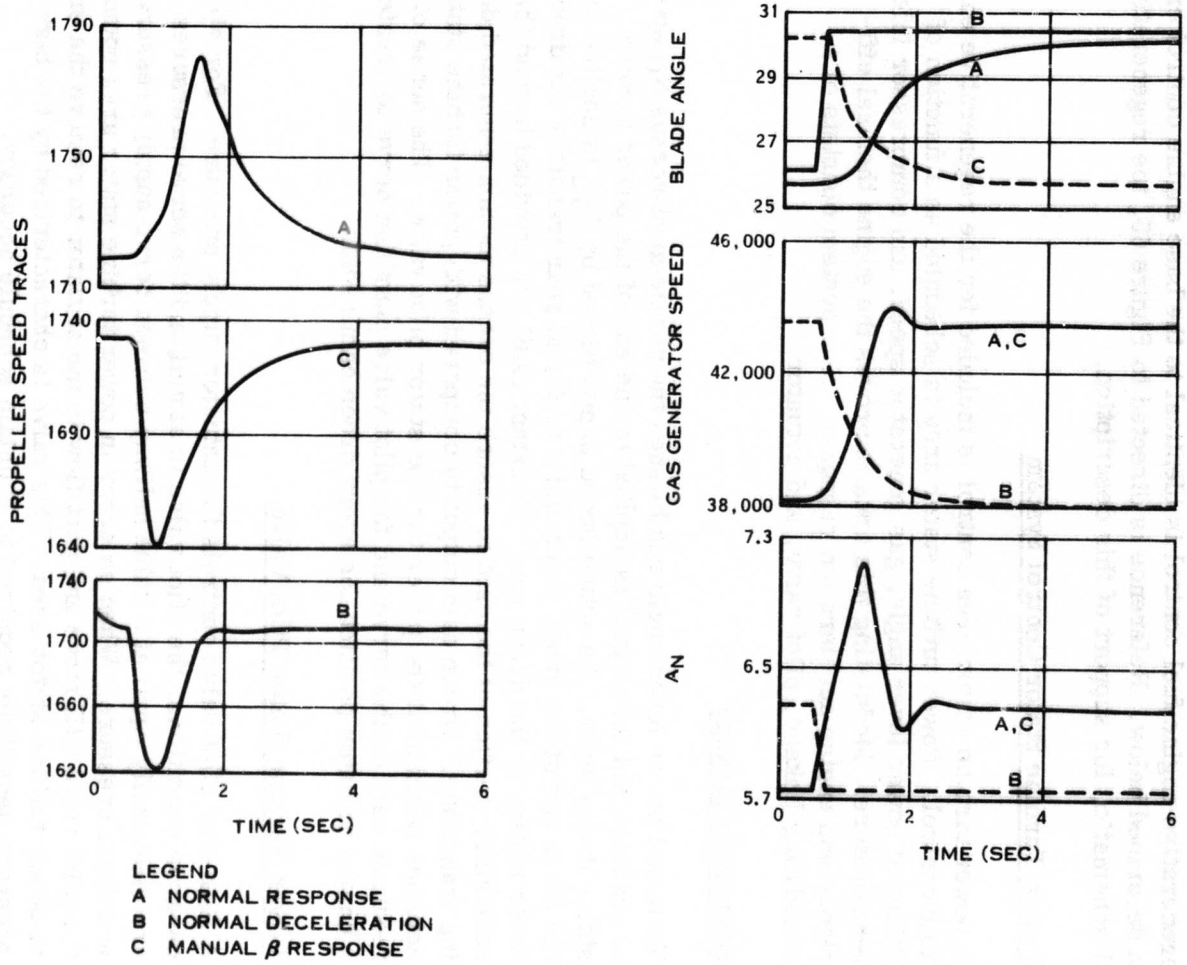

Figure 64. Propeller Control Mode Comparison - Regenerative Control.

Functional Description of Regenerative Engine Control

The regenerative engine fuel control is identical to the base engine control except as described below. Reference is directed to Figure 65, the regenerative control schematic, for support of this description.

Power Turbine Stator Control System

A power turbine stator area control is included for the regenerative engine control. Power turbine stator area is scheduled as a function of trimmed power lever angle, gas generator speed, and compressor inlet temperature. Modulating this area improves the engine thermal efficiency and engine acceleration response. The system consists of a scheduling linkage, pilot valve, and actuator.

Scheduling Linkage

Trimmed power lever angle establishes the nozzle-area-versus-N_G-speed droop lines, and this signal is applied to one end of the power turbine stator droop lever. An actual speed signal biased by T_{T2} is applied to the other end of the droop lever, and a rack and gear transfers net droop lever motion to the droop cam. Constant radii are provided beyond the scheduling portion of the cam to absorb the excess motion generated during transients. Droop cam output is compared with power turbine stator actuator position at the power turbine stator pilot valve. The sense of the feedback cam on the servo and the pilot valve plumbing serve to create a unique actuator position for every droop cam radius.

Power Turbine Stator Pilot Valve

A four-way pilot valve controls the actuator supply pressure. For all on-area conditions, the pilot valve is at null, and the servo pressures are essentially equal at a value halfway between servo supply pressure and drain pressure. When an error in power turbine stator area occurs, the pilot valve will move and port flow to the actuator to remove the error in power turbine stator area. This valve is characterized by the high pressure sensitivity required to maintain schedule accuracy.

Power Turbine Stator Actuator

The power turbine stator actuator is a full-area servo. Its output pushrod is connected to the engine area controlling linkage. Two seals with

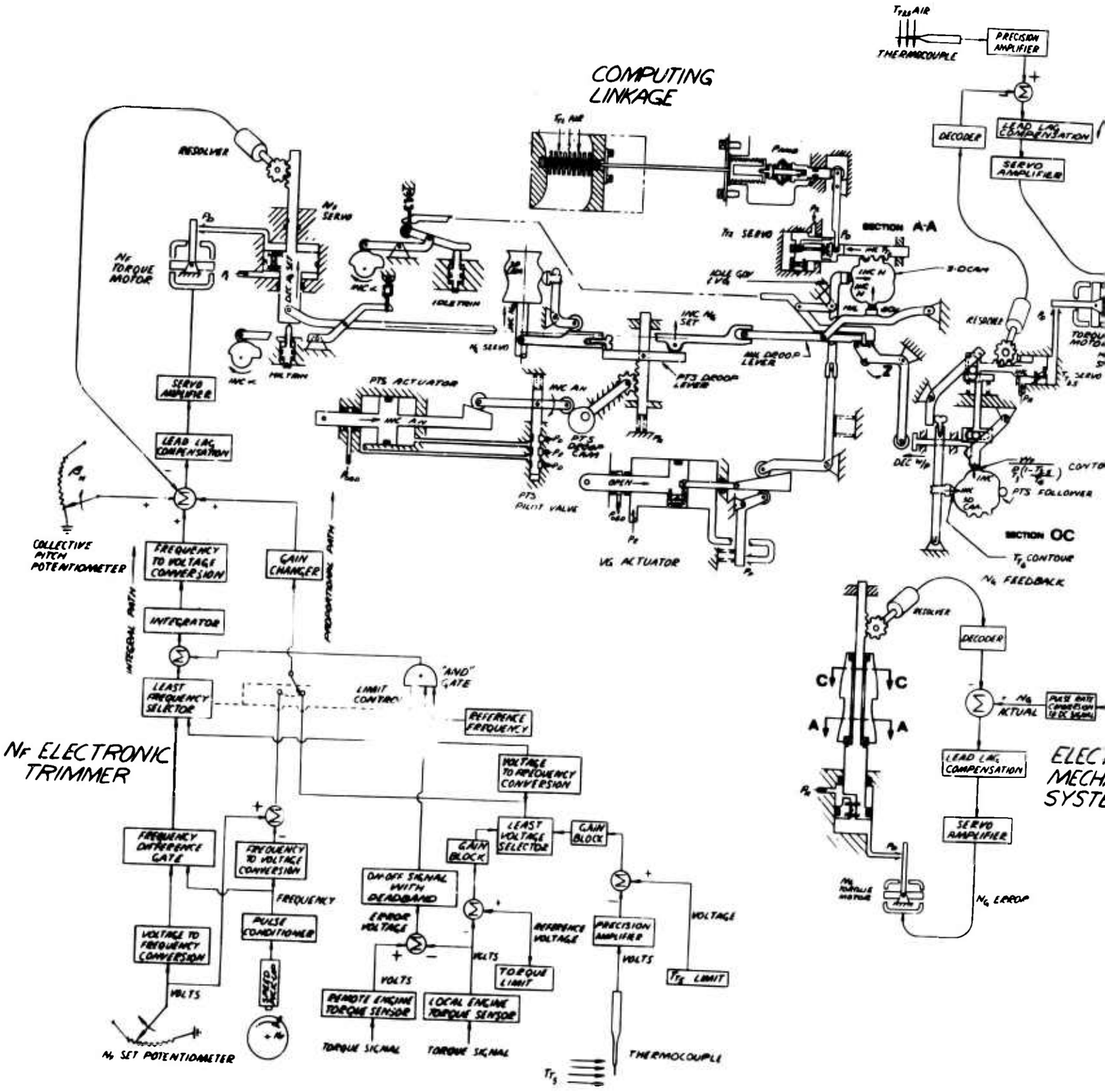

Figure 65. Regenerative Control Schematic.

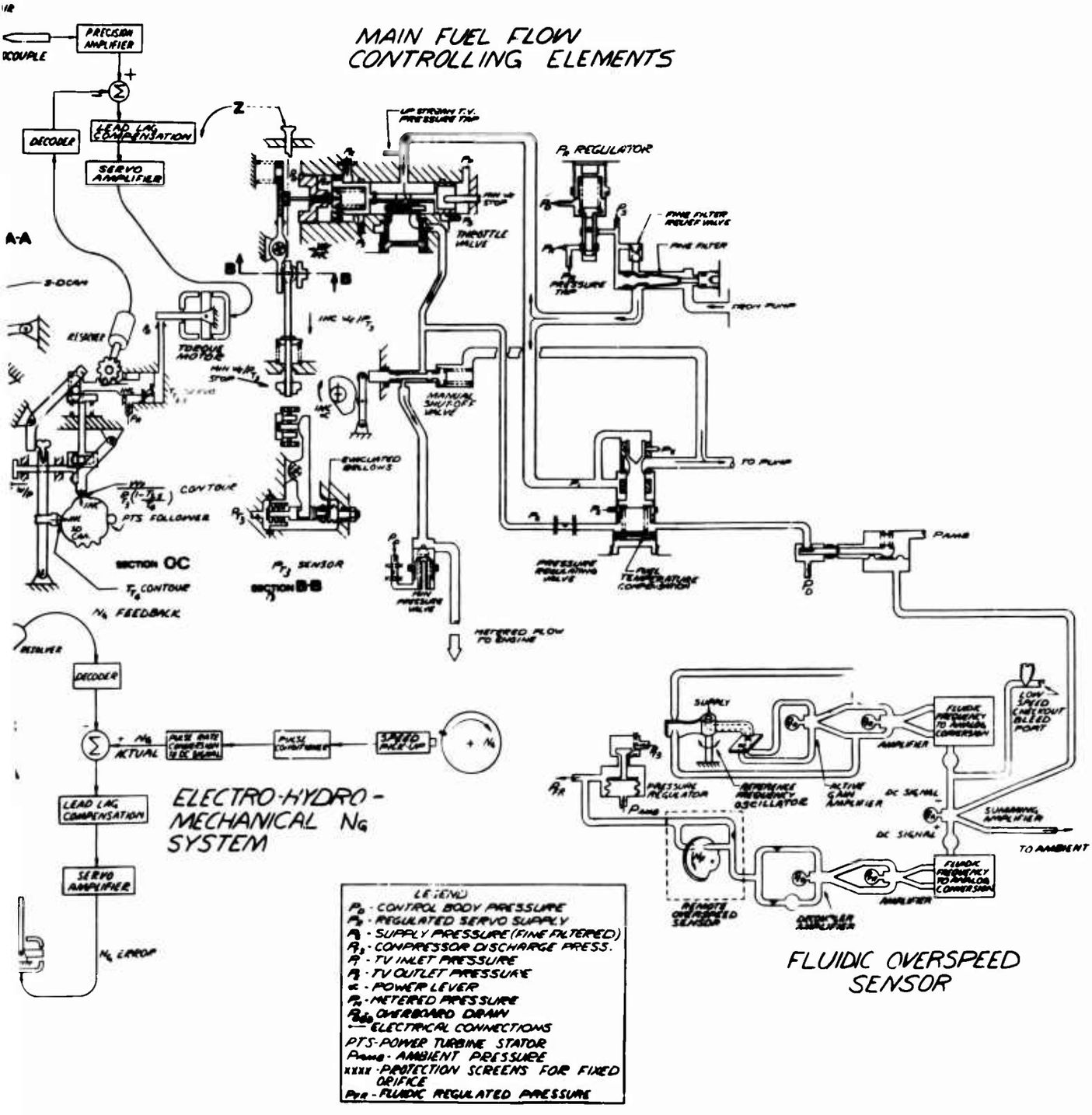
MAIN FUEL FLOW
CONTROLLING ELEMENTS
PRECISION AMPLIFIER
DECOUPLE
DECODER
LEAD LAG COMPENSATION
SERVO AMPLIFIER
Z
A-A
B-B
RESOLVER
TORQUE MOTOR
THROTTLE VALVE
MANUAL SHUTOFF VALVE
ENCLOSED BELLOWS
CONTOUR
PTS FOLLOWER
SECTION OC
SECTION B-B
P_{T_3} SENSOR
T_{t_6} CONTOUR
N_G FEEDBACK
P_R REGULATOR
FINE FILTER BYPASS VALVE
FINE FILTER
FROM PUMP
TO PUMP
P_{AMB}
PRESSURE REGULATING VALVE
FUEL TEMPERATURE COMPENSATION
METERED FLOW TO ENGINE
P_D
ACTUAL
PULSE RATE CONVERSION TO DC SIGNAL
PULSE CONDITIONER
SPEED PICK UP
$+N_G$
LEAD LAG COMPENSATION
SERVO AMPLIFIER
N_G ERROR
ELECTRO-HYDRO-MECHANICAL N_G SYSTEM
SUPPLY
FLUIDIC FREQUENCY TO ANALOG CONVERSION
AMPLIFIER
LOW SPEED CUTOUT BLEED PORT
PRESSURE REGULATOR
REFERENCE FREQUENCY OSCILLATOR
ACTIVE GAIN AMPLIFIER
DC SIGNAL
SUMMING AMPLIFIER
TO AMBIENT
REMOTE OVERSPEED SENSOR
OVERSPEED AMPLIFIER
FLUIDIC OVERSPEED SENSOR
LEGEND
P_D - CONTROL BODY PRESSURE
P_R - REGULATED SERVO SUPPLY
P_S - SUPPLY PRESSURE (FINE FILTERED)
P_{T_3} - COMPRESSOR DISCHARGE PRESS.
P_1 - TV INLET PRESSURE
P_2 - TV OUTLET PRESSURE
α - POWER LEVER
P_M - METERED PRESSURE
P_{OB} OVERBOARD DRAIN
⟵ ELECTRICAL CONNECTIONS
PTS - POWER TURBINE STATOR
P_{AMB} - AMBIENT PRESSURE
XXXX - PROTECTION SCREENS FOR FIXED ORIFICE
P_{FR} - FLUIDIC REGULATED PRESSURE

B

an overboard drain between them are provided on the output rod to contain leakage effectively. The feedback cam on the actuator rod serves to null the system.

Regenerative Acceleration Control System

For the regenerative engine, acceleration fuel ratio units Wf/P_{T3} are computed differently than for the base engine. Algebraically, the computation taking place in the regenerative system is:

$$\frac{W_f}{P_{T3}} = \frac{W_f}{P_{T3}\left(1 - \frac{T_{T3.5}}{T_{T4}}\right)} \times \left(1 - \frac{T_{T3.5}}{T_{T4}}\right) \qquad (1)$$

The fuel control measures $T_{T3.5}$ electrically, and T_{T4} is synthesized on the three-dimensional cam from T_{T2} and N_G signals. $T_{T3.5}$ is divided by T_{T4}, and the result is subtracted from unity. The resulting quantity is then multiplied by $W_f/P_{T3}\ (1-T_{T3.5}/T_{T4})$, which is scheduled from the three-dimensional cam as a function of T_{T2} and N_G, resulting in a W_f/P_{T3} signal. The system can be divided into a $T_{T3.5}$ sensor and servo, and the multiplying linkage.

$T_{T3.5}$ Sensor and Servo

$T_{T3.5}$ temperature is measured by a thermocouple set located at the regenerator outlet. The signal is amplified and compared with a $T_{T3.5}$ servo position signal via the resolver feedback path. Any difference between actual $T_{T3.5}$ and servo position causes the torque motor to modulate the flapper gap and reposition the $T_{T3.5}$ servo. The servo output shaft contains a roller track to enter the $T_{T3.5}$ signal into the computing linkage.

Multiplying Linkage

Two multiplications are effected by the linkage:

$$T_{T3.5} \times \frac{1}{T_{T4}} \quad \text{and} \left(1 - \frac{T_{T3.5}}{T_{T4}}\right) \times \frac{W_f}{P_{T3}\left(1 - \frac{T_{T3.5}}{T_{T4}}\right)} \qquad (2)$$

Both multiplications utilize the tangent trigonometric function in a right triangle (tan θ = length of opposite side/length of adjacent side). For the product of $T_{T3.5} \times 1/T_{T4}$, servo stroke is made proportional to $T_{T3.5}$, and a signal is taken from the three-dimensional cam to make the angular position of the T_{T4} lever proportional to $1/T_{T4}$. The position of the upper end of the pushrod thus becomes proportional to $T_{T3.5}/T_{T4}$. By changing references, the position of the lower end of the pushrod is then made proportional to $(1-T_{T3.5}/T_{T4})$. In a similar manner, the resulting function is multiplied by the W_f/P_{T3} $(1-T_{T3.5}/T_{T4})$ function to produce a pushrod position proportional to W_f/P_{T3}. The calculated acceleration limit ratio unit is then applied to the selection lever to produce its limit when applicable.

Regenerative T_{T2} Servo System

In the regenerative system, two three-dimensional cams are contained on the N_G servo and rotated as a function of T_{T2}. The extra cam loads involved compared to the base engine create the necessity for a servoed T_{T2} system. This system consists of the sensor assembly utilized on the base engine, with the addition of a servo and modified linkage.

T_{T2} Servo and Modified Linkage

The sensor bellows output motion changes a flapper gap which modulates pressure to stroke the servo. Servo motion repositions the flapper gap to its null setting. A rack and gear arrangement rotates the three-dimensional cam as a function of T_{T2}. The linkage modifications facilitate the use of the base engine T_{T2} sensor arrangement for the regenerative systems.

Physical Description of the Regenerative Engine Control

An arrangement drawing of a regenerative version of the proposed advanced control system is shown in Figure 66. To modify the base engine to the regenerative version, the base engine linkage access cover is replaced by a special cover containing the functions required to operate a regenerative cycle engine as described above. Section drawings on Figure 67 also show definition of the components that are affected by the change from base engine to regenerative engine. The estimated volume is 210 cubic inches.

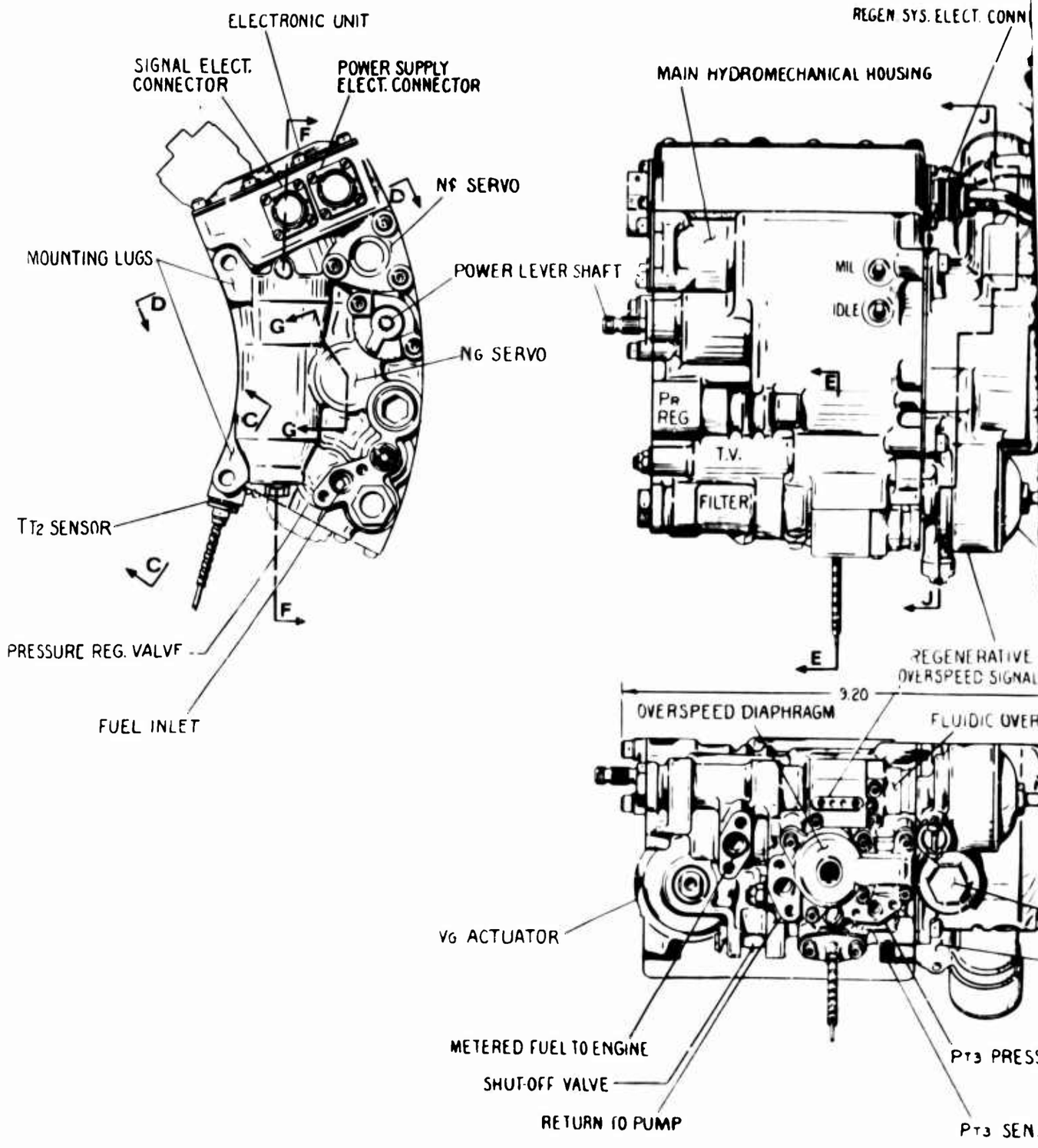

Figure 66. Regenerative Control Arrangement Drawing.

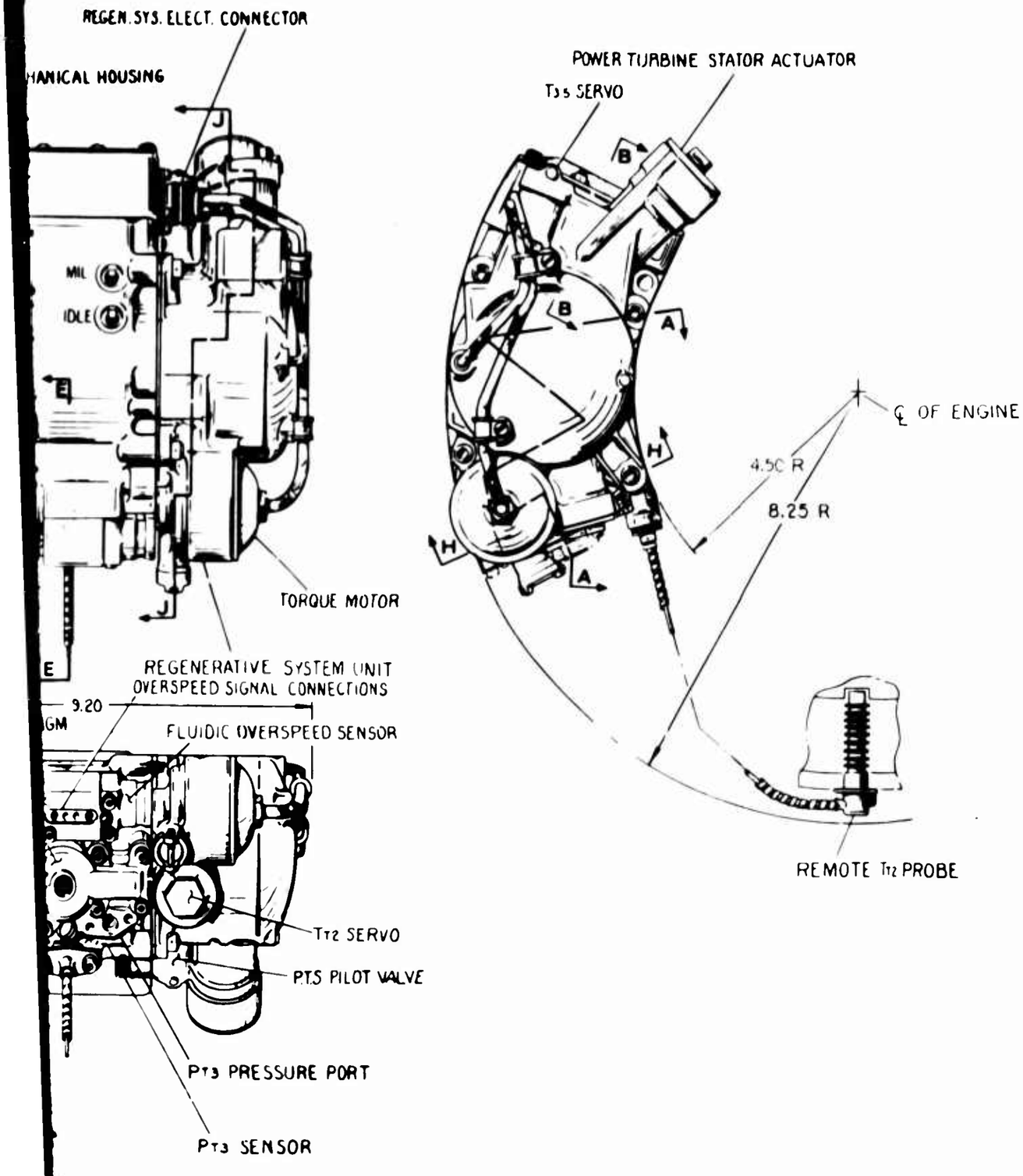
REGEN. SYS. ELECT. CONNECTOR
HANICAL HOUSING
MIL
IDLE
E
J
TORQUE MOTOR
REGENERATIVE SYSTEM UNIT
OVERSPEED SIGNAL CONNECTIONS
9.20
GM
FLUIDIC OVERSPEED SENSOR
Tt2 SERVO
PT5 PILOT VALVE
Pt3 PRESSURE PORT
Pt3 SENSOR
POWER TURBINE STATOR ACTUATOR
T35 SERVO
B
A
H
℄ OF ENGINE
4.50 R
8.25 R
REMOTE Tt2 PROBE

B

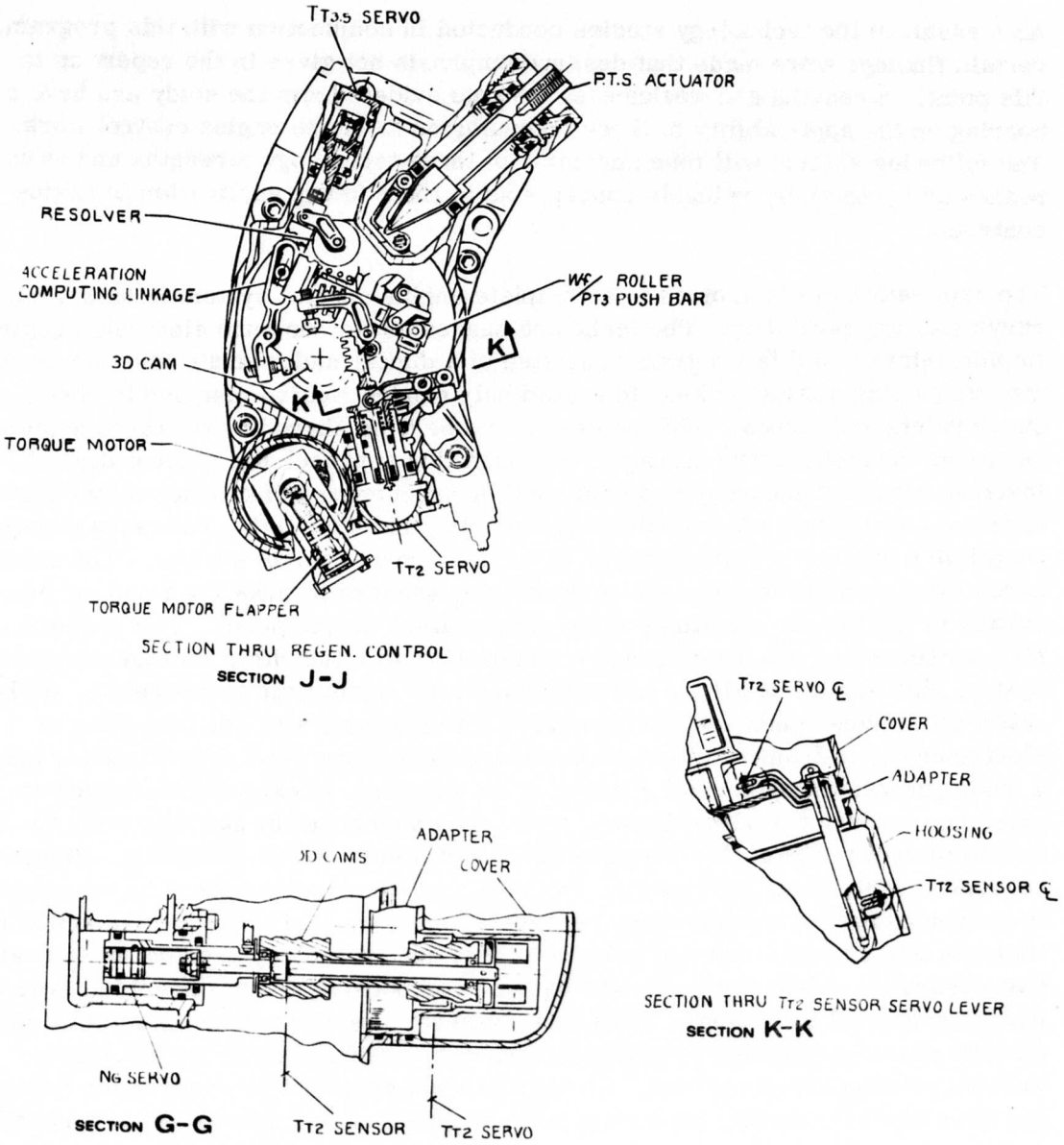

Figure 67. Regenerative Control Sectional Views.

TECHNOLOGY CAPABILITY FOR FUTURE APPLICATION

As a result of the technology studies conducted in conjunction with this program, certain findings were made that deserve emphasis not given in the report up to this point. Strengths and weaknesses became evident from the study and have a bearing on the applicability of these technologies to future engine control work. The following section will touch on some of these technology strengths and weaknesses and potentially valuable concepts as to their future application in engine controls.

The application of electronics to a complete engine control system is hampered by curve storage capability. The technique suggested for the pure electronic control implementation in this program consisted of a digital multivariate function generator employing a table look-up to a read-only nondestructive memory to obtain curve points and slopes. This system would be time shared by the three systems requiring bivariant curve storage. Although this approach has a great deal of merit in terms of accuracy and size, both nonrecurring and production costs are high and constitute a real disadvantage to using this approach. Pressure sensing constitutes another problem area in an all-electronic control system. The primary unresolved problem in this case is developing sensors to meet the required accuracy in the face of variations in the temperature environment. The problem of high nonrecurring costs mentioned in connection with the curve storage or memory system also applies to all the microminiaturized electronic components. In the trade-off studies conducted in conjunction with the program, the cost ratio of electronics to hydromechanical implementation appears to be approximately 2:1 for a basic gas generator control system. This condition is expected to remain in existence for at least several more years, at which time the gap may start to close. Another disadvantage of electronics is the lack of demonstrated reliability. Based on currently established information, reliability of electronics suffers by comparison to hydromechanical technology by perhaps as much as 10:1. Corrective action to improve this situation can and is being taken, and technology predictions indicate that eventually reliability rates will become competitive, or very nearly so, with the hydromechanical technology. This fact, however, remains to be established and until this is demonstrated by actual experience, a deficiency in the electronic technology must be recognized. Another general comment or reservation regarding the electronic technology as applied to engine controls relates to its generally poor compatibility with the harsh environment involved with mounting on a turbine engine. The temperature range usually requires cooling, vibration is an area of concern, and EMI from other electronic systems such as radar must be considered and dealt with successfully.

The fluidic technology, on the other hand, appears to indicate its greatest promise in the face of harsh environmental conditions. It appears that as environmental

factors such as temperature, vibration, EMI, and radiation become more severe, this technology becomes more competitive. At the reasonably mild environmental conditions imposed by this program, fluidics does not compete as a prime technology in the control system; however, fluidics may find application in specialty areas such as the simple fluidic N_F overspeed sensor employed in the final hybrid. In addition, should special program requirements dictate circumstances of an unusual nature, such as eliminating the possibility of a mechanical speed input to the control, fluidics may find application under these circumstances. The fluidic oscillator temperature sensor is a concept that, although not selected for this control system for reasons discussed in previous sections, under other conditions may find application to control systems for steady-state temperature limiting. One factor required to enhance the position of the fluidic technology, as far as application to engine controls is concerned, is demonstrated capability over a reasonably long-time duration of successful performance in the environment of engine air with military specification contaminate. In addition, further miniaturization would be of value in making the technology more acceptable. In the technology trade-off studies conducted as a part of this program, no size advantage was noted for fluidics. With the advent of further miniaturization, however, it would be necessary to prove that the contamination sensitivity situation was not worsened to the point where this became a problem. A last area of potential improvement for fluidics is in the area of interface devices. The applicability of the technology is dependent to a large degree upon its ability to interface with both electronics and hydromechanical actuators. The development of interface devices to permit this, with emphasis on accuracy as well as size and weight reduction, should improve the position of the fluidics technology.

The hydromechanical technology, by virture of the need for fuel regulation and metering, availability of a ready medium for actuation (high-pressure fuel) and vast experience, appears to enjoy a permanent role at least as a portion of engine fuel systems. This creates a slight advantage to employment of this technology in the fuel scheduling and computation system, since it is easier to remain in a single technology than it is to switch technologies and to require an interface device at each change. Certain areas of potential improvement exist for this technology, in spite of its long history in application to engine controls. Miniaturization, in spite of success in recent advanced control systems, has probably not yet reached the point of no further yield and effort should continue in this area.

Fuel control housings are an area where technology advance seems feasible. Recent control systems have resulted in housing-to-component weight ratios of 1:1. Perhaps with some advances in housing fabrication techniques, this situation could be improved, resulting in a lighter total engine control system.

ADDRESS IN PROPOSED SYSTEM TO SPECIFIC REQUIREMENTS

Certain specific control system requirements or areas of interest established by the work statement for this program require separate discussion concerning the extent of consideration received in this study program. These requirements are discussed in the following sections.

Adaptability of the Proposed Control System to Engine Analyzer Inputs

The final hybrid base engine control system defined by this program provides a large variety of parameters, many of which are available for monitoring in electrical form which may be of interest in engine health analysis. The extent to which these signals may be required is probably a function of whether the desired engine health analysis system is intended to be merely an assessment of health or, in addition to this determination, whether it is judged necessary to perform diagnostic analysis which would require the monitoring of additional functions. As implied above, not all of the functions are available in a directly usable form, assuming the analyzer would be electronic in nature. For these functions it would become necessary to add special transducers to convert the desired signal to the electrical form. Table XXV summarizes the suggested parameters for monitoring and indicates the availability of the signal, and the form in which it exists. As is noted in Table XXV, all electrical signals exist at the point where they would be monitored in analog voltage form. Although they have not been factored into this program in terms of weight, volume, etc., special connectors would be necessary on the control which would permit tapping into the pertinent signal lines to monitor these voltages. It should be noted that all of these signals mentioned, at some time, pass to an external connector in the form required. The signals which are not in electrical form are included in Table XXV because they are relatively important signals and probably would require monitoring. To monitor W_f, an electrical flow transducer would have to be plumbed into the external plumbing downstream of the control and, although there are some potential problems associated with this, it is feasible.

To monitor P_{T3} would require a similar installation of a transducer in an external plumbing line. In this case, a tee fitting would be supplied in the P_{T3} supply line for the purpose of installing an electrical pressure transducer. To monitor VG position the problem becomes more complex because a motion electrical transducer would be required. However, VG motion will exist externally in several positions throughout the engine linkage, and one of these positions should be accessible for installation of a position transducer, if required.

Greater emphasis on the initial design of a control system, with emphasis on increasing the number of available parameters and improving the availability of these parameters, probably would result in a system with improved capability for

interfacing with an engine analysis system over the system defined by this program. This is explained by the fact that in the design of this control system, interfacing with an engine analysis system was not a prime requirement. One of the recommendations discussed at the conclusion of this report describes a program for improving the capability of a control system for interfacing with an engine health analysis system.

TABLE XXV. SUGGESTED PARAMETERS FOR ENGINE HEALTH ANALYSIS

Parameter	Electrical Signal Exists	Transducer Required	Comments
N_F Act.	X		Analog voltage
W_f		X	Available in external plumbing
N_G Act.	X		Analog voltage
P_{T3}		X	Available in external plumbing
VG Position		X	External motion available
Trimmed N_G Set	X		Analog voltage
Collective Pitch	X		Analog voltage
N_F Set	X		Analog voltage
Local Torque	X		Analog voltage
Remote Torque	X		Analog voltage
T_{T5}	X		Analog voltage

Improved Vulnerability Resistance

Vulnerability of the engine control system, as considered throughout this program, consists not only of the vulnerability of the basic control package but also of the susceptibility of any portion of the system outside the basic package, the loss of which would result in rapid engine malfunction. In addition, the effect of damage

to external portions of the system (e.g., fuel lines) which would contribute to loss of the system, is considered.

Important factors that influence the vulnerability resistance of an engine control system include size, since this influences projected area and consequently frequency of damage from small-arms fire, resistance of the fuel system to penetration by small-arms fire, dependence of the engine control on functions located remote of the basic control, and the use of remote fuel lines to and from outside functions.

The first aspect of vulnerability previously mentioned, size, was a prime consideration throughout the conceptual design of this system, resulting in a final volume for the control system of 150 cubic inches, which represents an approximate 24 percent decrease in volume over comparable advanced control systems performing similar functions. This reduction in size should result in a comparable reduction in vulnerability.

The second aspect of vulnerability, resistance of the fuel system to penetration by small-arms fire, constitutes a real problem by being completely inconsistent with other program goals related to size and weight. This basic problem stems from the fact that the engine control system as currently conceived is basically a "soft" system; i.e., the lightweight aluminum housings normally used to house the components and provide flow passages will not withstand penetration by a projectile even of relatively low velocity. Corrective action to make the basic control housing resistant to armor-piercing small-arms fire by surrounding the control with protective armor, of even the most recently developed type, would result in an additional system weight burden between 8.5 and 15 pounds, depending upon whether a ceramic or a steel approach is taken. Assuming that the steel approach is rejected due to additional weight penalty (in spite of the fact that a ceramic covering would require replacement after each hit), the volume penalty would be approximately 100 cubic inches. A possible technique for eliminating this weight and volume penalty in a noncombat situation would be to fabricate a removable-type ceramic covering for the "soft" control, which then could be removed or added as mission conditions dictated.

Recognizing the typical engine installation conditions, this might represent a very difficult and time-consuming task to accomplish between missions. Another approach would involve fabrication of the control housings from steel; however, with the thickness of castable housing material required to resist penetration by small-arms fire, this approach would result in significantly more weight than the incorporation of ceramic armor. In addition, the capability for removal of the penalty under noncombat conditions is lost.

Dependence of the engine control upon functions located remote of the basic package can be controlled to some degree, and has been in the case of this control

system. With vulnerability an important factor in the trade-off studies, items such as a remote hydromechanical N_F control package with attendant hydraulic transfer lines are discouraged, resulting in a control package that is reasonably self-contained, except for the required, remotely sensed functions and a minimum of external fuel lines. This consideration, incidentally, represents a case for integration of the fuel pump within the confines of the fuel control housing.

Maintainability

The hybrid control was arranged in a manner to improve the ease of maintenance in two ways: first, field maintenance; second, depot maintenance.

For field maintenance, the control was designed to mount on a simplified three-point suspension as shown in Figure 51. This method of mounting reduces control removal time by eliminating the present-day, hard-to-get-at, hold-down screws that must be torqued to specific levels. The second step taken was to design the electronic power turbine governor control and the N_F overspeed controls as plug-in-type components. Both of these systems can be removed from the control without disturbing the hydromechanical section. Finally, all on-aircraft trimmers and adjustments are easily accessible through a small nacelle door.

Depot maintenance is also aided by the plug-in-type trimmer and overspeed governor because these units can be replaced quickly and the control recalibrated. In addition to this, the shutoff valve, pressure-regulating valve, P_r regulator, filter and T_{T2} sensor are removable from the outside of the main control body to reduce the effect their removal has on other components, such as linkage.

Failure Mode Considerations

The organization of an electrical control system for power turbines and the interrelationship of the power turbine control to the gas generator control may be implemented so that power turbine control system failures have different effects. As part of this study program, Hamilton Standard elected to gather from experienced helicopter manufacturers and operators the personal preferences they might have relative to how an electrical power turbine control system failure, in the event it occurred, would result in minimum danger to life or damage to the aircraft.

Three major helicopter manufacturers and a large commercial operator were contacted for this survey. The types of personnel contacted were flight test engineers, propulsion designers, propulsion analytical engineers, project engineers, and pilots. These people were asked to consider their preference for control mechanization on both single and multiengine helicopters for the following typical missions:

Search and Rescue	Tactical Weapons System
Heavy Lift	Antisubmarine
Personnel Transport	

It was assumed that a loss of power turbine reset capability to the gas generator control would occur during one of the following flight maneuvers:

Climb	Cruise
Descent	Hover
Autorotation	Bank

Five options for possible failure modes were then presented which might be available to the control designer in mechanizing the control system.

1. Hold the power setting which was set prior to the power turbine control failure or the last power setting ("fail-to-condition").

   A failure-detection circuit would be required to make the pilot aware of this failure prior to experiencing a lack of response to a change in power demand. Having this knowledge, he could then manually modulate gas generator power as required.

2. Fail to maximum gas generator power. This would be followed by a power turbine overspeed where an overspeed limiter set at 105 percent, for example, would then reset the gas generator. Manual modulation of gas generator settings up to the 105 percent power turbine speed is possible subsequent to this failure.

3. Fail to 90 percent gas generator power. The power turbine speed limiter would operate as in 2 above. Manual power setting to reach 100 percent power is available if needed.

4. Fail to some other percentage of gas generator power. Power turbine speed limiter would operate as in 2 above. Manual power setting to reach 100 percent power is available as needed.

5. Fail to shut down system.

The results of this survey showed a unanimous preference for a mode of control that caused the engine to go to maximum power if a failure occurred on single-

engine applications. This mode was desired regardless of the type of aircraft mission and for all of the flight maneuvers listed above. It was desired to have the limit be the topping power of the engine so that if an engine were derated for a particular installation the limit should be derated power. Some of the personnel contacted indicated they would trade off a somewhat higher failure rate if necessary to obtain a fail-to-high-power system as compared to a fail-to-condition system. All of the personnel contacted agreed that fail-to-lower-power or fail-to-shutdown systems were not acceptable.

The only group that indicated a fail-to-condition system might offer some advantages over a fail-to-high-power system was the commerical operator on a multiengine, single-rotor helicopter. One of his main concerns was on a heavy-lift mission where the aircraft may be hovering in relatively close quarters; the application of maximum power might cause a rapid change in the lateral position of the aircraft. On a dual rotor aircraft where a rapid change in power (torque) would not cause the aircraft to yaw, the fail-to-high power was preferred over the fail-to-condition system. Everyone agreed that the fail-to-condition system must have a failure detection circuit to warn the pilot of the failure before he demanded more power because of a change in maneuver. This is extremely critical for combat-type missions, where the normal procedure might be an autorotation descent with a flareout to hover before landing. Even with a detection circuit displaying a flashing light or giving an audio signal, there was much concern about the pilot's taking over manual control of the engine when he is preoccupied with picking his hover area and timing his flareout. The commercial operator, on the other hand, tends to fly the aircraft in a more conservative manner by making the transitions from one flight maneuver to another more gradually; therefore, he would have more time to transfer to a manual mode of engine power control from a fail-to-condition system.

It is concluded from this survey that the engine control system should be implemented in such a manner as to cause an automatic increase to high power in the event that a failure occurs in the electrical power turbine control system. For the aircraft missions and flight maneuvers noted above, this provides the minimum danger to the aircraft until the transition is made to manual control of the engine power. Although one operator expressed preference for a fail-to-condition system on multiengine, single-rotor applications, the fail-to-high-power system was much more desirable for an engine system than would be intended for use in both single and multiengine applications.

Failure mode considerations as applied to other portions of the control system include such protective measures as the addition of a failsafe plateau schedule at both high and low speed and high- and low-temperature portions of the three-dimensional scheduling cams. This permits operation at some preselected nominal condition in the event of a serious failure in either the speed or temperature system in

either direction. The fluidic N_F overspeed sensor provides protection against a multitude of failures when operating in this mode, which is the normal helicopter operating mode. As an example, in the event of a saturated throttle valve servo to maximum condition, the N_F overspeed sensor would be triggered, cutting back fuel flow downstream of the throttle valve, thus providing system protection. It was elected not to provide a manual mode of throttle valve operation as a backup failure protection, since the use of this system in some unforeseen circumstances might result in damage to the engine that would otherwise not have occurred.

Electromagnetic Interference (EMI) Susceptibility and Suppression Considerations

The EMI characteristics of the electronic engine control system are vital to the correct functioning of the device. The study control must incorporate an aggressive EMI control plan at the outset of the design to effectively eliminate its susceptibility to adjacent systems, not jeopardize adjacent systems and not interfere with its own internal operation. The purpose of the control plan is to direct the EMI design approach using MIL-STD-461 as a design guide. The above should consider test cell and aircraft electronic and electrical systems. For this reason, general considerations, such as those listed, have been applied to the study control and will be required when applying this control concept to hardware.

The primary source of EMI within the control and the units with which it interfaces are the following:

1. Power supply
2. Thermocouples
3. Magnetic speed pickup

The measures listed below should be taken to prevent undesirable reaction of the control as a result of susceptibility to radiated fields in the area of the control or its inputs. Shielding will achieve the required degree of attenuation of EMI radiation generated by the control itself (MIL-I-6181D).

1. The housing is to be designed as an integrally shielded box, with all mating surfaces (case, covers, etc.) finished with conductive coatings to inhibit corrosion by excluding humidity and to provide low-impedance mating surfaces. The internal surfaces should be finished to provide proper grounding surfaces, with the circuit ground being electrically connected to the case ground.

2. Apertures, where necessary, should be provided with components that are shielded and conductively mounted.

3. Aperture design should conform to the following figure of merit:

$$\frac{L}{D} = 2 \tag{3}$$

where L = aperture length in inches

D = aperture diameter in inches (or largest diagonal)

4. Connectors should be mounted on surfaces that are conductively coated and employ RF gasketing.

5. Cover mounting screws should be spot-faced and conductively coated.

6. Housing wall thicknesses should be based on shielding effectiveness necessary. Shielding effectiveness is expressed in db based upon the following equation:

$$S = A + R + B \tag{4}$$

where S = shielding effectiveness

A = absorption loss

R = reflection loss

B = degradation factor

7. Busses should be provided for power supply voltages used by the computer.

8. Insulation materials should be used to provide capacitance to ground for noise bypassing.

9. Electrical shields which reduce capacitive cross-coupling and minimize conducted and radiated electromagnetic interference should be used.

10. A layer of buss material, instead of wire (reduce L di/dt generation) should be used.

Provisions intended to ensure the proper installation of the peripheral equipment feeding, or being fed by, the control include:

1. Thermocouples should be shielded, since they are good noise pickups and operate at very low voltage levels.

2. Feed-through capacitors should be employed in the control to shunt any noise present on the thermocouple lines to ground.

3. Power input circuits - Low pass, T-section, EMI filters should be used on the alternator input, if necessary.

The bonding of interconnecting mechanical assemblies in the equipment is provided in the design of the housing. The bonding practices to be followed will be geared to MIL-B-5087B.

The ground philosophy to be used must:

1. Minimize or eliminate coupling into low-frequency, low-level circuits such as the sensors.

2. Reduce radiation and coupling of radio frequency interference.

3. Preclude the development of inter- and intra-equipment potentials which can cause sensitive-circuit malfunction or performance degradation.

With reference to bonding and grounding, the following provisions should be made:

1. AC power neutral from the alternator is to be grounded at the alternator only. The alternator housing is to be grounded to the engine.

2. Circuit ground is to be tied to case ground, which is in turn grounded to the engine.

3. Cable shields are to be terminated to ground at each end, and at all breaks by leads not exceeding 1 inch in length. Shields are to be peripherally terminated in a conductive connector backshell.

Decreased Contamination Sensitivity

A stated technical objective of this program, decreased contamination sensitivity, is assured by the incorporation of several proven features as well as by some new features of a promising nature, not yet evaluated. Contamination considerations relative to the prime fuel metering and computation system can be separated into those associated with the main flow components and those associated with the computation elements. The main flow elements must be designed to function in the presence of fuel contaminated in accordance with MIL-E-5007C. This is accomplished by the selection of materials with demonstrated capability of operation in this environment, such as through hardened AISI 440C for the metering valve plate and guide as well as the minimum pressurizing and shutoff valves. The pressure regulating valve, which sustains a much higher pressure drop and consequently high-velocity impingement of contaminant particles, would be flame plated with tungsten carbide for additional resistance. The computational elements are protected to a large degree by the incorporation of a high-efficiency, no maintenance, wash-type filter which provides at least 20-micron effective filtration to the servo supply fuel. Critical functions in the computational section are further protected by the incorporation of last-chance screens. The selection of the shear plate-type metering valve should represent an advantage in reduction of contamination sensitivity by the nature of its wiping action by the two plates in intimate contact tending to exclude contamination from the area of metal-to-metal relative motion. Careful attention to materials selection is required for corrosion resistance and all computing valves should be servoed to have unsticking forces in excess of 10 pounds.

Automatic Fuel Density Compensation

If left uncompensated, the variations of three fuel characteristics could cause improper engine operation with a scheduling control. These fuel characteristics are the heating value tolerance, the temperature effects on density, and the density variation with different types of fuel. It would be desirable to have all these variations automatically compensated so that they would not have an effect on engine operation. However, as a study of these variations has shown, full automatic compensation is neither necessary nor practical with the mode selected as a result of this study program.

Referring to Figure 68, it can be seen that the heating value tolerance is relatively small and, therefore, has a negligible effect on engine operation. This is not true of the temperature variation effect on fuel density. Fuel density tolerance is about ±6%. Present-day fuel controls compensate for this variation by the use of bimetallic discs in the metering valve pressure drop regulator. These discs fully compensate for temperature effects on density.

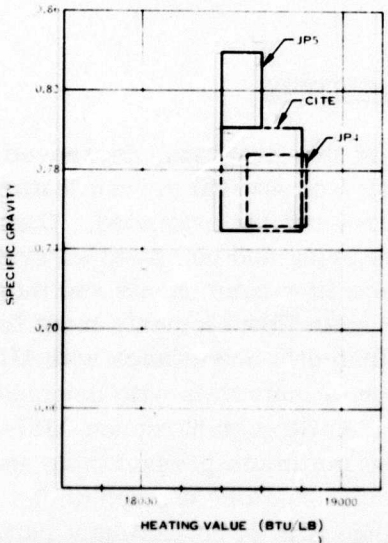

Figure 68. Fuel Specific Gravity and Heating Value Variation.

The third characteristic which is as critical as the temperature variation is the density variation between fuels. Presently, this is manually compensated for by an adjustment on the metering valve pressure drop regulator. Automatic compensation of this variation requires a device that produces a signal as a function of fuel density. An investigation has shown that devices of this type are relatively large and complicated compared to our simple position adjustment on the pressure drop regulator. It is therefore proposed from a practical standpoint that the present method of fuel-type compensation is sufficient.

An interesting fact to note is that if the T_{T4} closed-loop mode of engine control were used instead of the W_f/P_{T3} open-loop mode, heating value tolerance, temperature effects, and fuel type would not have to be compensated for at all. The T_{T4} limit would control the metered fuel flow regardless of variations in the fuel characteristics. However, because the beat T_{T4} sensor available was not accurate enough to meet the control specification and because of problems with engine stability discussed in the section on mode considerations and the gross transient analysis section, the T_{T4} mode could not be used as an adequate means of engine control.

Fly-By-Wire Capability

Fly-by-wire capability reflects the ability of the engine control system to interface with an automatic flight control system by making all normal pilot input parameters to the control system easily available in a form such that they could be interfaced with a master flight control system.

In the resulting hybrid control described in this report, the power turbine governing

system was best executed by the electronic technology. The results of this selection also give a second benefit in that both inputs, N_F speed set and collective pitch reset, are adaptable to fly by wire. In the proposed control, it was decided that both inputs would be aircraft mounted in the cockpit. This approach eliminates the need for complex temperature and deflection compensating linkage or cable systems between the cockpit and the fuel control. Thus, the N_F system is in reality a fly-by-wire system as it currently exists.

The other main input to the control is the gas generator power lever to the hydromechanical section. This is shown as a control shaft in the arrangement drawing and provisions have been made to adapt a stepper motor to this shaft for interfacing with an electrical signal to set N_G power lever. To reduce the loads on this motor and to permit a reasonably sized motor, the power lever torques have been kept under 10 inch-pounds. By these techniques it is believed that successful integration into a fly-by-wire system could be achieved.

CONCLUSIONS

The following represents a list of some of the major conclusions which have been drawn from this study program:

1. The best overall mode of engine control for this size range and type of engine, based on the assumptions made for sensor and probe capabilities up to the mid-1970's and based upon the estimated engine variations, is an open-loop scheduling W_f/P_{T3} gas generator control. To this gas generator control, an isochronous N_F governor with proportional-plus-integral action is added as a trimmer to reset the gas generator droop line to maintain N_F speed. Included in this trimmer are provisions for closed-loop, steady-state turbine discharge temperature limiting, torque limiting and local and remote engine torque-sharing.

2. The technology employed to implement this mode of control, based upon detailed trade-off studies conducted comparing electronics, fluidics and hydromechanical approaches to various functions of the control system, is a hybrid system consisting of a hydromechanical gas generator control with an electronic N_G speed sensor, an electronic N_F trimmer package with temperature limiting, torque sharing and limiting and a fluidic N_F overspeed sensor providing single speed backup N_F governing through the gas generator control. This technology selection is influenced by the selection and relative weighting value of the evaluation criteria factors as presented in Figure 1 and discussed in previous sections.

3. The mode of control would best be modified for optimum running of a regenerative version of the engine by the substitution of a W_f/P_{T3} $(1 - T_{T3.5}/T_{T4})$ schedule for the conventional acceleration schedule. A $T_{T3.5}$ sensor is added and an additional cam is required to schedule T_{T4} as a function of N_G and T_{T2}. This permits a fuel flow computation based upon the heat addition from the regenerator. In addition, a power turbine stator scheduling and actuation system is added to maintain constant high turbine inlet temperature over a wide range of operating conditions for improved efficiency of operation.

4. The control design resulting from this program has an estimated weight of 12.0 pounds and a volume of 150 cubic inches. This represents an approximate 19% reduction in weight and a 24% reduction in volume over comparable sized advanced control systems currently under development. Initial weight and volume goals established for the base engine control were 9.0 pounds and 137 cubic inches.

5. The projected production costs of the control design arrived at in this program are approximately equivalent to those for present advanced control systems. Although improvements in design for cost effectiveness were made, these are more than offset by increases in complexity in the form of added functions and requirements. This will probably remain a fact until engine performance can be sacrificed for control simplicity or additional pilot work-load.

6. The effect of technology advancements on this program and the effect a change in the usage date from the mid-1970's to 1980, for example, that would have on the program are uncertain. Certain technology advances currently nearing fruition such as the edge-tone fluidic oscillator, the optical pyrometer, fluidic computation circuitry and miniaturized electronic curve storage capability may find increased application in engine controls under certain conditions; however, with the requirements and ground rules as established for this program, recommendation for application to this program was not indicated. It is possible that by modification of the ground rules and/or weighted evaluation criteria in conjunction with an extension of the usage date to 1980,the outcome of the program would be changed, resulting in the application of one or more of these technology advances. With regard to the application of a completely closed-loop turbine inlet temperature control, however, it does not appear probable that the extension of the usage date to 1980 would allow the recommendation of this technique of engine control due to dynamic response problems inherent in the engine/control system combination.

RECOMMENDATIONS FOR FUTURE PROGRAMS

As a result of the work accomplished during this study program, several areas for future study and/or evaluation have become apparent. These recommendations fall into three categories:

Category I	Requires implementation and evaluation in order to lessen possible jeopardies in implementing the recommended control system
Category II	Extends the scope of the program now being reported on
Category III	Special technolcgy areas to establish applicability to engine control systems

CATEGORY I

Recommendations falling into the first category which represents concepts not currently in practice and requiring some degree of demonstration prior to application to an exploratory development program include:

1. 75,000 rpm. N_G Speed Sensor

   Current maximum engine gearbox output speeds (control sensor input speed) are approximately 4000 to 4500 rpm, with the highest reaching 6000 rpm. Advanced control systems currently under development are designed for input speeds up to 15,000 rpm. Because engine rotor speed tends to be inversly proportional to engine size, the new advanced small engines with high rotor speeds have to provide large reduction gearboxes to drive fuel controls and other engine accessories. In order to overcome this disadvantage, a goal of this program was either to drive the control mechanically at direct engine speed or to require no mechanical drive at all. To accomplish this, fluidic, electronic and hydromechanical flyweight sensors with a gear reduction in the control were reviewed. The electronic speed sensor was selected for application to this control.

   A program to pursue this activity would consist of additional study to explore the following areas. The maximum operating speed of mechanical sensors should be determined with particular emphasis on contact wear and bearing life. Further study of which electronic approach is preferable, ergine-driven alternator or magnetic pulse sensor, should be accomplished. Further accuracy study should also be accomplished on the fluidic speed sensor. The relative

merits of these speed-sensing methods from the viewpoint of cost, durability, accuracy and engine environment compatibility should be studied. Following this study, the most promising technique would be selected, and a concept would be designed for breadboard implementation. Sketches would be produced for manufacture of a prototype sensor. A sensor and test fixture would then be manufactured and assembled, followed by evaluation testing with primary emphasis on accuracy and response.

2. Develop a Shear-Type Metering Valve for Accurate Metering Down to 15 PPH

One of the requirements of this program is the need to meter fuel flow accurately down to 15 pounds per hour (established by the regenerative version of the 2-pound-per-second engine). To meet this rather stringent requirement and at the same time maintain the miniaturization required by the program, a new concept in metering was required. Accurate metering at low flows requires strict metering window configuration control and the elimination of metered leakage. The flat plate valve previously described appears to satisfy these requirements; however, additional design effort as well as evaluation testing is required to establish the validity of this design. Design analysis on the concept is required in the following areas:

a. The piston must be lapped to a bore in the housing. This is undesirable from a cost standpoint.

b. The piston must be antirotated which increases valve friction.

c. Distortion of the window plate during installation remains a potential problem.

d. The plate-loading flexures must be analyzed to insure that the plate remains seated on the valve under all conditions.

e. The effect of variations in parallelism between plate and spring seat requires further evaluation.

It is recommended that this design effort be pursued and that this be followed by prototype manufacturing and evaluation testing of a single system in a fixture.

3. Development of a New Shutoff and Minimum Pressurization System Design

The same problems of wide flow range and metering at extremely low flow levels also impose problems on the shutoff and minimum pressurization system. Some of these problems include stability of the minimum pressurization valve at low flow levels, reduction of power lever torque on the manual shutoff valve, elimination of internal leakage because of its significance to metered flow error, maintenance of zero external leakage and miniaturization of components consistent with program goals. The concept design (shown in the sectional views in Figure 52) proposed to accomplish these goals should be detail designed, prototype-manufactured and evaluation-tested in a fixture to ensure its adequacy in meeting design requirements.

4. Implementation of the Complete Control System

The advisability of a program to implement the complete control system concept as arrived at in this program is contingent to a large degree upon the immediacy of a requirement for this class and size of control system. The results of this program indicate a control system which, although different in many respects, is not radically different from new control systems currently under development for the 1500 hp class of advanced turboshaft engine. This results in a situation where, without the pressure of an immediate requirement, greater flexibility in the selection of a program to reduce program jeopardies is afforded. Possible approaches for the implementation of this program include:

a. Prototype implementation of the program base engine control system and subsequent demonstration running on an existing small engine.

b. The same as above except evaluation running would be on a computer simulation of an engine.

c. Prototype implementation of the regenerative version of the engine control system and demonstration running either on a regenerative engine or a computer simulation of a regenerative engine.

d. Modification of an existing new control system, such as one of the controls currently under development for the advanced 1500 hp Army turboshaft engines, to incorporate the regenerative

control concept arrived at under this study, and demonstration on a regenerative engine or a computer simulation.

CATEGORY II

Recommendations for future activity falling into the second category, which consist of broadening or extending the scope of the present program, include:

1. Integration of a Variable Displacement Fuel Pump With the Control System

A fuel pumping system was described in the section entitled Alternate Arrangement Scheme Involving Integration of Control System With Pump, which consisted of a variable stroke vane pump, modulated to maintain a constant metering head across the metering valve. This system offers distinct advantages in the area of reduction of fuel temperature rise at low-flow, high-speed conditions and the accompanying reductions in drive horsepower. In addition, recent developments in high-speed, contaminant-resistant vane pumps hold promise for the eventual achievement of speeds of 55,000 rpm and above, thus allowing the gearbox to be discarded. In view of these potential advantages it is recommended that a joint pump vendor/control vendor program be implemented to develop an integrated pumping system based on the variable-displacement vane concept. As was noted in the referenced section, this approach represents a true integration of the fuel pump into the control system, since pump delivery is modulated in response to a control fuel flow demand. As a result of the severe transient performance imposed by the necessity to supply fuel for variable geometry actuation, it is essential that the dynamic performance of the pump and control be defined as a total system rather than as separate components.

A program to develop this concept should emphasize very close coordination between the selected pump and control vendors to ensure a proper address to system integration. This is especially important during the design phase to ensure adequate resolution of the dynamic requirements referred to previously.

The development phase of the program would emphasize contamination resistance at very high speeds (55,000 rpm and above), dynamic performance and freedom from hydraulic interactions. In addition to the basic pump characteristics of flow, head, speed, etc., the requirements imposed by the loads of the pump actuator itself would be evaluated. The program could be conducted either in conjunction with the follow-on prototype design or by using existing fuel control components to create the pump/control subsystem.

2. Additional Regenerative Control Adaptability Work

Since it is anticipated that the ratio of regenerative engines to base engines in any particular size range would probably be on the order of 0.20 or less, it is important that the regenerative control concept impose as little burden as possible on the base engine in terms of weight, size, cost, etc. Based on the concept evolved during this study program it appears this penalty is between 0.50 and 1.00 pound; however, additional work is recommended to study the regenerative mode further to verify its adequacy and define this adaptability penalty.

3. Determine Effect of Control Simplification on Engine Performance and Pilot Work Load

Because of the obvious relationship between control complexity and control costs, it appears worthwhile to evaluate the various functions required of a control system of the type recommended by this program to determine the results (in terms of engine system performance and pilot work load) of either removing or decreasing the performance requirements of specific control functions. This is somewhat contrary to the trend toward increased complexity and performance in recent control systems. A study of this type might, however, indicate areas where for certain applications, the best payoff in reduced cost might be available at the least sacrifice in system performance.

4. Determine Optimum Control Organization for Ease of Propulsion System Analysis and Troubleshooting

The need is frequently expressed for the development of a system approach to automate and simplify the analysis of a propulsion system to determine its present performance relative to a standard or perhaps even to anticipate incipient problems. In the evaluation of the control system concept designed in this program, attention was given to making available such parameters as would assist in this analysis; however, this was not a prime factor in the design of the system. It is proposed that this problem be studied further to determine the additional parameters, form of organization and form of mechanization that would assist in this analysis and, based upon this information, to determine what the effect on the control system would be to optimize the design of the system with this need in mind. By conducting this evaluation, it would be possible to weigh the benefit of the increased potential for propulsion system analysis against the penalty involved in terms of control system complexity, cost, weight, etc.

5. Determine Effect of Variation in Weighted Evaluation Criteria on Program Outcome

As discussed previously in this report, the outcome of this program, particularly in the area of technology selection, is greatly influenced by the relative value of the weighted evaluation criteria as defined in Figure 1. Recognizing that different programs will have different emphasis it is recommended that the technology selection be repeated with various assignments of values to the weighting factors to determine the effect this would have on the makeup of the hybrid control system.

CATEGORY III

Two recommendations for follow-on programs fall into the third category relating to the pursuit of special technology advances to determine their capability for future application to control systems of the type defined by this program:

1. Determine the Effect of Environmental Factors on the Performance of the Fluidic Temperature Sensor

The accuracy of the basic fluidic oscillator as well as its performance potential for future engine control application has been discussed in detail in this report. One aspect of this sensor which does not appear to have received sufficient emphasis, however, is the effect of various environmental factors on sensor performance. Included for evaluation should be such factors as humidity, fuel air ratio, the long term effect of operation in combustion products and the length and configuration of inlet and signal lines.

2. Implementation of an Optical Radiation Pyrometer for the Environment of an Engine

This technique for turbine inlet temperature sensing appears to offer an accurate, fast-response approach to sensing actual metal temperature over a limited but high range of temperature. To prove the acceptability of this technique for a small engine control system, a program should be conducted to incorporate a working system of this type in a small engine. The system should be operated for an extended period of time to determine if potential problems associated with the engine environment such as temperature, vibration, lens sooting, electronic part stability and reliability can be overcome.

APPENDIX I
FLUIDIC N_F OVERSPEED SENSOR

GENERAL

A fluidic sensor and amplifier utilizing compressor discharge air as its prime power supply is particularly attractive as an overspeed protective device backing up an electromechanical prime control system. The high speed of response of fluidic amplifiers makes it possible to sense shaft speed directly with simple passive speed choppers in locations inaccessible by other means. The resultant frequency signals are processed by fluidic amplifiers and compared to a reference. An analog output signal is derived which is proportional to the deviation of shaft speed from the reference speed.

Test results on the functional blocks required to implement a fluidic overspeed sensor show that a fluidic sensor can operate reliably and accurately in the engine environment.

SENSOR OPERATION

A functional block diagram of the overspeed sensor is shown in Figure 69. The speed signal generator is a disc or drum mounted on the rotating shaft. The disc interrupts a jet of air between a supply nozzle and receiver once per revolution of the shaft. The resultant signal is a frequency (f_S) equal to the shaft rotational frequency. The decoupler amplifier amplifies the AC signal and removes undesired DC or slowly varying pressure signals appearing on the signal line. These undesired signals may be introduced by buildup of pressures in the sump containing the signal generator. The signal line is also pressurized through a dropping orifice from the supply to prevent ingestion of oil or other contaminants appearing in the sump. The output of the decoupler amplifier contains only the desired signal (f_S). This signal is processed by a frequency-to-analog circuit.

This frequency-to-analog (f/a) circuit is a pulse forming circuit, generating 2 pulses per input cycle. Averaging and smoothing these pulses in a filter yields an output pressure (P_O) directly proportional to shaft speed. The area of each pulse generated and hence the scale factor of the f/a converter are dependent on both the supply pressure and the temperature of the gas in the converter. An accurate determination of when f_S has reached the desired set speed then requires that P_O be compared against a reference which is also supply pressure and temperature dependent. This reference pressure (P_r) is generated by feeding the output of a fixed frequency oscillator to an f/a converter identical to the converter used in the primary sensing path. The outputs of the two converters are compared in a summing amplifier.

The output of the summing amplifier is proportional to the difference between the reference frequency and the signal frequency. The output is one polarity when $f_s < f_r$ and the opposite polarity when $f_s > f_r$.

The proportional range of the output is a function of both the gain and saturation level of the output amplifier. The range is selected to meet the particular application. Proportional ranges as low as ±1% to as high as ±20% of set speed are typical.

A key functional block in the sensor is the reference frequency oscillator. The output frequency must be independent of supply pressure, temperature and externally induced vibration. The basic frequency reference for this oscillator is a torsional reed with a very low damping factor. This reed is used in the feedback of fluidic amplifier to form a fluidic oscillator. The reed is dynamically balanced to make it insensitive to shock and vibration. The reference spring for the torsional reed is fabricated of a material with a modulus of elasticity independent of temperature over the range of concern. The particular oscillator which has been tested utilizes Ni-span C as the spring material. Almost complete independence of supply pressure is obtained by utilizing reeds with a damping factor on the order of 0.005.

Checkout of the sensor at speeds lower than the normal set speed is done by lowering the reference pressure P_r by bleeding flow through a bypass orifice. In normal operation the flow is blocked by a shutoff valve located at the end of a line connected to the low-speed checkout port. Opening the valve reduces the set speed to a value dependent on the size of the bypass orifice.

A circuit schematic of the overspeed sensor is shown in Figure 70. Amplifier number 1 provides the active gain required for the reference frequency oscillator. A jet pipe mounted on the torsional reed directs its output at two receivers which communicate with the control ports of the amplifier. The amplified signal is fed back as an exciting torque on the reed to sustain oscillation. The output of the oscillator is raised to the level required to drive the frequency to analog converter circuit by amplifier number 2. Amplifiers number 3 through number 5 convert the frequency to an analog output. Amplifier number 3 is a fluidic flip-flop used to convert the sinusoidal output of the oscillator to a square wave. Amplifier number 4 (flip-flop) and amplifier number 5 (fluidic rectifier), along with volumes V_1 and V_2 do the pulse forming. One pulse is formed at both the leading and trailing edges of the square wave. The area of the pulse is controlled by the volumes V_1 and V_2 and the supply pressure used on amplifiers number 4 and number 5. The pulses are filtered by volume V_3 to give a DC signal which can be applied to the input of the summing amplifier.

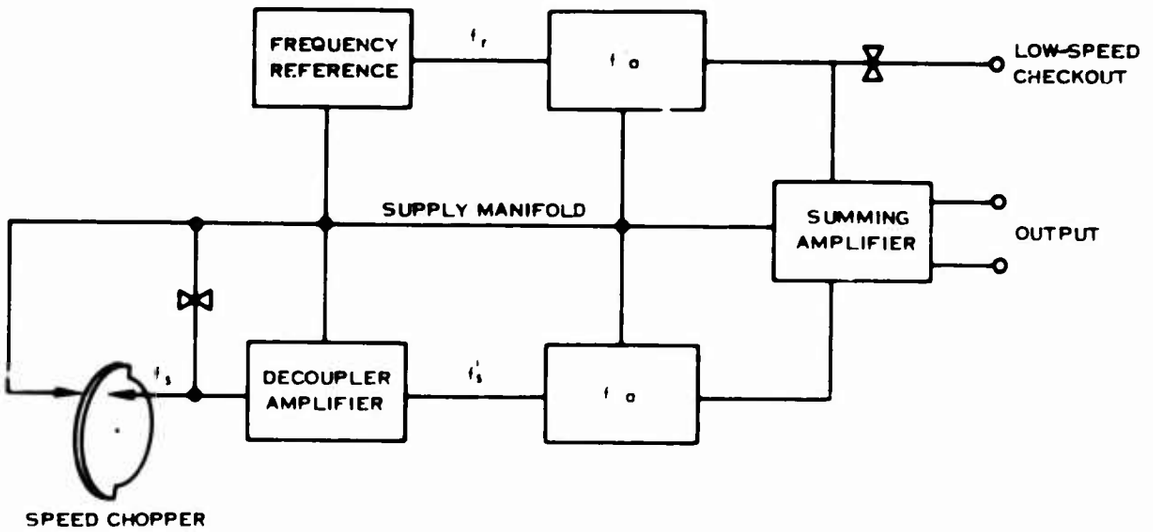

Figure 69. Block Diagram of N_F Overspeed Sensor.

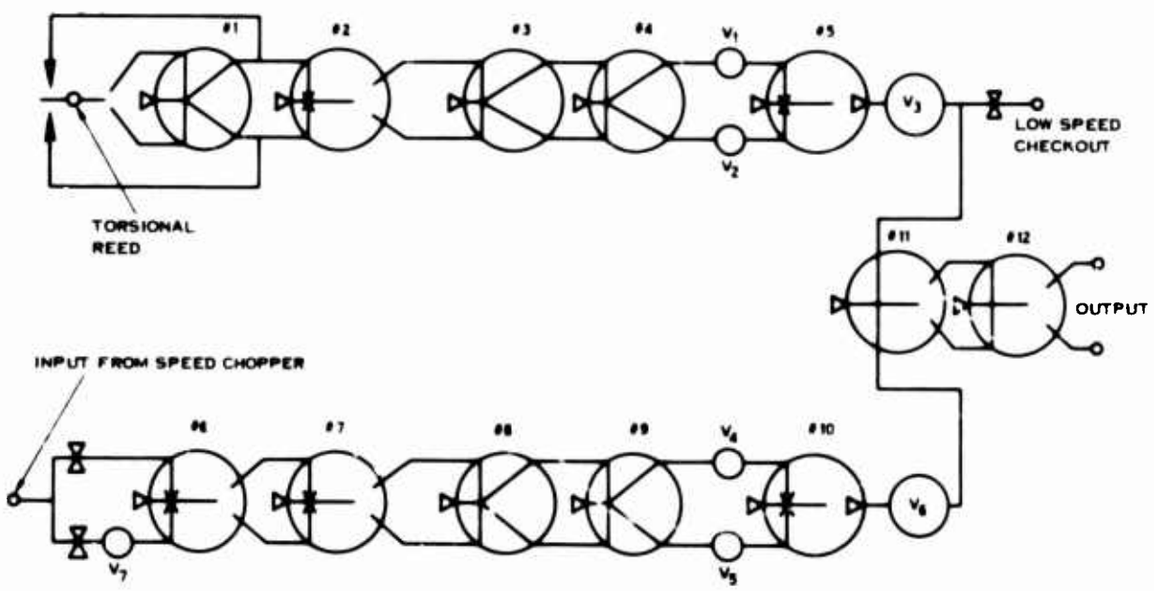

Figure 70. Circuit Schematic of N_F Overspeed Sensor.

Amplifier number 6 is used as the decoupler and also converts the single-sided signal from the speed chopper to a push-pull signal. This signal is further amplified by number 7 and used to drive the frequency-to-analog converter (amplifiers number 8 through number 10). The output of the converter is filtered by volume number 6 and applied to the summing amplifier.

The summing amplifier consists of one or more stages of proportional fluidic amplifiers. The number of amplifier stages in the summing amplifier is selected on the basis of the overall gain required.

A typical output characteristic obtained from a circuit similar to Figure 70 is shown in Figure 71. The linear range of the sensor is approximately ± 10% and the gain is 0.8 psi for a 1% speed change with a 25-psig supply to the sensor. Addition of one more stage to the summing amplifier will increase the gain to approximately 3 psi per percent speed change and reduce the linear range to ± 3%. Figure 72 is a plot of the reference oscillator frequency vs. ambient temperature. The oscillator frequency holds to within 0.1% to a temperature of 350°F. At temperatures in excess of 350°F, the oscillator frequency will drop off approximately 1% per 100°F increase in temperature. The oscillator frequency change with temperature is determined entirely by the characteristics of the Ni-span C material used as the torsional reed spring.

The overall tracking characteristics of the sensor versus temperature are shown in Figure 73. In this test, the set point was arbitrarily chosen as corresponding to a 5 psi output from the sensor. The change in speed required to hold the output was monitored. The change in set point was less than 0.5% over the temperature range tested.

Figure 74 shows the output of the frequency-to-analog converter in the primary sensing path. The output is linear in the design range of 400 to 600 Hz. The output begins to level off at 700 Hz because of saturation. The linear range can be extended by decreasing the area of the individual pulses.

Current hardware designs have been directed at sensors operating in the 20,000-to-30,000-rpm range. Mechanization of these sensors has been based on the use of standard 1-inch amplifier laminates with power nozzles of 0.02 by 0.02 inch and circuit components which have orifices or channels of at least 0.02 inch. The upper operating limit on a sensor mechanized as shown in Figure 70 and using 1-inch laminates is 80,000 rpm. This upper limit is fixed by the frequency response of the flip-flops used in the frequency-to-analog converters and the frequency reference for the reference oscillator. This range can be extended by two methods:

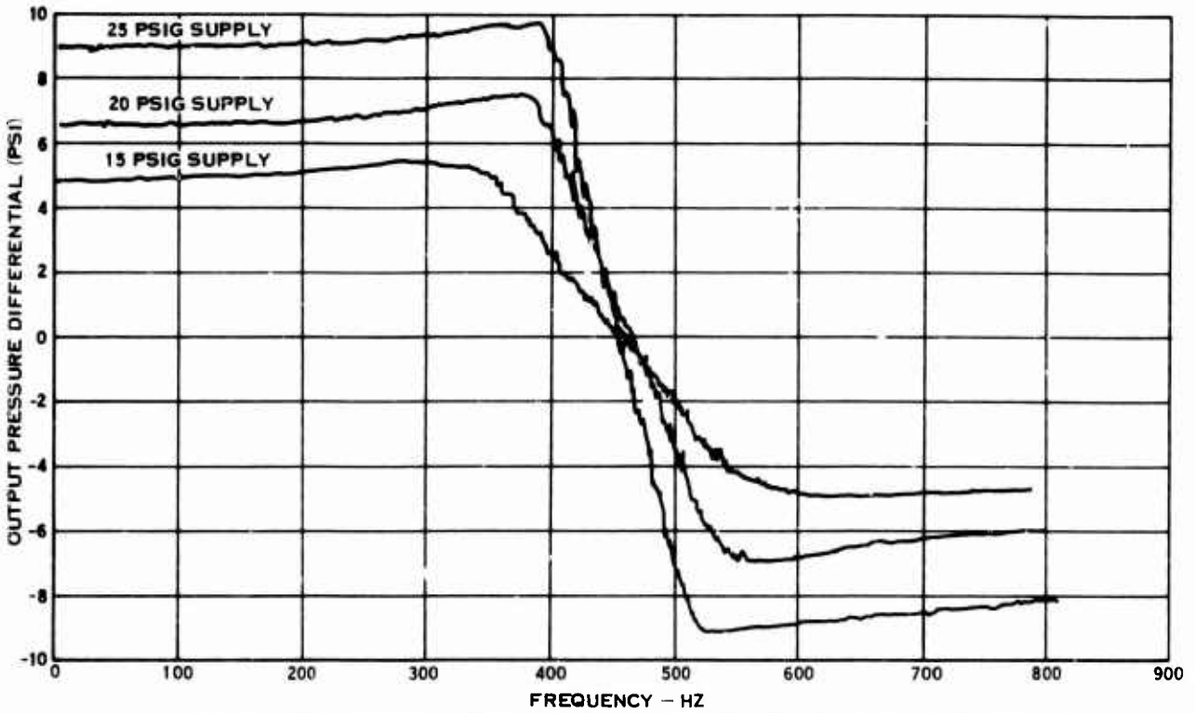

Figure 71. Typical Output Characteristic, N_F Overspeed Sensor.

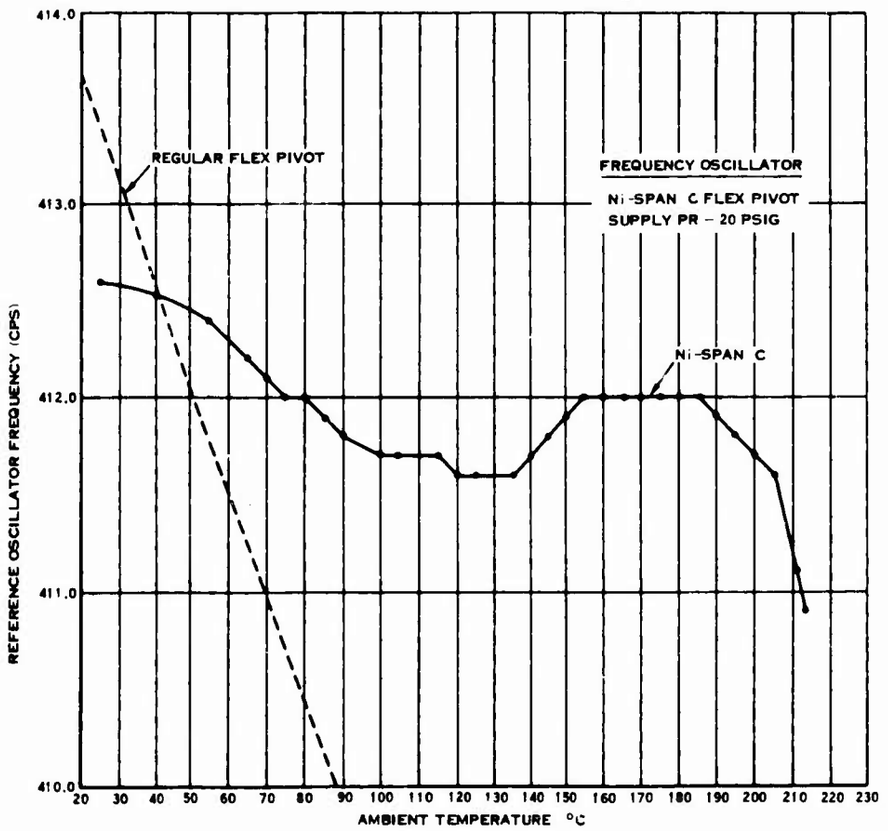

Figure 72. Reference Frequency vs Ambient Temperature, N_F Overspeed Sensor.

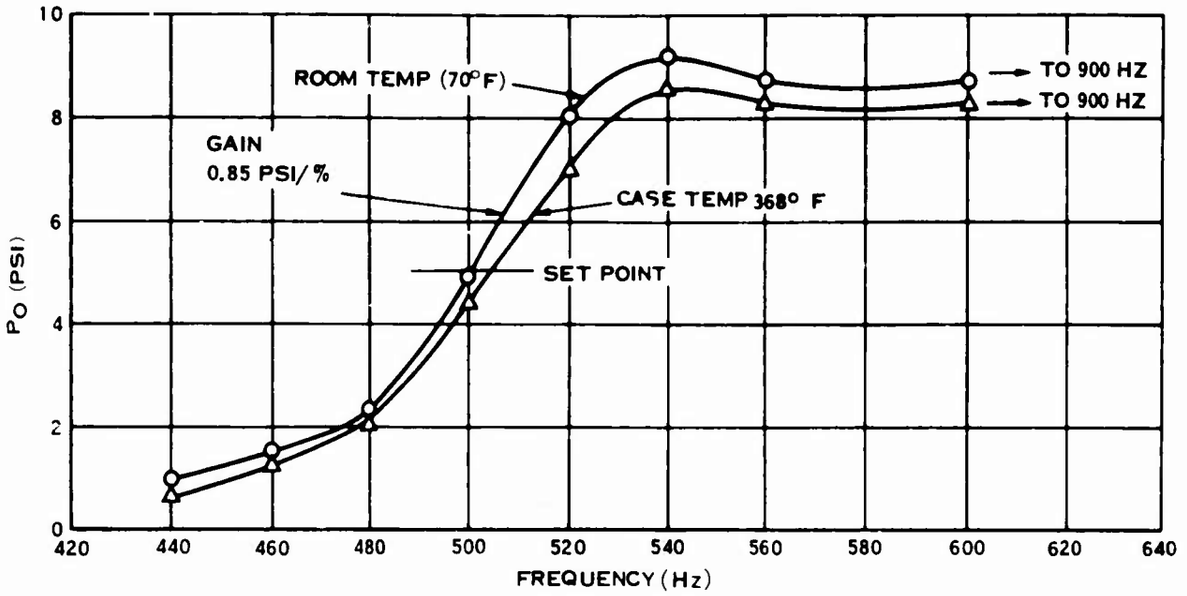

Figure 73. Temperature Effects on Set Point and Gain, N_F Overspeed Sensor.

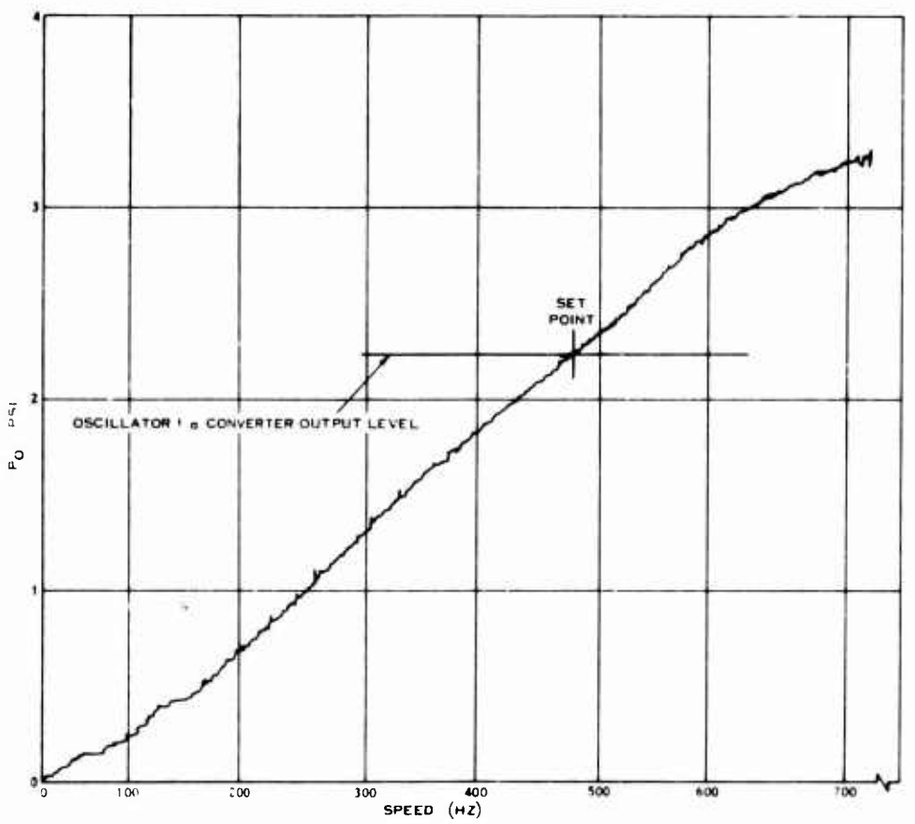

Figure 74. Frequency-to-Analog Converter Output vs Frequency, N_F Overspeed Sensor.

1. A frequency divider can be inserted between the frequency-to-analog converter and the decoupler amplifier in the primary speed sensing path. The frequency-to-analog converters and the reference oscillator would operate at one-half shaft speed. Standard 1-inch amplifiers would be used throughout.

2. The frequency response of the basic amplifiers can be increased by reducing the size of the amplifier. One-half-inch amplifier laminates (0.01-x 0.01-inch power nozzle) will increase the range to approximately 120,000 rpm. Other advantages to be gained by using the smaller amplifiers are a substantial weight saving and decreased gas consumption. These advantages may be offset by a greater susceptibility to failure because of contamination in the air supply. This approach is employed in the sensor shown in Figure 52.

HARDWARE DESCRIPTION

The packaging of the fluidic sensor is based on integrated circuit modules. Groups of amplifiers are selected on the basis of function or input-output considerations and combined into a module. The amplifiers as well as all interconnections within the modules are made up by stacking standard stainless steel laminations. The assembly is then diffusion-bonded to form a module which can be manifold mounted. The manifold is used to make interconnections between modules, input and output connections to the assembly and also contains all filter volumes too large to be incorporated in individual modules.

The overspeed sensor circuit is subdivided into three modules. The frequency reference plus the five fluidic amplifiers associated with the reference channel are combined in one module. The five fluidic amplifiers associated with the primary speed sensing are combined in a second module. The summing and output amplifiers are combined in the third module.

The stackup of the modules is shown in the hybrid control arrangement drawing, Figure 51, in the main body of this report.

APPENDIX II
FLUIDIC TURBINE INLET TEMPERATURE SENSOR

A schematic of the basic oscillator configuration is shown in Figure 75. The frequency of oscillation at a given temperature is fixed by the cavity length (L). Frequency dependence on supply pressure is minimized by choking chamber outlet nozzles to maintain a constant pressure ratio across the supply nozzle.

In the interest of minimizing size, weight, and the sensor purge time, the operating frequency of the sensor should be as high as possible. The maximum practical operating frequency is limited by the frequency response capability of the signal processing circuits. A technique which permits very high sensor frequencies with moderate signal frequencies is the use of two sensors with slightly different scale factors. The outputs of the two sensors are heterodyned and only the difference frequency, also proportional to the square root of temperature, is processed in the signal circuitry. Implementation of this technique is shown schematically in Figure 76.

In addition to reducing the signal frequency to workable levels, use of the two sensors permits dynamic compensation. The time response of a single sensor, to a step change in temperature, is characteristically about 0.02 second to reach 75 percent of the steady-state value (purge time); this is followed by a long thermal mass time constant (typically 40 seconds) to reach steady state. The dual sensor approach is based on the difference frequency; hence, by selecting the relative time constants of the individual sensors the time constant of the composite sensor can be compensated in the difference term.

Summarizing, the principal advantages of the dual oscillator type of sensor as opposed to a single oscillator sensor are:

1. Compensation for transient response is available
2. Steady-state heat losses can be compensated
3. Lower gas flows can be used for the same response
4. Lower signal frequencies are possible, thus easing transmission line and fluidic circuit coupling requirements

The output of the sensor is a pneumatic signal at a frequency equal to the difference frequency of the two oscillators. This difference frequency also varies

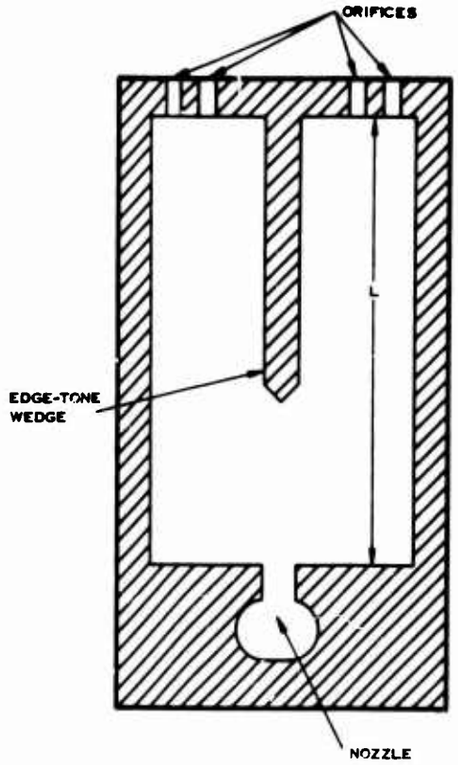

Figure 75. Schematic of Basic Fluidic T_{T4} Sensor Oscillator.

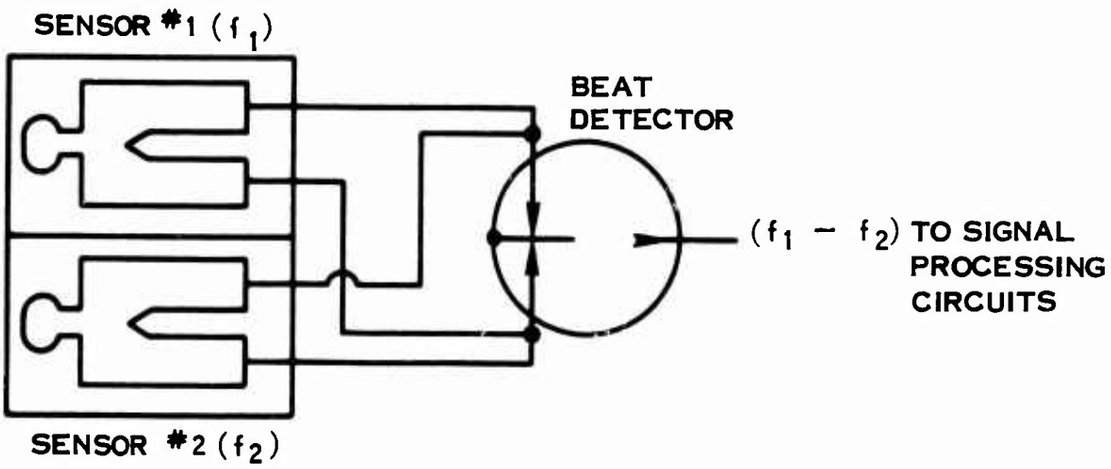

Figure 76. Schematic Diagram of Dual Fluidic T_{T4} Sensor.

directly as the square root of the absolute temperature T, since

$$F_1 - F_2 = K_1 \sqrt{T} - K_2 \sqrt{T} = (K_1 - K_2) \sqrt{T}$$

where F_1 and F_2 are oscillator frequencies and K_1 and K_2 are constants.

By this means, the output frequency is low even though the oscillators themselves are small and operate at a high frequency. The low frequency of the output permits transmission of the signal pneumatically for distances of up to 5 feet, permitting the use of a remote transducer.

The steady-state accuracy of this device is summarized in Table XXVI where the error sources are listed with their contributing error percentage and an RSS error total of ± 1.56% is indicated.

The material for the basic temperature sensor is Hastelloy-X. Heat transfer analyses show that the maximum temperature of the temperature sensor material will not exceed the reasonable upper limit of 1200°C, even with gas inlet temperatures of 1500°C. Furthermore, the dual sensor approach allows the heat loss terms to be partially compensated when a frequency difference is taken.

The signal line is a 1/8 in. O. D., 1/16 in. I. D. tube which may be bent around obstacles in order to connect the sensor and remote transducer. Line resonances do not present a problem since the line is small enough so that resonant oscillations are rapidly damped.

Previous discussions have described the dual oscillator temperature sensor and the means by which the dual oscillator principle permits compensation of the sensor for errors caused by environmental cooling both in transient and steady state. The following discussion elaborates on certain portions of the compensation principle. In summary, it is shown that in addition to compensating for steady-state environmental temperature changes and the transient effects of the heat transfer characteristics of the two oscillators, it is also possible to compensate for the transient effects of heat transfer in the inlet probe of the temperature sensor. It is further shown that heat transfer effects are mainly a function of forced convection coefficients and the specific heat of the sensor material.

The net heat flow between the gas inside the temperature sensor and the temperature sensor material is a function of the convection film heat transfer coefficient (h) and the thermal conductivity of the base material of the temperature sensor and the oxide film on its surface. In a transient analysis, the specific heat of the material of the sensor and of the gas must be considered. Table XXVII gives the heat transfer coefficients for the gas film, oxide film, and parent metal of a typical temperature sensor.

TABLE XXVI. STEADY-STATE ACCURACY ANALYSIS OF A DUAL-OSCILLATOR FLUIDIC T_{T4} SENSOR

Source of Steady-State Error	Error
1. Cold wall radiation losses	± 0.6%
2. Supply (compressor discharge) pressure range	± 0.8%
3. Dimensional variations	± 0.1%
4. Change in $\sqrt{\frac{\gamma g R_0}{M}}$ due to f/a temp.	± 0.2%
5. Change in $\sqrt{\frac{\gamma g R_0}{M}}$ due to humidity range	± 1.18%
RSS error	± 1.56% (45° @ 2900°R)

ENVIRONMENTAL RANGES FOR ERRORS

P_s = 27 to 300 psia

T = 2100°R to 3460°R

Humidity = 0 to 0.06 lb H_2O/ lb Air

TABLE XXVII. HEAT TRANSFER COEFFICIENTS OF A TYPICAL TEMPERATURE SENSOR

Medium	Coefficient (Btu/hr-ft^2-°F)	Conditions
Gas Film	137	37 lb/hr, 0.28 in. dia., 2000°F
Oxide Film	7,500	0.004 in. thick, k = 2.5 Btu/hr-ft-°F
Sensor Material	450	0.02 in. thick, k = 12 Btu/hr-ft-°F

It can be seen from the conduction coefficients listed above in Table XXVII that the most significant resistance to heat transfer is in the gas film. The resistance to heat flow of the oxide film is relatively insignificant, which is advantageous since otherwise the sensor characteristics would change with time due to oxide film buildup. The sensor material was assumed to be a metal such as Hastelloy-X or stainless steel, and its thermal resistance was found to be relatively insignificant compared to gas film thermal resistance in thicknesses below 0.02 inch. However, in larger thicknesses or for different materials such as ceramics, the sensor material must be considered in an exact analysis.

It is of interest also to calculate the thermal time constant of a typical temperature sensor. As a first assumption, let us take the time constant of a length of tubing having a 0.020-in. wall thickness (t), heat transfer coefficient (h), a specific heat (C_p) of 0.1 Btu lb/°F, and a density (ρ) of 0.3 lb/cu. in. The thermal time constant is given by the following equation:

$$T = \frac{C_p \rho t \times 144 \times 3600}{h} \qquad (6)$$

Inserting the appropriate values and letting h equal 137 Btu/hr-ft^2-°F, the time constant is 2.27 seconds. In most actual sensors, the time constant will be significantly larger than this due to larger wall thicknesses and lower gas flow rate. This is especially true at higher altitudes because of lower gas density.

The foregoing calculation of the thermal time constant points up the futility of attempting to obtain fast response of the temperature sensor solely by reducing the amount of material in the sensor and increasing the flow through the sensor. Furthermore, electronic compensation of the temperature sensor output becomes difficult because of the variation in thermal time constant with operating pressure and temperature.

The thermal time constant is only a small part of the whole story behind the transient response of the temperature sensor. Suppose that the tube in the foregoing analysis is a fluidic oscillator, which is the essential ingredient of a fluidic temperature sensor. The oscillation frequency is proportional to the square root of the absolute temperature of the gas in the oscillator or, if the temperature is not constant throughout the oscillator, the frequency is proportional to the square root of the average gas temperature. If the oscillator is initially operating at a gas temperature (T_o) and a step increase (ΔT) is initiated at the inlet to the oscillator, the oscillator continues to function at the initial frequency until all the old, low-temperature gas is flushed out and replaced by the new, higher temperature gas. Typically, these flushing times are very short. For a 3-inch long sensor inlet probe at a gas velocity of 220 feet per second, the flushing time is 1

millisecond. For a typical temperature sensor, including the fluid oscillator resonant cavities, the flushing time is approximately 3 milliseconds. These time lags are negligible compared to the desired response time of 0.5 second, and in the practical case the flushing can be assumed to be instantaneous.

The response of the temperature sensor is limited therefore by the heat exchanger between the walls of the sensor and the gas flowing through the sensor. The probe which extends into the gas stream for temperature measurement must also be considered in the transient analysis. For instance, suppose that the probe is 3 inches long and 0.28 inch diameter with a gas flow through the tube of 37 pounds per hour. Assume that the probe is at the initial gas temperature (T_o) and that a sudden step increase in gas temperature (ΔT) is introduced. Instantaneously (ignoring flushing time), the temperature at the exit of the tube (T_e) is lower than the temperature at the inlet of the tube because of heat transfer from the gas to the walls of the tube. The exit temperature can be found from the following heat balance:

$$\left(\frac{T_o + \Delta T + T_e}{2} - T_o \right) h \; A_w = (T_o + \Delta T - T_e) \; C_p \; M \qquad (7)$$

In this equation, M is the gas flow rate, A_w is the wall area of the tube, and C_p is the gas specific heat. The left side of the equation is the heat transfer from the gas to the tube. The right-hand side of the equation represents the heat lost by the gas. Average temperature difference rather than log mean temperature difference has been used for simplicity. The error incurred is small if the temperature drop is small.

Only a certain proportion of the step increase in temperature which occurs at the inlet to the tube is seen instantaneously at the exit of the tube. If that proportion is designated as R then

$$T_e = T_o + R \, \Delta T \qquad (8)$$

Substituting and solving for R

$$R = \frac{2 \, C_p \, M - h \, A_w}{2 \, C_p \, M + h \, A_w} \qquad (9)$$

Again assuming a tube of 0.28 inch I.D. and 3 inches long, h = 137 Btu's per hour per square foot per °F, gas flow of 37 pounds per hour, and the gas specific heat of 0.24 Btu/lb/°F:

$R = 0.75$

Thus, it is seen that significant error can be introduced during a temperature transient just due to heat transfer within the temperature sensor probe. Similarly, additional transient error occurs within the fluidic oscillator of the temperature sensor. By keeping the distance traveled by the gas from the inlet to the oscillator exit short, these transient errors can be minimized but not eliminated. Other means of compensation are required.

The response of the fluidic temperature sensor probe to a step change in gas temperature at the inlet of the probe is therefore given by

$$\frac{\Delta T_{out}}{\Delta T_{in}} = 1 + (1-R)\, e^{\frac{-t}{\tau}} \tag{10}$$

or

$$\frac{\Delta T_{out}}{\Delta T_{in}} = 1 - D\, e^{\frac{-t}{\tau}} \qquad \text{where } D = 1-R \tag{11}$$

Typically, $R = 0.85$, $D = 0.15$, and $\tau = 5$ seconds. This, it must be remembered, is the transient response of the outlet temperature of the probe which is the inlet temperature of the fluidic oscillators in the fluidic temperature sensor. An additional and similar response occurs within the fluidic oscillators except that in this case the average temperature within the oscillator is of interest rather than the exit temperature.

It will now be shown how the dual-oscillator temperature sensor principle permits compensation of the thermal lags in the temperature sensor, including the temperature sensor inlet probe. The response of the temperature sensor can be determined from the block diagram of Figure 77. In this diagram the zero subscript refers to the inlet probe, the 1 subscript refers to the high frequency oscillator and the 2 subscript refers to the low-frequency oscillator. Each section of the temperature sensor indicated by the dotted lines has a response characteristic as given by the previous equation. The individual oscillator frequency is some constant, K, times the square root of the average temperature of the gas in the oscillator. These two frequencies are heterodyned, and the resulting difference frequency squared times $\frac{1}{K_1 - K_2}$ gives the indicated gas temperature which, ideally, is equal to the actual gas temperature.

For an initial analysis it will be assumed that all of the time constants in the block diagram of Figure 77 are equal; that is, $\tau_0 = \tau_1 = \tau_2 = \tau$. Note that these time constants in the actual sensor can indeed be made equal by adjusting the mass

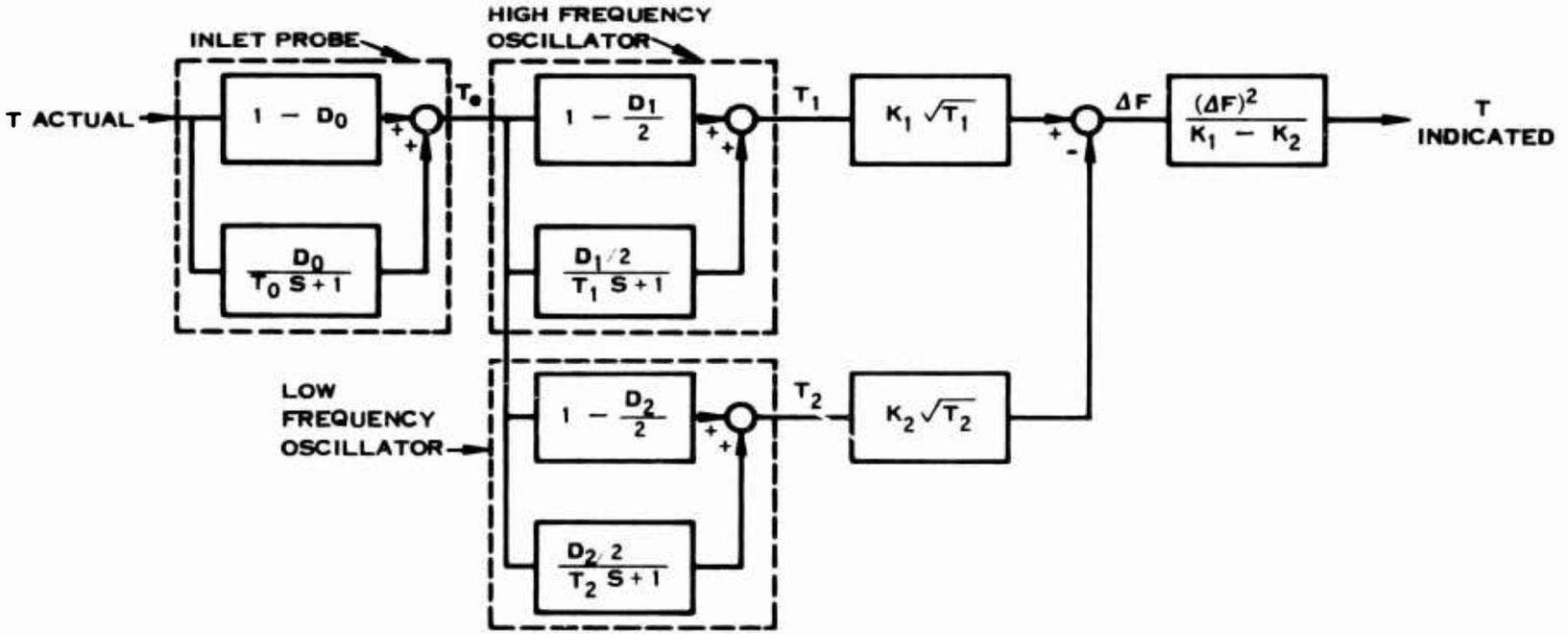

Figure 77. Block Diagram of a Dual-Oscillator Fluidic Temperature Sensor for Response Analysis.

effective at each location in the fluidic temperature sensor, in spite of the fact that the heat transfer coefficient is probably different at each location.

Using the Laplace transform, the response of the temperature sensor to a step change in inlet temperature can be determined. The response of the high-frequency sensor is given by the following equation:

$$\Delta T_1 = \Delta T\left[1 + \left(-\frac{D_1}{2} - D_o + \frac{D_oD_1}{2} + \frac{D_oD_1t}{2\tau}\right) e^{-\frac{t}{\tau}}\right] \tag{12}$$

In this equation, ΔT represents the step change in inlet gas temperature and ΔT_1 represents the resulting change in the average gas temperature in the high frequency oscillator. (In this analysis the temperature sensor is assumed to be perfectly insulated so that external heat losses can be neglected.) Similarly, the change in average temperature of the low-frequency oscillator is

$$\Delta T_2 = \Delta T\left[1 + \left(-\frac{D_2}{2} - D_o + \frac{D_oD_2}{2} + \frac{D_oD_2t}{2\tau}\right) e^{-\frac{t}{\tau}}\right] \tag{13}$$

Examination of the above equation shows that the thermal response of the individual oscillator combined with the thermal response of the probe is similar in characteristic to the response of the probe alone in that an initial step occurs instantaneously with a long settling time to final output. In the case of the oscillator, however, the initial instantaneous step is smaller than it would be if the probe responded instantaneously to the step change in inlet temperature.

In order to be able to handle these equations more readily, let

$$\Delta_1 = \left(\frac{D_1}{2} - D_o + \frac{D_oD_1}{2} + \frac{D_oD_1t}{2\tau}\right) e^{-\frac{t}{\tau}} \tag{14}$$

$$\Delta_2 = \left(-\frac{D_2}{2} - D_o + \frac{D_oD_2}{2} + \frac{D_oD_2t}{2\tau}\right) e^{-\frac{t}{\tau}} \tag{15}$$

Therefore,

$$\Delta T_1 = \Delta T\,(1 + \Delta_1) \tag{16}$$

$$\Delta T_2 = \Delta T\,(1 + \Delta_2) \tag{17}$$

The difference frequency is given by

$$F = K_1\sqrt{T_1} - K_2\sqrt{T_2} \tag{18}$$

If we make the assumption that Δ_1 and Δ_2 are small relative to unity, then the square root of $1 + \Delta$ can be approximated by $1 + \Delta/2$. Therefore, it follows that

$$\Delta F = \sqrt{\Delta T}\ (K_1 - K_2) + \sqrt{\Delta T}\left(\frac{\Delta_1 K_1}{2} - \frac{\Delta_2 K_2}{2}\right) \tag{19}$$

From this it follows that the indicated temperature is equal to the actual temperature if

$$\Delta_1 K_1 = \Delta_2 K_2 \tag{20}$$

Substituting for Δ_1 and Δ_2 and rearranging terms we have

$$D_1 = D_2\ \frac{K_2}{K_1} + D_o\left(1 - \frac{K_2}{K_1}\right) \Big/ \left(\frac{1}{-\frac{1}{2} + \frac{D_o}{2} + \frac{D_o t}{2\tau}}\right) \tag{21}$$

This equation gives the relationship required between D_1 and D_2 in order to have the temperature sensor perfectly compensated for transient response. Unfortunately, this relationship is a function of time, t. Since the greatest transient error in the temperature sensor occurs at time $t = 0$, it is reasonable to evaluate this equation at that time. Also, for illustrative purpose, let $K_2/K_1 = 0.85$. This equation can now be plotted as shown in Figure 78 for various values of D_o. Also on this figure, the same equation is evaluated for time $t = \tau$. This illustrates that the time effect on the relationship between D_1 and D_2 is small provided D_o is small. In other words, if the temperature sensor probe length is short, resulting in less than 20% temperature drop ($D_o = 0.2$) upon initiation of a step increase in gas temperature, then the temperature sensor can be effectively compensated to obtain accurate transient response. This analysis not only points out the need for having a short distance between probe inlet and temperature sensor oscillator nozzles but also shows that the sensor and probe must be designed as a system, not individually, for accurate transient compensation.

At one point in this analysis it was assumed that the thermal time constants of the probe, high-frequency oscillator, and low-frequency oscillator were equal. It is possible that making these time constants unequal, in the correct proportion, could compensate for the time element in the equation for the relationship between D_1 and D_2. No attempt has been made in this direction. A more sophisticated computer analysis would be required.

Now let us look at the reasonableness of the relationship between D_1 and D_2. In the initial phase of development of fluidic temperature sensors, the inlet probe and its effect on the sensor were ignored, $D_o = 0$. This means that if

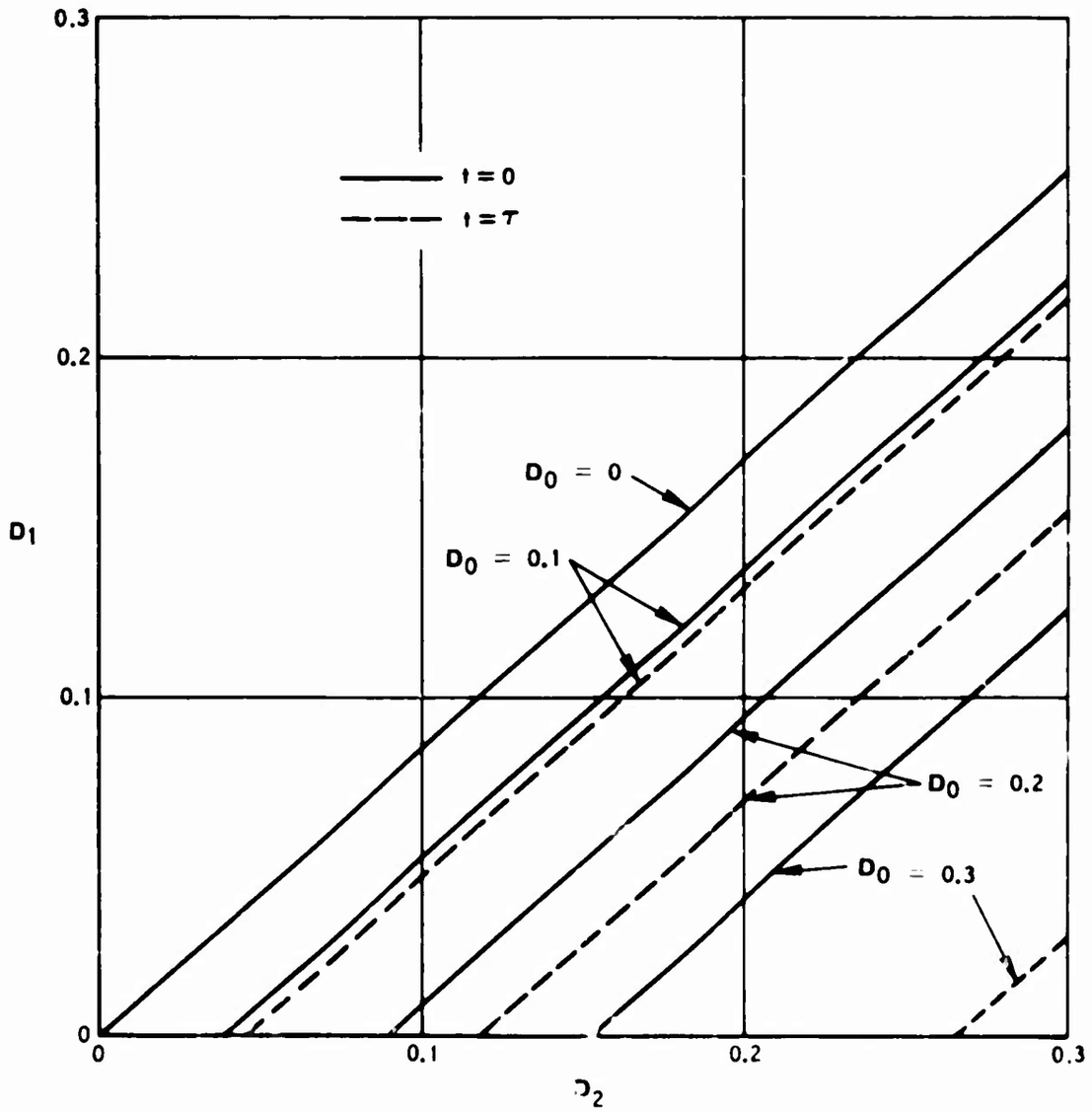

Figure 78. Relationship of Temperature Drop Coefficients for Transient Compensation of a Fluidic Temperature Sensor.

D_1 = 0.1 (10% average temperature drop through the high-frequency oscillator) then D_2 should equal 0.118 (11.8% average temperature drop through the low-frequency oscillator). The lower percent temperature drop through the high-frequency oscillator could be obtained by doubling the flow through the high frequency oscillator. Since the forced convection heat transfer coefficient (h) varies as the 0.8 power of flow, the temperature drop through the oscillator varies approximately as the 0.2 power of flow. Therefore, doubling the flow in the high-frequency oscillator results in D_1 being about 20% less than D_2, which is theoretically the desired relationship. However, if the effect of the temperature sensor probe is considered so that D_o = 0.1, then it is desired that D_2 = 0.155 if D_1 = 0.1. Using the same compensation technique, this requires that the flow through the high-frequency oscillator be about nine times the flow through the low frequency oscillator. This is not easy to achieve. It would be preferable to route the gas for the high frequency oscillator separately from the gas for the low frequency oscillator in order to deliberately obtain a higher temperature drop for the gas entering the low frequency oscillator. This must be done with care so as not to introduce steady-state errors.

The foregoing analysis contains several approximations and ignores many second-order effects. For purposes of illustration, this is adequate. In a final design, more sophisticated techniques of analysis would be required. Even so, it is unlikely that exact compensation can be achieved under all possible operating conditions of the temperature sensor. Since a simple fluidic temperature sensor can be expected to have an initial transient error of approximately 30% (D = 0.3) decreasing to zero transient error with a time constant in the order of 10 or 20 seconds, it will be assumed that the dual-oscillator temperature sensor can be compensated to achieve a response which results in a 10% initial transient error. This says that the transient error must be 67% compensated.

It will be noted that the inaccuracy discussed above is an inability of the temperature sensor to reproduce exactly a given step change in temperature of the inlet gas. This inaccuracy, when put on an absolute accuracy basis, is a function of the step magnitude.

Suppose for instance that a step change in turbine inlet temperature occurred from an initial value of 1500°F to a final value of 2500°F. The change is 1000°F. Assuming that the temperature sensor reproduces the step within 10%, the error of the sensor is 100°F or 4% of the final output temperature on an absolute accuracy basis. Since temperature steps of this order of magnitude are hardly likely to occur, the temperature sensor accuracy obtainable with "67% compensation" provides adequate response.

Fluidic Oscillator Temperature Sensor Test

As discussed previously in this report, the use of a fluidic oscillator as a means for sensing turbine inlet gas temperature was rejected on the basis of the number of areas of jeopardy outstanding at this time. In the interests of evaluating the magnitude of these factors, a test program has been established based on the fabrication by Hamilton Standard of an advanced fluidic edge-tone oscillator design evolved by the Harry Diamond Laboratories.

The test probe is of sandwich construction and consists of an oscillator plate mounted between appropriate inlet, outlet and sensing manifolds as shown in Figure 79. High temperature testing was conducted using a jet engine combustion can to simulate exposure to combustion products. The test probe was mounted across the burner duct on the combustor centerline and 1.5 inches downstream of the end of the combustion frame tube. Testing was initiated at an inlet temperature of 300° F and was followed by runs at 600°, 900° and 1200° F. An immediate loss in signal amplitude was observed when burning was initiated and this effect was accentuated as temperature was increased. The increasing level of burner noise is evident in the photographs of Figure 80 and had the effect of inducing more and more data scatter in the frequency readings of Figure 81. This was due to the uncertainty of triggering the frequency counter, in spite of the use of a variable band pass filter which was optimized at each frequency reading.

Loss of signal from two out of the five oscillators tested was experienced after 10 hours running. Disassembly indicated that while the basic oscillators were in good condition, appreciable quantities of soft carbon were present in the oscillator cavities. Carbon accumulation in the nonflowing areas of the resonant cavities of the oscillator could affect the Eigen frequency of the cavity, thus reducing the amplifying effect of the cavity on the basic edge-tone oscillation. Testing will be resumed to accumulate additional hours of endurance running on the five oscillators, together with an evaluation of water content effects, etc. This should allow much more definitive conclusions to be drawn than are currently possible. At this time, however, it is possible to draw some preliminary conclusions:

1. The basic Harry Diamond Laboratory oscillator design has a clean output signal with low pressure sensitivity (<1% of full scale) and represents a good basis for advanced sensor designs for specific applications.

2. The relatively high frequency output presents no transduction problems, while at the same time being desirable from the point of view of overcoming burner noise. Reduction in frequency would require operation of the oscillator in areas of ever increasing burner noise (up to 180 db at 50 Hz).

3. Improved methods of attenuating burner noise entering the probe will be required on future designs to eliminate the erratic counter triggering currently being experienced.

Address to these problems in future probe designs will result in a more usable component for engine control use. Remaining areas of concern would then center on materials for high temperature (recognizing that the engine designer's expedient of using cooling air is not open to the sensor designer) and the effects of humidity, fuel-air ratio, hydrocarbon content of fuel, etc.

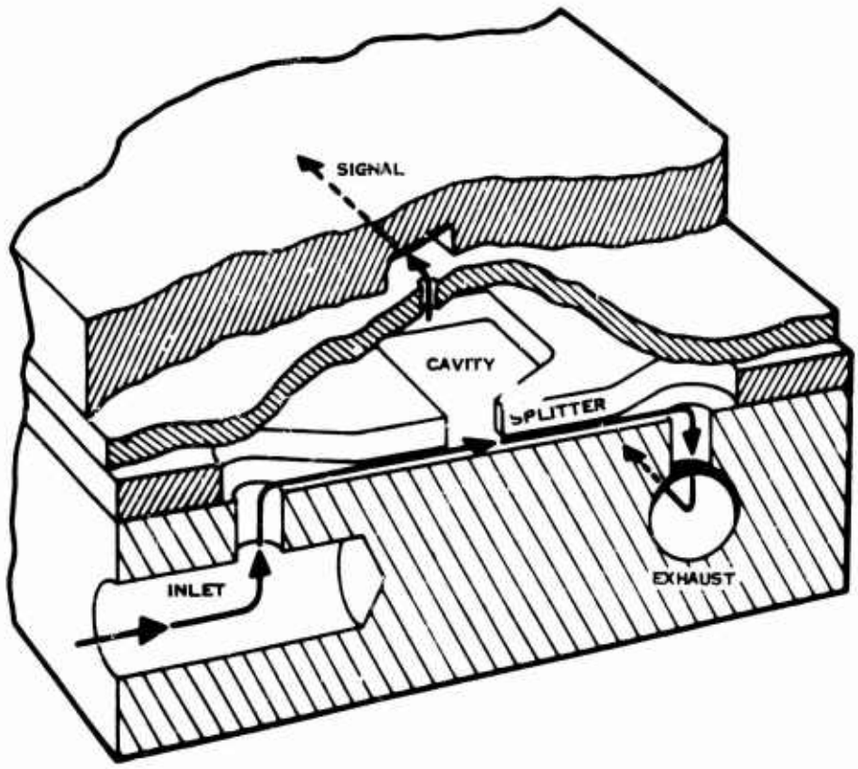

Figure 79. Partial View of Fluidic Oscillator Temperature Probe.

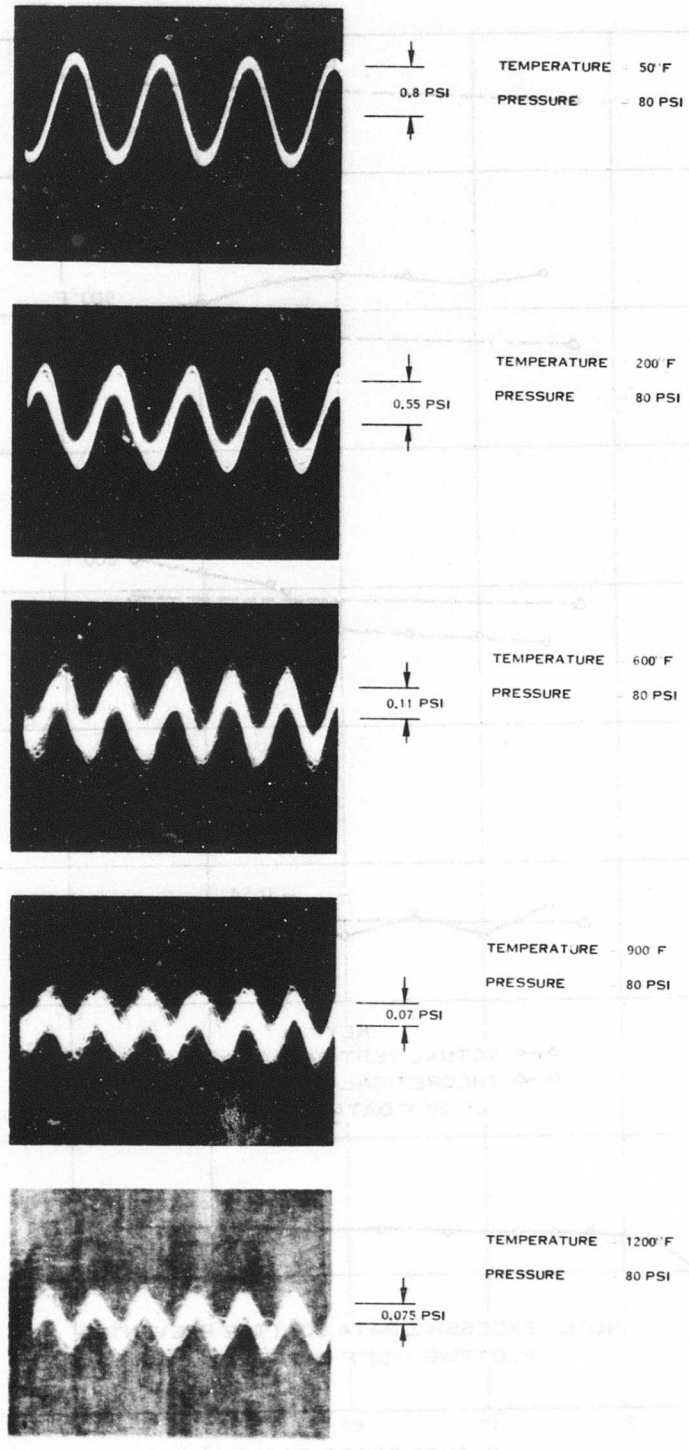

Figure 80. Signal Characteristics of Fluidic Oscillator Temperature Probe in Burner Rig.

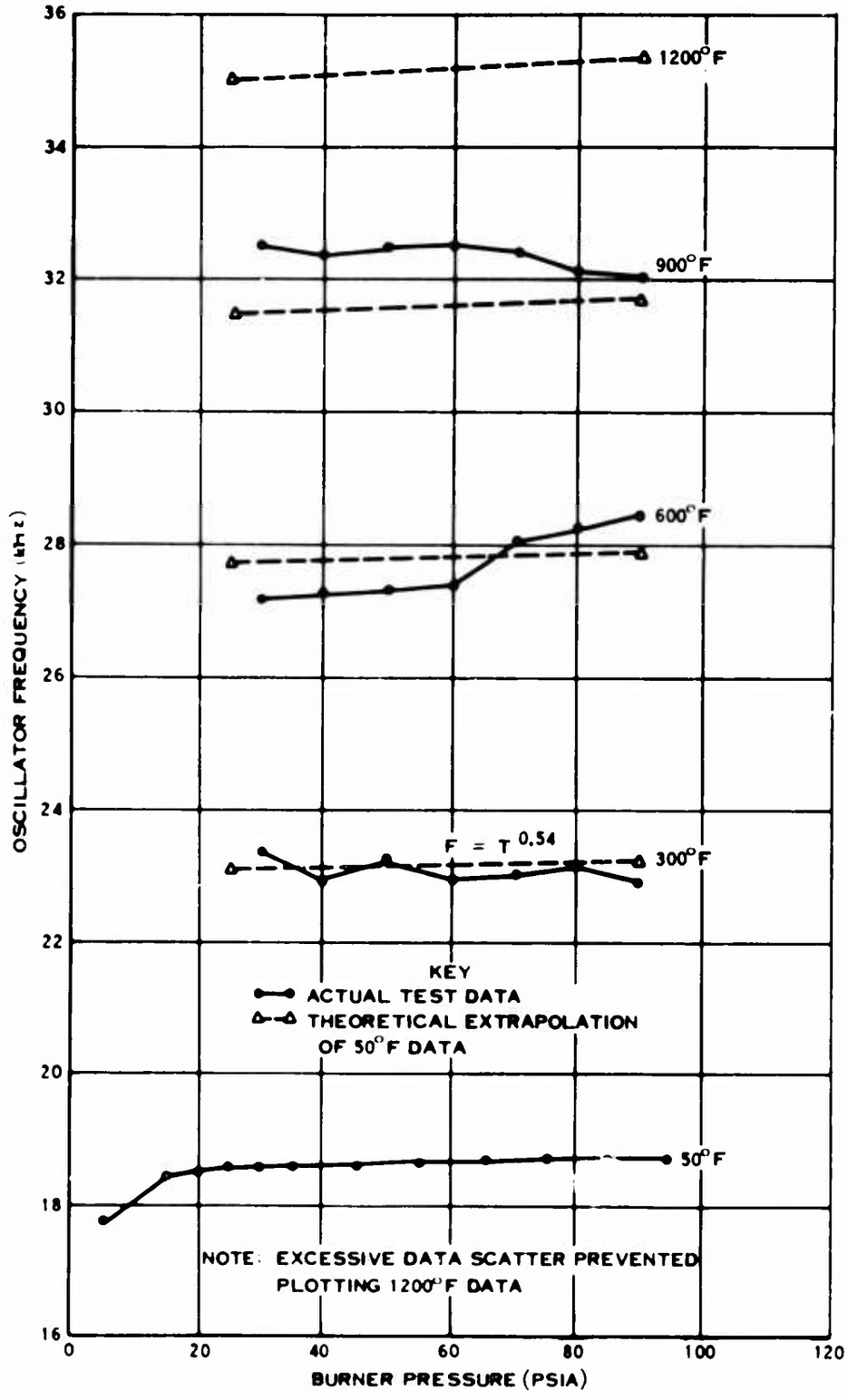

Figure 81. Test Data Fluidic Oscillator Temperature Probe in Burner Rig.

APPENDIX III
FLUIDIC N_G SPEED SENSOR STUDY

GENERAL

The corrected speed servo positions an actuator and fuel control cam motion as a function of $N_G\sqrt{\theta_{T2}}$. Pressure pulses from a shaft-mounted chopper are applied to a Helmholtz resonator purged with T_{T2} air. A phase discriminator circuit converts the fluidic frequency signals to a differential pressure which through an interface drives an actuator, positions a cam, and resets the resonator geometry to match its resonant frequency to shaft speed.

To a first approximation, the differential pressure at the output of the fluidic circuitry is given by

$$\Delta P_o = K\,(\omega - \omega_r) \tag{22}$$

where ω is the input frequency, ω_r is the resonant frequency of the resonator (a function of geometry (x) and temperature (T)), and the K terms are constants. Thus,

$$\Delta P_o = K_1\,(\omega - K_2\, f(x)\,\sqrt{T}) \tag{23}$$

On a linearized basis,

$$\Delta\Delta P_o = K_1 \Delta\omega - K_3\Delta T - K_4\Delta X \tag{24}$$

The loop is then connected as shown in Figure 82.

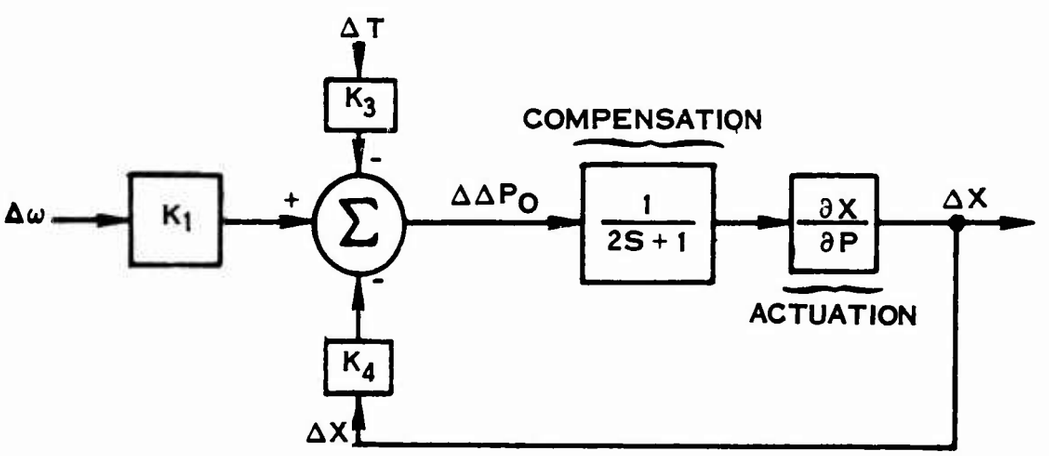

Figure 82. Simplified Block Diagram of Fluidic N_G Speed Loop.

To improve system accuracy the loop is closed around the actuator, and a 0.5-radian/second lag is added for stability. In the block diagram note that increasing speed increases ΔX and increasing temperature decreases ΔX, which is the desired action for the corrected speed loop. If all of the significant dynamics and estimated gains are included, the block becomes as shown in Figure 83.

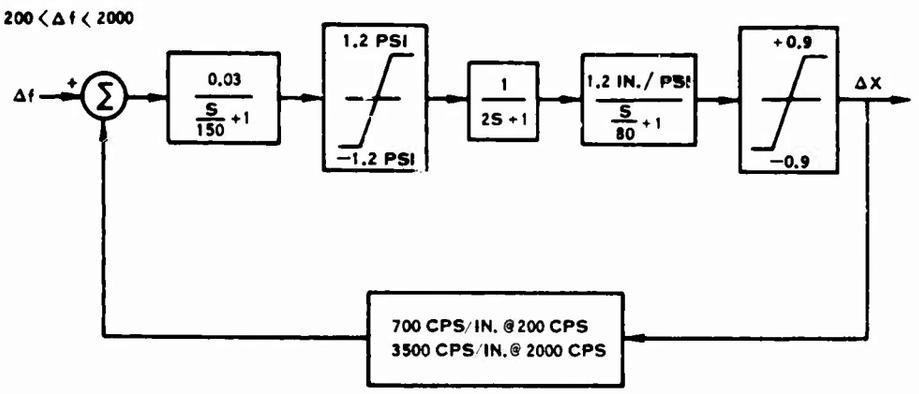

Figure 83. Block Diagram of Fluidic N_G Speed Loop Showing Significant Dynamics And Gains.

For convenience, Δf is chosen to be corrected speed.

Probably the most stringent design requirement is the need to vary the resonator's resonant frequency over a 10:1 speed range. To maintain reasonable physical dimensions, the nominal shaft speeds of 100 to 1000 cps were doubled to 200 to 2000 cps. In addition, both the resonator capacitance and inductance are varied simultaneously. Figure 45 shows the selected configuration. The components are shown full size, and the package arrangement has been folded out to show the cross-sectional detail.

A brief summary of the system characteristics is shown in Table XXVIII.

TABLE XXVIII. SUMMARY OF FLUIDIC N_G SPEED LOOP CHARACTERISTICS

Characteristic	Definition
Shaft speed range	100 to 1000 cps
Output motion	0 to 1.44 in.
Weight	1.5 lb
Fluidic air supply pressure	6 psig
Air consumption	0.00091 lb/sec
Static accuracy	±1.1% @ 1000 cps +1.6% @ 100 cps
Dynamic error*	15%
Loop response	13 to 65 rad/sec

*Max error for a 3-sec speed ramp from 10% to 100% speed.

DETAILED CIRCUIT DESIGN

Resonator Transfer Function

The electrical equivalent for the resonator circuit is a parallel combination of inductance and capacitance as shown in Figure 84.

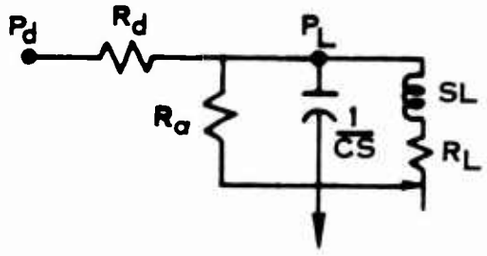

Figure 84. Electrical Equivalent for Fluidic N_G Resonator Circuit.

R_d and R_a are the resistances of the driver orifice and pickoff amplifier, C is the pneumatic capacitance (volume), L is the inductance, R_L is the resistance of the inductor and s is the Laplace operator. The complete transfer function between driving pressure P_d and resonator pressure P_L is:

$$G = \frac{P_L}{P_d} = \frac{R_a(R_L + sL)}{R_dR_aLCs^2 + s[(R_a + R_d)L + R_dR_LR_aC] + R_dR_a + R_dR_L + R_aR_L} \qquad (25)$$

For a reasonable selection of circuit parameters,

$$R_a \approx R_d >> R_L$$

$$R_dR_a >> R_dR_L >> R_aR_L$$

and transfer function becomes (divide by R_dR_a):

$$G = \frac{\frac{1}{R_d}(R_L + sL)}{LCs^2 + \left[\left(\frac{R_a + R_d}{R_aR_d}\right)L + R_LC\right]s + 1} \qquad (26)$$

A further simplification can be made if the Q of the inductor (ratio of reactance to resistance) is high (say, $Q \geq 10$); then

$$G = \frac{\left(L/R_d\right) s}{\frac{s^2}{LC} + \left(\frac{R_a + R_d}{R_a R_d}\left(\frac{L}{C}\right) + R_L\right) \quad Cs + 1} \tag{27}$$

Generally,

$$R_a \approx R_d \approx 25{,}000 \text{ sec/in.}^2$$

Also for the geometry shown in Figure 45,

$$\frac{L}{C} \approx 35{,}000 \text{ sec}^2/\text{in.}^4$$

If inductor resistance is low, a typical average value is

$$R_L \approx 30 \text{ sec/in.}^2$$

The coefficient of s in the resonator transfer function determines the damping or Q of the resonator. From a gain and accuracy standpoint, very low damping (high Q) is desirable since a high Q circuit will exhibit a very rapid change in phase with frequency.

Evaluating the coefficient of s,

$$\frac{R_a + R_D}{R_a R_d}\left(\frac{L}{C}\right) + R_L = \frac{25{,}000 + 25{,}000}{25{,}000 \quad (25{,}000)} \quad (35{,}000) + 30 \tag{28}$$

$$= 2.8 + 30 \approx 30$$

Thus the circuit parameter limiting the resonator Q is the inductor resistance R_L. In terms of Q, the resonator pressure gain is

$$G = \frac{\left(\frac{L}{R_d}\right) s}{\frac{s^2}{\omega_R{}^2} + \frac{1}{\omega_R Q} \quad s + 1} \tag{29}$$

At resonance $\omega = \omega_r$ the gain of the quadratic denominator is equal to the circuit Q; thus,

$$G = \frac{QL}{R_d} \quad \omega_r \tag{30}$$

It can further be shown that the phase (ϕ) vs. frequency slope is

$$\frac{d\phi}{d\omega} = \frac{2Q}{\omega R} \tag{31}$$

The resonant frequency of the resonator will be set by varying both the inductance and capacitance. The inductors are ten discrete holes 0.1 inch in diameter and 0.4 inch long. At the low set point speed one hole is open and at approximately 50% speed all ten holes are open; further variation in LC is obtained by varying only the capacitance volume. Figure 85 shows the speed vs. displacement relation. The solid curve is the relation obtained if the inductance is programmed over the entire stroke. The dotted curve, used in the recommended design, was adopted because of the lower change in feedback gain over the desired speed range.

THE PHASE DISCRIMINATOR CIRCUITRY

Figure 86 shows the circuit configuration assumed in the analysis. Amplifiers 1 and 2 detect and amplify the resonator pressure signal and compare this signal to reference signal R_2 across rectifiers 3 and 4. Generally the control pressure to amplifier number 1 will vary in amplitude as the set point is varied (refer to equation 30) to maintain constant gain. Amplifier number 2 will be set to saturate over the full range of operation.

For maximum and minimum set points the circuit parameters shown in Table XXIX were established.

TABLE XXIX. SUMMARY OF FLUIDIC N_G SYSTEM CIRCUIT PARAMETERS.

Parameter	Min Speed	Max Speed
Input Frequency	200	2000
Q	4.27	42.7
L	0.154	0.0154
ω	1255	12550
R_d	21200	21200
G_{RES}	0.039	0.39
$G_1\ G_2\ G_{RES}$	0.39	0.39

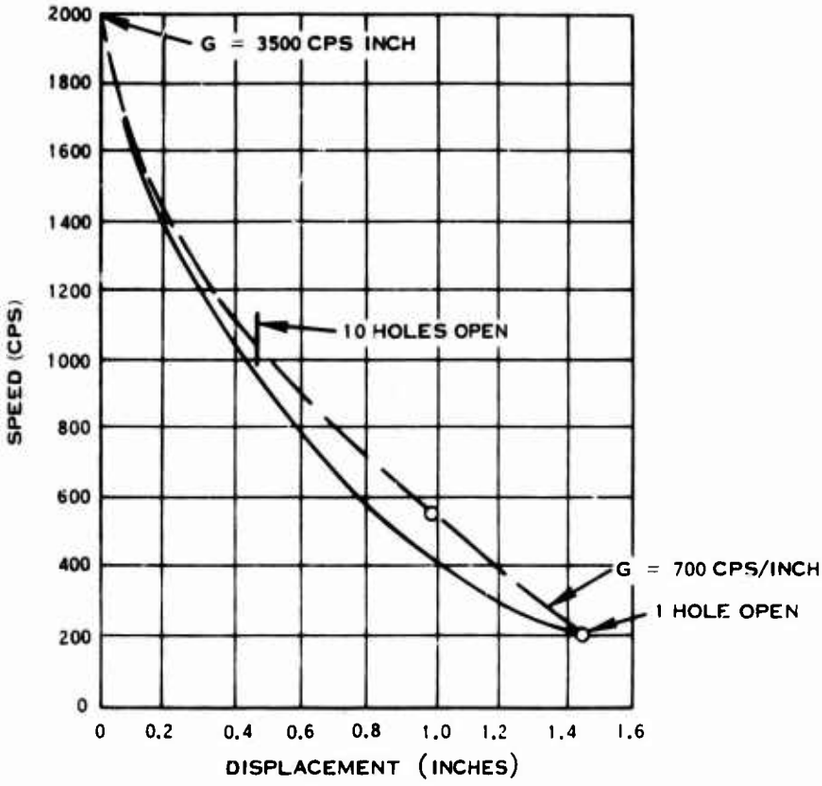

Figure 85. Speed vs. Displacement for Fluidic N_G Speed Sensor System.

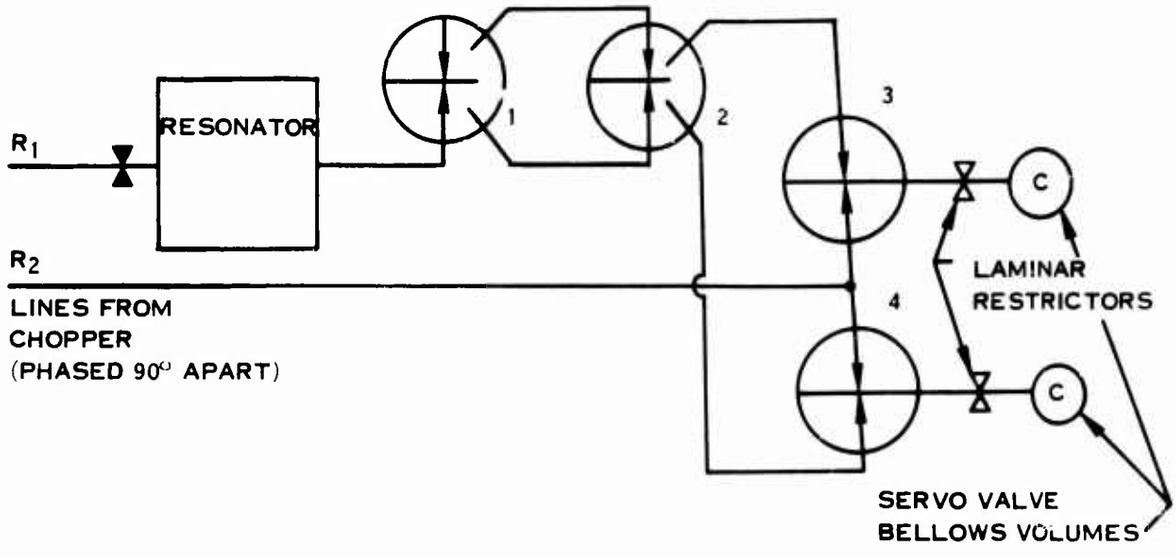

Figure 86. Fluidic N_G Speed System Circuitry.

The resonator gain can be computed from equation (30); G_1G_2, the product of gains for amplifiers number 1 and number 2, varies from 10 at 200 cps to 1 at 2000 cps. Thus, the amplifiers saturate at all amplitudes above that at 200 cps. The change in rectifier output pressure with phase is computed at 90° phase change through the resonator. Assuming ±3 psi is applied to the resonator, the amplitude at the output of amplifier 2 is ±3 x 0.39 ≃ ±1.2 psi and the pressures across rectifiers number 3 and 4 are as shown in Figure 87.

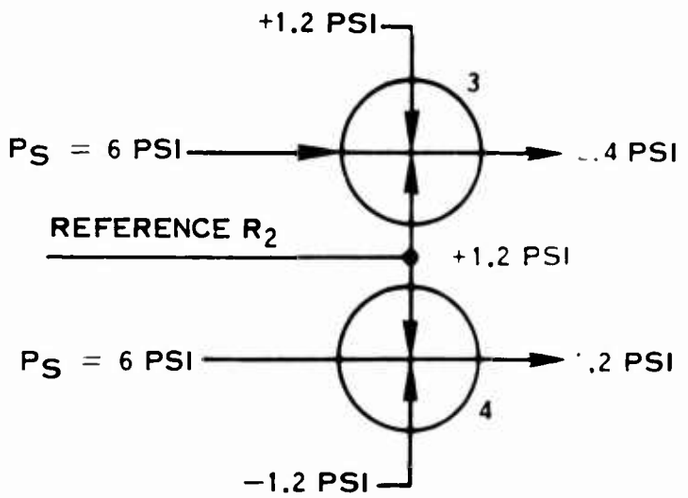

Figure 87. Pressure Summary Across System Rectifiers Fluidic N_G System

Rectifier number 3 undergoes no deflection of the power jet since the control pressures are in phase and hence full pressure is recovered at the output (actually about 40% of supply pressure P_S). The wave form at the output of rectifier number 4 is approximately triangular with a time average value one-half that of rectifier number 3. Thus the change in differential pressure with phase is

$$\frac{\Delta P}{\Delta \phi} = \frac{2.4 - 1.2 \text{ psi}}{90^\circ} = 0.0133 \ \frac{\text{psi}}{\text{deg}}$$

The complete gain between input frequency is

$$\frac{\Delta P}{\Delta \omega} = \frac{\Delta P}{\Delta \phi} \times \frac{\Delta \phi}{\Delta \omega} \tag{32}$$

$\Delta \phi / \Delta \omega$ can be obtained from equation (31) and expressed as a function of Q. A more convenient expression than equation (32) is

$$\frac{\Delta P}{\Delta f} = \frac{360}{\pi} \frac{\Delta P}{\Delta \phi} \frac{Q}{f} \tag{33}$$

where the input frequency (f) is in cps. Since Q varies directly with frequency and since $\Delta P/\Delta \phi$ is constant the gain between frequency and pressure is constant.

Substituting values,

$$\frac{\Delta P}{\Delta f} = 0.0326 \text{ psi/cps}$$

Position Loop

The output of the phase discriminator directly drives the cam position loop. The input diaphragm volumes filter the frequency ripple as well as providing a [illegible] time constant lag (effective integration) for stability and high static gain. Closing the position loop eliminates much of the hysteresis deadband and sensitivity to friction and loading in the servo.

ERROR ANALYSIS

There are five major static error sources in the corrected speed loop in addition to the dynamic error previously discussed:

1. Gain changes in the forward loop caused mainly by variations in regulated supply pressure

2. Temperature effects on the fluidic circuitry causing some extraneous phase lag between the resonator and circuit output

3. Temperature effects within the resonator varying the resonant frequency and hence set point

4. Threshold in the position loop

5. Mechanical deadband in linkages external to the position loop

A summary of the errors at maximum and minimum speeds is shown in Table XXX.

1. Gain Change Effects

   A pressure regulation accuracy of ±10% was assumed. Since pressure sensitive gain changes occur in the forward loop, the percent of error in the closed loop is reduced.

   At 200 cps (loop gain ≈ 15), the scale factor between position and speed varies ±0.67% between the limits 695 and 705 in./cps. The equivalent displacement error is ±0.0019 inch.

At 2000 cps (loop gain ≈ 75) the scale factor stability is greatly increased at the higher loop gain and an error of ±0.00076 inch is computed.

TABLE XXX. ACCURACY SUMMARY FLUIDIC N_G SPEED SYSTEM

	N = 200 cps Position	N = 2000 cps Position
Error Source	Error - mils	Error - mils
(1)	1.90	0.76
(2)	1.52	3.02
(3)	2.15	4.30
(4)	2.70	2.70
(5)	2.00	2.00
RSS	4.67 (1.65% N)	6.27 (1.1% N)

Item (4) was computed and item (5) was arbitrarily assumed to be ±0.002 in. Error sources (1), (2), and (3) are discussed further below.

2. Temperature Effects - Circuitry

In both temperature error sources, (2) and (3), a range of supply temperatures 600° to 1200°R was assumed. Approximate heat loss calculations (based on a 1-foot length of supply tubing to the circuitry) reduced the variation to 560° to 920°R. A nominal design temperature of 790°R was selected and errors computed for temperature variations from that point.

As a general rule all pneumatic phase lag varies with temperature; for most common circuits this phase lag varies inversely proportional to $\sqrt{T}$. In the phase discriminator circuit, ideally the only phase lag should occur across the resonator; this condition is approached for very high Q resonators. Referring to the circuit schematic Figure 86, amplifiers number 1 and number 2 in series will have a nominal transport lag of approximately 0.00025 second.

A convenient formula relating the change in set point speed to temperature is

$$\frac{\Delta\omega}{\omega_o} = \frac{\omega_o \tau_o}{4Q} \quad \frac{\Delta T}{T_o} \tag{34}$$

where τ_o = nominal transport lag at T_o, ω_o = set point speed, and T'_o = nominal temperature.

At both maximum and minimum speed settings, the speed error is ±1.06%. Theoretically, this error could be compensated by unbalancing the two reference line lengths (transmitting speed pulses to the circuitry) or by adding dummy amplifiers in the R_2 reference leg. For conservatism it has been assumed that only one-half of the error would be compensated, which corresponds to position errors of 1.52 and 3.02 mils for the 200 and 2000 cps set points.

3. Temperature Effects - Resonator

The temperature of the purge air within the resonator is raised a small amount as a result of the driver gas introduced into the resonator. The actual temperature can be computed by a simple energy balance:

$$W_{purge}\, C_p\, (T_{T2}) + W_{driver}\; C_p T_d = (W_p + W_d)\, C_p\, T_x \qquad (35)$$

where T_x = actual temperature inside the resonator, T_d = temperature of driver gas, and C_p = specific heat at constant pressure. Assuming the temperature variation of 560° to 920°R and a ratio of purge-to-driver flow of 10/1, errors in T_x are ±3% on temperature which is equivalent to ±1.5% on speed.

Actually some tracking will be obtained (i.e., T_{driver} vs N_G) due to the compressor relations between temperature and speed so that the computed error of ±1.5% was reduced by one half to a value of ±0.75% corresponding to 2.15 and 4.30 mils at 200 and 2000 cps.

Lower error could possibly be achieved by increasing the purge flow and decreasing the driver flow.

APPENDIX IV
PURE TECHNOLOGY IMPLEMENTATION OF CONTROL - ELECTRONICS

INTRODUCTION

The proposed system uses advanced state-of-the-art electronics for the generation of operating schedules and for the free-turbine speed, torque and temperature trimming. It also takes advantage of the hydromechanical devices where they have proven superior to their electronic counterparts. The electronic control is optimized by the use of digital, pulse rate and analog technologies resulting in a system which satisfies the response, accuracy and reliability requirements of the specification. Advanced packaging techniques ensure that the control adequately meets the environmental, volume and weight specifications.

SYSTEM DEFINITION

The engine control system proposed herein is a schedule type controller with droop correction, topping governor loops on power turbine speed and torque, torque sharing control between engines and stator vane angle control. A schedule type control was selected for several reasons:

1. Such controls are simple and inherently stable.

2. No accurate and durable temperature sensor is currently available for temperatures of 2900°R, the peak temperature of the engine.

3. Since there is no sensor available to detect incipient compressor surge directly, the schedule control of the stator vane angle was considered to be superior to any existing closed-loop control.

The input to the fuel control actuator is a position signal proportional to the desired fuel flow ratio (W_f/P_{T3}) units. The fuel flow is controlled by a pilot valve actuated by a stepping motor via a variable linkage. This linkage is modified by P_{T3} to accomplish the desired multiplication and yield W_f.

The compressor stator vanes are positioned by an electrohydraulic actuator as a function of the gas generator speed and the ambient temperature. Provision is made to accept a temperature-limiting loop on T_{T5}, at the present time, or on T_{T4}, whenever a suitable temperature sensor becomes available.

CONTROL MODE DEFINITION

The functional block diagram of the system is shown in Figure 35. This section discusses the function of the various sections of the system.

When the W_f/P_{T3} demanded by power lever angle (PLA) setting is less than that demanded by the trimmer section, the fuel flow is controlled by the PLA schedule. This schedule yields a signal proportional to the desired N_G gas generator speed as a function of the PLA and the ambient temperature. The N_G-sensed signal is fed back to establish a droop-type control which stabilizes the gain of the engine and improves its time response. The error in the N_G loop is used as the fuel flow ratio unit signal subject to the acceleration and deceleration limits.

The acceleration limit is a function of the gas generator speed and the ambient temperature.

The deceleration limit is a constant number of fuel flow ratio units. The trimmer section takes over control when its fuel demand is less than that of the PLA schedule. It consists of a power turbine speed governing loop, a load-limiting loop and a torque-sharing loop. The torque sharing loop serves to equalize the load between the two engines, reducing unbalance and excessive wear and improving efficiency. The errors from the three feedback comparators are compared, and the largest negative error signal is passed through a proportional-plus-integral path to generate the output of the trimmer section.

The exhaust gas temperature (T_{T5}) or turbine inlet temperature (T_{T4}) limiting can be incorporated in the trimmer section.

The two sections are combined in a least select gate which passes the smallest of three signals: one from the trimmer section, a second from the PLA schedule and the third from the acceleration schedule. Finally, a most select gate takes care of the deceleration limit to prevent engine flame-out. The output of this gate becomes the input signal to the fuel valve actuator loop.

The fuel valve actuator loop yields a displacement proportional to the desired fuel ratio units. This displacement moves the fuel valve via a linkage whose ratio is adjusted to be proportional to the burner pressure, P_{T3}. The output of the linkage is proportional to the desired fuel flow, W_f.

The variable geometry (VG) is scheduled as a function of the gas generator speed and the ambient temperature. The stator vanes are driven by an electrohydraulic actuator, requiring a DC input to exploit the power density of hydraulic devices.

Below 10% full gas generator speed, the fuel control system is inactive. Between 10% and 20% insufficient electrical power is available to operate the entire control system. Hence, during this period, only the sections absolutely essential for operation (i.e., the fuel control actuator and VG actuator), are connected to

the power supply. At the same time, the fuel control valve actuator loop is given the minimum W_f/P_{T3} signal, and the VG positioning loop the full open signal. As soon as the gas generator reaches 20% of full speed, the entire system is switched on in normal control.

IMPLEMENTATION - ELECTRONIC CONTROL

The control system is implemented by a hybrid digital-analog-pulse rate technique. The schedules are generated by a time-shared digital multivariate function generator. The variable stator vanes are positioned by an electrohydraulic actuator to take full advantage of the power density of these devices. The rest of the system is implemented by pulse rate modulation with the fuel valve being driven by a stepping motor through a rack-and-pinion coupling.

The proposed digital multivariate function generator (DMFG) is unique in concept and, except for costly full digital computer-type approaches, it is the only general-purpose electronic device currently available for this purpose. It can closely approximate any multivariate function whether discontinuous or analytic. The hardware requirements are influenced by the accuracy requirements of the application and by the characteristics of the function to be generated, but they are small compared with other methods of implementation of the same functions.

This design is based on the principle of the total derivative:

$$z = z_i + \frac{\partial z}{\partial x} dx + \frac{\partial z}{\partial y} dy = z_i + dz \tag{36}$$

or in terms of finite differences,

$$z = z_i + s_{xi}\Delta x + s_{yi} \Delta y = z_i + \Delta z \tag{37}$$

where x, y, and z represent the coordinates of a three-dimensional system, and s_{xi} and s_{yi} are the slopes associated with Δx and Δx at (x_i, y_i). 's' is not necessarily identical to the value of the partial derivative at point 'i'; it may be an artificial value to provide the best approximation over the interval. Figure 88 gives a pictorial description of the techniques.

The DMFG employs table look-up to find the values of z_i, s_{xi} and s_{yi}; the values of z_i are in one table, and the values of the slopes in another. A third table is used for the necessary multiplications.

The truncated values of x_i and y_i are used in the look-up process, and the residues of the truncation are used as the respective errors $(\Delta x, \Delta y)$. In the suggested implementation scheme, each input variable is converted into a nine-bit binary

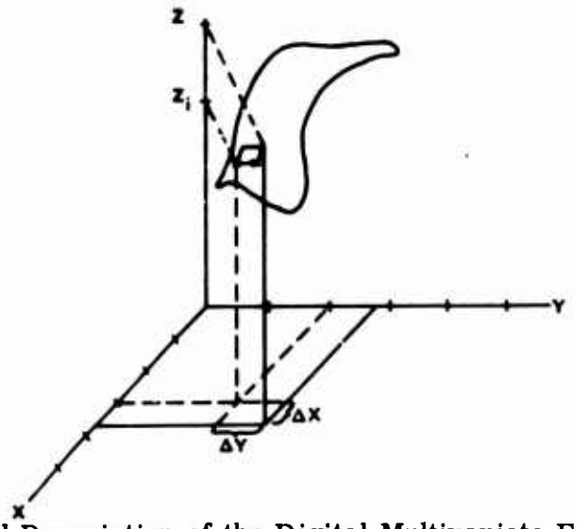

Figure 88. Pictorial Description of the Digital Multivariate Function Generator.

number of which the first three to five bits (depending on the relative resolution required) are used as the input to the look-up tables. The outputs of the tables are eight-bit binary numbers. The output of the slope table is divided into four-bit words, each containing a sign bit and three value bits. The value bits of the slopes are used in conjunction with the four- to six-bit residue of the corresponding input variable to enter the multiplication table and obtain the corrections (+ or -). These are then added to the eight-bit number obtained from the base map to yield the final result.

The outputs are fed into the appropriate buffers from which they are converted into either pulse rate signals, for the acceleration and N_G schedules, or an analog voltage, for the VG schedule. The ambient temperature input signal is converted into a pulse rate signal by a voltage-controlled oscillator (VCO).

Pulse rate modulation was selected as the basic implementation technique of the system because of its inherent accuracy and high reliability. The analog implementation suffers from low reliability when high accuracy is required. The complete digital computer approach entails prohibitive costs and excessive size.

Pulse rate components are also amenable to modern packaging techniques because of the standard sizes in which these components are manufactured. Only with such components could the accuracy, reliability and size demanded from the control system be achieved. To attain these objectives, monolithic components which are common to all pulse rate systems will be used. The electronic components, except the power supply, will be metal oxide semiconductor (MOS) based. MOS devices are easier to build, less costly, require less power to run, and, consequently, are expected to be more reliable than bipolar-type devices. The chief drawback of MOS devices, slower operating speeds, causes no problem in this application.

The W_f/P_{T3} signal drives a position loop with a stepping motor used as a power device. A stepping motor was selected primarily to allow the direct use of the pulse rate signal as input to the loop. The stepping motors currently available can accept and follow the necessary slew rate, are sufficiently small, can survive the environment, and are sufficiently reliable. The resolution achieved at the output is 1/2% so that any limit cycle resulting from the output granularity will be of small amplitude and long period.

The proportional path and the subsequent summation of the trimmer section are implemented by analog technique. This approach has various advantages:

1. By converting from pulse rate to analog and later reconverting to pulse rate, the number of clock phases required by the entire system is reduced; hence, the allowable pulse width is increased.

2. Nonlinear gain characteristics are more easily implemented by analog than by pulse rate technique.

3. The analog lead-lag compensation is more trouble-free than the equivalent pulse rate compensation.

Despite the added conversion hardware, the number of components, and hence reliability, remains virtually unchanged. This approach is acceptable because the proportional path does not require high accuracy and because errors added downstream of the integrator do not affect the steady-state accuracy.

POWER SUPPLY

The power supply for the electronic fuel control shown schematically in Figure 89 generates four DC voltages, assuming a constant current alternator as the power source. The four voltages generated are +15, -15, -12, and -10 volts. The alternator provides unregulated AC power, the voltage of which is rectified, filtered, and regulated to generate DC power as the first step in the regulation. This voltage is applied to a static inverter; the secondary coils yield the four regulated and constant frequency AC voltages, which are then rectified, filtered and further regulated by series regulators to generate the precision voltages required by the control system. The DC voltages are used to drive a sine wave generator which supplies the power to the resolvers and/or LVDT's.

A shunt regulator is used to minimize the effect of the varying voltage of the constant current alternator. This regulator dissipates very little power since it operates in the switching mode. It also minimizes the undesirable effects of the high reactance of the constant current alternator. The -12-volt supply is fed back to a voltage controlled oscillator which controls the duty cycle of the shunt regulator. The switching is performed after the three-phase bridge rectifier so that DC rather than AC is being switched.

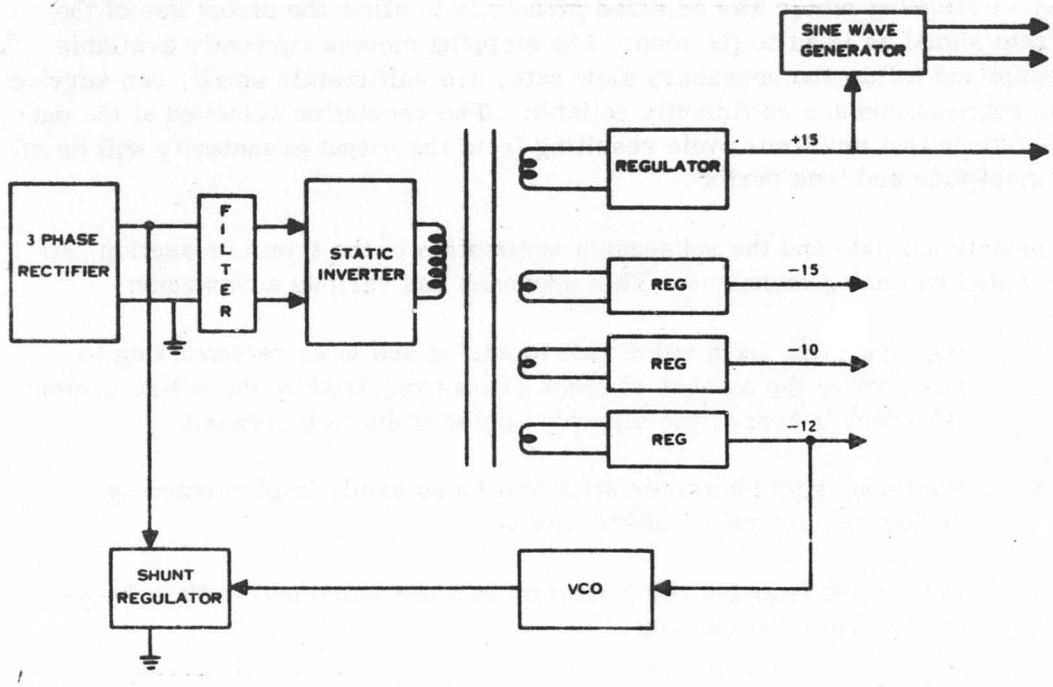

Figure 89. Electronic Control Power Supply Schematic.

A constant current alternator was assumed as the power source primarily because of its small size. The AC output current of the alternator is constant over the speed range from 20 to 100%. Provided the load impedance is constant, the output voltage and the current reach their rated values at 20% speed, and they increase by 25% at 100% speed. The problem with this type of alternator is that the high source reactance results in voltage spikes when the load is dropped suddenly. Special protective measures are added to provide for this condition.

SENSORS

Five kinds of parameters are monitored for the engine control: speed, temperature, torque, position and pressure. All of the sensor signals, except the pressure signal which is utilized in a mechanical linkage, must be transformed into electrical signals, preferably pulse trains. The speeds of the turbines are sensed by pulse pickups which yield pulse trains with frequencies directly proportional to the speeds of the turbines. The output signals of the pickups must be conditioned to provide pulse shapes that can be used in the standard logic elements. The accuracy of the signals depends on the available pulse frequencies and the time available for counting pulses in the control system where necessary. Typical maximum pulse rates available are 10 to 20 kHz.

Of the currently available sensors for ambient temperature, the platinum resistance probe presents the most desirable features for accuracy, simplicity and durability. The output of this probe is an analog voltage proportional to the temperature with a typical accuracy of ±1°F for the required range of -65°to 180°F. This signal must be converted into a digital number either by a VCO and a counter or a direct A/D converter. In this implementation, the former method is selected.

There are several torque sensors available on the market and it appears that one with 1 to 2% accuracy could be supplied for the environmental conditions specified. The exact type of the sensor depends largely on the physical constraints so that the final selection should be made in conjunction with the engine supplier.

The actuator position and the PLA will be sensed by resolvers to ensure sufficient accuracy and reliability in the given environment. The tolerance of these devices is typically 0.2%.

ACCURACY

All the accuracy requirements set down in the specifications are satisfied by the electronic control system. An attempt was made to specify sensors and other components in such a manner that the resulting accuracies would not result in excessive complication and cost. As mentioned before, the pulse rate components contribute no offset errors. Such errors that do occur are of random nature; e.g., a pulse lost or added in a counter because of uneven pulse rate. The main sources of error are the analog sensors, the transducers and the function generator. The granularity of the output stepping motor contributes a small random error and it may result in a small limit cycle in the reset mode.

The accuracy of the function generator is characterized by the following error source. Large errors occur where the rate of change of the partial derivatives (slopes of contour curves) is the greatest, i.e., at break points or jumps in the contour curves or where the contour curves have small radii of curvature. Significant errors can also be introduced by the granularity of the slopes and by their limited range. Further errors are introduced by the granularity of the input word (these are usually negligible) and by errors of the input signal; the effect on the output is determined by the slopes of the contour curves at the particular point. Since the contribution of each factor varies from point to point over the operating range, the total error band cannot be calculated by summing the errors from the individual factors.

In order to provide a proper description of the accuracy of the approximation, each map, or function, must be examined individually. Several potential worst error points must be selected on the basis of the qualitative considerations described above, and the actual errors must be calculated. The largest of these errors becomes the value of the total error band.

A set of three maps associated with engine control was analyzed for total error band. The most difficult one to approximate was the engine acceleration map. Two total error bands were determined: one for the section of the map over which the controller must operate (15 - 100% maximum speed), the other for the entire map. (The first one is 0.8%, the other 5% (expressed as ratios of the maximum value of the output.) The great difference between the two error bands results from the presence of a sharp corner associated with a steep slope in the 10-15% speed range. With due consideration to the worst case point, the 5% error band could be somewhat reduced without impairing the error band determined for the rest of the map. The examination of the engine speed schedule and the VG schedule indicated that their error bands do not exceed 0.5%.

These schedule maps were compared with the equivalent maps of other engines and were found to pose problems at least as severe. Therefore, it is likely that all engine schedules could be approximated by the digital multivariate function generator with at least as good an accuracy as outlined above.

In the schedule function generator, the 1°F tolerance of the temperature probe, the 0.5% error of the VCO and the 0.6% error of the pulse rate-to-digital converter result in 1.0% RSS error in the acceleration limit schedule. The total error band of the PLA schedule is 0.8%.

The accuracy of the N_G loop is determined by the accuracy requirements of the PLA schedule mode. Since the tolerance of the PLA schedule mode is 1% and the errors through the function generator amount to 0.8%, the allowable error for the N_G loop is 0.5% considering the error on an RSS basis. The total error of the loop is calculated by referring errors from all sources to the output and then dividing the total by the loop gain. In the present design, the only source of error is the N_G servo loop feedback path,and its contribution is 0.27% output/% actuator position. This ratio is inversely proportional to the N_G loop gain.

The error in the fuel control actuator loop must be less than 1.5% in order to satisfy the N_G loop tolerance. In order to achieve this accuracy, the position of the actuator is sensed by a resolver with a tolerance of 1.2% at limited travel.

In the trimmer section, all errors originate upstream of the integrator. All errors entering downstream of it, or in the proportional path, are eliminated by the integral action. Consequently, the N_F loop will maintain the speed within a 0.3% total error band, the Q_{PT} limiting loop will be accurate within 1.45% (sensor accuracy of 1% was assumed), and the Q_{PT} torque sharing loop will have an accuracy of 2.2%. (The torque loops suffer from the 2.5:1 reduction of authority relative to the N_F governing loop, and the torque sharing from the contribution of errors from the sensors on both engines.)

PACKAGING

The pure electronic control package is depicted in Figure 36 and is divided into an electronic section and a hydraulic section. The electronic section is located on the far side of the fuel control so that the hydromechanical section is interposed between the electronic package and the engine. The first advantage of this arrangement is that the housing of the hydromechanical section, which serves as a fuel drain cavity, can be used as a heat sink for the electronics package at a maximum fuel temperature of 200°F. Only in this way can the acceptable electronic component temperatures be guaranteed. The second advantage of the arrangement is that, since the heavier section is mounted directly to the engine, the resulting lower vibration forces allow lighter construction. The third advantage is improved maintainability: the electronics package can be easily separated from the hydromechanical section so that repairs and tests can be made without the danger of fuel contamination. The electronics package could even be removed from the engine without necessitating the removal of the hydromechanical section.

The electronics will be divided into two sections: a power supply section and a control section. There will be three printed wiring cards, one for the power supply and two for the control. The control section contains twenty 1-1/4-inch-square hybrid modules plus a few small discrete components. The power supply contains discrete components, a 1-1/2-inch diameter transformer, three stud-mounted diodes and an oscillator module. Bosses are provided for mounting the printed wiring cards and brackets for diodes. The 1-1/2 inch diameter transformer will be mounted directly to the base plate, and wired to the power supply card.

The aluminum h[illegible]te of the electronics unit will extend beyond the housing walls at four co[illegible], providing ears by which the unit can be mounted to the hydromechanical housing by means of six number 10-32 screws.

The control section will be separated from the power supply by an electromagnetic interference shield. The entire control will be covered to provide dust and EMI protection.

Two connectors will be provided: one for leads to the alternator and another for all other leads.

The total package weight, including both electronic and hydraulic package, is 10.65 pounds.

RELIABILITY

By 1972, the mean time between failures (MTBF) of the electronic section of this control is expected to be 12,900 hours. The failure rate of the semiconductor

components is affected by the number of welded (soldered) leads associated with the component. A reduction in the total failure rate can be achieved by implementing various system operations with monolithic semiconductor devices. At present, the metal oxide semiconductor (MOS) technology provides a feasible opportunity for this approach.

The failure rates upon which the above number is based are those estimated for 1972 and are lower than those established at present because of several factors. Past trends in product development in the electrical industry have demonstrated an improvement factor of 2 per 5 years. Further improvements are obtained by implementing a stringent part control program which includes detailed procurement specifications, qualification inspections, 100% electrical tests and a 100% burn in. By these methods "infant mortality" can be virtually eliminated, and poorly manufactured parts are kept from use in the product. An end item screening program is also suggested to provide two benefits: 1) reduce failures in the field, and 2) improve structural and electrical design as indicated by the results of the program thereby improving the performance and the reliability of the system.

As a program advances, it will be possible to obtain further improvements by part improvement programs, specification control measures, and screening requirements at the part and the system level.

The total pure electronic control reliability consists of the electronic components plus the hydromechanical fuel metering components. This total reliability is expected to be 9,500 hours MTBF.

FAILURE MODE ANALYSIS

Volume and weight considerations have made it impractical to consider a complete redundancy approach (duplication or triplication with majority voting). Furthermore, there is at present insufficient information to assess which parts of the system are more vulnerable than others.

For failures upstream of the stepper motor, a "backup" mode is suggested. This could take the form of a DC winding in the output stepper motor. In the event of a failure, the pilot would switch to the manual backup mode and control the position of the valve by means of a DC voltage, derived directly from the alternator, with a separate power lever or, alternately, a potentiometer on the main power lever. The switchover to backup mode could be made automatic by gating the fault signals into a master "failure" gate.

Alternately, or in addition, at the expense of additional hardware, the existing power lever could control the W_f/P_{T3} multiplier linkage directly in the backup mode. This would necessitate a clutch mechanism but would provide a measure of control in the event of a complete power supply failure.

APPENDIX V
PURE TECHNOLOGY IMPLEMENTATION OF CONTROL - FLUIDICS

GENERAL

Some of the basic types of fluidic circuits utilized in the proposed pure fluidic control system as shown in Figure 34 are discussed with respect to performance and accuracy with particular emphasis on fluidic interface devices. A reliability analysis of the complete control system is also presented. A discussion of the fluidic gas generator speed servo was previously introduced in Appendix III and an analysis of the fluidic turbine inlet temperature sensor was presented in Appendix II.

One of the more significant fluidic inaccuracy sources results from supply pressure variations. Most of the data presented was taken with circuitry not specifically designed for operation over a wide range of supply conditions; thus, it is anticipated that if a particular loop of circuit were developed for the specific conditions to be encountered in the present application, tighter accuracy specifications might be possible.

SIGNAL SUMMING - OPERATIONAL AMPLIFIER

Summing two or more differential signals is done resistively through a proportional amplifier, analogous to electronic signal summing. Differential signal summing has proven to be much more tolerant to minor supply pressure fluctuations, bias signals, etc. than single-ended summing. Typical summation configurations are illustrated in Figure 90.

The operational amplifier is the basic element used in all amplifying, summing, and wave shaping (lead, lag, integration, etc.) applications. The basic equation describing its function is:

$$\frac{\text{Output}}{\text{Input}} = \frac{Z_f}{Z_i} \frac{GH}{1 + GH} \tag{38}$$

where GH = the open-loop amplifier gain

Z_f, Z_i = feedback and input impedances.

In general, Z_f and Z_i can be complex impedances involving resistance capacitance and inductance (e.g., a capacitor feedback element will make a lead network).

Temperature and pressure changes cause two effects: the loop gain changes (GH)

and time constants in the Z_f and Z_i circuits change. Loop gain effects are small; as GH varies, the ratio of GH/1 + HG variation is reduced by 1/GH. That is, for a loop gain of 20 and a power supply variation of +20%, a variation of ±1% can be expected in GH/1+GH. Steady-state changes in Z_f/Z_i can be neglected since both feedback and input resistors are the same temperature levels. (They are physically in the same assembly.)

Time constants vary with temperature; the time constant of an RC network varies as

$$\tau \alpha \frac{1}{\sqrt{\theta}} \quad \text{for square law resistors} \tag{39}$$

or

$$\tau \alpha \theta^{.7} \quad \text{for laminar resistors} \tag{40}$$

where Θ is the relative absolute temperature.

In an amplifier network, the total resistance communicating with the capacitor elements generally includes the amplifier input and output resistance (square law) so that generally the laminar exponent of 0.7 is reduced to possibly 0.5.

Assuming ±20% changes in the power supply pressure and a 2:1 variation in temperature, the accuracy of the operational amplifier circuits is

±1% on gain

and ±19% on time constants

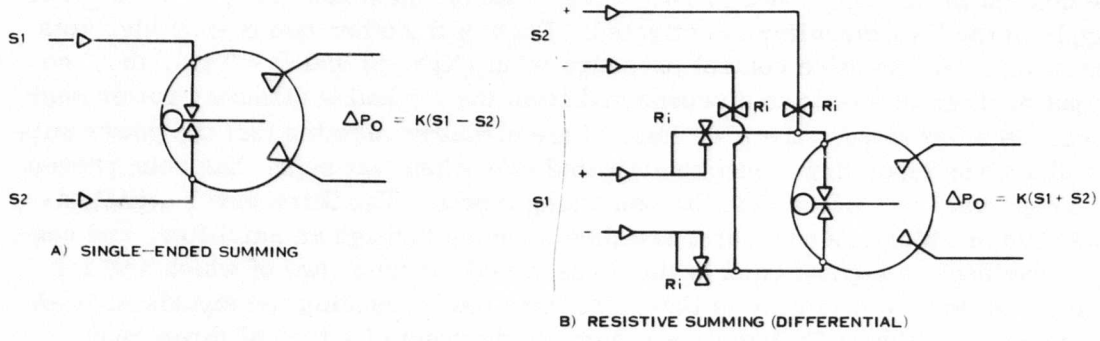

Figure 90. Schematic of Fluidic Summing Techniques.

SIGNAL SELECTION

Two-Input Selection

Signal selection can be performed by fluidic circuitry. The selector compares analog input signals and performs the necessary logic to let either the highest or lowest of the two signals pass. The two signals are compared in a summing amplifier. The output polarity of the comparator switches a flip-flop; the output is the power supply for amplifiers in series with each input channel. Depending on the flip-flop output connections, the result is that only the power supply associated with either the highest or lowest error signal is permitted to pass. All signals are summed into a gain block and negative feedback is applied back to the inputs. Loss of accuracy is not therefore incurred by passing the signals through the selector.

Three-Input Selection

Three-input signal selection requires more complicated fluidic logic and circuitry. The logic is best illustrated with an example. The selector involved is designed to compare three input error signals, N_F, Q, T_{T4}, and to permit only the lowest signal to pass. Referring to the circuit diagram in Figure 91, the three signals are compared with each other in three summing amplifier flip-flop branches and six digital signals, $N_F > Q$, $Q > N_F$, $N_F > T_{T4}$, $T_{T4} > N_F$, $T_{T4} > Q$, and $Q > T_{T4}$ are produced. These six digital signals are then compared in three or-nor elements which results in an AND function. Assume T_{T4} is approaching its limiting value and its error signal is the lowest of the three inputs. The or-nor element whose output is the power supply of the circuitry connected with T_{T4} has the control inputs $T_{T4} > Q$ and $T_{T4} > N_F$, both of which are zero, and the power supply of the T_{T4} circuitry is activated. Each of the other two or-nor elements has at least one positive control pressure input ($N_F > T_{T4}$ and $Q > T_{T4}$), thus the output of these elements is disconnected from the N_F and Q circuitry power supplies. In other words, the AND logic of the circuitry dictates that the power supply of a given input signal will be activated only when that signal has been proven by comparison to be less than the remaining inputs. The three error signal inputs (two of which are now zero) are then summed through an amplifier, and negative feedback is applied back to the three signal circuits (two of which are dormant). No loss of accuracy is therefore incurred by passing the signals through the selector. Figure 91 depicts a schematic diagram of a typical three-input selector.

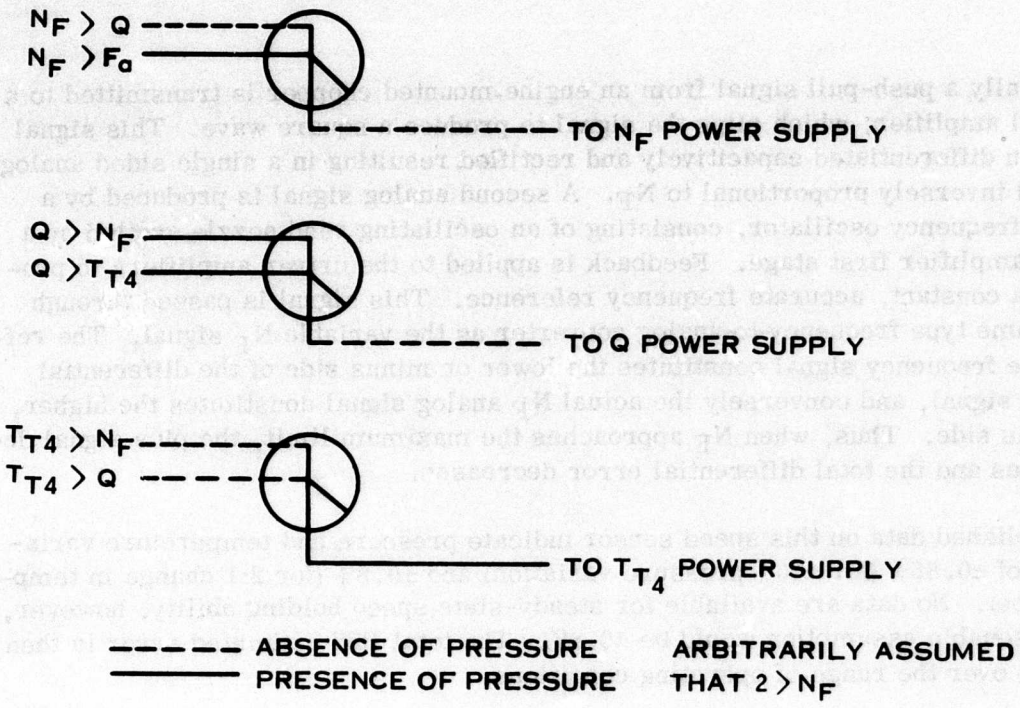

Figure 91. Fluidic Three-Input Selector, Partial-Circuit Diagram.

In the selector approach used, feedback around the selector will be employed so that the same accuracy of analog computation can be assumed as for the operational amplifier. In addition, an error is further introduced by the digital amplifier following the input summing amplifier. The digital amplifier is a memory type of element (flip-flop) having a hysteresis band of about ±10%. If one amplifier stage (a gain of five) precedes the flip-flop, the hysteresis referred back to the input is 2%. If two parameters are near the same limit value, 2% of hysteresis between limits will occur. If the hysteresis is undesirable, additional amplifier stages can be added which will reduce the hysteresis a factor of five for each added stage.

REAL SPEED SENSOR

The real speed sensor is designed to produce an analog signal proportional to real speed of the power turbine (N_P). This signal is then compared to a reference frequency analog signal, and a real speed error signal used for governing N_F results.

Basically, a push-pull signal from an engine-mounted chopper is transmitted to a digital amplifier, which clips the signal to produce a square wave. This signal is then differentiated capacitively and rectified, resulting in a single-sided analog signal inversely proportional to N_F. A second analog signal is produced by a fixed frequency oscillator, consisting of an oscillating reed nozzle excited by a fluid amplifier first stage. Feedback is applied to the driver amplifiers to produce a constant, accurate frequency reference. This signal is passed through the same type frequency-to-analog converter as the variable N_F signal. The reference frequency signal constitutes the lower or minus side of the differential error signal, and conversely the actual N_F analog signal constitutes the higher, or plus side. Thus, when N_F approaches the maximum limit, the plus signal decreases and the total differential error decreases.

Unpublished data on this speed sensor indicate pressure and temperature variations of ±0.85% (for ±20% pressure variation) and ±0.8% (for 2:1 change in temperature). No data are available for steady-state speed holding ability; however, a reasonable assumption would be ±0.8%. The total RSS estimated error is then ±1.2% over the range of operating conditions.

MECHANICAL-MOTION-TO-FLUIDIC TRANSDUCER

Mechanical-motion-to-fluidic-signal transducers are required to introduce the following inputs into the fluidic fuel control circuit.

1. β_H collective
2. $\frac{W_f}{P_{T3}}$ cam schedule
3. Stator vane cam schedule

The requirement of the transducers is to produce a proportional fluidic output as a function of input motion. The accuracy of the transducer desired is on the order of ±0.25%. Repeatability, hysteresis, ambient temperature and pressure, and supply pressure effects are included in the accuracy.

A transducer capable of meeting the accuracy requirement in a reasonably small size package is shown in Figure 92.

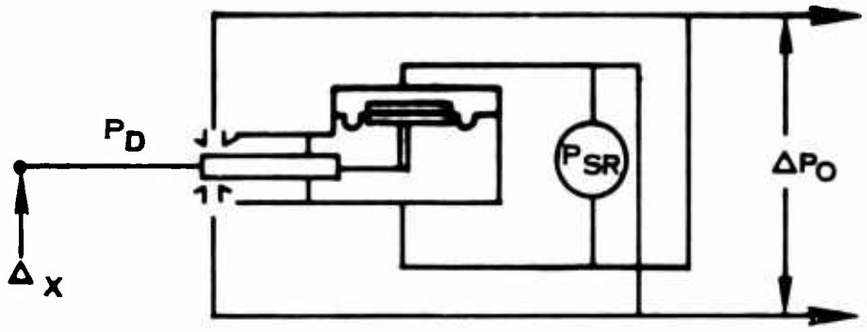

Figure 92. Schematic of Mechanical Motion to Fluidic Signal Transducer.

The transducer is a force (or torque) balance device in which the input motion, converted to torque through the wire cantilever spring, is nulled by the output pressure acting on a diaphragm area. The input and feedback torques are summed mechanically in a frictionless flex-pivot and isolation member. Mechanical motion is converted to proportional fluidic pressure by the deflection of the flapper. The flapper deflection unbalances the impedance in the fluidic bridge circuit to produce a differential output pressure.

Accuracy

The factors that affect accuracy are discussed below.

Ambient pressure

The transducer is designed so that it is insensitive to variations in ambient pressure.

Temperature

Temperature effects within the transducer can be made negligible by transducer design. A significant source of temperature error can result from thermal gradients between the input and transducer position reference points. Assuming a thermal gradient of 5°F, a distance of 0.5 inch from base reference to input point, and aluminum as the material, a position input error of 0.000035 inch can result. Assuming an input of ±0.2 inch, a 5°F thermal gradient will result in ±0.175% accuracy.

Fluidic Supply Pressure

Variation in the fluidic supply pressure changes the flapper-nozzle gain directly. Hence, the transducer accuracy is influenced through changes in the loop gain. The loop gain of the transducer is defined as

$$GH = \frac{1}{k_\theta} \frac{\partial P_o}{\partial \theta_n} (2 \ell_f A_f) \tag{41}$$

where k = torque gradient of flapper, in. lb/rad

$\frac{\partial P_o}{\partial \theta_n}$ = pressure gain of flapper-nozzle, psi/rad

ℓ_f = feedback lever, in.

A_f = feedback diaphragm area, $in.^2$

Assuming typical values for the parameters involved as follows,

k_θ = 5 in. lb/rad

$\frac{\partial P_o}{\partial \theta_n}$ = 1000 psi/rad (P_s = 10 psia)

ℓ_f = 0.75 in.

A_f = 0.2 $in.^2$

then GH = 60.

Assuming that the fluidic supply pressure is regulated to ±10%, then the accuracy of the transducer with GH = 60 is +0.15%, -0.18%.

Hysteresis

The flexing members of the transducer have approximately 2% hysteresis. Assuming 0.04 in.-lb torque will saturate the flapper deflection, a 2% hysteresis is equivalent to 8×10^{-5} in.-lb torque. The maximum hysteresis referred to output pressure through the previously assumed feedback gain of 0.3 in. lb/psi is 2.67×10^{-4} psi. The accuracy due to 2% hysteresis for a maximum fluidic signal of 5 psid is 0.006%. Hysteresis is insignificant due to the gains available in the transducer.

Friction

The transducer is designed for negligible friction.

Mechanical Tolerance

Error due to mechanical design tolerances can occur at the input cam, follower and linkages. Assuming tolerances on the order of ±0.0005 inch and maximum transducer motion of ±0.2 inch, the effect of tolerance on accuracy is ±0.25%.

Accuracy Summary

Accuracy of the mechanical-motion-to-fluidic-signal transducer is summarized in Table XXXI.

TABLE XXXI. TRANSDUCER ACCURACY SUMMARY

ERROR SOURCE	ERROR
Ambient Pressure	negligible
Temperature	0.175%
Fluidic Supply Pressure	0.18%
Hysteresis	0.006%
Friction	negligible
Mechanical Tolerance	0.25%
RSS Total	0.354%

Size and Weight

A mechanical motion to fluidic transducer providing accuracies on the order of 0.4 to 0.5% will occupy a space of 1.75 cubic inches (1 inch x 1 inch x 1-3/4 inch) and will weigh approximately 0.2 pound.

Gas Flow Required

The gas flow required is equivalent to that through a 2.5×10^{-4} square-inch orifice. At 20 psia output pressure, the flow is 1.08×10^{-4} pounds/second at 200°F.

FLUIDIC-TO-HYDROMECHANICAL TRANSDUCERS

Fluidic-to-hydromechanical transducers are required to amplify the output of the

fluidic fuel control circuit and provide interface with hydromechanical servoactuators. Fluidic-to-hydromechanical interfaces are required for the following actuation functions:

1. T_{T2} servo
2. Corrected N_G servo
3. Stator vane servo
4. Main fuel valve servo

The specific interface function desired is to transduce a pneumatic pressure signal of low-pressure level to a proportional mechanical motion while working against a high force load. The accuracy, load, and displacement requirements dictate the use of an interface device equivalent to a fluidic input hydraulic servo valve actuator, typical of that shown for the stator vane servoactuator in Figure 34.

Accuracy

Ambient pressure, temperature, fuel reference and drain pressures, hysteresis, friction and loading influence the transducer-servoactuator position accuracy. These effects are discussed as follows:

Ambient Pressure

Significant errors can be introduced into the fluidic input stage by ambient pressure variations if appreciable differential areas are exposed to ambient pressure. The transducer is designed so that it is insensitive to this effect.

Temperature

Effects of temperature on accuracy are negligible due to symmetry (push-pull) in design. No significant thermal gradients are anticipated to cause excessive null shift.

Fuel Reference Pressure

Variation in the fuel reference pressure (200 to 800 psi) can influence the transducer-servoactuator position accuracy. Since the actuator stiffness (load sensitivity) is a function of the valve pressure gain which is also dependent upon the reference pressure, sufficient pressure gain must be provided to meet the accuracy requirements at minimum reference pressure. The stiffness of the servoactuator is defined as:

$$\frac{\Delta F}{\Delta y} = 2A_p \ell_f r_f K_f K_v \left(\frac{\partial P_o}{\partial V}\right) \qquad (42)$$

where A_p = actuator piston area, inch^2

ℓ_f = feedback lever ratio, inch/inch

r_f = feedback arm, inch

K_f = feedback spring rate, pound/inch

K_v = transducer - valve gain, inch/inch pound

$\frac{\partial P_o}{\partial V}$ = pressure gain of spool valve, psi/inch

Assuming typical values for the parameters involved as follows,

A_p = 0.33 inch^2 (50-lb force capability at 150 psid)

ℓ_f = 0.5 inch/inch

r_f = 0.75 inch

K_f = 5 pound/inch

K_v = 0.25 inch/inch pound

$\frac{\partial P_o}{\partial V}$ = 15 x 10^4 psi/inch at P_R = 200 psi

then $\frac{\Delta F}{\Delta y}$ = 4.6 x 10^4 pound/inch

Assuming an actuator stroke of 1.0 inch and 50 pound load (friction plus output force) an accuracy of 0.1% is possible.

Variation in hydraulic reference pressure is also reflected in actuator accuracy through changes in the spool valve flow gain. Thus, the actuator loop gain changes with reference pressure are analyzed.

The loop gain of the transducer-servovalve actuator is defined as

$$GH = K_v \frac{\partial Q}{\partial V} \left(\frac{1}{A_p}\right) (r_f \ell_f K_f) \qquad (43)$$

where the parameters are as defined previously, and $\frac{\partial Q}{\partial V}$ = spool valve flow gain in cubic inches per second.

Assuming $\frac{\partial Q}{\partial V}$ = 50 cis/inch and the previously used values for the other parameters, GH = 71.

For a change in ΔP across the valve of 195 to 250 psid, the actuator accuracy is 0.2%.

Hydraulic Case Pressure, Friction and Loading

The hydraulic case pressure acting upon unbalanced actuator rod areas, friction, and loading affect position accuracy. Their effect on accuracy is dependent upon the actuator stiffness as discussed previously. The combined loading for 0.1% accuracy is less than 50 lb.

Hysteresis

The flexing members of the transducer and servovalve have approximately 2% hysteresis. Assuming that 0.1 in.-lb torque will saturate the flapper deflection, a 2% hysteresis is equivalent to 0.002 in.-lb torque input. The maximum hysteresis referred to output motion through the foregoing feedback gain of 1.87 in. lb/in. is 0.00107 in. The accuracy due to 2% hysteresis for a maximum of 1.0 inch is 0.1%.

Accuracy Summary

Accuracy of the fluidic-to-hydromechanical transducer is summarized in Table XXXII.

TABLE XXXII. ACCURACY SUMMARY, FLUIDIC TO HYDROMECHANICAL TRANSDUCER

ERROR SOURCE	ERROR
Hydraulic Reference Pressure (Friction and Load)	0.1%
(Flow Gain)	0.2%
Hysteresis	0.1%
RSS Total	0.245%

Size and Weight

The size and weight of the fluidic input servoactuator to provide 50 lb force and 1 inch displacement are estimated as follows:

	Size	Weight
Transducer and flapper nozzle	1.75 $in.^3$	0.2 lb
Spool valve	0.5 $in.^3$	0.1 lb
Actuator and feedback	3.1 $in.^3$	0.6 lb
Total	5.35 $in.^3$	0.9 lb

Gas Flow Required

The fluidic input flow comes from the fluidic fuel control circuit. Since the transducer is a blocked (high impedance) load on the circuit, negligible flow is required.

ELECTROMAGNETIC-TO-FLUIDIC TRANSDUCER

Analog-electrical-to-fluidic-signal transducers are required to introduce the electrical torque sensor outputs into the fluidic fuel control circuit.

This transducer shown in Figure 93 is basically the same in perfc rmance characteristics as the mechanical motion to fluidic transducer. The only difference is that input torque is developed by current input to an electromagnetic torque motor.

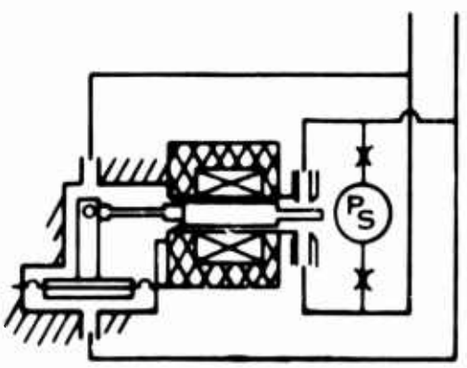

Figure 93. Analog Electrical to Fluidic Signal Transducer

Accuracy

The factors that affect accuracy are identical to those previously discussed for the mechanical-motion-to-fluidic transducer. The estimated RSS accuracy is of the same order, 0.4% for the design parameters discussed.

Size and Weight

An electromagnetic-to-fluidic transducer providing accuracy on the order of 0.4 to 0.5% will occupy a space of 2.5 cubin inches (1 inch x 1-1/4 inches x 2 inches) and weigh approximately 0.35 pound.

Gas Flow Required

The gas flow required at 20 psia output pressure is approximately 1×10^{-4} pound/second at 200°F.

Pure Fluidic Control Reliability

By necessity, quantitative reliability determinations of fluidic control systems must be based on speculative and extrapolated analysis due to the relative newness of the state of the art and the scarcity of pertinent data. The elimination of many moving parts and the apparent tolerance to a wide range of adverse environments give intuitive confidence in fluid amplifier control reliability.

In order to provide some quantitative indication of fluid amplifier reliability, failure risk analysis has been performed. Included within the scope of this analysis has been (1) the underlying failure modes associated with the individual fluidic and mechanical elements, (2) the underlying mechanism of failures, and (3) the effects of such failures on the performance of the related control function.

Determination of Failure Rates

Analysis of the control loops indicates that fluid amplifier components are the dominant elements in the control loops. These elements vary in function and complexity as well as in their effect on system performance. They can, however, be individually broken down into detail design features, such as orifices or nozzles, and pneumatic connections, and their dominant failure mechanism identified. Standard reliability handbooks and methods (Naval FARADA, MIL Handbook 217, etc.) can be used to approximate MTBF for the associated mechanical, pneumatic, and

hydraulic elements also in each loop. Most of the failure rates assumed in this analysis have been based on an analogous reliability study performed for the USAF Aeropropulsion Laboratory (Contract No. AF33(657)-10705 SA4) entitled Control Research Program for the Variable Compressor and Turbine Components Program. The degree of extrapolation is reemphasized in this reference, although the results of the present analysis are considered to represent a reasonable measure of fluidic system reliability. Explanation and qualification of USAF Control Research data are as follows:

Fluid Amplifier Contamination

Contamination refers to the plugging or geometric variation of an amplifier port resulting from the introduction of foreign material. Assuming a 20-mil orifice with an anticipated filtration level of between 1.0 and 1.5 mils, a failure rate of 0.30×10^{-6} failures/hour was assumed. This estimate is considered somewhat conservative since contamination due to fluid breakdown or gumming, as with hydraulic systems, will not occur.

Fluid Amplifier Crossport Leakage

Crossport leakage refers to critical leakages occurring at the cover and circuit channel, such as between the power supply and the control channel. One crossport leakage failure rate is assumed for each amplifier. The failure rate of 0.02×10^{-4} failure/hour was chosen based on FARADA experience with case-welded seals. This constitutes a pessimistic approximation since the use of diffusion bonding in the manufacturing process will tend to minimize the susceptibility to crossport leakage.

External Leakage and Breakage

This failure mechanism refers to failure of the external pneumatic connections to the fluid amplifier module. A failure rate of 0.03×10^{-6} for leaks and 0.01×10^{-6} for breaks is assumed based on FARADA data for pneumatic joints. A high degree of circuit integration will tend to minimize these failure mechanisms.

Restrictor Contamination

Contamination resulting in plugging and geometry changing will be the dominant failure mechanism in fluidic restrictors (resistances). Restrictors are considered to be simple capillary tubes, and a failure rate of 0.35×10^{-6} is assigned. This is based on 20-mil capillaries and a filtration level of between 1.0 and 1.5 mils.

Fluid Capacitance

The dominant mode of failure for a fluid capacitor is assumed to be contamination of the element chamber. Thus, for chamber contamination of a fixed resonator, a failure rate of 0.15×10^{-6} is assumed.

Frictionless Pivot

This device has been treated as two leaf springs and the pertinent failure mechanisms appear to be fatigue and plastic deformation. Failure rates of 0.15×10^{-6} and 0.05×10^{-6}, respectively, have been assumed.

Torsional Pendulum

The failure mechanism of the torsional pendulum is approximated by that of a simple leaf spring. A failure rate of 0.15×10^{-6} for fatigue and 0.05×10^{-6} for plastic deformation has been assumed.

Reed Reference

Again using the leaf spring approximation, failure rates of 0.15×10^{-6} and 0.05×10^{-6} are assumed for fatigue and plastic deformation modes of failure.

Diaphragm

Pertinent failure mechanisms appear to be fatigue and overstress, and a failure rate of 0.8×10^{-6} is assumed.

Helical Spring

Fatigue and overstress appear to be the dominant failure mechanisms, and a collective failure rate of 0.15×10^{-6} is assumed, considering levels of stress expected.

Reference Screw

A position change is the outstanding failure, and a failure rate of 0.10×10^{-6} is assumed.

Helmholtz Resonator

Contamination of the driving amplifier inlet ports appears to be the dominant failure mechanism, and a failure rate of 0.35×10^{-6} is assumed. Contamination of the aspirator is assumed to be negligible, considering the

relative size of the ports involved.

Table XXXIII is a summary of control elements employed, the predominant failure mechanism associated with each, and the failure rate assumed for each element.

TABLE XXXIII. FAILURE RATES - FLUID AMPLIFIER CONTROL

Component	Failure Mechanism	Failures/hour x 10^6
Fluid Amplifier	Contamination per 20 mil port	0.30
	Leakage, crossport per element	0.20
	Leakage, external per connection	0.03
	Breakage, external per connection	0.01
Capacitor	Contamination - Fouling, plugging	0.15
Resistors - Capillary	Contamination - Fouling, plugging	0.35
Frictionless Pivot	Fatigue	0.15
	Plastic deformation	0.05
Torsional Pendulum	Leaf spring fatigue	0.15
	Plastic deformation	0.05
Reed Reference	Fatigue	0.15
Helmholtz Resonator (Piston-cylinder)	Contamination	0.35
Diaphragm	Fatigue, overstress	0.8
Helical Spring	Fatigue, overstress, Plastic deformation	0.15
Reference Screw	Change position	0.10
Pressure Regulator	Full-open or full-shut failure	0.50
Air Filter	Fatigue, pitting, overstress	0.20
Check Valve	Spring fatigue	0.15
	Face, seat abrasion	0.30
Actuator	Sticking, inoperative	0.21

The combined failure rate for the entire fluidic control system has been determined to be 69.02 failures per million hours, resulting in a MTBF of 14,490 hours.

In many cases, hard over failure modes are designated for fluidic elements operating on frequency signals. This simply signifies a hard over signal each half cycle.

The analysis has been simplified to some extent, and some minor modes of failure may have been inadvertently overlooked. However, final results can be safely assumed to represent the order of magnitude of fluidic-hydromechanical reliability of this particular system.

Unclassified

Security Classification

DOCUMENT CONTROL DATA - R & D

(Security classification of title, body of abstract and indexing annotation must be entered when the overall report is classified)

1. ORIGINATING ACTIVITY (Corporate author)	2a. REPORT SECURITY CLASSIFICATION
Hamilton Standard Division of United Aircraft Corp. Windsor Locks, Connecticut	Unclassified 2b. GROUP

3. REPORT TITLE

STUDY OF AN ADVANCED CONTROL SYSTEM FOR SMALL FREE-TURBINE ENGINES

4. DESCRIPTIVE NOTES (Type of report and inclusive dates)

Final Report Study and Concept Design Program - 1 July 1968 - 31 December 1969

5. AUTHOR(S) (First name, middle initial, last name)

Thomas L. Soule
Donald E. Anschutz
Melvin L. Perkins

6. REPORT DATE	7a. TOTAL NO. OF PAGES	7b. NO. OF REFS
June 1969	276	0

8a. CONTRACT OR GRANT NO.	9a. ORIGINATOR'S REPORT NUMBER(S)
DAA J02-68-C-0041 b. PROJECT NO. 1G162203D144 c. d.	USAAVLABS Technical Report 69-41 9b. OTHER REPORT NO(S) (Any other numbers that may be assigned this report) HSER 5300

10. DISTRIBUTION STATEMENT

This document is subject to special export controls and each transmittal to foreign governments or foreign nationals may be made only with prior approval of US Army Aviation Materiel Laboratories, Fort Eustis, Virginia 23604.

11. SUPPLEMENTARY NOTES	12. SPONSORING MILITARY ACTIVITY
	US Army Aviation Materiel Laboratories Fort Eustis, Virginia

13. ABSTRACT

Advanced small free-turbine engines in the 2-to-5-pps airflow class have undergone vast improvements in performance, permitting large reductions in overall size. Effort is required to optimize performance and to miniaturize the engine control system to keep pace with these improvements.

This study program was undertaken to conceptually design an advanced engine control system for this class of engine, providing all the required functions consistent with an advanced system and to accommodate, with mimimum hardware change, such variants as regenerative cycle and/or variable turbine geometry. Study effort to determine the optimum control for the small engine of the mid 1970's fell into two major categories: mode selection and technology selection. Ten modes of control were evaluated, with the selected mode consisting of a $W_f/PT3$-scheduling gas generator control and an isochronous N_F-governing control with turbine-discharge-temperature limiting.

Technology selection consisted of reviewing electronic, fluidic, and hydromechanical technologies against a weighted set of evaluation criteria for application to the proposed system. This resulted in the selection of a hydromechanical gas generator control and an electronic N_F control with fluidic N_F overspeed sensing.

DD FORM 1 NOV 68 1473 REPLACES DD FORM 1473, 1 JAN 64, WHICH IS OBSOLETE FOR ARMY USE.

Unclassified

Security Classification

14. KEY WORDS	LINK A		LINK B		LINK C	
	ROLE	WT	ROLE	WT	ROLE	WT
Engine Control System						
Gas Generator Control						
Regenerative Engine						
Hydromechanical Technology						
Fluidic Technology						
Electronic Technology						
Mode of Control						
Turbine Inlet Temperature Sensor						
Influence Coefficient Summary						
Ng Speed Sensor						
Technology Trade-Off Studies						
Base Engine						
Vulnerability						
Pure Technology Implementation						
Hybrid Control						
Power-Turbine Governing						